

T 394

Microwave Electronics

**Investigations on Reconfigurable
Dual Frequency Microstrip Antennas Controlled by
PIN Diodes and Varactors**

Thesis submitted to
Cochin University of Science and Technology

in partial fulfilment of the requirements

for the award of the degree of

DOCTOR OF PHILOSOPHY

by

Shynu S.V.

Under the guidance of

Prof. K. Vasudevan

Department of Electronics
Cochin University of Science and Technology
Cochin 6820 22
India



October 2006

CERTIFICATE

Certified that the work presented in this thesis entitled “Investigations on Reconfigurable Dual Frequency Microstrip Antennas Controlled by PIN Diodes and Varactors” is based on the bonafide research work done by Mr. Shynu S.V. under my guidance in the Centre for Research in Electromagnetics and Antennas (CREMA), Department of Electronics, Cochin University of Science and Technology, Cochin 682 022, and has not been included in any other thesis submitted previously for the award of any degree.

Cochin-22
October 20, 2006



Prof. K. Vasudevan
Supervising Guide
Centre for Research in Electromagnetics
and Antennas (CREMA)
Department of Electronics
Cochin University of Science and Technology
Cochin-22

DECLARATION

I hereby declare that the present work entitled “Investigations on Reconfigurable Dual Frequency Microstrip Antennas Controlled by PIN Diodes and Varactors” is based on the original work done by me under the guidance of Prof. K. Vasudevan, Centre for Research in Electromagnetics and Antennas (CREMA), Department of Electronics, Cochin University of Science and Technology, Cochin-22 and has not been included in any other thesis submitted previously for the award of any degree.

Cochin-22

October 20, 2006



Shynu S.V.

ACKNOWLEDGEMENT

With immense pleasure I extend deep sense of gratitude to my supervising guide, Prof. K. Vasudevan, Centre for Research in Electromagnetics and Antennas (CREMA), Department of Electronics, Cochin University of Science and Technology for his excellent guidance and constant encouragement throughout the course.

I thank Prof. K.G Nair, Director C-SiS, Cochin University of Science and Technology for his constant support and encouragement.

I am thankful to Prof. P. Mohanan, Department of Electronics, and Dr. C.K. Aanandan, Reader, Department of Electronics, Cochin University of Science and Technology for providing the necessary facilities and for their valuable suggestions in shaping my research work.

I remember with gratitude Prof. K.T. Mathew, Prof. K.G. Balakrishnan Nair, Prof. P.R.S Pillai and Dr. Tessamma Thomas for their support and encouragement of my work and also grateful to Dr. Rajaveerappa, Mrs. M.H Supriya and Mr. James Kurian, faculty members, Department of Electronics for their support and help.

I am thankful to all the non-teaching staff of the Department of Electronics for their sincere co-operation.

I am extremely thankful to all the Research Scholars and Project Staff of the Department of Electronics, from whom I have benefited immensely towards the accomplishment of this work.

I wish to thank Kerala State Council for Science Technology and Environment (KSCSTE), Govt. of Kerala, for providing Junior Research Fellowship (JRF). I also acknowledge University Grants Commission (UGC), Govt. of India for financial assistance at the later stages of my research work.

I am extremely grateful to my parents, brother, my wife and well-wishers for the support and encouragement rendered to me. Above all, I thank the supreme power without whose blessings and kindness I cannot achieve anything in this world.

Shyru S.V.

CONTENTS

1. INTRODUCTION	1- 24
1.1 Microstrip Antennas	4
1.1.1 Advantages and Limitations	4
1.1.2 Radiation Mechanism	6
1.1.3 Analytical Models for Microstrip Antennas	7
1.1.3.1 Transmission Line Model	7
1.1.3.2 Cavity Model	8
1.2 Various Microstrip Antenna Configurations	9
1.2.1 Microstrip Patch Antennas	9
1.2.2 Microstrip Dipoles	10
1.2.3 Printed Slot Antennas	10
1.2.4 Microstrip Travelling Wave Antennas	11
1.3 Feeding Techniques	11
1.3.1 Coaxial Feed or Probe Coupling	12
1.3.2 Microstrip Line Feed	13
1.3.3 Proximity Coupled Microstrip Feed	13
1.3.4 Aperture Coupled Microstrip Feed	14
1.3.5 Coplanar Waveguide Feed	15
1.4 Full Wave Analysis of Microstrip Antennas	15
1.4.1 Spectral Domain Full-Wave Analysis	16
1.4.2 Mixed Potential Integral Equation Analysis (MPIE)	16
1.4.3 Finite Difference Time Domain Analysis	16
1.5 Dual Frequency Microstrip Antenna Technologies	17
1.5.1 Multi-Patch Dual-Frequency Antennas	19
1.5.2 Reactively Loaded Antennas	19
1.5.3 Orthogonal-Mode Dual Frequency Patch Antennas	19
1.6 Current Reconfigurable Antenna Technologies	20
1.6.1 Mechanical Tuning	20
1.6.2 Magnetic Tuning	21
1.6.3 Electronic Tuning	21
1.7 Reconfigurable Microstrip Antennas	22
1.8 Motivation and Development of Subject of Research	23
1.9 Thesis Overview	24
2. A BRIEF REVIEW OF PAST WORK	26- 47
2.1 Microstrip Antenna Technology	29
2.2 Dual Frequency Microstrip Antenna Design	37
2.3 Reconfigurable Antenna Techniques	40
2.4 Analysis of Microstrip Antennas	45

3. METHODOLOGY – EXPERIMENTAL AND THEORETICAL ANALYSIS	49 - 74
3.1 <i>Fabrication of the Microstrip Antenna</i>	51
3.1.1 <i>Selection of Substrate Material</i>	51
3.1.2 <i>Photolithography</i>	52
3.1.3 <i>Integration of Semiconductor Devices</i>	53
3.2 <i>Excitation Technique</i>	53
3.3 <i>Facilities Used for Antenna Measurements</i>	54
3.3.1 <i>HP 8510C Vector Network Analyzer</i>	54
3.3.2 <i>Anechoic Chamber</i>	55
3.4 <i>Antenna Measurements</i>	56
3.4.1 <i>Measurement of Resonant Frequency, S-Parameters and Bandwidth</i>	56
3.4.2 <i>Measurement of Radiation Pattern</i>	57
3.4.3 <i>Gain</i>	59
3.4.4 <i>Polarization</i>	59
3.5 <i>Antenna Design and Analysis Using FDTD Method</i>	60
3.5.1 <i>Simulation Steps</i>	61
3.5.2 <i>Basic Concepts</i>	62
3.5.3 <i>FDTD Problem Definition</i>	65
3.5.4 <i>FDTD Principal Equations</i>	66
3.5.5 <i>Source Consideration</i>	68
3.5.6 <i>Absorbing Boundary conditions</i>	70
3.5.7 <i>Scattering Parameters</i>	72
3.5.8 <i>Computational Domain and Implementation of 3D-FDTD</i>	72
3.6 <i>Electromagnetic Simulation Using IE3D™</i>	73
4. EXPERIMENTAL AND THEORETICAL INVESTIGATIONS ON RECONFIGURABLE DUAL FREQUENCY MICROSTRIP ANTENNAS USING PIN DIODES	75 - 183
4.1 <i>Design of the Passive Dual Frequency Dual Polarized Square Microstrip Patch Antenna</i>	79
4.1.1 <i>Design Concepts</i>	79
4.1.2 <i>Staircase Approximation in FDTD</i>	81
4.1.3 <i>Antenna Geometry</i>	82
4.1.4 <i>Excitation Technique</i>	84
4.1.5 <i>Mechanical Frequency Tuning</i>	85
4.1.6 <i>Antenna Dimensions and Its Effect on Dual Resonant Modes</i>	87
4.1.6.1 <i>Frequency Tuning by Tailoring the Slot Arm Length</i>	89
4.1.6.2 <i>Improvement in Area Reduction</i>	91
4.1.6.3 <i>Variation of Input Impedance</i>	92
4.1.6.4 <i>Variation of Frequency Ratio</i>	93
4.1.6.5 <i>Effect of Slot Arm Width, w_s</i>	94
4.1.7 <i>Dual Polarized Operation of the Proposed Antenna Design</i>	95
4.1.8 <i>Radiation Pattern and Gain</i>	96
4.1.9 <i>Dual Slot Arm Loaded Patch Antenna</i>	97

4.1.10	<i>Dual Frequency Patch with Orthogonal Slot Arms</i>	100
4.1.11	<i>Determination of Square Patch and Slot Arm Lengths for Particular Dual Operating Frequencies</i>	103
4.2	<i>Reconfigurable Dual Frequency Microstrip Antenna Design using PIN Diodes</i>	108
4.2.1	<i>PIN Diode Switch</i>	108
4.2.2	<i>Single Slot Arm Loaded Reconfigurable Dual Frequency Microstrip Antenna</i>	109
4.2.2.1	<i>Variation of Resonant Frequencies with PIN Diode Position</i>	112
4.2.2.2	<i>Loading Effect of PIN Diode on Antenna Resonant Frequencies</i>	114
4.2.2.3	<i>Theoretical Analysis of Reconfigurable Microstrip Antenna using FDTD</i>	116
4.2.2.4	<i>Polarization and Gain</i>	118
4.2.2.5	<i>Radiation Characteristics</i>	120
4.2.2.6	<i>Summary of the Characteristics of Single Slot Reconfigurable Microstrip Antenna with PIN diode</i>	121
4.2.3	<i>Dual Slot Arm Reconfigurable Microstrip Antenna Design for Tunable Frequency Ratio</i>	122
4.2.3.1	<i>Antenna Configuration</i>	123
4.2.3.2	<i>Operational Mechanism</i>	124
4.2.3.3	<i>Antenna Resonant Frequencies</i>	125
4.2.3.4	<i>Study on reconfigurable resonant frequency variations with different x_1 and x_2 combinations</i>	129
4.2.3.5	<i>Antenna Polarization and Gain</i>	
4.2.3.6	<i>Radiation Characteristics</i>	133
5.	INVESTIGATIONS ON RECONFIGURABLE DUAL FREQUENCY MICROSTRIP ANTENNAS USING VARACTOR DIODES	139-181
5.1	<i>Varactor Controlled Single Slot Arm Loaded Reconfigurable Dual Frequency Microstrip Antenna</i>	142
5.1.1	<i>Frequency Tuning</i>	143
5.1.2	<i>Variation of Dual Resonant Frequencies with Varactor Reverse Bias</i>	144
5.1.3	<i>Antenna Size Reduction</i>	146
5.1.4	<i>Study of the Resonant Behavior of the Antenna at Different Varactor Positions</i>	146
5.1.5	<i>Polarization, Gain and Radiation Pattern</i>	147
5.2	<i>Computation of Resonant Frequencies of Varactor Tuned Reconfigurable Antenna</i>	150
5.3	<i>Varactor Controlled Reconfigurable Dual Frequency Microstrip Antenna Design for Frequency Ratio Tuning</i>	153
5.3.1	<i>Antenna Geometry</i>	153
5.3.2	<i>Variation of Resonant Frequencies with Varactor Reverse Bias</i>	154
5.3.3	<i>Polarization and Gain</i>	156
5.4	<i>Experimental Investigations on Varactor Loaded Reconfigurable Microstrip Antennas for Enhanced Dual Frequency Tuning and Area Reduction</i>	159

5.4.1	<i>Varactor Controlled Microstrip Antenna with Dual Orthogonal Slot Arms</i>	160
5.4.2	<i>Triple Slot Arm Loaded Reconfigurable Dual Frequency Microstrip Antenna Using Varactors</i>	164
5.4.3	<i>Four Slot Arm Loaded Varactor Controlled Reconfigurable Microstrip Antenna</i>	167
5.4.4	<i>Eight Slot Arm Loaded Varactor Controlled Reconfigurable Microstrip Antenna</i>	171
5.5	<i>Independent Frequency Tuning in Hexagonal Slot Loaded Microstrip Antenna Using Modified Slot Arm</i>	176
5.5.1	<i>C-Shaped Slot Loaded Reconfigurable Microstrip Antenna</i>	176
5.5.1.1	<i>Independent Tuning of Dual Resonant Modes</i>	178
5.5.2	<i>Meandered Slot Arm Loaded Reconfigurable Microstrip Antenna</i>	181
6.	CONCLUSIONS AND SUGGESTIONS FOR FUTURE WORK	185 - 190
6.1	<i>Inferences from Passive Dual-Frequency Microstrip Antenna</i>	187
6.2	<i>PIN Diode Controlled Reconfigurable Dual Frequency Microstrip Antennas</i>	188
6.3	<i>Varactor Controlled Reconfigurable Dual Frequency Microstrip Antenna Designs</i>	189
6.4	<i>Independent Control of Dual Operating Frequencies</i>	189
6.5	<i>Suggestion for Future Work</i>	190
	REFERENCES	191 - 205
	LIST OF PUBLICATION OF THE AUTHOR	207 - 209
	RESUME OF THE AUTHOR	210 - 211
	INDEX	212 - 215

LIST OF FIGURES

Chapter 1

Figure 1.1	The basic microstrip antenna geometry	5
Figure 1.2	Charge distributions on a microstrip antenna	7
Figure 1.3	Basic microstrip patch antenna shapes	9
Figure 1.4	Configuration of a microstrip printed dipole	10
Figure 1.5	Basic printed slot antenna shapes with feed structures	10
Figure 1.6	Microstrip traveling wave antennas	11
Figure 1.7	Coaxial probe fed microstrip antenna	12
Figure 1.8	Microstrip line fed patch	13
Figure 1.9	Proximity coupling method and its equivalent circuit	14
Figure 1.10	Exploded view of an aperture coupled microstrip patch	14
Figure 1.11	Tuning using shorting posts	20
Figure 1.12	Mechanical tuning of patch using dual stubs	21
Figure 1.13	Electronic tuning using varactor diodes	22

Chapter 3

Figure 3.1	Different stages in the photolithographic process of antenna fabrication	53
Figure 3.2	Block diagram of HP8510C Vector Network Analyzer	54
Figure 3.3	Experimental setup for the measurement of return loss and resonant frequency	56
Figure 3.4	Experimental setup for measuring the radiation characteristics of the antenna	58
Figure 3.6	Field component placements in the FDTD unit cell	64
Figure 3.7	FDTD Source with source Resistance ' R_s '	69
Figure 3.8	The computational domain for the propose dual frequency microstrip antenna	72

Chapter 4

Figure 4.1	Staircase meshing employed in the hexagonal slot boundary	81
Figure 4.2	Actual plot showing the close view of the fine mesh and staircase along the slant sides of the hexagonal slot	82
Figure 4.3	Computed and experimental return loss behavior of the square patch with hexagonal slot on its centre	83
Figure 4.4	Geometry of the proposed passive dual frequency dual polarized microstrip antenna electromagnetically coupled to a 50Ω microstrip line. $L = 4\text{cm}$, $l_1 = l_2 = 0.8\text{cm}$, $l_x = 1\text{cm}$, $w_x = 0.1\text{cm}$, $b = 0.16\text{cm}$ and $\epsilon_r = 3.98a$	84
Figure 4.5	FD'ID computed surface current distribution of the hexagonal slot loaded single slot arm square microstrip patch antenna showing the simultaneous excitation of TM ₁₀ and TM ₀₁ mode	86

- Figure 4.6** Surface current density plots for the (a) TM_{10} and (b) TM_{01} resonant modes at frequencies, $f_{10} = 1.56$ GHz and $f_{01} = 1.705$ GHz. It is seen that the current densities are excited in orthogonal planes. (simulated using IE3D) 86
- Figure 4.7** Return loss performance of the standard 4×4 cm square patch with and without embedded regular hexagonal shaped slot 88
- Figure 4.8** Theoretical simulated and measured return loss for the two resonant frequencies. The antenna dimensions are, $L = 4$ cm, $l_1 = l_2 = 0.8$ cm, $l_x = 1$ cm, $w_x = 0.1$ cm, $h = 0.16$ cm and $\epsilon_r = 3.98$ 89
- Figure 4.9** Plot showing the experimental variation of f_1 (TM_{10}) and f_2 (TM_{01}) frequencies with change in slot arm length. $L = 4$ cm, $l_1 = l_2 = 0.8$ cm, $w_x = 0.1$ cm, $h = 0.16$ cm and $\epsilon_r = 3.98$ 90
- Figure 4.10** Variation of frequency ratio with change in slot arm length. $L = 4$ cm, $l_1 = l_2 = 0.8$ cm, $w_x = 0.1$ cm, $h = 0.16$ cm and $\epsilon_r = 3.98$ 93
- Figure 4.11** Plot showing the FDTD computed variation of f_1 (TM_{10}) and f_2 (TM_{01}) frequencies with change in slot arm width w_x . ($L = 4$ cm, $l_1 = l_2 = 0.8$ cm, $l_x = 1$ cm, $h = 0.16$ cm and $\epsilon_r = 3.98$) 94
- Figure.4.12** Variation of received power with frequency for the two orthogonal polarization planes for first and second resonant modes. The antenna dimensions are, $L = 4$ cm, $l_1 = l_2 = 0.8$ cm, $l_x = 1$ cm, $w_x = 0.1$ cm, $h = 0.16$ cm and $\epsilon_r = 3.98$ 96
- Figure .4.13** Measured E and H plane radiation pattern of the proposed antenna for (a) $f_1 = 1.56$ GHz and (b) $f_2 = 1.705$ GHz. The antenna dimensions are, $L = 4$ cm, $l_1 = l_2 = 0.8$ cm, $l_x = 1$ cm, $w_x = 0.1$ cm, $h = 0.16$ cm and $\epsilon_r = 3.98$ 97
- Figure 4.14** Geometry of the dual slot arm loaded square microstrip patch antenna. $L = 4$ cm, $l_1 = l_2 = 0.8$ cm, $w_x = 0.1$ cm, $h = 0.16$ cm and $\epsilon_r = 3.98$ a 97
- Figure 4.15** Comparison of frequency tuning between single and dual slot arm loaded square microstrip patch antennas. The common antenna parameters are $L = 4$ cm, $l_1 = l_2 = 0.8$ cm, $w_x = 0.1$ cm, $h = 0.16$ cm, $l_x = l_y$ and 98
- Figure 4.16** Frequency ratio variations with slot arm length for the proposed single and dual slot arm designs. The antenna dimensions are same as in fig. 4.14 100
- Figure 4.17** Geometry of the orthogonal slot arm loaded square microstrip patch antenna. $L = 4$ cm, $l_1 = l_2 = 0.8$ cm, $w_x = 0.1$ cm, $h = 0.16$ cm, $l_x = 1$ cm and $\epsilon_r = 3.98$ a 101
- Figure 4.18** Plot showing the variation of two resonant frequencies of the proposed antenna with single and orthogonal slot arms. The antenna parameters are $L = 4$ cm, $l_1 = l_2 = 0.8$ cm, $w_x = 0.1$ cm, $h = 0.16$ cm, $l_x = 1$ cm and $\epsilon_r = 3.98$ a. l_y is kept constant at 10mm for later case. 103
- Figure 4.19** Graphs showing the variation of experimental and theoretical square patch and slot arm dimensions for different dual operating frequency pairs 107
- Figure 4.20** Geometry of the reconfigurable dual frequency dual polarized microstrip antenna controlled by a PIN diode. The antenna parameters

are $L = 4\text{cm}$, $l_1 = l_2 = 0.8\text{cm}$, $l_3 = 12\text{cm}$, $w_1 = 0.1\text{cm}$, $h = 0.16\text{cm}$ and $\epsilon_r = 3.98$. PIN diode is placed at 0.7mm from the hexagon edge 110

Figure 4.21 Measured reflection co-efficient of the reconfigurable dual frequency microstrip antenna for PIN diode ON and OFF states. The antenna parameters are $L = 4\text{cm}$, $l_1 = l_2 = 0.8\text{cm}$, $l_3 = 12\text{cm}$, $w_1 = 0.1\text{cm}$, $h = 0.16\text{cm}$ and $\epsilon_r = 3.98$. PIN diode is placed at 0.7mm from the hexagon edge. 111

Figure 4.22 Experimental and simulated return loss of the PIN diode controlled reconfigurable microstrip antenna in (a) OFF and (b) ON states. The diode is positioned at 0.7mm from the hexagonal slot 116

Figure 4.23 Computed surface electric field distribution in the entire computational domain when the PIN diode is in the ON state 117

Figure 4.24 Comparison of experimental and theoretical (FDTD) computed dual resonant frequency values for PIN ON and PIN OFF states of the proposed reconfigurable antenna. 118

Figure 4.25 Variation of received power with frequency for the two orthogonal polarization planes for both diode states. The antenna parameters are $L = 4\text{cm}$, $l_1 = l_2 = 0.8\text{cm}$, $l_3 = 12\text{cm}$, $w_1 = 0.1\text{cm}$, $h = 0.16\text{cm}$ and $\epsilon_r = 3.98$. PIN diode is placed at 0.7mm from the hexagon edge 119

Figure 4.26 Measured gain of the single slot arm reconfigurable dual frequency microstrip antenna at $f_1 = 1.57\text{GHz}$ (PIN ON) and $f_2 = 1.96\text{GHz}$ (PIN OFF). The antenna parameters are $L = 4\text{cm}$, $l_1 = l_2 = 0.8\text{cm}$, $l_3 = 12\text{cm}$, $w_1 = 0.1\text{cm}$, $h = 0.16\text{cm}$ and $\epsilon_r = 3.98$. PIN diode is placed at 0.7mm from the hexagon edge. 119

Figure 4.27 Measured radiation pattern of the single slot arm loaded reconfigurable antenna controlled by PIN diodes 120

Figure 4.28 Layout of the dual slot arm loaded reconfigurable microstrip antenna. The antenna parameters are $L = 4\text{cm}$, $l_1 = l_2 = 0.8\text{cm}$, $x_1 = 0\text{cm}$, $x_2 = 0.8\text{cm}$, $l_3 = l_h = 1.2\text{cm}$, $w_1 = 0.1\text{cm}$, $h = 0.16\text{cm}$ and $\epsilon_r = 3.98$ 123

Figure 4.29 Measured return loss of the antenna for all the three PIN diode states. ($L = 4\text{cm}$, $l_1 = l_2 = 0.8\text{cm}$, $x_1 = 0\text{cm}$, $x_2 = 0.8\text{cm}$, $w_1 = 0.1\text{cm}$, $h = 0.16\text{cm}$ and $\epsilon_r = 3.98$). 126

Figure 4.30 Simulated (IE3D) return loss of the antenna for all the three PIN diode states. ($L = 4\text{cm}$, $l_1 = l_2 = 0.8\text{cm}$, $x_1 = 0\text{cm}$, $x_2 = 0.8\text{cm}$, $w_1 = 0.1\text{cm}$, $h = 0.16\text{cm}$ and $\epsilon_r = 3.98$). 127

Figure 4.31 3-dimensional electric field distributions in the surface of the patch in D1 and D2 OFF state showing the excited resonant modes 127

Figure 4.32 FDTD computed surface current distribution for (a) PIN D2 ON and (b) D1 & D2 OFF 128

Figure 4.33 Measured and theoretical (FDTD) computed return loss behavior of the reconfigurable microstrip antenna with two vertical slot arms 128

Figure 4.34 Variation of received power with frequency for the two orthogonal polarization planes for all the three pin diode states. (a) D1 and D2 OFF (b) D1 ON (c) D2 ON 134

Figure 4.35 Measured E and H plane radiation patterns of the proposed antenna in different PIN diode states (contd. in next page.) 136

Figure 5.1	Geometry of the single slot arm reconfigurable dual frequency dual polarized microstrip antenna with Varactor diode. The antenna parameters are $L = 4\text{cm}$, $l_1 = l_2 = 0.8\text{cm}$, $l_3 = 12\text{cm}$, $w_1 = 0.1\text{cm}$, $h = 0.16\text{cm}$ and $\epsilon_r = 3.98$. Varactor diode is placed in the tip of the extending slot arm.	142
Figure 5.2	Measured return loss of the dual frequency Varactor controlled reconfigurable microstrip antenna for different bias voltage. ($L = 4\text{cm}$, $l_1 = l_2 = 0.8\text{cm}$, $l_3 = 1.2\text{m}$, $w_1 = 0.1\text{cm}$, $h = 0.16\text{cm}$ and $\epsilon_r = 3.98$)	143
Figure 5.3	Experimental and simulated variation of resonant frequencies with Varactor reverse bias voltage, (a) First resonant frequency, f_1 (b) Second resonant frequency, f_2	145
Figure 5.4	Measured return loss of the dual frequency Varactor controlled reconfigurable microstrip antenna at two different diode positions. ($L = 4\text{cm}$, $l_1 = l_2 = 0.8\text{cm}$, $l_3 = 1.2\text{m}$, $w_1 = 0.1\text{cm}$, $h = 0.16\text{cm}$ and $\epsilon_r = 3.98$)	147
Figure 5.5	Variation of received power with frequency for the two orthogonal polarization planes at different Varactor diode bias. (a) 0V (b) 15V (c) 30V	148
Figure 5.6	Measured gain plot of the antenna for first and second resonant frequencies	149
Figure 5.7	Measured E and H-plane radiation patterns of the proposed antenna for different varactor bias voltages	150
Figure 5.8	Plot showing the experimental and theoretical variation of first and second resonant frequencies with the applied varactor reverse bias	153
Figure 5.9	Reconfigurable dual frequency microstrip antenna controlled by varactor diodes for frequency ratio tuning. ($L = 4\text{cm}$, $l_1 = l_2 = 0.8\text{cm}$, $l_3 = l_4 = 1.1\text{cm}$, $w_1 = 0.1\text{cm}$, $h = 0.16\text{cm}$ and $\epsilon_r = 3.98$).	154
Figure 5.10	Measured return loss of the antenna for different varactor reverse bias voltages. ($L = 4\text{cm}$, $l_1 = l_2 = 0.8\text{cm}$, $l_3 = l_4 = 1.1\text{cm}$, $w_1 = 0.1\text{cm}$, $h = 0.16\text{cm}$ and $\epsilon_r = 3.98$).	154
Figure 5.11	Variation of first and second resonant frequencies with varactor reverse bias.	155
Figure 5.12	Variation of received power with frequency for the two orthogonal polarization planes at different Varactor bias voltages	157
Figure 5.13	Measured E and H-plane radiation patterns of the reconfigurable antenna at 0V, 15V and 29V	158
Figure 5.14	Reconfigurable dual frequency microstrip antenna configuration with orthogonal slot arms. ($L = 4\text{cm}$, $l_1 = l_2 = 0.8\text{cm}$, $l_3 = 1.1\text{cm}$, $l_4 = 1.5\text{cm}$, $w_1 = 0.1\text{cm}$, $h = 0.16\text{cm}$ and $\epsilon_r = 3.98$).	160
Figure 5.15	Return loss characteristics of the varactor tuned orthogonal slot arm loaded microstrip antenna	161
Figure 5.16	Variation of first and second resonant frequencies with varactor reverse bias	162
Figure 5.17	Measured received power in the two orthogonal polarization planes	163
Figure 5.18	Measured radiation pattern for the dual modes	164
Figure 5.19	Geometry of the proposed varactor controlled microstrip antenna with three slot arms ($L = 4\text{cm}$, $l_1 = l_2 = 0.8\text{cm}$, $l_3 = l_4 = 1.1\text{cm}$, $l_5 = 1.5\text{cm}$, $w_1 = 0.1\text{cm}$, $h = 0.16\text{cm}$ and $\epsilon_r = 3.98$).	165

Figure 5.20	Measured return loss of the antenna for different varactor reverse bias voltages. ($L = 4\text{cm}$, $l_1 = l_2 = 0.8\text{cm}$, $l_a = l_b = 1.1\text{cm}$, $l_c = 1.5\text{cm}$, $w_a = 0.1\text{cm}$, $h = 0.16\text{cm}$ and $\epsilon_r = 3.98$).	165
Figure 5.21	Variation of resonant frequencies with varactor reverse bias voltage, (a) f_1 (b) f_2	166
Figure 5.22	Measured E and H-plane radiation patterns at $f_1 = 1.432\text{GHz}$ and $f_2 = 1.76\text{GHz}$ of the antenna, for $V = -15\text{volt}$	167
Figure 5.23	Four slot arm loaded reconfigurable dual frequency microstrip antenna controlled by varactor diodes. Antenna parameters are $L = 4\text{cm}$, $l_1 = l_2 = 0.8\text{cm}$, $l_a = l_c = 1.1\text{cm}$, $l_b = l_d = 1.5\text{cm}$, $w_a = 0.1\text{cm}$, $h = 0.16\text{cm}$ and $\epsilon_r = 3.98$.	168
Figure 5.24	Measured return loss, (S_{11}) of the four slot arm antenna configuration for different varactor reverse bias voltages	169
Figure 5.25	Variation of resonant frequencies for the four slot arm reconfigurable antenna design with varactors reverse voltage. (a) First resonant frequency, f_1 (b) Second resonant frequency, f_2	170
Figure 5.26	Geometry of the eight slot arm reconfigurable microstrip antenna controlled by varactor diodes	172
Figure 5.27	Measured return loss of the antenna for different varactor reverse bias voltages. ($L = 4\text{cm}$, $l_1 = l_2 = 0.8\text{cm}$, $l_a = 1.1\text{cm}$, $l_b = 1.5\text{cm}$, $w_a = 0.1\text{cm}$, $h = 0.16\text{cm}$ and $\epsilon_r = 3.98$).	173
Figure 5.28	Variation of resonant frequencies with varactor reverse bias voltage, (a) f_1 (b) f_2	173
Figure 5.29	Variation received power with frequency in two orthogonal polarization planes for $V = 15\text{V}$	174
Figure 5.30	Schematic diagram of proposed reconfigurable microstrip antenna (a) Top view, (b) Side view. The antenna parameters are $L = 40\text{mm}$, $l_1 = 8\text{mm}$, $h = 1.6\text{mm}$, $w_a = 1\text{mm}$, $x_1 = 10\text{mm}$, $x_2 = 16\text{mm}$, $\epsilon_r = 3.95$	177
Figure 5.31	Variation of resonant frequencies with 'C' slot dimension (a) $x_1 = 16\text{mm}$ and x_2 varying (b) $x_2 = 10\text{mm}$ and x_1 varying	178
Figure 5.32	Return loss performance of reconfigurable antenna for $x_1 = 10\text{mm}$ and $x_2 = 16\text{mm}$	179
Figure 5.33	Variation of resonant frequencies, f_1 and f_2 with varactors bias voltage.	180
Figure 5.34	Measured E and H-plane radiation patterns at $f_1 = 1.504\text{GHz}$ and $f_2 = 1.768\text{GHz}$ of the antenna, for $V = 9\text{volt}$.	181
Figure 5.35	Geometry of the proposed tunable microstrip antenna controlled by varactor diode. ($L = 4\text{cm}$, $l_1 = l_2 = 0.8\text{cm}$, $x_1 = 1.6\text{cm}$, $x_2 = 0.4\text{cm}$, $w_a = 0.1\text{cm}$, $h = 0.16\text{cm}$ and $\epsilon_r = 3.98$)	182
Figure 5.36	Measured return loss of the antenna for different varactor reverse bias voltages. ($L = 4\text{cm}$, $l_1 = l_2 = 0.8\text{cm}$, $x_1 = 1.6\text{cm}$, $x_2 = 0.4\text{cm}$, $w_a = 0.1\text{cm}$, $h = 0.16\text{cm}$ and $\epsilon_r = 3.98$).	182
Figure 5.37	Variation of resonant frequencies with varactor reverse bias voltage, (a) f_1 (b) f_2	183
Figure 5.38	Measured E and H-plane radiation patterns at $f_1 = 1.168\text{GHz}$ and $f_2 = 1.68\text{GHz}$ of the antenna, for $V = -15\text{volt}$	183

LIST OF TABLES

Chapter 1

Table 1.1	Various types of dual frequency microstrip antennas	18
------------------	---	----

Chapter 4

Table 4.1	Dual frequency performance of the proposed antenna with variation in slot arm slot length. The antenna parameters are: $L = 4\text{cm}$, $l_1 = l_2 = 0.8\text{cm}$, $w_s = 0.1\text{cm}$, $b = 0.16\text{cm}$ and $\epsilon_r = 3.98$	90
Table 4.2	Percentage area reduction for the two resonant frequencies for different slot arm length, compared to standard rectangular patches. The antenna parameters are: $L = 4\text{cm}$, $l_1 = l_2 = 0.8\text{cm}$, $w_s = 0.1\text{cm}$, $b = 0.16\text{cm}$ and $\epsilon_r = 3.98$	91
Table 4.3	Variation of complex input impedance for TM_{10} and TM_{c1} resonant modes with slot arm length. The antenna parameters are: $L = 4\text{cm}$, $l_1 = l_2 = 0.8\text{cm}$, $w_s = 0.1\text{cm}$, $b = 0.16\text{cm}$ and $\epsilon_r = 3.98$. The feed position is kept unchanged as in figure 4.1.	92
Table 4.4	Dual frequency performance of the proposed antenna with variation in slot arm width w_s . The antenna parameters are: $L = 4\text{cm}$, $l_1 = l_2 = 0.8\text{cm}$, $l_a = 1\text{cm}$, $b = 0.16\text{cm}$ and $\epsilon_r = 3.98$	95
Table 4.5	Measured dual frequency operation of the dual slot arm loaded patch with variation in slot arm length. The antenna parameters are: $L = 4\text{cm}$, $l_1 = l_2 = 0.8\text{cm}$, $l_a = l_b$, $b = 0.16\text{cm}$ and $\epsilon_r = 3.98$	99
Table 4.6	Measured dual frequency operation of the orthogonal slot arm loaded microstrip antenna. The antenna parameters are: $L = 4\text{cm}$, $l_1 = l_2 = 0.8\text{cm}$, $b = 0.16\text{cm}$ and $\epsilon_r = 3.98$	102
Table 4.7	Dual frequency operation of the single slot arm loaded antenna at different PIN diode position on the slot arm	113
Table 4.8	Comparison of experimental and simulated (IE3D) resonant frequencies for PIN diode ON and OFF states	115
Table 4.9	Measured half-power beam-width in the two principal planes	121
Table 4.10	Summary of single slot arm reconfigurable microstrip antenna parameters	122
Table 4.11	Measured resonant frequencies and corresponding -10dB bandwidths	126
Table 4.12	Variation in dual frequency operation with PIN diode position (antenna shown in fig. 4.28)	130
Table 4.13	Variation in impedance bandwidth with PIN diode position (antenna shown in fig. 4.28)	131
Table 4.14	Percentage area reduction of the dual slot arm reconfigurable antenna design (antenna shown in fig. 4.28)	132
Table 4.15	Measured half-power beam width in degrees for first and second resonant frequencies for all PIN-diode states	135

Table 4.16	Maximum radiation direction in degrees for first and second resonant frequencies for all PIN-diode states	137
Table 4.17	Summary of dual slot arm reconfigurable microstrip antenna characteristics	138

Chapter 5

Table 5.1	Resonant frequencies, percentage bandwidth and frequency ratio of the proposed Varactor tuned antenna with bias voltage	144
Table 5.2	Summary of percentage area reduction of the new dual slot arm reconfigurable antenna design	146
Table 5.3	Measured frequency ratio and percentage bandwidths at different varactor bias	156
Table 5.4	Overview of dual slot arm loaded reconfigurable microstrip antenna with varactor diode control	159
Table 5.5	Measured bandwidths and frequency ratios	162
Table 5.6	Measured percentage area reduction for the two resonant modes	163
Table 5.7	Percentage area reduction for the dual resonant modes at different varactor bias voltages	166
Table 5.8	Area reduction at various reverse voltages	171
Table 5.9	Comparison between two and four slot arm	171
Table 5.10	Percentage area reduction at different varactor reverse bias voltages	174
Table 5.11	Comparison of antenna properties for all the two, three, four and eight slot arm loaded reconfigurable microstrip antenna designs	175
Table 5.12	Percentage area reduction offered by the c-slot loaded reconfigurable antenna design	180

CHAPTER

1

INTRODUCTION

Contents

1.1	<i>Microstrip Antennas</i>	4
1.1.1	<i>Advantages and Limitations</i>	4
1.1.2	<i>Radiation Mechanism</i>	6
1.1.3	<i>Analytical Models for Microstrip Antennas</i>	7
1.2	<i>Various Microstrip Antenna Configurations</i>	9
1.2.1	<i>Microstrip Patch Antennas</i>	9
1.2.2	<i>Microstrip Dipoles</i>	10
1.2.3	<i>Printed Slot Antennas</i>	10
1.2.4	<i>Microstrip Travelling Wave Antennas</i>	11
1.3	<i>Feeding Techniques</i>	11
1.3.1	<i>Coaxial Feed or Probe Coupling</i>	12
1.3.2	<i>Microstrip Line Feed</i>	13
1.3.3	<i>Proximity Coupled Microstrip Feed</i>	13
1.3.4	<i>Aperture Coupled Microstrip Feed</i>	14
1.3.5	<i>Coplanar Waveguide Feed</i>	15
1.4	<i>Full Wave Analysis of Microstrip Antennas</i>	15
1.4.1	<i>Spectral Domain Full-Wave Analysis</i>	16
1.4.2	<i>Mixed Potential Integral Equation Analysis (MPIE)</i>	16
1.4.3	<i>Finite Difference Time Domain Analysis</i>	16
1.5	<i>Dual-Frequency Microstrip Antenna Technologies</i>	17
1.5.1	<i>Multi-Patch Dual-Frequency Antennas</i>	19
1.5.2	<i>Reactively Loaded Antennas</i>	19
1.5.3	<i>Orthogonal-Mode Dual Frequency Patch Antennas</i>	19
1.6	<i>Current Reconfigurable Antenna Technologies</i>	20
1.6.1	<i>Mechanical Tuning</i>	20
1.6.2	<i>Magnetic Tuning</i>	21
1.6.3	<i>Electronic Tuning</i>	21
1.7	<i>Reconfigurable Microstrip Antennas</i>	22
1.8	<i>Motivation and Development of Subject of Research</i>	23
1.9	<i>Thesis Overview</i>	24

Today the world lives in a completely dependent environment, where the use of modern communication systems is becoming essential in everyday routine. In particular, the field of wireless communications is experiencing unprecedented growth evident from the increase in use of cellular phones, Wireless Local Area Networks (WLAN), Global Positioning Systems (GPS) and Satellite Telephones. Moreover, advancement in electronic warfare revolutionized the wireless communications through cutting edge technologies like Space-Based Radar, Communication Satellites, and Electronic Intelligence.

Antenna technology is one of the vital elements in this wireless communication systems. Antennas interface between space and circuitry; form the transition between space waves and electric currents; convert electrons to photons and vice versa. They are structures carefully designed for radiating electromagnetic energy effectively in a prescribed manner. Without an efficient antenna, electromagnetic energy would be localized and wireless transmission of information over long distances would be impossible.

Although, James Clerk Maxwell's paper of 1865 set out the theory of electromagnetic radiation in strictly simple and symmetric mathematical form, the mechanistic analogies, which formed the basis of his work, were undoubtedly a hindrance to the general acceptance of the theory. The concept was finally unraveled in a classical series of experiments by Heinrich Hertz in 1886. In one stroke he conceived, built and tested the first radio complete with the first antennas, a half-wave dipole for transmitting and a square loop for receiving [1]. Following Hertz, Sir Oliver Lodge designed the first biconical antenna, while Guglielmo Marconi erected enormous monoconical antennas of wire for long wave transatlantic communication. Almost at the same time Jagadis Chandra Bose experimented at very short waves with the first horn

antennas [2]. New types of antennas gradually appeared such as slots, helices, flat spirals, conical spirals and log periodics.

1.1 Microstrip Antennas

The concept of planar antennas dates back to 1953, when Deschamps in USA first proposed it [3]. Gutton and Baissinot in France acquired a patent for a 'flat aerial' for ultra high frequencies during 1955 [4]. Shortly thereafter, Lewin investigated radiation from stripline discontinuities [5]. Further studies in basic rectangular and square microstrip patch configurations were undertaken by Kaloi in late 1960's. However, a well built study was only reported in 1970 when Byron proposed a strip radiator separated from a ground plane by a dielectric substrate for phased array applications. He used a half wavelength wide strip, fed coaxially at the radiating edges, as the basic array element [6]. Later, a microstrip element was patented by Munson and data on basic rectangular and circular microstrip patches were published by Howell [7, 8]. Additional works on basic microstrip patch elements were reported in 1975 by Garvin, Howell, Weinschel and Janes and Wilson. Munson's earlier works concentrated on the development of low-profile antennas on rockets and missiles and this gave birth to a new antenna industry with potential applications [9-12].

To a large extent, the development of microstrip antennas has been driven by systems requirements for antennas with low profile, light weight, easy integrability into arrays or with microwave integrated circuits, or polarization diversity. Thus microstrip antennas have found applications in both the military and civil sectors.

1.1.1 Advantages and Limitations

A microstrip antenna in its simple configuration consists of a radiating metallic patch of copper or gold on one side of a dielectric substrate which has a ground plane on the other side as in fig. 1.1.

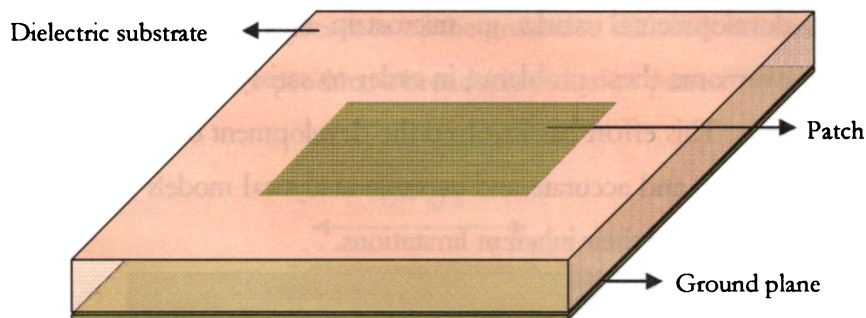


Figure 1.1 The basic microstrip antenna geometry.

The geometry of the patch can assume any shape, but regular shapes are generally used to simplify the analysis and performance prediction. Several advantages compared to conventional microwave antennas augmented their use in satellites and missiles, un-manned air crafts, personal communication systems and remote sensing radars and radiometers [13]. Some of the principal advantages are their light weight, thin profile and low fabrication cost. This makes them readily amenable to mass production. Linear and circular polarizations are possible by simply adjusting the feeding mechanism or by placing shorting pins at appropriate position. Dual frequency and dual polarizations can be easily achieved by reactive loading such as carving slots on the radiating patch.

However, the disadvantages of the original microstrip antenna configurations include narrow bandwidth, spurious feed radiation, poor polarization purity, limited power capacity, tolerance problems and excitation of surface waves. Poor efficiency and reduced gain adds to the above and makes these antennas incompatible for long range applications. But some of these limitations can be minimized by using special design techniques. For example, bandwidth can be increased by using stacked patch configuration or by coplanar parasitic elements [14]. An array configuration is used to overcome lower gain and lower power handling limitations. Photonic band gap structures are used to surmount surface wave associated limitations such as poor efficiency and radiation pattern degradation [15].

Much of the developmental works in microstrip antennas thus focused on experiments to overcome these problems, in order to satisfy increasingly stringent system requirements. This effort has involved the development of novel microstrip antenna configurations, and accurate and versatile analytical models to design and optimize and to understand their inherent limitations.

1.1.2 Radiation Mechanism

Radiation from a microstrip antenna can be determined from the field distribution between the patch metallization and ground plane. The energization of the patch will establish a charge distribution on the upper and lower surfaces of the patch, as well as on the surface of the ground plane. Fig 1.2 shows the charge distribution for rectangular patch geometry. The repulsive forces between like charges on the bottom surface of the patch tend to push some charges from the bottom of it, around its edges, to its top surface. This movement of charges creates current densities on the top and bottom of the microstrip patch. As the dielectric substrate is usually electrically thin, electric field components parallel to the ground plane must be very small throughout the substrate. The patch element resonates when its length is nearly $\lambda/2$, leading to relatively large current and field amplitudes.

In view of the equivalence theorem, the antenna can be viewed as a cavity with slot type radiators at $x = 0$ and $x = L$, with equivalent magnetic currents,

$$\vec{M} = \vec{E} \times n \quad (1.1)$$

radiating in the presence of the dielectric substrate. Alternatively, radiation can be considered as being generated by the induced surface current density,

$$\vec{J}_s = n \times \vec{H} \quad (1.2)$$

on the patch element in the presence of the grounded dielectric substrate. In either case the equivalent sources produce a broadside radiation pattern.

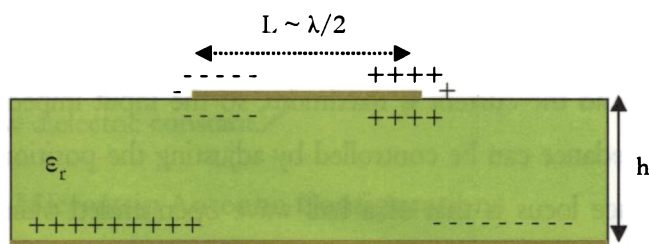


Figure 1.2 Charge distributions on a microstrip antenna

1.1.3 Analytical Models for Microstrip Antennas

These analytical models treat the microstrip antenna as a lossy cavity, or as a loaded transmission line resonator. These models involve several simplifying approximations, so that they are easy to use and can provide useful information on antenna patterns, impedance, efficiency and bandwidth. Even though their accuracy and versatility are much less compared to full wave analysis, these simple models can provide an insight into the operation of microstrip antennas.

1.1.3.1 Transmission Line Model

In terms of transmission line model, the antenna is viewed as a length of open-circuited transmission line with light loading at the ends to account for fringing fields and radiation [16-18]. The voltage and current on this equivalent transmission line can be approximated as,

$$\text{voltage, } V(x) = V_0 \cos \frac{\pi x}{L} \quad (1.3)$$

$$\text{current, } I(x) = \frac{V_0}{Z_0} \sin \frac{\pi x}{L} \quad (1.4)$$

The results give a simple explanation for the input impedance variation of the antenna, $Z_{in} = V/I$. That is, for a feed point at the radiating edge, ($x = 0$ or $x = L$) the voltage is a maximum and the current is a minimum, and thus the input impedance is a maximum. For the feed point at the center of the patch, ($x = L/2$), the voltage is zero and the current is maximum, so the input impedance is zero. Thus the input impedance can be controlled by adjusting the position of the feed point. The impedance locus is that of a half-wave open ended transmission line resonator, which can be modeled as a parallel RLC network. The resonant patch element is sometimes made in a different shape, but the principles of operation are essentially the same as for the rectangular patch.

1.1.3.2 Cavity Model

In the cavity model the perimeter of the patch is approximated as a magnetic wall, for which the electric and magnetic fields of the dominant resonant mode can be expressed as,

$$\text{vertical electrical field, } E_z = E_0 \cos \frac{\pi x}{L} \quad (1.5)$$

$$\text{transverse magnetic field, } H_y = H_0 \sin \frac{\pi x}{L} \quad (1.6)$$

Higher order resonant modes have more variations in the x or y directions. This result ignores the effect of fringing fields at the edges of the patch, so an ad hoc correction factor must be applied to the patch length to obtain accurate resonant frequencies. Also an effective dielectric loss-tangent is used to account for power lost due to radiation [19, 20].

The magnetic wall approximation of the cavity model and the open end approximation of the transmission line model become more realistic as the substrate becomes thinner. This implies that the Q of a patch antenna on a thin

substrate is large, and that the bandwidth is small. Also, the current on the patch element is in very close proximity to its negative image caused by the presence of the ground plane. This causes near-cancellation of the radiated fields and the relatively large stored energy below the patch. This performance leads us to conclude that microstrip antennas operate best when the substrate is electrically thick with a low dielectric constant.✓

1.2 Various Microstrip Antenna Configurations

All microstrip antennas can be divided into four basic categories: microstrip patch antennas, microstrip dipoles, printed slot antennas and microstrip traveling wave antennas. The major characteristics of each are described below.

1.2.1 Microstrip Patch Antennas

A microstrip patch antenna consists of a conducting patch of any planar or non-planar geometry on one side of a dielectric substrate with a ground plane on the other side. The basic configurations used in practice are shown in fig. 1.3. All these patches behave like a dipole and therefore their radiation characteristics are similar. They have gain typically in between 5 and 6dB and exhibit a 3dB beamwidth between 70° and 90° .

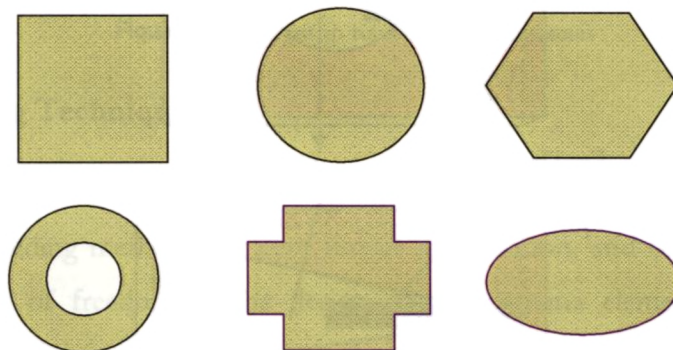


Figure 1.3 Basic microstrip patch antenna shapes

1.2.2 Microstrip Dipoles

Microstrip dipoles have a geometry similar to the rectangular patch antenna except that their length to width ratio is always less than $0.05 \lambda_0$. A typical bow-tie shaped printed dipole with its feeding mechanism is depicted in figure 1.4. The radiation patterns of the dipole and patch are similar owing to similar longitudinal current distributions. However, the radiation resistance, bandwidth and cross-polar radiation differ widely from that of microstrip patches.

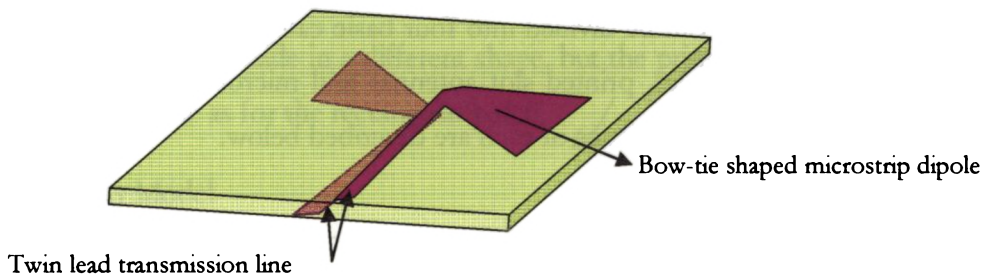


Figure 1.4 Configuration of a microstrip printed dipole

1.2.3 Printed Slot Antennas

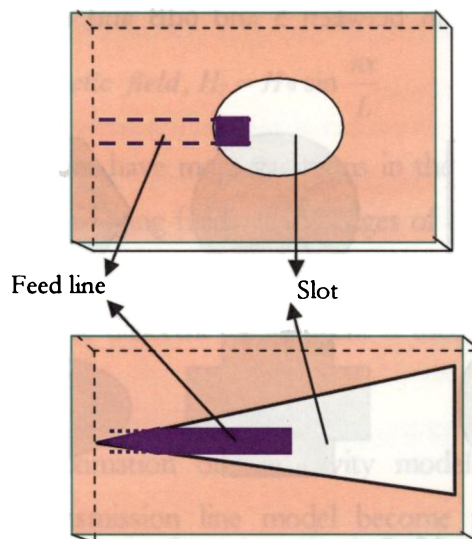


Figure 1.5 Basic printed slot antenna shapes with feed structures

Printed slot antenna consists of a slot in the ground plane of a grounded substrate. They can be fed either by a microstrip line or a co-planar wave guide. Most of the microstrip patch geometries can be realized in the form of a printed slot. Slot antennas are generally bidirectional radiators; i.e, they radiate on both sides of the slot. Tapered and circular microstrip slot antennas with the feeding mechanisms are shown in fig. 1.5.

1.2.4 Microstrip Travelling Wave Antennas

They consist of chain shaped periodic conductors or a long microstrip line of sufficient width to support a TE mode. To avoid the standing waves, the other end of the traveling-wave antenna is terminated in a matched load. Traveling-wave antennas can be designed so that the main beam lies in any direction from broadside to end fire. Various microstrip traveling-wave antennas are shown in figure 1.6.

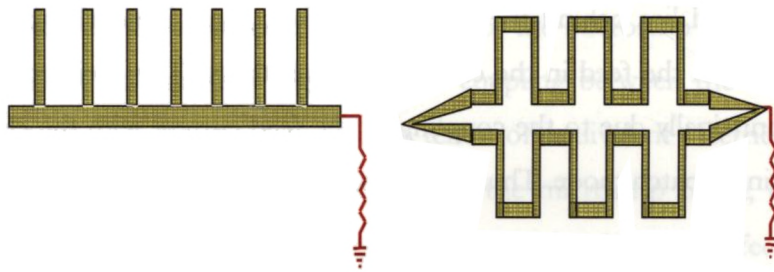


Figure 1.6 Microstrip traveling wave antennas

1.3 Feeding Techniques

Early microstrip antennas used either a microstrip feed line or a coaxial probe feed. These two feeding methods are very similar in operation, and offer essentially a single degree of freedom in the design of the antenna element through the positioning of the feed point to adjust the input impedance level. Other feeding techniques includes proximity-coupled feed, aperture coupled microstrip feed and coplanar waveguide feed.

1.3.1 Coaxial Feed or Probe Coupling

It is the basic mechanism used for microwave power coupling [3, 13, and 17]. The probe can be an inner conductor of a coaxial line feeding. It is attached to the back side of the printed circuit board, and the coaxial center conductor after passing through the substrate is soldered to the patch metallization. A typical rectangular patch antenna with a coaxial SMA connector is shown in fig. 1.7.

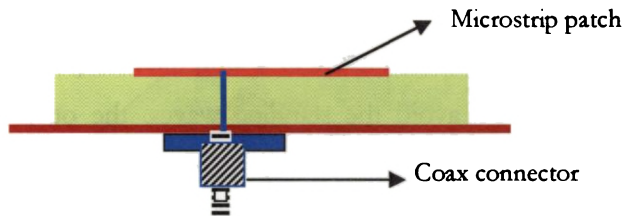


Figure 1.7 Coaxial probe fed microstrip antenna

Since the feed lies behind the radiating surface, there is no chance of unwanted radiation from the feed in the case of thin substrates. The excitation of the patch occurs principally due to the coupling of the feed current with the electric field of the dominant patch mode. Thus the coupling constant is given by,

$$\text{Coupling} \approx \int_v E_z J_z dv \approx \cos \frac{\pi s}{L} \quad (1.7)$$

where L is the resonant length of the patch and s is the offset of the feed point from the patch edge. This result shows that maximum coupling occurs for a feed at a radiating edge of the patch ($s = 0$ or L). Such direct contact feeding methods have the advantage of simplicity, but they have several disadvantages. Even though the probe primarily excites the dominant mode, due to its inherent asymmetry some higher order modes are also generated, which in turn produce cross polarized radiation. Moreover, in an array having thousands of elements, a large number of coaxial solder joints will make fabrication difficult and lower the reliability.

1.3.2 Microstrip Line Feed

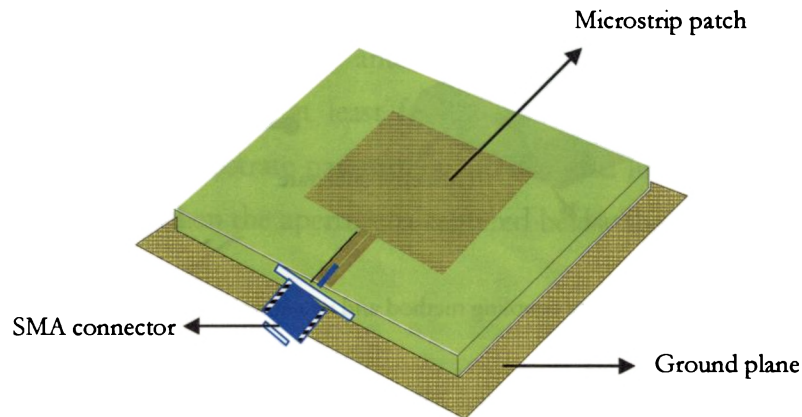


Figure 1.8 Microstrip line fed patch

A microstrip line on the same substrate appears to be a natural choice to feed a patch as the patch can be considered an extension of the microstrip line, and both can be fabricated simultaneously (fig. 1.8). The coupling between the microstrip line and the patch edge can be described in terms of equivalent electric current density, J_z associated with the magnetic field of the microstrip patch, coupling with E_z of the patch antenna. The same equation given for the coaxial feed above governs the coupling constant [3].

1.3.3 Proximity Coupled Microstrip Feed

Proximity feed uses a two layer substrate with a microstrip line on the lower substrate, terminating in an opening below the patch which is printed on the upper substrate as shown in the fig. 1.9. This kind of feeding has the advantage of allowing the patch to exist on a relatively thick substrate, for improved bandwidth, while the feed line sees an effectively thinner substrate, which reduces spurious radiation and coupling.

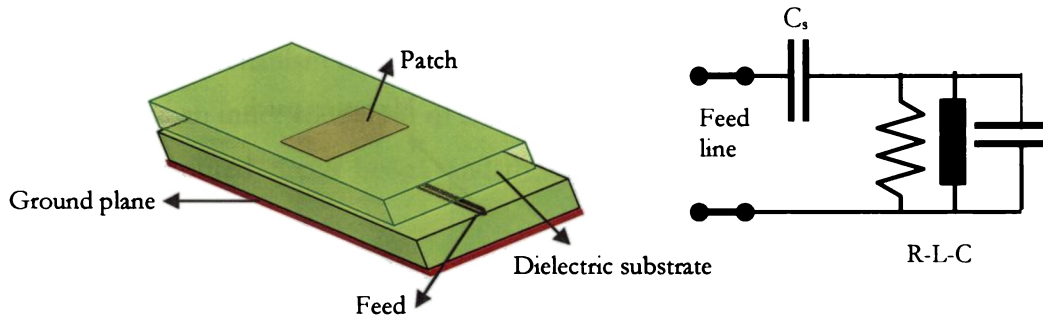


Figure 1.9 Proximity coupling method and its equivalent circuit

The proximity coupled patch has at least two degrees of freedom, making it easy for determining the exact impedance match. The capacitive nature of this feeding method is reflected in the fact that the equivalent circuit shown in figure 1.9 has a capacitor in series with the parallel RLC resonator that represents the patch. This can be used to impedance match the antenna as well as to aid in the tuning of the element for improved bandwidth [3, 21].

1.3.4 Aperture Coupled Microstrip Feed

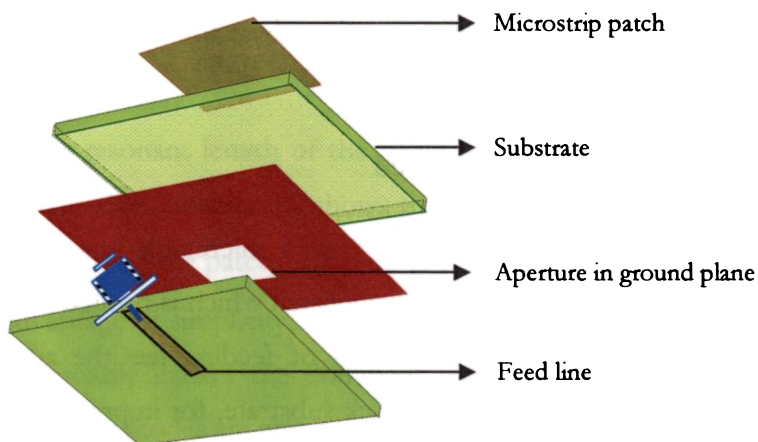


Figure 1.10 Exploded view of an aperture coupled microstrip patch

It consists of a microstrip feed line on the bottom substrate coupled through a small aperture in the ground plane, to a microstrip patch on the top substrate (fig. 1.10). Here the ground plane eliminates spurious radiation from the feed away from interfering with the antenna pattern or polarization purity [22, 23]. This type of feeding has at least four degrees of freedom: the slot size, its position, the feed substrate parameters and the feed line width. The maximum coupling occurs when the aperture is centered below the patch, where magnetic field is maximum.

1.3.5 Coplanar Waveguide Feed

Since both the coplanar waveguide (CPW) and the microstrip antennas belong to the planar geometry, integrating microstrip antennas with microwave monolithic integrated circuits (MMIC) can be easily done by feeding it with CPW. An advantage of a CPW feed is that the radiation from the feed structure is negligible since the coplanar waveguide is excited in the odd mode [13].

1.4 Full Wave Analysis of Microstrip Antennas

The analytical models of the microstrip antennas explained earlier suffer from a number of limitations. Some of the above mentioned feed configurations such as proximity coupled and aperture coupled microstrip feeds are difficult to be modeled. Only single mode analysis has been carried out in transmission line analysis and therefore cross-polarized radiation from a patch antenna has not been predicted. Most of these limitations can be overcome in the full-wave techniques. Full wave techniques usually assume that the substrate is infinite in extent in the lateral dimensions, and enforce the proper boundary conditions at the air-dielectric interface. This is most commonly done by using the exact Green's function for the dielectric substrate, which allows space wave radiation, surface wave modes, dielectric loss and coupling to the external elements to be

included in the model. The most popular full-wave techniques are described below:

1.4.1 Spectral Domain Full-Wave Analysis

This approach uses the exact Green's function for the mixed dielectric nature of the microstrip antenna. The Green's function is employed in the electric field integral equation formulation to satisfy the boundary conditions at the patch metallization. The resulting integral equations are discretized into a set of linear equations by means of the moment method to yield a matrix equation [24, 25]. The solution of this matrix equation provides the current distribution on the patch. Near and far-field characteristics of the antenna are then obtained from the current distribution and the Green's functions.

1.4.2 Mixed Potential Integral Equation (MPIE) Analysis

It is computationally more efficient than the integral equation analysis in the spectral domain. As the name suggests, different types of potential Green's functions are employed in MPIE to set up the integral equation. Among several choices, Sommerfield's choice of potentials is the most popular approach for solving straightfield media problems [26].

1.4.3 Finite Difference Time Domain Analysis




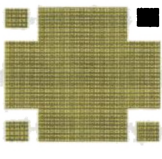

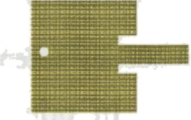




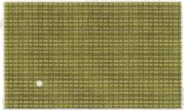


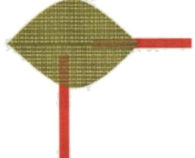
The complicated analytical pre-processing and modeling in the above two methods makes them highly intricate in modeling complex patch geometries. Mathematically, FDTD is just a direct discretization and implementation of Maxwell's curl equations in time and space and therefore analytical pre-processing and modeling are totally absent [27,28]. FDTD simulation of any problem includes dividing the region under consideration into different material properties (by modeling the proper antenna structure to be analyzed) and finally

terminating the unbounded region by absorbing boundary conditions to prevent the electric and magnetic fields from reflecting. Next, the physical space of the problem is discretized in the form of cubes (or cuboids) with dimensions Δx , Δy , Δz and the time of simulation is also divided into Δt interval steps. The source of electromagnetic energy is then introduced into the physical domain in the form of pulse or a plane wave and allowed to interact with the structure and finally the time domain information is processed to determine the electromagnetic behavior of the structure.

1.5 Dual-Frequency Microstrip Antenna Technologies

Dual frequency antennas exhibit a dual resonant behavior in a single radiating structure. In principle, these planar antennas should operate with similar features, both in terms of radiation and impedance matching, at two separate frequencies. Most of the dual-frequency patch antennas found in the literature can be subdivided into three major categories namely multi-patch, reactively loaded and orthogonal modes as shown in table 1.1.

Table 1.1 Various types of dual frequency microstrip antennas

Multi-Patch	Stacked		
	Co-planar		
Reactively Loaded	Stubs		
	Pins and Capacitors		
	Slots		
Orthogonal Modes	Single-point		
	Dual-point		

1.5.1 Multi-Patch Dual-Frequency Antennas

In these structures, the dual-frequency operation is obtained by means of multiple radiating elements [29-31]. These antennas can operate with same polarization at the two frequencies, as well as with a dual polarization. Multi-patch dual-frequency antennas can also be obtained by printing more resonators on the same substrate.

1.5.2 Reactively Loaded Antennas

This approach was first used by W.F. Richards, where an adjustable coaxial stub was employed [32]. The simplest way is to connect a stub to one of the radiating edge of the patch, in such a way as to introduce a further resonant length that is responsible for the second operating frequency. Different kinds of reactive loads like notches, pins, capacitors and slots can be used for dual frequency generation [33, 34].

1.5.3 Orthogonal-Mode Dual Frequency Patch Antennas

As is well known, a simple rectangular patch can be regarded as a cavity with magnetic walls on the radiating edges. The first three modes with same polarization can be indicated as TM_{10} , TM_{20} and TM_{30} . TM_{10} is the mode typically used in practical applications; TM_{20} and TM_{30} are associated with a frequency approximately twice and triple of that of the TM_{10} mode [34]. Unfortunately, owing to the behavior of the radiating currents, the TM_{20} and TM_{30} modes are of little use due to their distortion in broadside radiation patterns; TM_{20} pattern has a broadside null, and the TM_{30} pattern has grating lobes. Also, simultaneous matching of these same polarizations resonant modes with a single feed is generally worse in microstrip antennas. Thus the simplest way to operate at dual frequencies is to use the first resonance of the two orthogonal dimensions of the rectangular patch, i.e, the TM_{10} and TM_{01} modes. Since dual polarization is an increasingly important requirement of modern communication systems the excitation of these orthogonal resonant modes with a single feed will be of great advantage [35, 36].

1.6 Current Reconfigurable Antenna Technologies

The last few years have seen an exponential growth in the development of reconfigurable antennas. Reconfigurable antennas are defined as those antennas whose aperture can be dynamically modified to enable different functions at different times. The development efforts include the use of mechanical tuning, magnetic tuning and electronic tuning.

1.6.1 Mechanical Tuning

The earlier forms of reconfigurable antennas were all based on mechanical tuning with shorting pins, stubs and air-gaps [13, 37]. The shorting pins are introduced in between the ground plane and patch metallization as in fig. 1.11. This presents an inductance and thus this type of tuning increases resonant frequency of the patch. This technique was first introduced by Schaubert et al [38].

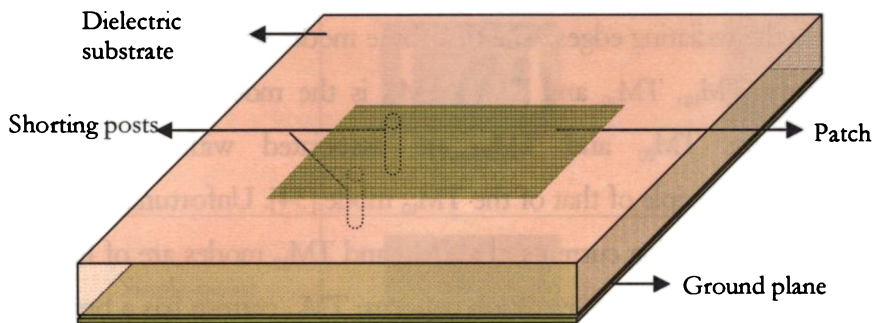


Figure 1.11 Tuning using shorting posts

Printed or co-axial transmission line stub attached to the antenna can be used for frequency tuning by varying its length mechanically. In this technique, tuning is only possible from a lower frequency to a higher frequency owing to the destructive nature of trimming. The two-stub approach is the widely used stub

tuning technique. Patch antenna with dual stubs for mechanical frequency tuning is shown in fig. 1.12. Another method of mechanical tuning involves an adjustable air gap introduced between the substrate and ground plane. The idea was first proposed by Dahele and Lee [39]. Here the effective dielectric constant of the patch is varied by adjusting the thickness of the air layer, resulting in a new resonant frequency.

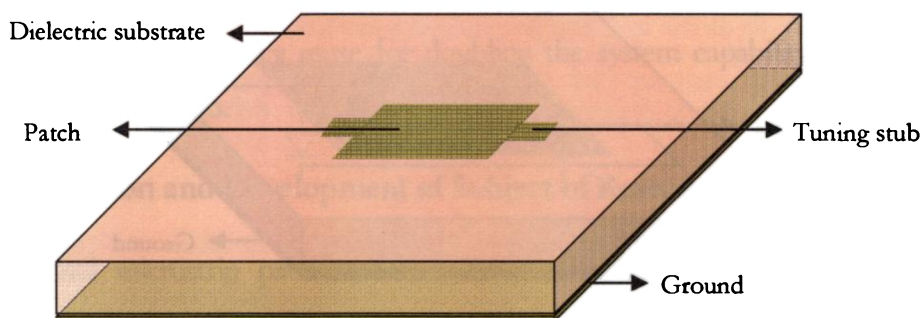


Figure 1.12 Mechanical tuning of patch using dual stubs

1.6.2 Magnetic Tuning

Magnetic tuning is generally accomplished by biasing the substrate. Henderson et al. used a biased ferrite substrate to control the radiation pattern of a microstrip antenna [40]. Later Pozar and Sanchez have reported a rectangular microstrip antenna, printed on a ferrite substrate, whose operating frequency can be tuned by varying the strength of a dc magnetic biasing field applied to the substrate [41].

1.6.3 Electronic Tuning

Electronic tuning is the most reliable and highly efficient method of tuning used in reconfigurable antennas. In recent years, electronically reconfigurable antennas have received significant attention for their applications in communications, electronic surveillance and countermeasures by adapting their properties to achieve

selectivity in frequency, bandwidth, polarization and gain [42-46]. In particular, preliminary studies have been carried out to demonstrate electronic tunability for different antenna structures. In all these designs electronic tuning of the antenna is achieved by using either varactor diodes (fig. 1.13), switching pin diodes or microelectromechanical switches (MEMS) [47].

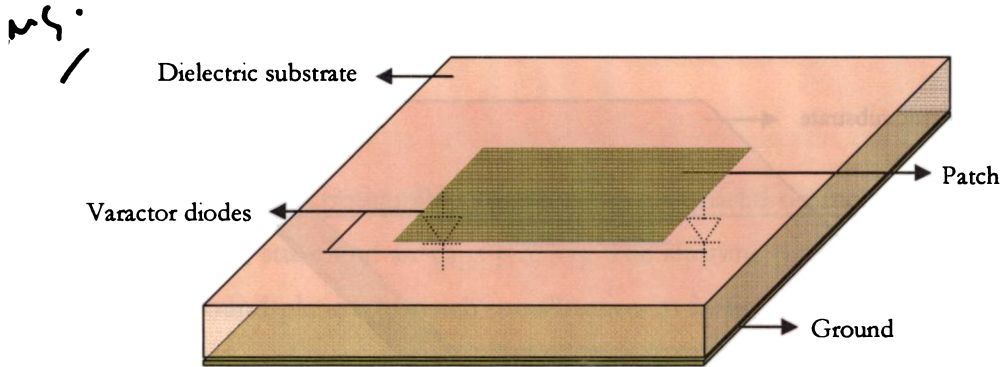


Figure 1.13 Electronic tuning using varactor diodes

MEMS were started to be used in tunable circuits in the early 1990s. MEMS have very little loss at RF and microwave frequencies and can handle higher power levels. However, they have some disadvantages including low tunability, slow switching speed (2-100 μs), and high bias voltage (50-100 V). In addition, they require hermetically sealed packaging, which is expensive and hard to integrate with antennas and other circuits. Semiconductor diodes are still the dominant devices for making electronically reconfigurable antennas. They are very small in size (in μm s), very fast ($<1\mu\text{s}$ for pin diode), and have large tunability. In addition, they can be easily integrated with other circuits for example in monolithic microwave integrated circuits (MMIC).

1.7 Reconfigurable Microstrip Antennas

Reconfigurable microstrip antennas have the potential to add substantial degrees of freedom and functionality to mobile communication applications and electronic

intelligence. This is achieved mainly by electronically reconfiguring the antenna parameters like radiation pattern, polarization or resonant frequency [48].

In pattern-reconfigurable microstrip antennas, operating frequency and bandwidth is maintained while changing radiation patterns. Manipulation of an antenna radiation pattern can be used to avoid noise sources or intentional jamming, improve security by directing signals only towards intended users and serves as a switched diversity system. Polarization reconfigurable microstrip antennas are utilized mainly in frequency reuse for doubling the system capability in satellite communication systems.

1.8 Motivation and Development of Subject of Research

Conventional microstrip patch antennas have a number of inherent practical limitations which make them incompatible for use in modern wireless communication systems. The foremost disadvantage is the limitation in bandwidth due to the resonant nature of the patch structure. Moreover, this narrow bandwidth makes their input impedance very sensitive to manufacturing errors and substrate material tolerances. In applications where the increased bandwidth is needed for operating at two sub bands, a valid alternative to the broadening of total bandwidth is provided by dual-frequency patch antennas. Satellite base communication, air route surveillance, GPS and mobile satellite personal communication systems require dual frequency multipolarization microstrip antennas.

However, the rapid growth of modern communication systems demands the ability to design frequency agile RF front ends for operation in various frequency bands. Reconfigurable dual-frequency microstrip antennas can be used to cover these multiple functions with a single antenna aperture. This will increase antenna efficiency and signal processing speed while maintaining high degree of flexibility.

Such common aperture antennas find applications in space-based radar, unmanned aerial vehicles (UAV), communication satellites, synthetic aperture radar (SAR), electronic intelligence and other sensing applications. Tunable RF and microwave components are thus in large demand due to their frequency agile characteristics. These requirements impose significant challenges on current tunable antenna and circuit technologies and illustrate the need for new reconfigurable antennas with simple and efficient switching mechanism. Therefore the main objectives of this research work are to devise and analyze compact electronically reconfigurable dual frequency microstrip antennas with simple and efficient tuning mechanisms.

1.9 Thesis Overview

In this work, we investigate novel designs of compact electronically reconfigurable dual frequency microstrip antennas with a single feed operating mainly in L-band. The strict requirements of a constant input impedance, gain, radiation pattern and polarization can only be met, if both the passive antenna structure and the tuning mechanism are carefully designed and integrated into the final reconfigurable antenna design. PIN diodes and varactor diodes are used for the switching/tuning mechanism. A brief introduction on different types of microstrip antennas, their feeding, analysis and various tuning mechanisms is provided in Chapter 1.

Chapter 2 gives a brief review of past works carried out in the field of microstrip antennas. Various dual frequency microstrip antenna design techniques and reconfigurable antenna schemes are also discussed.

In Chapter 3, the methodology adopted for the investigations are described. The development of the FDTD technique used for the theoretical analysis of the reconfigurable dual frequency microstrip antenna is depicted in detail. The photolithographic technique used for the microstrip antenna fabrication is also included. The measurement of different antenna characteristics like resonant

frequency, bandwidth, radiation pattern, polarization and gain are illustrated. Electromagnetic modeling of reconfigurable microstrip antennas using the method of moment based software, IE3D is also explained.

The vital passive antenna design and the reconfigurable antenna design using PIN diodes are described in Chapter 4. All the experimental and theoretical investigations carried out in these reconfigurable antenna configurations are portrayed in detail here. Theoretical interpretations of the developed passive and reconfigurable antenna designs are explained using the full wave approach based on FDTD modeling. A semi empirical design equation is given for the passive antenna.

Chapter 5 describes the detailed experimental studies on various varactor loaded reconfigurable dual frequency microstrip antennas. A theory based on transmission line model is given for the reconfigurable antenna configurations with varactor diode loading.

The conclusion drawn from the experimental and theoretical investigations and the scope for further work are described in Chapter 6.

CHAPTER

2

A BRIEF REVIEW OF PAST WORK

Contents

<i>2.1 Microstrip Antenna Technology</i>	29
<i>2.2 Dual Frequency Microstrip Antenna Design</i>	37
<i>2.3 Reconfigurable Antenna Techniques</i>	40
<i>2.4 Analysis of Microstrip Antennas</i>	45

This chapter gives a brief review of literature relating to microstrip antenna design in a historical perspective. The theoretical and experimental aspects of different types of microstrip antennas are covered in the first section. A review of various dual frequency microstrip antenna design techniques is given in the second section with emphasis on slot loaded patch antennas. The third section covers different reconfigurable antenna techniques employed recently in modern communication and military systems, and the emphasis is given to electronically reconfigurable microstrip antennas with semiconductor diode tuning. The final section covers various analytical and full wave solutions of microstrip antennas and reconfigurable antennas. Finite difference time domain (FDTD) analysis of various microstrip antennas is thoroughly examined in this section.

2.1 Microstrip Antenna Technology

This section describes analytical and experimental design approaches for microstrip antenna elements, and provides a comprehensive survey of the state of microstrip antenna element technology. Several practical techniques are outlined for modifying the basic element for special purpose applications such as conformal arrays and wide band communications.

The idea of planar microstrip radiators was first proposed by G. A. Deschamps [49] in USA and by Gutton and Baissinot in France [50]. Shortly thereafter, Lewin [51] investigated radiation from stripline discontinuities. Additional studies were undertaken by Kaloj in the late 1960s, who studied basic rectangular and square microstrip configurations [4]. However, work was not reported in the literature until the early 1970s, when a conducting strip radiator separated from a ground plane by a dielectric substrate was described by Byron [6]. Shortly thereafter, a microstrip antenna element was patented by Munson [7] and data on basic rectangular and circular microstrip patch antennas were published by Howell [8].

Microstrip geometries for use with cylindrical S-band arrays on rockets were later developed by Weinschel [52]. Sanford [53] showed that the microstrip element could be used in conformal array designs for L-band applications. The early works by Munson on the development of microstrip antennas on rockets and missiles showed that this was a practical concept for use in many antenna system problems, and thereby gave birth to a new antenna industry.

Mathematical modeling of the basic microstrip antenna geometries was initially carried out by the application of transmission line analogies to simple rectangular patches fed at the center of the radiating wall by Munson and Derneryd [54, 55]. Carver reported the measurements and analysis of the radiation pattern of a circular patch microstrip antenna [56]. Although the transmission line model is easy to use, it suffers from numerous disadvantages. It is only useful for patches of rectangular shape, and an unknown constant called fringe factor must be empirically determined, it ignores field variations along the radiating edge and it is not adaptable to the inclusion of the feed. These limitations are eliminated in the modal expansion analysis.

Lo et al [57] in 1977 published the modal expansion technique to analyze rectangular, circular, semicircular and triangular patch geometries. Here the patch is considered as a thin cavity with leaky magnetic walls. The impedance boundary conditions are imposed on the four walls and the stored and radiated energy were investigated in terms of complex wall admittances. Similar analytical papers on basic patch geometries were later published by Derneryd [58], Chen and Long [59], and Carver and Coffey [60]. Thus by 1978, the microstrip patch antenna became much more widely known and used in a variety of communication systems. This was accompanied by increased attention by the theoretical community to improved mathematical models which could be used for design.

As the microstrip antenna technology developed further, many new substrate materials were also invented with dielectric constants ranging from 1.17 to 25 and loss tangents from 0.0001 to 0.004. A comparative data on most available substrates were later published by Carver and Mink [4].

The basic microstrip antenna geometries like rectangular and circular have been modified to other shapes such as pentagon and hexagon [11, 61]. For these geometries the modal expansion technique is a more cumbersome analysis method than a direct numerical method, due to the difficulty in finding the appropriate orthogonal mode vectors. In recent years several numerical techniques applied to the microstrip antenna have been proposed, including the method of moments by Newman [62, 63], the uni-moment Monte Carlo method [64], the finite element techniques [60], and the direct form of network analogs method [65]. The effect of radiation and other losses are represented in terms of either an artificially increased substrate loss tangent or by the more elegant method of impedance boundary conditions at the walls [66, 67]. The method of moments is used in connection with Richmond's reaction method [68] to determine the unknown surface currents flowing on the walls forming the microstrip patch, ground plane and magnetic walls.

The transmission line model, cavity model and the multi-port network model all come under the reduced analysis category, which uses one or more significant approximations to simplify the problem. The multi-port network model generalizes the cavity model [69]. Drawbacks of these models include limited accuracy for resonant frequency and input impedance for substrates that are not very thin [70], and their limited capacity to handle related problems such as mutual coupling, large arrays, surface wave effects and different substrate configurations.

The numerical analysis of the fields interior to the microstrip antenna cavity can also be carried out using a finite element approach [60]. This is a variational

method in which a minimization process automatically seeks out the solution which is closest to the true analytical solution.

Deshpande and Bailey [25] used the spectral domain full wave approach which uses the exact Green's function for the mixed dielectric nature of the microstrip antenna. Various patch geometries and feed structures were analyzed using this technique. The analysis of a rectangular patch and a circular disc were studied by Chew, Aberle and Bailey [71-73].

In addition to standard rectangular and circular patch antennas, several modified patch geometries were developed by researchers for different applications. One of the requirements is the generation of circular polarization. Various shapes for microstrip antennas capable of circular polarization operation have been reported in literature [74, 75]. Design of circularly polarized patch antennas fabricated on ferrite substrate was demonstrated by Tsang and Langlely [76].

In 1981 rigorous experimental studies were carried out by Schen [77] and Long [78] on elliptical shaped printed antennas with circular polarization generation. Later in 1988, Haneishi and Yoshida [79] designed a circularly polarized rectangular microstrip antenna with a single point feed. Huang [80] used an array of linearly polarized elements to obtain circular polarization.

The serious limitation of narrow bandwidth of microstrip antennas was fixed by researchers using a variety of innovative patch designs and feed modifications. Pozar [81] proposed the aperture coupling of microstrip patch antennas for improved impedance bandwidth and reduced spurious radiation. Basic aperture coupled patch antenna geometries were analyzed using various techniques including the integral equation method [82-85], cavity model [86-88], transmission line model [89, 90] and modal expansion method [91].

The use of stacked patches in order to increase the impedance bandwidth was first proposed by Long and Walton [29]. Here an upper patch with a slightly different dimension was proximity coupled to the lower excited patch. Impedance bandwidth up to 30% had been achieved with probe fed stacked patches [92, 93] and up to 67% for aperture coupled stacked patches [94, 95]. The larger bandwidth in each case corresponds to relatively thicker substrate.

A set of coplanar resonators with slightly different resonant frequencies were used by Kumar, Entsehladen and Aanandan to obtain broadband performance [96-98].

Pues and Van de Capelle [99] obtained a bandwidth of about 12% using a passive coplanar matching network. Similar techniques used by Paschen [100] produced a bandwidth of more than 25%, which was sufficient to cover the GPS bands with a single radiating element.

Wong and Lin [101] studied the loading effect of a chip resistor mounted at the edge of a rectangular patch. The 10dB return loss bandwidth of this patch antenna was found to be about 4.9 times that of a patch without the resistor loading [102].

As the telephone handsets for mobile communications needed compact antennas, several designs were proposed to reduce the size of existed microstrip patches. In 1989, Kossiavas et al [103] proposed a small C-shaped patch element for applications at 413MHz.

Vandenbosch in 1995 [104] presented a capacitive matching of small microstrip antennas with rigorous theoretical analysis to calculate the input impedance. This method allows separation of the analysis of the capacitive feeding from the analysis of the radiating patch. Later in 1997, Corbett and Murch [105], proposed a capacitively loaded planar inverted F- antenna (PIFA) for mobile telephone handsets. They found the capacitive load reduces the resonance length of the PIFA from $\lambda/4$

to less than $\lambda/8$. A design with a bandwidth of 178MHz centered at 1.8GHz was provided to demonstrate that compact antennas for mobile telephone handsets can be constructed using this approach.

K. L. Wong and Cheng Pan in 1997 [106] used a shorting pin in a triangular microstrip patch fed with a coaxial probe, to reduce its size at 1.9GHz band. They obtained a reduction of 78% in the linear dimension of the microstrip antenna.

Different slot loaded patch geometries were suggested by this time to make the conventional microstrip patch antennas more compact. The addition of shorting pins and chip resistors further brought down the size. J. H. Lu et al [107], in 1997 proposed a slot coupled triangular microstrip patch antenna with a shorting pin or chip resistor loading. This technique of chip resistor loading provided a much broader operating bandwidth as compared to regular patches or shorted patch antennas.

Small broadband rectangular microstrip patch antenna with a chip resistor at its edge was proposed by K. L. Wong and Y. F. Lin [108], for increased bandwidth and size reduction. The design was applicable to both probe fed and microstrip line fed antenna configurations.

C. Y. Huang et al [109] reported a broadband circular polarization operation of a single feed slot coupled microstrip antenna using an inclined nonlinear coupling slot. This nonlinear slot, end loaded with two V – shaped slots, significantly broadens the bandwidth to about 2.1 times that obtained using a simple inclined coupling slot.

A novel folded rectangular microstrip patch antenna was designed by K. M. Luk et al [110]. Compared with a conventional patch antenna with the same surface area, the resonant frequency was reduced by 37%. The cross-polarization level was also near -20dB.

Wen Hsu [111] investigated a novel disk sector microstrip antenna with specific flare angles for circular polarization operation. Their results showed that by suitably selecting the flare angle of the disk sector microstrip patch, right hand or left hand circular polarization can easily be obtained using a single coaxial probe feed.

S. K. Satpathy et al [112], studied different shorted variations of triangular microstrip patch antennas. The increased size reduction was achieved by partially shorting the curved edges of the sectoral antennas.

A novel two layer rectangular patch antenna had been designed and tested with a 5% bandwidth by R. Chair et al [113]. Compared with a basic single layer patch antenna with the same projection area, the resonant frequency was reduced by 39%.

Bandwidth enhancement of a single layer, single patch rectangular microstrip patch antenna was achieved by J. Y. Sze et al [114], by embedding a pair of double bent slots close to the patch's non-radiating edges and an additional bent slot centered to the patch's center line. An antenna bandwidth up to about 2.8 times that of a conventional unslotted rectangular patch had been obtained.

C. S. Hong [115] designed a small size annular slot antenna with miniaturized slot shrunk by a loaded capacitor. The antenna had the advantages of a good impedance bandwidth and good linearly polarized radiation patterns after chip capacitor loading. A 23.4% slot antenna area size reduction had been achieved with this type of capacitor loading compared with the ordinary slot antenna.

M. C. Liang et al [116] proposed a frequency varying microstrip patch antenna design with a loaded capacitor. Unlike traditional patch size reduction schemes, this capacitor – loaded design does not significantly affect the radiated power efficiency of the antenna. In some cases the maximum radiated power can even be improved.

A novel internal square microstrip patch antenna for 3G IMT – 2000 mobile handsets was first investigated by Y. J. Wang [117]. By introducing a single shorting pin and a thin rectangular slot perforated in a square patch, this probe fed antenna realized an impedance bandwidth of 25.6% with dual frequency operation, which thoroughly covers the 3G IMT – 2000 frequency spectra.

In 2001, Jaume Anguera et al [118] proposed a systematic design method for broad band single patch antenna input impedance prediction. This mathematical approach allowed designing an optimum feed that enhances the impedance bandwidth.

J. P. Lee and S. O. Park [119] in 2002 put forward a small size and high gain meander line antenna for Bluetooth applications. The bandwidth of this design was about 9% at 2.44GHz and the gain was 2.73dBi. They achieved a size reduction of 35% compared to conventional patch antennas.

A novel and broadband semi disk microstrip antenna suitable for a portable and compact terminal integrated with the 3G IMT-2000 cellular system, DECT mobile system, and Bluetooth wireless technology was discussed both theoretically and experimentally by Y. J. Wang [120]. The reduced dimensions of the proposed antenna were achieved by using a single cylindrical shorting pin, while the broadband characteristics were obtained through a narrow rectangular slot which induced two resonant frequencies sufficiently close to each other.

Aaron Shackelford et al [121] in 2003 examined several designs for small size wide-bandwidth microstrip antennas. The designs were presented based on a U-slot patch and an L-probe-fed patch. Several techniques were utilized to reduce the resonant length of these wideband microstrip patch antennas: increasing the dielectric constant of the microwave substrate material, a shorting wall or shorting pin between the conducting patch and the ground plane. A size reduction of 94% and bandwidth of 20% were attained by these techniques.

A numerically efficient substitute for the general transmission line model of microstrip antennas was suggested by S. K. Roy [122] in 2000. Here the fringe factor determines the accuracy of the resonant frequency calculation. In 2004, Schubler, Jens Freese and Jakoby [123], derived design equations for compact planar antennas using LH – transmission lines. This model allows preliminary design studies and was able to improve the understanding of the connection between bandwidth and radiation impedance.

2.2 Dual Frequency Microstrip Antenna Design

Dual frequency microstrip patch antennas may provide an alternative to large bandwidth planar antennas, in applications in which large bandwidth is really needed for operating at two separate transmit-receive bands. On the other hand, modern communication systems, such as those for satellite links (GPS, Vehicular etc.), as well as emerging applications like wireless local area networks (WLAN), often require antennas with compactness and low-cost, thus rendering planar technology useful, and sometimes unavoidable. Furthermore, thanks to their lightness, patch antennas are well suitable for systems to be mounted on airborne platforms, like synthetic aperture radar (SAR) and scatterometers. Despite the convenience that they may provide in terms of space and cost, not much importance has been given to dual frequency microstrip antennas. This is possibly due to the relative complexity of the feeding network which is required, in particular for array applications. An excellent review of dual frequency microstrip antennas was given by S. Maci and Biffi Gentili [34] in the year 1997.

Wang and Lo [124] were the first to use shorting pins and slots in a rectangular microstrip patch to generate dual frequency operation. The upper and lower frequencies showed similar broadside radiation characteristics.

In 1993, Yazidi et al [88] designed an aperture coupled rectangular microstrip patch antenna with a pair of symmetrical slots. The excited modes of the antenna depend on the type and position of the feed. By choosing aperture coupling with a centered slot, the even modes were not excited.

If two orthogonal linear polarizations at separate frequencies are required, the simplest antenna for this is a rectangular patch antenna fed at the diagonal for exciting the (1, 0) and (0, 1) modes. The frequencies of these modes are determined by the respective lengths of the patch. Impedance matching for these two resonant frequencies can be easily achieved with a single feed. Salvador et al [125], proposed a new configuration of dual frequency planar antenna operating at S and X bands. They used a cross patch sub array and the geometry had two symmetry planes to provide radiation in double-linear polarization by using a proper feeding system.

K. L. Wong and G. B. Hsieh [126] suggested a dual frequency circular microstrip antenna with a pair of arc shaped slots excited with a single co-axial feed. Frequency ratio ranging from 1.38 to 1.58 were implemented and studied.

A slot loaded bow-tie microstrip antenna for dual frequency operation was proposed by K. L. Wong and W. S. Chen [127]. Frequency ratios within the range 2 to 3 were obtained with a single probe feed.

Chen [128] demonstrated a single probe fed dual frequency rectangular microstrip antenna with a square slot at its center. This technique was one of the simplest methods of dual frequency generation in a rectangular patch with dual linear polarization. The excited frequencies were orthogonally polarized.

E. Lee et al [129] developed a compact dual-band dual-polarization microstrip patch antenna for application in terrestrial cellular communication and satellite mobile. The two operating frequencies showed different polarization and radiation characteristics. Bandwidths of 2 and 4% respectively, had been obtained in the two resonant modes.

J. H. Lu [130] demonstrated a dual – frequency rectangular microstrip patch antenna with embedded spur lines and integrated reactive loading. The two operating frequencies had the same polarization planes and frequency ratios of 1.1 to 1.6 were achieved with a single feed.

Jui – Han Lu [131] described novel dual – frequency design of single feed equilateral triangular microstrip antenna having same polarization planes and similar radiation characteristics.

Guo et al [132] demonstrated a dual band patch antenna using slot loaded and short-circuited size reduction techniques. By controlling the short plane width, the two resonant frequencies can be significantly reduced and the frequency ratio was tunable in the range 1.6 to 2.2.

A slot loaded dual – frequency rectangular microstrip patch antenna with a single feed was also proposed by **J. H. Lu** [133]. By varying the angle and the horizontal section length of the bent slots, the frequency ratio was tunable in a range from about 1.28 to 1.79.

X. Yang [134] derived analytical expressions for the input and mutual impedance of two kinds of dual – polarization square – patch antenna double fed at the orthogonal edges using the Green's function approach based on the planar circuit principle. The frequency characteristics of the input impedance, VSWR and isolation were analyzed and verified by experimental data.

C. Tang et al [135] designed a broadband dual frequency V-shape microstrip patch antenna with impedance bandwidths up to 10%.

A dual band GSM – 900/DCS – 1800, personal communication handset microstrip antenna with a spur-line filter and a shorting pin was proposed by **M. M. Vazquez et al** [136]. It consists of a PIFA like rectangular patch with a shorting pin close to

the corner of the patch. The spur line generated a second resonant mode lower than that of the rectangular patch.

A slot coupled chip capacitor loaded square microstrip patch antenna for dual frequency operation was proposed by G. S. Binoy et al [137]. The design provided an enhanced area reduction of 64 and 36% respectively, for the two operating frequencies and good cross-polarization levels.

2.3 Reconfigurable Antenna Techniques

With ever increasing demand for reliable wireless communications, the need for efficient use of electromagnetic spectrum is on the rise. Conventional broadband antennas discussed above never satisfy all these demands. The reconfigurable antennas have shown strong potential in this field due to its low cost and flexibility. This section depicts the recent advancements in reconfigurable antenna technology.

In 1991, Kawasaki and Itoh [138] demonstrated a novel idea of electronic tuning with the help of integrated FET components in a microstrip slot antenna. By changing the bias voltages, the reactance of the FET varied and the length of the slot was tuned electronically. 10% tuning of the center frequency was obtained with negligible changes in the radiation pattern. The 50Ω matching point of the center feed line was difficult to maintain, since the reactive circuits made of MESFETs affected the field distribution of the slot antenna.

Rainville and Harackiewicz [139] proposed a magnetic tuning scheme for a single feed square microstrip patch antenna fabricated on a ferrite film. The application of a small in-plane magnetic field tuned the frequency and the phase of one of the polarization.

The bandwidth extension approaches in tunable dipole antennas were illustrated by D. J. Roscoe et al [140] in 1993. They integrated beam lead diodes to the original

printed dipole and its parasitic patches so as to present low or high impedances according to its bias states. This produced a multi frequency antenna which was controlled by an applied bias voltage.

Egor Alekseev et al [141], invented InGaAs/InP PIN diodes for microwave and millimeter wave switching and limiting applications. DC and microwave characterization of the PIN diodes demonstrated low turn-on voltage (0.46 V), low insertion loss (<1.2dB up to 38GHz) and high switching cut-off frequency (17THz) as necessary for microwave and millimeter – wave switching and limiting applications.

M. A. Forman and Z. B. Popovic [142] designed a tunable second – resonance cross – slot antenna for use in active array applications. The resonant frequency can be mechanically tuned over a 45% bandwidth or electrically tuned over a 10% bandwidth with an integrated varactor diode.

A varactor loaded electronically tunable microstrip patch antenna with a probe feed was presented by S. H. Al-Charchafchi and M. Frances [143]. An effective impedance bandwidth of 50% was achieved centered on a frequency of 2.2GHz. A simple transmission line model was used to predict the resonant frequency.

Various radio frequency applications involving microelectromechanical systems (MEMS) were studied thoroughly by Elliott R. Brown [144] in 1998. RF MEMS are the new class of passive devices (e.g. switches) and circuit components (e.g. tunable transmission lines) controlled by MEMS. Several applications of these types of switches were analyzed here, including switchable routing in RF system front-ends and time-delay networks. The promising concept of reconfigurable antennas controlled by these MEMS was discussed in detail.

N. Fayyaz et al [145] designed a novel electronically tunable rectangular patch antenna with one octave bandwidth for applications in multi-band communication

systems and frequency hopping systems. The layout of the antenna consisted of a rectangular patch antenna divided into two sections and connected using varactor diodes. However, a wide tuning range resulted in mismatching in a larger range of frequencies because the feed point was fixed mechanically.

Kolsrud et al [146] proposed a dual – frequency electronically tunable CPW – fed coplanar strip dipole antenna with varactor control. Dual frequency operation of the dipole antenna was realized by introducing a small gap in the length of the dipole. Varactors were integrated with this dipole to tune the antenna, by applying reverse bias. But a wideband CPW – to – CPS balun was needed to feed the antenna in order to achieve better matching.

S. Sharma and B. R. Vishvakarma [147] studied a new MOS capacitor loaded frequency agile microstrip patch antenna in which the operating frequency of the rectangular microstrip antenna was electronically controlled by the bias voltage of the MOS capacitor. Theoretical investigations based on a modal expansion cavity model were carried out for different MOS structures. The larger frequency variation was achieved with lower variation in the bias voltage as compared with the varactor diode.

MEMS – switched reconfigurable multi-band antenna design and modeling were thoroughly studied by W. H. Weedon et al [148] in 1999. A general adaptive reconfigurable feed design methodology was proposed for designing and tuning the feed structure for each configuration independently. However, their research was limited to simulating the MEMS switches as ideal switches, and building separate antennas to simulate the OPEN and CLOSED configurations.

B. C. C. Chang et al [149] developed a reconfigurable leaky mode patch antenna controlled by PIN diode switches. Different radiation configurations were obtained by switching the antenna with PIN diodes. When the switches were turned on, the

entire microstrip structure functioned as a leaky mode antenna, while, when the switches were turned off, the segmented pieces of microstrips converted into ordinary patch antennas.

A prototype of a reconfigurable patch module array connected using MEMS switches were proposed by W. H. Weedon et al [150] for dual band application in L and X bands. Stripline power dividers and blind via transitions were developed to demonstrate feed structures that could be located below the radiating aperture.

Fan Yang and Y. Rahmat-Samii [151] put forward the concept of a patch antenna with switchable slot for dual frequency operation. A slot was incorporated into the patch and a PIN diode was utilized to switch the slot on or off, for achieving dual frequency operation. The antenna was designed for same polarization at two frequencies and for a small and flexible frequency ratio. Similar radiation patterns were observed at the two operating bands.

A planar microstrip line fed reconfigurable slot antenna with a series of PIN diode switches were proposed by D. Peroulis et al [152]. The tuning of the operating frequency was realized by varying the electrical length of the slot using the loaded PIN diodes. The antenna was capable of radiating at four different frequencies ranging from 550 to 900MHz. Unlike other reconfigurable antenna designs discussed earlier, this configuration never used any special matching network. It was demonstrated that the radiation pattern, efficiency and polarization remained essentially unaffected by the frequency tuning.

F. Yang and Y. Rahmat-Samii [153] devised a novel reconfigurable patch antenna using switchable slots for circular polarization diversity. Two orthogonal slots were incorporated into the patch and two pin diodes were utilized to switch the slots on or off. Right hand and left hand circular polarizations were generated by suitably

switching the diodes on and off. The design was well suitable for wireless communication applications and future planetary missions.

The influence of the PIN diode bias current on the microstrip reconfigurable antenna efficiency was studied by J. M. Laheurte et al [154]. A drop in radiation efficiency was observed for inadequate values of the PIN diode bias current. A trade off between the dc – consumption of the diodes and the antenna gain was demonstrated. A simple resistor model was used for the TLM analysis of the antenna.

G. H. Huff et al [155] illustrated a novel radiation pattern and frequency reconfigurable single turn square spiral microstrip antenna. The basic antenna at 3.7GHz operates with a linear polarization. One set of connections provided a re-directed radiation pattern while maintaining a common operating impedance bandwidth. The second set of connections resulted in an operation at a higher band at 6GHz with broadside patterns.

Aly Fathy et al [156] reported an innovative reconfigurable antenna concept with significant practical relevance based on dynamic definition of metal-like conductive plasma channels in high resistivity silicon that were activated by the injection of dc-current. These dynamically defined plasma reconfigurable antennas enable frequency hopping, beam shaping and steering without the complexity of RF-feed structures.

W. H. Chen et al [157] proposed a dual-band planar-reconfigurable antenna for wireless communications. The concept of pattern steering in several given directions was demonstrated using ideal switches.

The design of reconfigurable slot antennas was well illustrated by D. Peroulis et al [158]. A single-fed resonant slot antenna, loaded with a series of PIN diode switches constitutes the fundamental structure. An effective bandwidth of 1.7:1

was obtained through this tuning without using a reconfigurable matching network. The radiation pattern, efficiency and polarization remained essentially unaffected by the frequency tuning.

2.4 Analysis of Microstrip Antennas

Various analytical and full wave methods for the analysis of microstrip antennas were already discussed in sections 1.1.3 and 1.4. Among them, the finite difference time domain (FDTD) method is arguably the most popular numerical method for the solution of problems in electromagnetics.

Reineix and B. Jecko [159] were the first to apply the FDTD method to the analyses of microstrip antennas. Modifications had been made on the classical FDTD method in order to study the microstrip antennas. All frequency dependent parameters of a rectangular microstrip patch antenna were predicted using this method.

Leveque et al [160] modeled frequency dispersive microstrip antennas while Wu et al [161] used the FDTD method to accurately measure the reflection co-efficient of various microstrip antenna configurations.

Uehara and Kagoshima [162] presented an analysis of the mutual coupling between two microstrip antennas while Oonishi et al [163] and Kashiwa et al [164] used one of the conformal FDTD approaches to analyze microstrip antennas on a curved surface.

In 1992, Luebbers et al [165] and Chen et al [166] analyzed hand-held antennas using an FDTD model of a monopole antenna on a conducting or dielectric box. Sheen et al [167] presented FDTD results for various microstrip structures, including a rectangular patch antenna, a low-pass filter and a branch line coupler.

In 1995, Bilge Belentepe [168] derived a simple equivalent circuit model to represent an electromagnetically coupled microstrip patch antenna. This model allows the use of different dielectric constants for the substrate on which the patch and the microstrip line were printed.

D. Lee and S. Lee [169] proposed a design of a coaxially fed circularly polarized rectangular microstrip patch antenna using a genetic algorithm. They derived the objective function from the cavity model and optimized the size and feeding point of the antenna using the genetic algorithm.

H. T. Chen and K. L. Wong [170] analyzed probe-fed spherical-circular microstrip antennas using cavity model theory. Theoretical formulation of the input impedance and far-field radiation were discussed in detail.

D. L. Sengupta [171] used a uniform transmission line model to determine the resonant frequency of a coaxial probe-fed rectangular patch antenna tuned by a number of passive metallic posts suitably placed within the antenna boundary. An approximate expression was given for the resonant frequency as a function of the post location and number, and other characteristic parameters of the antenna.

B. Beker et al in 1994 [172] proposed quasi-static electromagnetic models for analysis and design of microwave capacitors and integrated circuit packages. The theoretical background for modeling of open 3-D boundaries with finite difference method was reviewed thoroughly in this paper.

Radiation and scattering analyses of a slot-coupled patch antenna loaded with a MESFET oscillator was verified by C. C. Huang and T. H. Chu [173]. In the analysis, the antenna was represented by its equivalent circuit model based on the reciprocity theorem and method of moments. A circuit equation of the MESFET oscillator was then analyzed using the Volterra series technique to acquire the oscillating frequency and the output radiation power.

Luebbers and Langdon [174] demonstrated a simple feed model that reduces time steps needed for FDTD antenna and microstrip calculations. The approach was based on using a source with an internal resistance to excite the problem.

Mehmet Kara [175] derived formulas for the computation of the far-field radiation patterns of rectangular microstrip antenna elements with thick substrates. Three closed form formulas were presented for the calculation of the E-plane radiation pattern, derived from two-slot models. The H-plane pattern was calculated from both two-slot and cavity models.

K. M. Krishnaiah and C. J. Railton [176] proposed a novel method of updating the sub-grid boundary fields by replacing the grid discontinuity with an equivalent circuit. The stability and accuracy of this new scheme was demonstrated through calculation of the cut-off wavelength of a dielectric slab loaded waveguide for various slab thickness.

M. J. White [177] developed a novel multi-grid FDTD code for three-dimensional applications which focuses a large number of cells of small dimensions in the region of interest. The simulation required the construction of two grid regions; a coarse-grid region and a fine-grid region surrounding the area of interest.

F. Bilotti et al [178] designed a multi-frequency patch antenna using a combined numerical procedure with method of moments and genetic algorithm. Method of moments was applied to analyze rectangular patches fed by a coaxial probe and suspended over a ground plane. Then the impedance matrix of such a structure was manipulated by a genetic algorithm optimization procedure.

A simple and efficient method to incorporate non-linear bipolar junction transistors (BJT) into finite difference time domain (FDTD) framework was presented by F. Kung and H. T. Chuah [179].

CHAPTER

3

METHODOLOGY FOR EXPERIMENTAL AND THEORETICAL ANALYSIS

Contents

3.1	<i>Fabrication of the Microstrip Antenna</i>	51
3.1.1	<i>Selection of Substrate Material</i>	51
3.1.2	<i>Photolithography</i>	52
3.1.3	<i>Integration of Semiconductor Devices</i>	53
3.2	<i>Excitation Technique</i>	53
3.3	<i>Facilities Used for Antenna Measurements</i>	54
3.3.1	<i>HP 8510C Vector Network Analyzer</i>	54
3.3.2	<i>Anechoic Chamber</i>	55
3.4	<i>Antenna Measurements</i>	56
3.4.1	<i>Measurement of Resonant Frequency, S-Parameters and Bandwidth</i>	56
3.4.2	<i>Measurement of Radiation Pattern</i>	57
3.4.3	<i>Gain</i>	59
3.4.4	<i>Polarization</i>	59
3.5	<i>Antenna Design and Analysis Using FDTD Method</i>	60
3.5.1	<i>Simulation Steps</i>	61
3.5.2	<i>Basic Concepts</i>	62
3.5.3	<i>FDTD Problem Definition</i>	65
3.5.4	<i>FDTD Principal Equations</i>	66
3.5.5	<i>Source Consideration</i>	68
3.5.6	<i>Absorbing Boundary conditions</i>	70
3.5.7	<i>Scattering Parameters</i>	72
3.5.8	<i>Computational Domain and Implementation of 3D-FDTD</i>	72
3.6	<i>Electromagnetic Simulation Using IE3D™</i>	73

This chapter briefly describes the fabrication procedures and various experimental facilities used for the study of the proposed electronically reconfigurable microstrip antenna. The different measurement techniques for determining the antenna parameters are also portrayed in this chapter. The chapter concludes with a concise description of the theoretical and electromagnetic simulation approaches employed to analyze the experimental results.

3.1 Fabrication of the Microstrip Antenna

The various steps employed in the fabrication of the reconfigurable microstrip antenna are listed below.

3.1.1 Selection of Substrate Material

The first procedure in the microstrip antenna fabrication is the selection of suitable substrate with electrical and material properties matching the required application. The dielectric constant and loss tangent and their variation with temperature and frequency are important in fabrication. A large range of polytetrafluoroethylene (PTFE), polystyrene, polyolefin, polyphenylene, alumina, sapphire, quartz, ferromagnetic, rutile and semiconductor substrates permit considerable flexibility in the choice of substrates for a particular application. There is no ideal substrate; rather, the choice depends on the application. Traditional microstrip antennas at microwave frequencies use substrates such as PTFE and quartz for good radiation efficiency. These offer excellent electrical performance, but the resulting substrate costs are often too high. So we selected FR4, a widely used substrate material for microwave applications. It is low cost, easily available and most suitable for effortless fabrication.

3.1.2 Photolithography

Since the dimensions of the patch antennas are critical in microwave frequencies, photolithographic techniques were used to fabricate the desired antenna configurations in the selected substrate. Photolithography or Optical lithography is the process of transferring geometric shapes from a photo-mask to the surface of a substrate. The major procedures involved in this technique are explained below.

In the first step, the double side copper coated FR4 substrates are chemically cleaned with acetone or chloroform to remove particulate matter on the surface as well as any traces of organic, ionic, and metallic impurities. A very thin film of photoresist is applied with the help of a spinner. There are two types of photoresist; positive and negative. For positive resists, the resist is exposed with UV light wherever the underlying material is to be removed. In these resists, exposure to the UV light changes the chemical structure of the resist so that it becomes more soluble in the developer solution. The exposed resist is then washed away by the developer solution, leaving windows of the bare underlying metallic region. The photomask, therefore, contains an exact copy of the pattern which is to remain on the substrate. The negative resist on the other hand, remains on the surface wherever it is exposed, and the developer solution removes only the unexposed portions. Masks used for negative photoresist, therefore, contains the inverse (or photographic "negative") of the pattern to be transferred. After developing, the unwanted metallic portions are cleared using ferric chloride solution. Fig. 3.1 shows the different steps involved in the procedure.

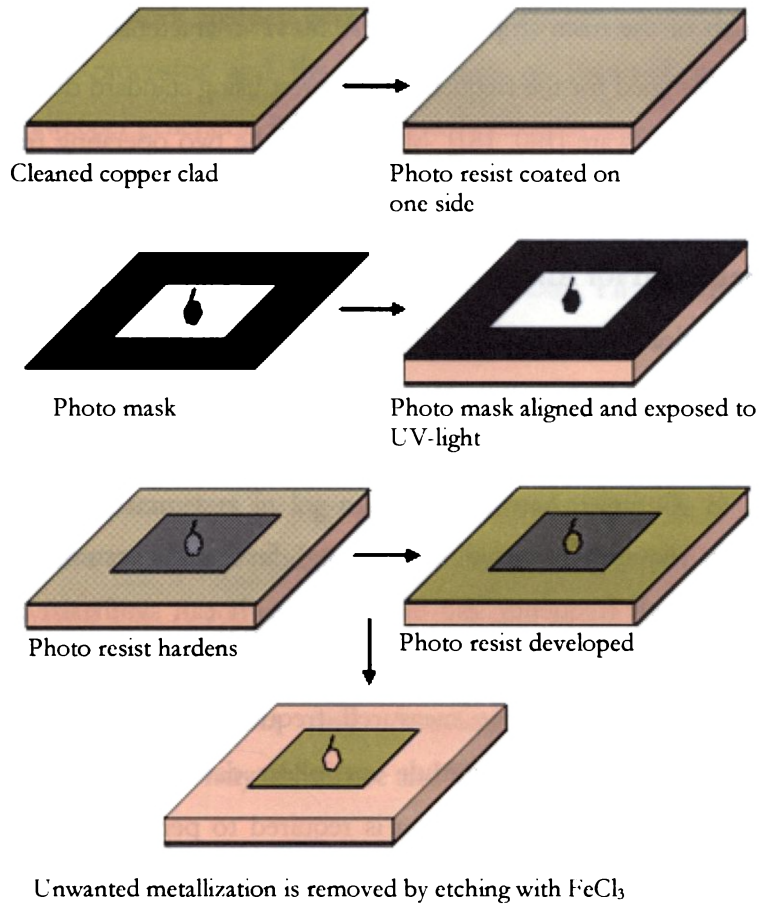


Figure 3.1 Different stages in the photolithographic process of antenna fabrication

3.1.3 Integration of Semiconductor Devices

Two types of frequency reconfigurable antenna designs; one involving PIN diodes and the other with varactor diodes were fabricated for the studies. A high precision soldering station with temperature control is used to integrate the non-linear smd components into the surface of the fabricated patch antenna.

3.2 Excitation Technique

In the present work, proximity coupling (electromagnetic coupling) with a 50Ω microstrip line is used to excite the patch antenna as described in section 1.3.3. The

length and width of the microstrip feed line at 50Ω characteristic impedance, with ground plane is designed for the frequency of interest using standard design equations and HP AppCAD software [180, 181]. Matching of the two operating frequencies is simply obtained by moving the patch along the surface of the microstrip feed line.

3.3 Facilities Used for Antenna Measurements

A concise description of the basic facilities used for the antenna measurements is presented below.

3.3.1 HP 8510C Vector Network Analyzer

It is the main equipment used for taking fast and accurate microwave measurements in both frequency and time domain. It can synthesize frequencies from 45MHz to 50GHz. The time domain response is displayed by taking the Inverse Fourier transform of the measured frequency data. The time domain characterization requires both magnitude and phase data to perform the Inverse Fourier transform. Moreover, phase data is required to perform the vector error correction for measurement accuracy [182].

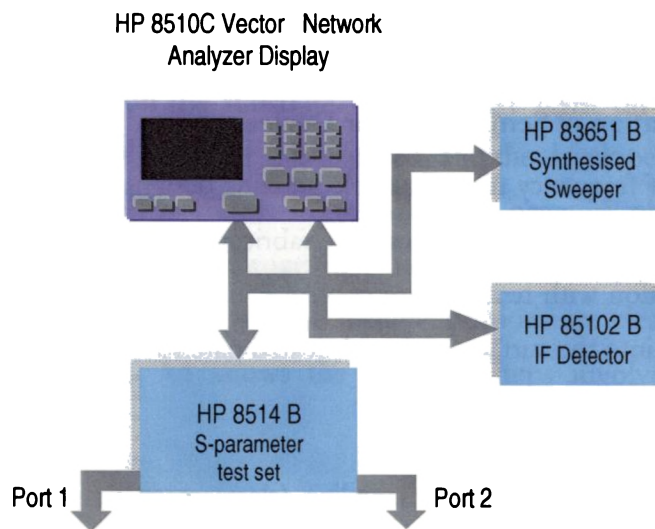


Figure 3.2 Block diagram of HP8510C Vector Network Analyzer

The HP 8510C network analyzer consists of a microwave generator, S-parameter test set, signal processor and the display unit, as depicted in fig. 3.2. The synthesized sweeper generator, HP 83651B, uses an open loop YIG tuned element to generate the RF stimulus. The frequencies can be synthesized in step-mode or ramp-mode, depending on the desired measurement accuracy. The antenna under test is connected to the two-port S-parameter Test Unit, HP 8514B. This module isolates the incident, reflected and transmitted signals at the two ports. The signals are then down converted to an intermediate frequency, and fed to the IF detector. These signals are suitably processed to display the magnitude and phase information of S-parameters in log-magnitude, linear-magnitude or Smith Chart formats. All these constituent modules of the network analyzer are connected using the GPIB system bus. A completely automated data acquisition is made possible using the HP-BASIC based MERLSOFT, developed indigenously at the Center for Research in Electromagnetics and Antennas (CREMA), Department of Electronics, Cochin University of Science and Technology.

3.3.2 Anechoic Chamber

The free space environment required in antenna pattern measurements is realized by making use of the anechoic chamber. The tapered chamber with an average chamber reflectivity of -35dB is used for making antenna measurements. The absorbers used in building the chamber are made from high quality, low density foam, infused with dielectrically and magnetically lossy medium. The wall of the chamber is covered with carbon black impregnated polyurethane foam based pyramidal and flat absorbers of appropriate sizes. Aluminum sheets are used to shield the chamber from electromagnetic interference from other equipments. The polyurethane foam structure gives the geometrical impedance matching, while the dispersed carbon provides the required attenuation, for a wide frequency range of 500MHz to 18GHz.

3.4 Antenna Measurements

Various antenna parameters like resonant frequency, S-parameters, bandwidth, gain, polarization, radiation pattern etc. are measured using different experimental setups as described below.

3.4.1 Measurement of Resonant Frequency, S-Parameters and Bandwidth

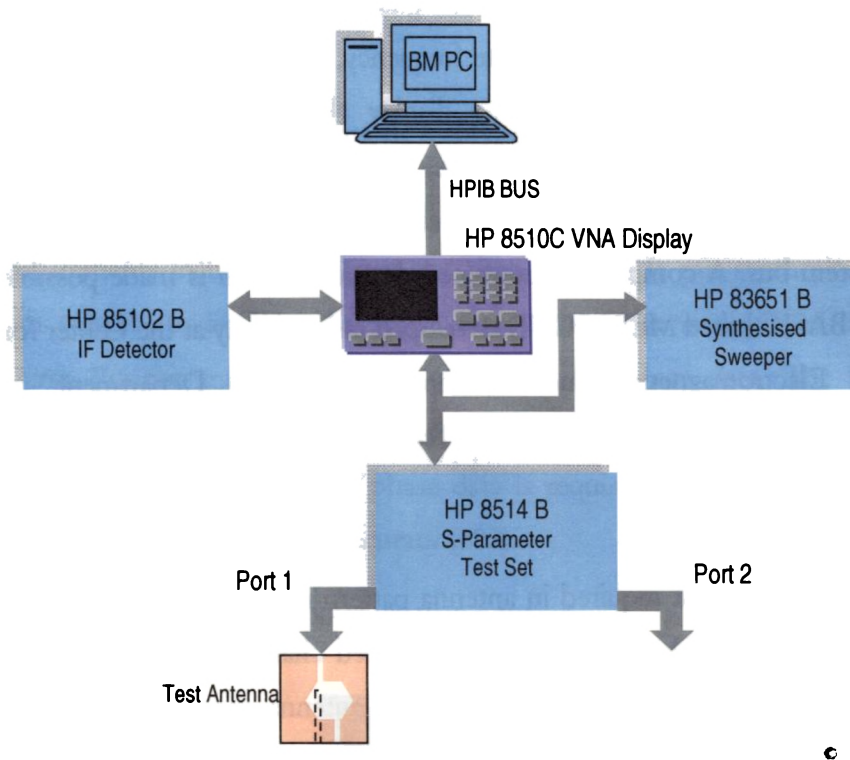


Figure 3.3 Experimental setup for the measurement of return loss and resonant frequency

The port-1 of the vector network analyzer is calibrated by using the suitable standard short, open and thru loads. Proper phase delay is introduced while calibrating, to ensure that the reference plane for all measurements in the desired frequency range is actually at 0° , thus taking care of probable cable length variations. The reconfigurable antenna is then connected to the first port of the network analyzer S-parameter test set as shown in the figure. The magnitude and

phase of the measured S11 logmag data is the acquired and stored in ASCII format in the computer using the MERLSOFT. The resonant frequencies are determined from the return loss curves in logmag form, by identifying those frequencies for which the curve shows maximum dip. The experimental setup for these measurements is given in fig. 3.3.

The return loss is the number in dB that the reflected signal is below the incident signal. As the VSWR=2 corresponds to the reflection coefficient, $\rho = \frac{VSWR + 1}{VSWR - 1} = \frac{1}{3}$, then $20\log(1/3) \approx -10dB$. Thus 2:1 bandwidths are determined by observing the range of frequencies (Δf_r) about the resonant frequency, f_r for which the return loss curves show a -10dB value. The bandwidth is then calculated as $\frac{\Delta f_r}{f_r}$ [182]. The input impedance of the microstrip antenna at the given frequencies are determined directly from the Smith Chart display in the network analyzer, where after calibration the center corresponds to 50Ω .

3.4.2 Measurement of Radiation Pattern

Radiation pattern measurement is carried out using the setup consisting of both the network analyzer and anechoic chamber as depicted in fig. 3.4. An automatic turn table assembly kept in the quiet zone is used to mount the test antenna inside the anechoic chamber. The principal E and H-plane radiation patterns (with both co and cross-polar patterns) of the test antenna are measured by keeping the test antenna inside the chamber in the receiving mode. The block diagram of the experimental setup used for this measurement is shown in figure. A standard wideband ridge horn antenna is used as the transmitter. The horn is then connected to port-1 and the test antenna in port-2 of the s-parameter test set. The analyzer is configured to make the S21 measurements in the step mode with proper averaging.

The radiation patterns of the antenna under test at multiple frequency points can be measured in a single rotation of the positioner using MERLISOFT.

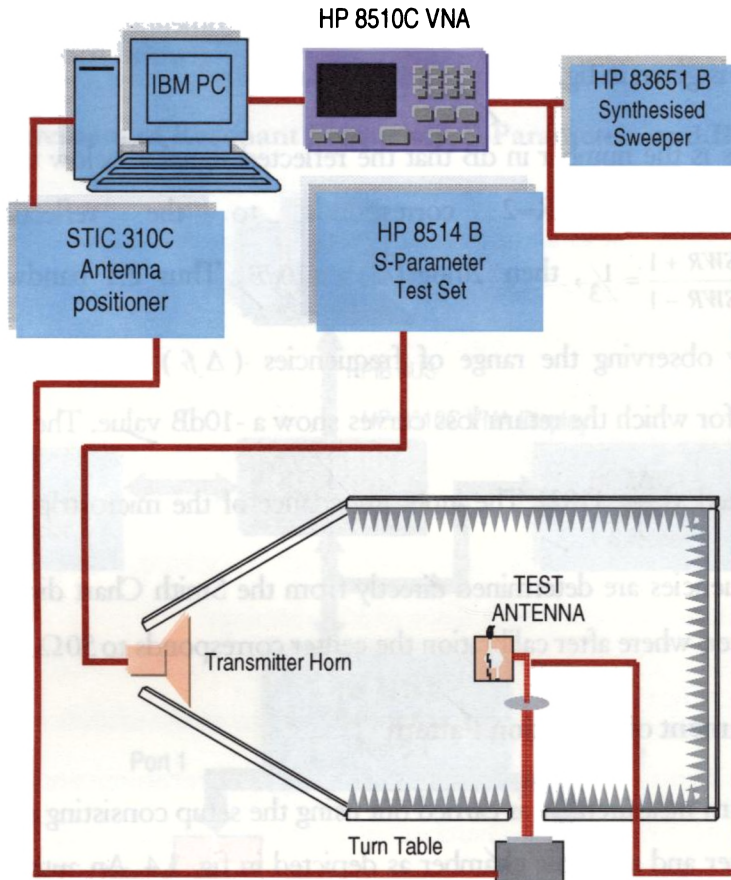


Figure 3.4 Experimental setup for measuring the radiation characteristics of the antenna

With the test and horn antennae aligned in bore sight for maximum reception and polarization matched, the response calibration is performed for the frequency of interest and saved in the cal set. To eliminate the spurious reflections from the neighborhood that are likely to interfere with the measured signal, a gate is turned on in the analyzer. This is done by switching it into the time domain and providing a gate span depending on the largest dimension of the test antenna. The turntable

is then set to rotate the desired angle using the positioner. The positioner will stop at each step angle and take the S21 measurements till it reaches the stop angle. Measurements are repeated in the principal planes for both the co and cross-polar orientations of the test antenna and horn. From the stored data, different radiation characteristics like half-power beam-width, cross-polar level etc. in the respective planes are estimated.

3.4.3 Gain

The gain of the antenna under test is measured using the gain transfer method, utilizing a reference antenna of known gain. The experimental setup for the measurement of gain is same as that used for the radiation pattern measurement. A standard antenna with known gain G_s operating in the same frequency band as the test antenna is used as the reference antenna. S21 measurements are then carried out to determine the reference power with the wideband horn as transmitter and the reference antenna as receiver. A thru response calibration is performed for the frequency band of interest and saved in a new cal set. This is taken as the reference gain response (0dB). The reference antenna is then replaced with the test antenna, retaining the earlier bore sight alignment. S21 is then measured with the new calibration on and the power received in dB, P_r is recorded. The gain G_t of the test antenna is calculated from the stored data based on Friis-transmission formula as, $G_t(dB) = G_s(dB) + P_r(dB)$,

3.4.4 Polarization

Polarization of an antenna in a given direction is the polarization of the wave radiated (or transmitted) by the antenna, which is that property of an electromagnetic wave describing the time varying direction and relative magnitude of the electric field vector at a fixed location in space, and the sense in which it is traced as observed along the direction of propagation. The experimental setup for polarization measurements is

similar as that for the radiation pattern. The designed reconfigurable antenna is kept in the transmitting mode and the wide band standard horn is used as receiver. RF signal and a DC voltage source are applied to the test antenna in the transmitting mode and the power received by the wide band horn, in the vertical plane is stored as a function of frequency. The transmitting antenna is then rotated 90° to record the received power as a function of frequency in the horizontal plane. The analysis of the recorded data in both the planes gives the polarization of the two resonant frequencies of the test antenna.

3.5 Antenna Design and Analysis Using FDTD Method

The finite difference time domain method (FDTD) is used to determine whether the initial dual frequency hexagonal slot loaded microstrip antenna configuration is suitable for the earlier mentioned applications in L-band. The staircase approximation in the 3D-FDTD method is employed to analyze the four slant edges of the embedded hexagonal slot. Various steps involved in the extraction of the antenna parameters along with the assumptions taken in the implementation of the algorithm are also described.

K. S. Yee was the first to propose a modified form of the Transmission Line Matrix method, which is now known as the FDTD method [28]. It determines the frequency response over a wide spectrum whereas many other simulation methods require different models and / or techniques for different frequency spectra. FDTD enables the accurate characterization of complex inhomogeneous structures for which analytical methods are hardly suited. This method is formulated by discretizing Maxwell's curl equations over a finite volume and approximating the derivatives with central difference approximations. Field, voltage or current samples are taken from fixed points in the FDTD grid and Fast Fourier Transform (FFT) is employed to compute the frequency domain information. Further post processing can be done to estimate the S-parameters,

resonant frequencies, input impedance and modes of resonance. A detailed description of the different procedures involved in the current FDTD method of antenna analysis is described in the following sections.

Since the proposed antenna geometry also includes slant edges which are not parallel to the FDTD cell edges, staircase approximation is required to model the patch antenna. This is realized by defining a series of zero valued E_x and E_y components in the FDTD grid which best fit the contour. Thus the original field update equations for the grid will remain the same as the conventional one.

An FDTD algorithm for designing the antenna is generated. The antenna geometry is divided into cells for which necessary boundary conditions are applied. The finite difference time domain method permits the analysis of interactions of electromagnetic waves with material bodies of the desired shapes.

A Matlab™ [183], based 3D-FDTD computer program is developed for the design and analysis of the proposed microstrip antenna configurations. From the geometrical dimensions and substrate parameters, this source code will compute the resonant frequencies, electric field variations along the periphery of the patch and input impedance.

3.5.1 Simulation Steps

Initially a 3-dimensional model is defined to represent the physical structure including conductors, dielectrics and boundaries. Next, an applied pulse, either a sine wave or a Gaussian pulse, acts as the input stimulus for the source. Then at increments of time, E and H fields are calculated. After each increment the input electric field amplitude is calculated and the E and H fields are again recalculated. This step continues until the E and H fields in the entire domain decays to zero.

After completing the stimulus a Fast Fourier Transform (FFT) extracts the frequency information from the transient response. The location of the transient data depends on the required system response. Thus, for the reflection co-efficient data of the dual frequency hexagonal slot loaded square microstrip patch antenna, the input and reflected waves at the source are monitored.

3.5.2 Basic Concepts

Applications of FDTD techniques to various electromagnetic problems are available in literature [160-164]. In the case of arbitrary shaped patches application of Yee's algorithm has been found to be extremely accurate in finding the current and field distribution across the patch. One practical difficulty with this method is that for devices containing small structures or strongly varying fields, it needs very fine mesh. When using finer meshes it needs longer CPU time and memory. An improved method for reducing the number of time steps is implemented by Lubbers *et al.* [174]. This is based on using a source with an external resistance to excite the circuit.

FDTD method has been used extensively for the solution of two and three dimensional scattering problems. The method has been applied to calculate the frequency dependent characteristics of microstrip discontinuities. Analysis of microstrip discontinuities has great importance, since complicated circuits can be realized by interconnecting the microstrip lines with these discontinuities and using transmission lines and network theory. If the discontinuities are too close to each other the use of network concept will not be accurate due to the interaction of evanescent waves. To analyze the circuits accurately the entire structure has to be simulated in one computation. In time domain analysis a broadband pulse may be used as the excitation and frequency domain parameters may be calculated over the entire frequency range of interest by Fourier Transform of the transient results [27].

The formulation of the FDTD method begins by considering the differential formulae of Maxwell's curl equations which govern the propagation of electromagnetic waves. The media are assumed to be piecewise uniform, isotropic and homogeneous.

$$-\frac{\partial B}{\partial t} = \nabla \times E \quad (3.1)$$

$$\frac{\partial D}{\partial t} = \nabla \times H - J \quad (3.2)$$

$$B = \mu H \quad (3.3)$$

$$D = \varepsilon E \quad (3.4)$$

manually

In Cartesian co-ordinate system the above equations may be written as

$$-\frac{\partial B_x}{\partial t} = \frac{\partial E_z}{\partial y} - \frac{\partial E_y}{\partial z} \quad (3.5)$$

$$-\frac{\partial B_y}{\partial t} = \frac{\partial E_x}{\partial z} - \frac{\partial E_z}{\partial x} \quad (3.6)$$

$$-\frac{\partial B_z}{\partial t} = \frac{\partial E_y}{\partial x} - \frac{\partial E_x}{\partial y} \quad (3.7)$$

$$\frac{\partial D_x}{\partial t} = \frac{\partial H_z}{\partial y} - \frac{\partial H_y}{\partial z} - J_x \quad (3.8)$$

$$\frac{\partial D_y}{\partial t} = \frac{\partial H_x}{\partial z} - \frac{\partial H_z}{\partial x} - J_y \quad (3.9)$$

$$\frac{\partial D_z}{\partial t} = \frac{\partial H_y}{\partial x} - \frac{\partial H_x}{\partial y} - J_z \quad (3.10)$$

The system of six coupled partial difference equations forms the basis of the FDTD numerical algorithm for electromagnetic wave interaction with general three dimensional objects.

The basic Yee algorithm helps to solve both electric and magnetic fields in time and space using the Maxwell's curl equations. The grid points for the E -field and H -field are chosen as shown in fig. 3.5. The boundary condition for a perfectly conducting surface is that the tangential components of the electric field vanish at the boundary. This implies that the normal component of the magnetic field vanishes on the surfaces. The conducting surfaces will therefore be approximated by a collection of surfaces of cubes, the sides of which are parallel to the coordinate axes. Plane surfaces perpendicular to the x -axis will be chosen so as to contain points where E_x and E_y are defined [27].

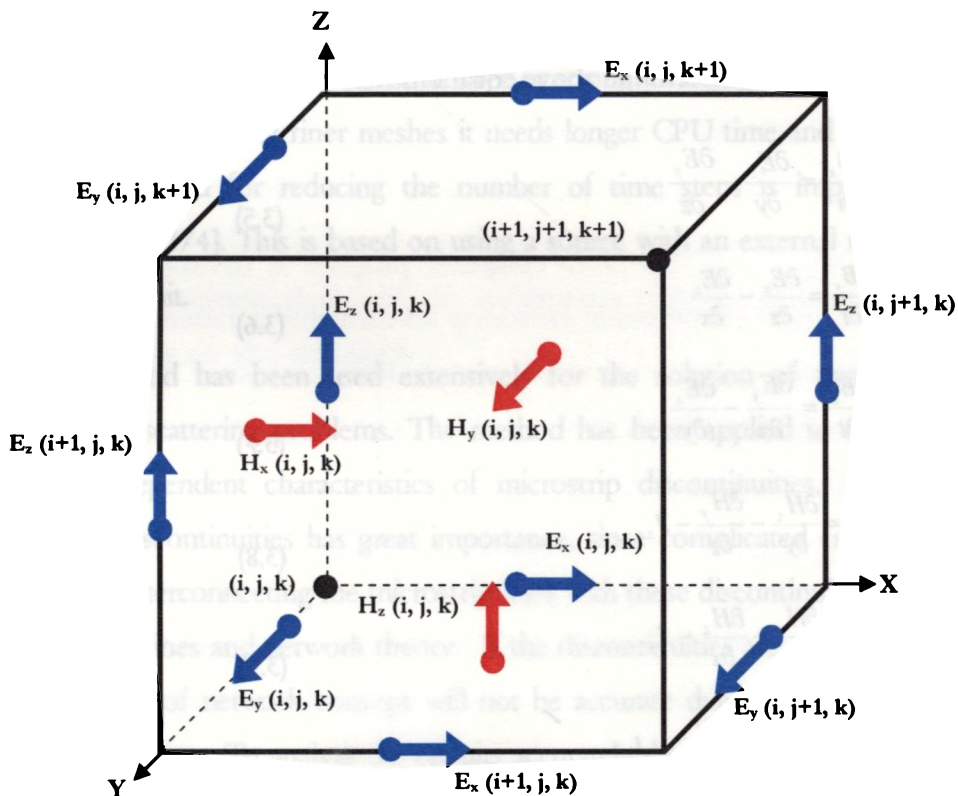


Figure 3.5 Field component placements in the FDTD unit cell

Each Yee cell contains six field components E_x, E_y, E_z and H_x, H_y, H_z . The Yee algorithm centers its \bar{E} and \bar{H} components in a three dimensional space so that every \bar{E} component is surrounded by four circulating \bar{H} components and every \bar{H} component by four circulating \bar{E} components.

The co-ordinate indexing scheme denotes cells in the x, y and z directions as i, j and k respectively. The cell dimensions are, Δ_x, Δ_y and Δ_z , which can vary as a function of x, y and z to more closely conform to objects with curved edges or surfaces. For accurate simulation, cells with edges of length $\lambda_m/10$ or less is required with $\lambda_m/20$ as the recommended size. Here λ_m is the wavelength of an isotropic material contained within the cell of interest. This discretization allows a sufficient number of field samples as a function of spatial distance, to yield an accurate representation of the actual field.

3.5.3 FDTD Problem Definition

The FDTD method is formulated by discretizing Maxwell's equations over a finite volume and approximating the derivatives with centered difference approximations. Conducting surfaces are treated by setting the tangential electric field components to be zero. The walls are treated separately to prevent reflections from the mesh terminations. In the present analysis, space grids are selected such that the electromagnetic field does not vary significantly over one increment. The notation used for analysis are generalized into three spatial dimensions, space points in a uniform rectangular lattice being represented as,

$$(i, j, k) = (i\Delta_x, j\Delta_y, k\Delta_z)$$

Here Δ_x, Δ_y , and Δ_z are the lattice space increments in the x, y, and z directions.

The aim of the present analysis is to model the L-strip fed antennas accurately and efficiently.

3.5.4 FDTD Principal Equations

The antenna geometry is divided into fixed rectangular field locations and each conducting surfaces are treated by setting the tangential electric field component to zero. The six field locations are interleaved in space as shown in Fig. 3.5, which is a drawing of the FDTD unit cell. The entire computational domain is formed by stacking these rectangular cells into a rectangular volume. The x , y , and z dimensions of the unit cell are Δx , Δy , and Δz respectively. This field arrangement has an advantage that the centered differences are realized in the calculation of each field component and the boundary condition of tangential field component is automatically satisfied at the dielectric material interfaces.

Since there are six field components within the unit cell, six field components touching the shaded upper eighth of the unit cell in the figure are considered to be a unit node with subscript indices (i, j, k) in the x , y , and z directions. The notation implicitly assumes the $\pm 1/2$ space indices and thus simplified the notation. The time step is indicated with subscripts, n . The explicit finite difference approximations to (3.5) to (3.10) are as given by Sheen *et al.* [167]

$$H_x^{n+1/2} = H_x^{n-1/2} + \frac{\Delta t}{\mu \Delta z} (E_y^n_{i,j,k} - E_y^n_{i,j,k-1}) - \frac{\Delta t}{\mu \Delta y} (E_z^n_{i,j,k} - E_z^n_{i,j+1,k}) \quad (3.11)$$

$$H_y^{n+1/2} = H_y^{n-1/2} + \frac{\Delta t}{\mu \Delta x} (E_z^n_{i,j,k} - E_z^n_{i-1,j,k}) - \frac{\Delta t}{\mu \Delta z} (E_x^n_{i,j,k} - E_x^n_{i,j,k-1}) \quad (3.12)$$

$$H_z^{n+1/2} = H_z^{n-1/2} + \frac{\Delta t}{\mu \Delta y} (E_x^n{}_{i,j,k} - E_x^n{}_{i,j-1,k}) - \frac{\Delta t}{\mu \Delta x} (E_y^n{}_{i,j,k} - E_y^n{}_{i-1,j,k}) \quad (3.13)$$

$$E_x^{n+1}{}_{i,j,k} = E_x^n{}_{i,j,k} + \frac{\Delta t}{\varepsilon \Delta y} (H_z^{n+1/2}{}_{i,j,k+1} - H_z^{n+1/2}{}_{i,j,k}) - \frac{\Delta t}{\varepsilon \Delta z} (H_y^{n+1/2}{}_{i,j,k+1} - H_y^{n+1/2}{}_{i,j,k}) \quad (3.14)$$

$$E_y^{n+1}{}_{i,j,k} = E_y^n{}_{i,j,k} + \frac{\Delta t}{\varepsilon \Delta z} (H_x^{n+1/2}{}_{i,j,k+1} - H_x^{n+1/2}{}_{i,j,k}) - \frac{\Delta t}{\varepsilon \Delta x} (H_z^{n+1/2}{}_{i+1,j,k} - H_z^{n+1/2}{}_{i,j,k}) \quad (3.15)$$

$$E_z^{n+1}{}_{i,j,k} = E_z^n{}_{i,j,k} + \frac{\Delta t}{\varepsilon \Delta x} (H_y^{n+1/2}{}_{i+1,j,k} - H_y^{n+1/2}{}_{i,j,k}) - \frac{\Delta t}{\varepsilon \Delta y} (H_x^{n+1/2}{}_{i,j+1,k} - H_x^{n+1/2}{}_{i,j,k}) \quad (3.16)$$

The half time steps indicate that \bar{E} and \bar{H} are alternatively calculated in order to achieve centered differences for the time derivatives. This algorithm is referred to as 'leap-frog' algorithm. Here the permittivity and permeability are set to appropriate values depending on the location of each field component. For the electric field component in the air-dielectric interface the average of two permittivities $(\varepsilon_0 + \varepsilon_1) / 2$, where ε_0 and ε_1 are the permittivity of the free space and medium is used. The error is second order in both space and time steps and are proportional to Δt , and the global error is $O(\Delta t^2)$. The maximum time step is limited by the Courant Stability criterion of the finite difference equations [27]

$$\Delta t \leq \frac{1}{v_{\max}} \left(\frac{1}{\Delta x^2} + \frac{1}{\Delta y^2} + \frac{1}{\Delta z^2} \right)^{-1/2} \quad \text{or the same angle,} \quad (3.17)$$

where v_{\max} is the maximum velocity of light in the computational volume.

3.5.5 Source Consideration

The time dependence of the source is chosen depending on the problem to be solved. For applications where frequency dependent data is to be generated, a pulse is used such that its frequency content covers the desired frequency range. The usable highest frequency is limited by the size of the Yee's cell. A Gaussian pulse has a smooth waveform in time, and its Fourier Transform is also a Gaussian pulse centered at zero frequency. This unique property makes it a perfect choice for investigating the frequency dependent characteristics of the microstrip discontinuities via Fourier Transform of the pulse response.

To simulate, a voltage source excitation is necessary to impose the vertical electric field in a rectangular region above the ground plane. The launched wave has a nearly unit amplitude and is Gaussian which is given by

$$f_s(t) = e^{-(t-t_0)^2 / T^2} \quad (3.18)$$

where, T is the half width and t_0 is the time delay.

The choice of t_0 and T is such that the truncation of the source pulse does not introduce unwanted high frequencies in the spectrum and does not waste computation time on determining values of the fields that are essentially zero. Usually the width of the pulse is chosen to be at least 20 points per wavelength at the highest frequency of interest. However, if we proceed straight way, the computational time is large to achieve the stability condition. Lubbers *et al.* [174] introduced a new concept to reduce the computational time, by introducing a source resistance R_s in series with the voltage source.

The equivalent circuit for a voltage source which includes an internal source resistance R_s is illustrated in fig. 3.6.

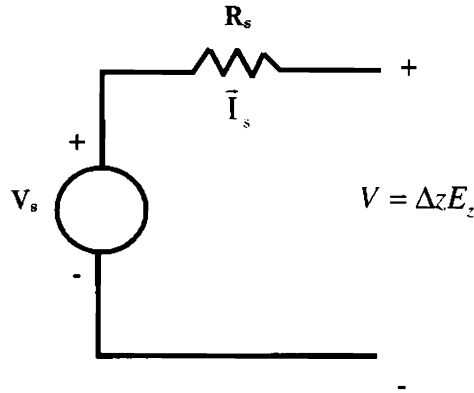


Figure 3.6 FDTD Source with source resistance ' R_s '

If the source resistance R_s is set to zero then the FDTD electric field at the source is given by

$$E_s^n(i_s, j_s, k_s) = V_s (n \Delta t) / \Delta z \quad (3.19)$$

Where V_s is the Gaussian pulse.

When the source resistance is included, the calculation of source field at each time step is complicated. To determine the terminal voltage V of fig. 3.6, the current through the source must be determined. The current through the source is given by

$$I_s^{n-1/2} = [H_x^{n-1/2}(i_s, j_s - 1, k_s) - H_x^{n-1/2}(i_s, j_s, k_s)] \Delta x + [H_y^{n-1/2}(i_s, j_s, k_s) - H_y^{n-1/2}(i_s - 1, j_s, k_s)] \Delta y \quad (3.20)$$

And the electric source field is given by

$$E_s^n(i_s, j_s, k_s) = V_s (n \Delta t) / \Delta z + I_s^{n-1/2} R_s / \Delta z \quad (3.21)$$

The value of the source resistance cannot be too large since instabilities may occur due to negligence of the displacement current through the FDTD cell containing the source.

Once the pulse amplitude drops, the source voltage becomes essentially zero, any reflections from the antenna which returns to the source, is totally reflected back. The inclusion of an internal resistance to the source provides an additional loss mechanism to dissipate energy introduced into the calculation space that will reduce the computational time appreciably.

3.5.6 Absorbing Boundary conditions

Absorbing boundary conditions are applied at the boundary mesh walls of finite difference, to simulate an unbounded space. The most common, and generally most practical, method used to derive absorbing boundary conditions are based on asymptotic expansion of one-way wave equation. Many researchers have developed theories to these approximate boundary conditions [27].

The difference equations cannot be used to evaluate the field components tangential to the outer boundaries since they would require the values of field components outside the mesh. One of the six mesh boundaries is a ground plane and its tangential electric field values are forced to zero. The tangential electric field components on other five mesh walls are represented in such a way that the outgoing waves are not reflected using the absorbing boundary conditions. For this structure the pulses on the microstrip line will be considered as incident normally to the mesh walls. This results in a simple approximate continuous absorbing boundary condition that the tangential fields on the outer boundaries will obey the one-dimensional wave equation in the direction normal to the mesh wall. For the y -normal wall the one dimensional wave equation is

$$\left(\frac{\partial}{\partial y} - \frac{1}{v} \frac{\partial}{\partial t} \right) E_{\text{tan}} = 0 \quad (3.22)$$

This equation is Mur's first order approximate boundary condition and may be easily discretized using only field components on or just inside the mesh walls, yielding an implicit finite difference equation [27].

$$E_0^{n+1} = E_1^n + \frac{v\Delta t - \Delta y}{v\Delta t + \Delta y} (E_1^{n+1} - E_0^n) \quad (5.23)$$

Here E_0 is the tangential electric field components on the mesh wall and E_1 represents the tangential electric field components one node inside the mesh wall. The normal incidence assumption is not valid for the fringing fields which are propagating tangential to the wall and therefore the side walls should be far away, so that the fringing fields are negligible at the walls. Also the radiation will not be exactly normal to the mesh walls. ✓

Finite difference equations are used with the above boundary and source conditions to simulate the propagation of broadband Gaussian pulse on the microstrip structure. The most important aspects of the time domain algorithm are as follows:

- Initially at $t = n = 0$ all the fields are forced to zero
- The following steps are repeated until the response is ≈ 0
 - Gaussian excitation is imposed at port
 - $H^{n+1/2}$ is calculated from the finite difference equations
 - $E^{n+1/2}$ is calculated from the finite difference equations
 - Tangential E is set to zero on conductors
 - Save the desired field quantities
 - Increment the time $n \rightarrow n+1$
 - Update the equation ✓
- Compute scattering matrix co-efficients from time domain results

To eliminate the reflections from the circuit, by the source wall, the circuit is placed a sufficient distance away from the source. After the Gaussian pulse has been launched, the absorbing boundary condition is switched on at the boundary walls.

3.5.7 Scattering Parameters

The frequency dependent scattering coefficients can be calculated from $[V]^r = [S] \cdot [V]^i$, where $[V]^r$ and $[V]^i$ are the reflected and incident voltage vectors and $[S]$ is the scattering matrix. To obtain the scattering parameters $S_{11}(\omega)$, the incident and reflected voltage must be known. To obtain the incident waveform the calculation is performed using only the port microstrip line which will be of infinite extent and the incident wave form is noted. This incident waveform is subtracted from total waveform to get the reflected waveform from the port. The scattering parameters, S_{jk} is obtained by calculating the Fourier Transform of these transient waveforms.

$$S_{jk}(\omega) = \frac{FT[V_j(t)]}{FT[V_k(t)]} \quad (3.24)$$

The reference planes are selected far away from the circuit discontinuities to eliminate evanescent waves. These distances are included in the circuit so that no phase correction is performed for scattering coefficients.

3.5.8 Computational Domain and Implementation of 3D-FDTD

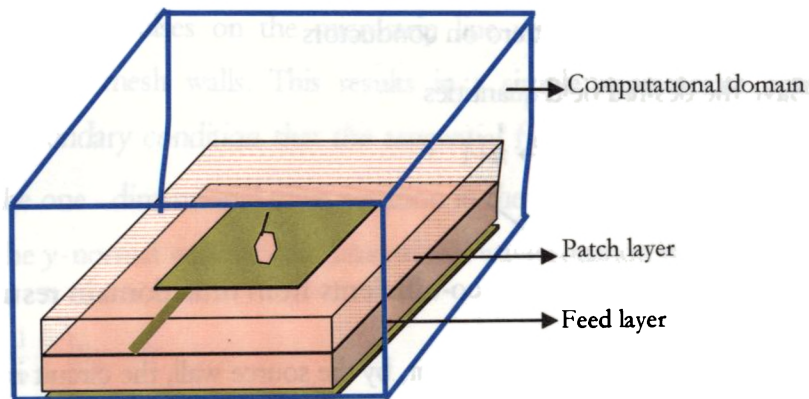


Figure 3.7 The computational domain for the dual frequency microstrip antenna

Fig. 3.7 illustrates the 3D-FDTD computational domain. The whole of the computational domain is then filled with the earlier described Yee cells. The ground plane, the feed surface and the patch metallization are then treated as Perfect Electric Conductors (PEC). The four slant edges of the hexagonal slot are modeled as staircases. The FDTD simulation of the microstrip antenna then involves direct application of finite difference equations, along with the source excitation and absorbing boundary conditions.

To excite the patch, the time delayed Gaussian pulse is assigned to the feed. The cell size, Δz along the height of the substrate is chosen in such a way that it exactly matches the thickness. Additional cells are included in the z direction to model the free space above the patch surface. The grid size along the x and y directions are chosen to make possible the antenna geometry with minimum discretization error. The spatial parameters used are $\Delta x = 0.4\text{mm}$, $\Delta y = 0.4\text{mm}$ and $\Delta z = 0.4\text{mm}$. The total spatial dimensions of the computational domain is taken as $N_x = N_y = 285$ and $N_z = 20$. The Gaussian half-width and the time delay are selected following the criteria given in section 3.5.5. The time delay, t_0 is chosen as three times the Gaussian half-width, T so as to ensure a smooth transition from zero to the maximum value of 1. The simulation is then performed for a maximum time steps of 4600, in an Intel 1.6GHz Centrino™, HP-Notebook with 768MB RAM.

3.6 Electromagnetic Simulation Using IE3D™

IE3D [184] is the most versatile, easy to use, efficient and accurate electromagnetic simulation tool available nowadays. The primary formulation of the IE3D is an integral equation obtained through the use of Green's functions. The reconfigurable microstrip antenna designs are modeled in IE3D for determining the antenna parameters like, resonant frequency, radiation pattern, gain, radiation efficiency etc. The results are found to be in reasonably good agreement with the experimental and FDTD results.

The modeling of the PIN and Varactor diodes and the integration into the patch antenna are described in chapter-4 and chapter-5.

In its product family, the following programs were used:

- Mgrid – A design environment where it is possible to define infinite lateral substrate planes, and build thin conducting surfaces in arbitrary 3D directions.
- Modua – An S-parameter viewing program.
- Curview – A 3D viewer of the conducting surfaces with the possibility of e.g. view current distribution animations, mean values or gradients of currents at the conductors.
- Patternview – A radiation pattern viewer.

When a design has been made in Mgrid, connection ports are defined. At the ports, incident signals are applied with the frequencies chosen for simulation. The simulation program uses the moment method, i.e. an integral equation obtained through the use of Green's functions. Thus, the electric and magnetic currents can be calculated. When the current distribution at the metal surfaces is defined, the S-parameters can be calculated. The radiation pattern can then be derived from the current distribution. When the design has been made in Zealand's Mgrid design program, the program divides the design in cells at which boundary values are calculated. The maximum frequency for which the simulation is to be made determines the size of the cells. A recommended value is 20 cells per wavelength (for the media with the shortest wavelength).

All unknowns (boundary values) are to be solved by inverting a matrix of this gigantic equation system. This means that the system memory requirement is proportional to the square of the number of unknowns, and the time consumption to the cube of the number of unknowns.

CHAPTER

4

EXPERIMENTAL AND THEORETICAL INVESTIGATIONS ON RECONFIGURABLE DUAL FREQUENCY MICROSTRIP ANTENNAS USING PIN DIODES

Contents

4.1	<i>Design of the Passive Dual Frequency Dual Polarized Square Microstrip Patch Antenna</i>	79
4.1.1	<i>Design Concepts</i>	79
4.1.2	<i>Staircase Approximation in FDTD</i>	81
4.1.3	<i>Antenna Geometry</i>	82
4.1.4	<i>Excitation Technique</i>	84
4.1.5	<i>Mechanical Frequency Tuning</i>	85
4.1.6	<i>Antenna Dimensions and Its Effect on Dual Resonant Modes</i>	87
4.1.7	<i>Dual Polarized Operation of the Proposed Antenna Design</i>	95
4.1.8	<i>Radiation Pattern and Gain</i>	96
4.1.9	<i>Dual Slot Arm Loaded Patch Antenna</i>	97
4.1.10	<i>Dual Frequency Patch with Orthogonal Slot Arms</i>	100
4.1.11	<i>Determination of Square Patch and Slot Arm Lengths for Particular Dual Operating Frequencies</i>	103
4.2	<i>Reconfigurable Dual Frequency Microstrip Antenna Design using PIN Diodes</i>	108
4.2.1	<i>PIN Diode Switch</i>	108
4.2.2	<i>Single Slot Arm Loaded Reconfigurable Dual Frequency Microstrip Antenna</i>	109
4.2.3	<i>Dual Slot Arm Reconfigurable Microstrip Antenna Design for Tunable Frequency Ratio</i>	122

This chapter describes the detailed design and experimental investigations carried out on the proposed electronically reconfigurable dual frequency microstrip antennas. The aim of the study is to develop compact electronically reconfigurable dual frequency microstrip antennas with dual orthogonal polarizations and excited with a single feed.

The important design considerations throughout this study are:

- compactness of the patch
- tuning of operating frequencies in a comparatively wide range without the use of any matching networks
- simplified switching/tuning mechanism directly integrated into the radiating patch and thus avoiding the use of any transmission lines between non-linear components and patch

The microstrip antenna proposed in this work utilizes two tuning schemes involving PIN diodes and Varactors in order to achieve frequency reconfiguration. The strict requirements of constant gain, radiation pattern and polarization in the entire tuning range are achieved by suitably designing the initial patch antenna and the tuning mechanism. The single feeding mechanism for simultaneous excitation of the two resonant frequencies, adds to the compactness of the system.

The last few years have seen an exponential growth in the development of reconfigurable antennas. Reconfigurable antennas are defined as those antennas whose aperture can be dynamically modified to enable different functions at different times. Reconfigurable antennas have recently received significant attention for their applications in communications, electronic surveillance and countermeasures, by adapting their properties to achieve selectivity in

frequency, bandwidth, polarization and gain. Compared to broad band antennas, reconfigurable antennas offer the advantages of compact size, similar radiation pattern for all designed frequency bands, efficient use of electromagnetic spectrum and frequency selectivity useful for reducing the adverse effects of co-site interference and jamming. Dual frequency reconfigurable microstrip antennas can offer additional advantages of frequency reuse for doubling the system capability and polarization diversity for good performance of reception and transmission or to integrate the receiving and transmitting functions into one antenna for reducing the antenna size.

Electronic tuning of dual frequency microstrip antennas to achieve desired frequency ratio values or simultaneous tuning of both the frequencies is thus studied in detail. Moreover a novel independent frequency selection design is also incorporated in the proposed antenna configuration. ✓

The outline of the elaborate studies conducted in this chapter is as follows:

- Design of the original passive dual frequency dual polarized square microstrip antenna with a single feed excitation using the FDTD method
- Mechanical tuning of the operating frequencies by varying the inserted slot dimensions in the square patch
- Electronic control of the operating frequencies and frequency ratios with embedded PIN diode switches
- Varactor controlled frequency tuning mechanism for more flexible dual frequency operations
- Independent control of the dual resonant frequencies of the reconfigurable microstrip antenna by using modified slot shapes.

4.1 Design of the Passive Dual Frequency Dual Polarized Square Microstrip Patch Antenna

As the aim is to devise reconfigurable dual-frequency microstrip antennas having high tuning ranges, with single feed, the original passive antenna design is vital. The design must ensure good matching below -10dB for both resonant modes, even when the frequencies are shifted a great extent by applying the electronic tuning mechanisms. Moreover, the patch design must include appropriate slot geometries in order to include the PIN diodes or Varactors for frequency reconfiguration. Keeping this and the above described applications in mind, the original patch antenna is developed as follows.

As the main applications fall under the L-band of the microwave spectrum we designed the original patch in the higher L-band of 1.885GHz. The antenna size at these frequencies becomes critical and therefore requires special consideration. A compact planar geometry is best suited since three-dimensional, large and bulky structures are in general undesirable, especially for personal communication and military applications. The 3-dimensional FDTD algorithm described in chapter-3 is used to design and predict the resonant characteristics of the antenna. Thorough experimental studies are then carried out to verify the theoretical predictions. A generalized FDTD code written in MATLABTM is developed for the initial design and optimization of the microstrip antenna.

4.1.1 Design Concepts

In principle, dual-frequency planar antennas should operate with similar features, both in terms of radiation characteristics and impedance matching, at two separate frequencies. A simple square or rectangular patch can be regarded as a cavity with magnetic walls on the radiating edges. The first three resonant modes for this patch with same polarization are TM_{10} , TM_{20} and TM_{30} where TM denotes the magnetic field transverse with respect to the interface normal. TM_{10} is the mode typically

used in practical applications while, TM_{20} and TM_{30} are associated with a frequency approximately twice and triple of that of the TM_{10} mode. Unfortunately, owing to the behavior of the radiating currents, the TM_{20} and TM_{30} modes are of with little use due to their distortion in broadside radiation patterns; TM_{20} pattern has a broadside null, and the TM_{30} pattern has grating lobes. Also, simultaneous matching of these same polarizations resonant modes with a single feed is generally difficult in microstrip antennas. Thus the simplest way to operate at dual frequencies is to use the first resonance of the two orthogonal dimensions of the square patch, i.e., the TM_{10} and TM_{01} modes. Thus, these two orthogonal resonant modes can be generated, in the simplest case, by a square patch with a slight perturbation in one of its resonant dimension. Since dual polarization is an increasingly important requirement of modern communication systems the excitation of these orthogonal resonant modes with a single feed will be an interesting feature to be studied in detail.

The important characteristic of these square patch antenna is its capability of simultaneous matching of the input impedance at the two resonant frequencies with a single feed. This can be easily achieved by a proximity coupling from a microstrip feed line, which is slightly displaced from the two principal axes of the square patch.

Furthermore, the compactness of the so designed square patch antenna can be enhanced by increasing the current density paths of the two orthogonal resonant modes by adding symmetric slot structures in the centre of the patch. Several slot geometries were considered and the regular hexagonal shape slot is selected in an attempt to achieve better size reduction. Both the newly developed FDTD code and a commercially available method of moment based software (IE3D™) are used to optimize the dimension and orientation of the hexagonal slot in the square patch.

4.1.2 Staircase Approximation in FDTD

Microstrip patches with patch edges parallel to the grid lines can be accurately modeled using the classical Yee FDTD approach, if the grid is accurately fine enough. Thus, inclined and curved boundaries of the geometry must be approximated using various methods.

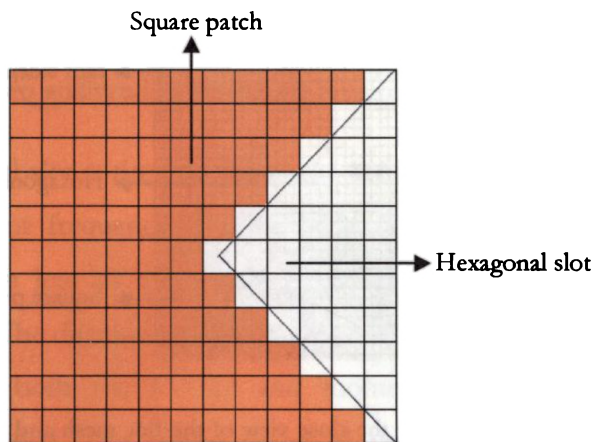


Figure 4.1 Staircase meshing employed in the hexagonal slot boundary

As there are four slant edges in a hexagonal slot embedded in the square patch, staircase approximation is employed to define the boundary between the square patch and the hexagonal slot. That is, in the FDTD grid based on Yee algorithm, the microstrip surface edges which are not parallel to the FDTD cell edges are approximated as either completely covered by metal or as totally uncovered. Thus, this scheme leads to the metallic patch edge being defined as a staircase boundary with steps of dimensions equal to that of the Yee cell dimensions (fig. 4.1).

The update equations for the grid will remain the same as the conventional one. But the complicated patch geometry involves complex mesh generation and therefore an automated fine mesh generation is included in the FDTD algorithm to

generate the required meshes in accordance with the co-ordinates. In order to increase the accuracy of the results, very fine gridding is used through out the study. Fig. 4.2 depicts the generated surface plot of the patch geometry embedded with the hexagonal slot and protruding arm.

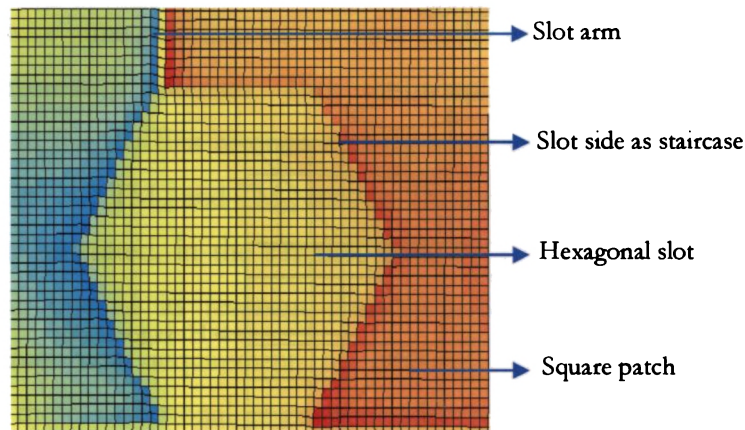


Figure 4.2 Actual plot showing the close view of the fine mesh and staircase along the slant sides of the hexagonal slot

The designed square patch with embedded hexagonal slot now resonates at a much lower frequency than that of the square patch. Dual frequency operation is achieved by perturbing the fundamental resonant mode of the patch with a narrow rectangular slot, thus splitting it into two distinct orthogonal resonant modes (TM_{10} and TM_{01}).

4.1.3 Antenna Geometry

The above described design concepts are used to develop a dual-frequency square microstrip patch antenna with a single feed excitation. A suitable microwave substrate material of dielectric constant $\epsilon_r = 3.98$ and height $h = 1.6\text{mm}$ is selected in accordance with the guidelines already discussed in section 3.1.1. The length of the square patch, L is arbitrarily determined by the standard formula,

$$L = \frac{c}{2 fr \sqrt{\epsilon_{eff}}} \quad (4.1)$$

where fr is the resonant frequency, c is the velocity of electromagnetic waves and ϵ_{eff} is the effective dielectric constant. The 3D-FDTD code described in section 3.5 is then used to accurately find the square patch dimension and its dependence on substrate thickness and dielectric constant. The optimized length of the square patch is found to be 4cm at a resonance frequency of 1.885 GHz. The effect of the hexagonal slot is then analyzed by modeling it using the staircase approximation.

A regular hexagonal slot is then carved at the centre of the patch in an attempt to reduce the resonant frequency to 1.74 GHz. The theoretically computed and experimental return loss of the square patch with embedded hexagonal slot is plotted in fig. 4.3. The dimensions (l_1 and l_2) and orientation of the hexagonal slot is determined using both the FDTD and moment method code (IE3D), and experimentally verified. The configuration of the new compact dual frequency microstrip antenna is shown in fig 4.4

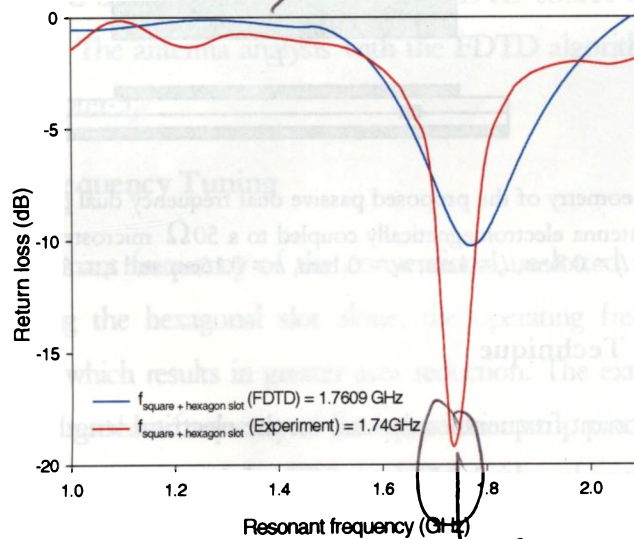


Figure 4.3 Computed and experimental return loss behavior of the square patch with hexagonal slot on its centre

v

Different hexagonal dimensions are then tried within the square patch and the one with side dimensions of 0.8cm resonating at 1.74GHz is selected because of its better matching and reduced size.

A slot arm of length l_a and width w_a is introduced in the edge of the hexagonal slot as shown in the fig. 4.4 in order to excite dual resonant frequencies. The slot arm is placed in the top corner of the central hexagonal slot to get maximum impedance matching for both frequencies at a single feed position and to tune the TM_{10} mode without much affecting the orthogonal TM_{01} mode.

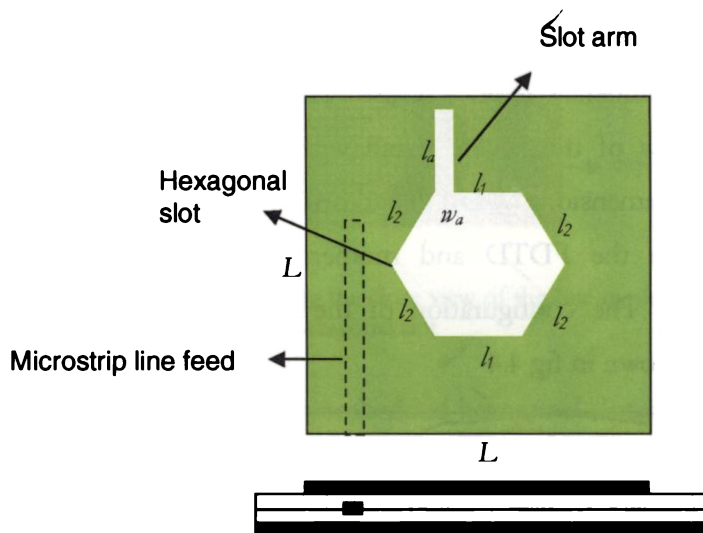


Figure 4.4 Geometry of the proposed passive dual frequency dual polarized microstrip antenna electromagnetically coupled to a 50Ω microstrip line. $L = 4\text{cm}$, $l_1 = l_2 = 0.8\text{cm}$, $l_a = 1\text{cm}$, $w_a = 0.1\text{cm}$, $b = 0.16\text{cm}$ and $\epsilon_r = 3.98$

4.1.4 Excitation Technique

Since the two resonant frequencies depend on the electrical lengths of two orthogonal dimensions of the square patch, determination of the common matching point inside the patch is difficult. Hence, electromagnetic coupling is employed to excite the two resonant modes with good matching. The optimum matching location can be easily determined by sliding the patch along the surface of the feed line. The microstrip feed

line is etched on a substrate of same dielectric constant and thickness as used for the construction of the square patch antenna. As the characteristic line impedance Z_0 is determined by the width of the microstrip line w and its substrate dielectric constant ϵ_{eff} , we have the standard design equations,

$$Z_0 = \frac{Z}{\sqrt{\epsilon_{eff}}} \ln\left(\frac{8h}{w} + \frac{w}{4h}\right) \Omega \quad \text{when } w/h \leq 1 \quad (4.2)$$

// and the same way for

where, h is the substrate thickness. For $w/h \geq 1$, we have,

$$Z_0 = \frac{Z}{\sqrt{\epsilon_{eff}}} \left(\frac{w}{h} + 1.393 + 0.667 \ln\left(\frac{w}{h} + 1.444\right) \right) \Omega \quad (4.3)$$

where Z is the characteristic impedance of the free space. All the passive and reconfigurable antennas are fabricated on FR-4 substrate of dielectric constant 3.98 and thickness 0.16cm. For this substrate, the width w of the feed line corresponding to characteristic impedance 50Ω is found to be 3mm. The size of the feed ground plane is also optimized as 11.4 x 11.4 cm using the moment method code as well as the indigenously developed FDTD source code for better antenna performance. The antenna analysis with the FDTD algorithm has already been described in chapter-3,

4.1.5 Mechanical Frequency Tuning

The fundamental resonant frequency of the conventional unslotted square patch is 1.885GHz. By loading the hexagonal slot alone, the operating frequency can be lowered to 1.74GHz, which results in greater area reduction. The extended slot arm splits the fundamental resonant frequency of the square microstrip patch with hexagon alone, into two separate resonant modes, TM_{10} and TM_{01} with orthogonal polarization planes. This is evident from the surface current density plot of the square patch with hexagonal and protruding slot arm obtained from FDTD analysis (fig. 4.5) and IE3D (fig. 4.6).

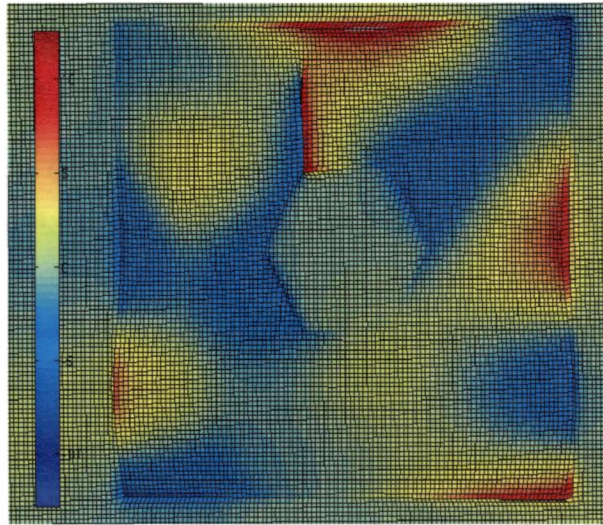


Figure 4.5 FDTD computed surface current distribution of the hexagonal slot loaded single slot arm square microstrip patch antenna showing the simultaneous excitation of TM₁₀ and TM₀₁ mode

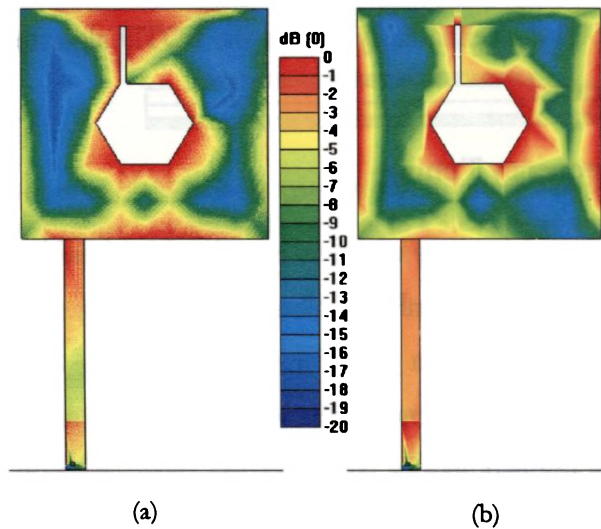


Figure 4.6 Surface current density plots for the (a) TM₁₀ and (b) TM₀₁ resonant modes at frequencies, $f_{10} = 1.56$ GHz and $f_{01} = 1.705$ GHz. It is seen that the current densities are excited in orthogonal planes. (simulated using IE3D)

Thus the central hexagonal slot with the protruding slot arm considerably increases the effective lengths of the two excited resonant modes, TM_{10} and TM_{01} , and the excited patch surface current densities are perturbed in such a way that these two modes can be excited for dual frequency operation with a single feed. Thus by varying the length of the protruding slot arm, the first resonant mode, TM_{10} can be tuned without much affecting the second resonant mode, giving different frequency ratios. This concept can be made use in the mechanical tuning of the first operating frequency by tailoring the effective length of the slot arm. The length of this protruding slot mainly determines the first resonant mode.

However, besides the slot arm, both the hexagonal slot and the square patch itself can be tailored for obtaining different frequencies. But this idea has not been considered here as the concept of electronic tuning with integrated PIN and Varactors is the major theme of this research work.

4.1.6 Antenna Dimensions and Its Effect on Dual Resonant Modes

Various theoretical and experimental studies are conducted in order to determine the variation of the two excited resonant modes with the antenna dimensions. The first and second resonant frequencies f_{10} and f_{01} purely depends on the horizontal and vertical dimensions of the square patch as in the case of a standard rectangular patch. But the inclusion of the hexagonal slot at the centre of the square patch modifies the effective horizontal and vertical electrical lengths of the patch. A regular hexagonal slot modifies these lengths equally and the currents paths of TM_{10} and TM_{01} are brought to 1.74GHz from 1.885GHz of the square patch. This is evident from the computed return loss of the square patch with and without the embedded hexagonal slot shown in fig. 4.7.

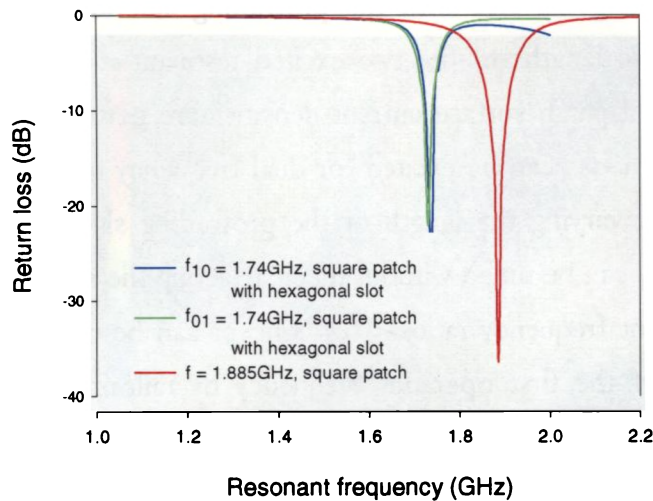


Figure 4.7 Return loss performance of the standard 4 x 4 cm square patch with and without embedded regular hexagonal shaped slot

The slot arm is then carved with its length, $l_a = 1\text{cm}$ and width, $w_a = 0.1\text{cm}$ as depicted in fig. 4.4. As explained earlier, this generates two orthogonal resonant modes, where the first resonant frequency, f_{10} now purely depends on the horizontal effective length modified by the length and width of the slot arm. It is observed that as the effective resonating length increases, the resonant frequency decreases, which in turn give greater size reduction.

Figure 4.8 shows the theoretical (FDTD), simulated (IE3D) and experimental, dual resonant frequencies excited by the inclusion of the slot arm to the hexagonal slot loaded patch. The introduction of the extended slot arm simultaneously excites TM_{10} and TM_{01} (say, f_1 and f_2 respectively) where $f_1 = 1.56\text{GHz}$ and $f_2 = 1.705\text{GHz}$. Thus the hexagonal slot with extended arm increased the effective lengths of the two resonant modes (TM_{10} and TM_{01}) and the excited patch surface current densities are perturbed in such a way that these two modes are excited for dual frequency dual polarized operation. The frequency ratio (f_2/f_1) is very low and

found to be 1.09. Bandwidths of 1.923% and 1.76% are obtained for the first and second resonant frequencies respectively.

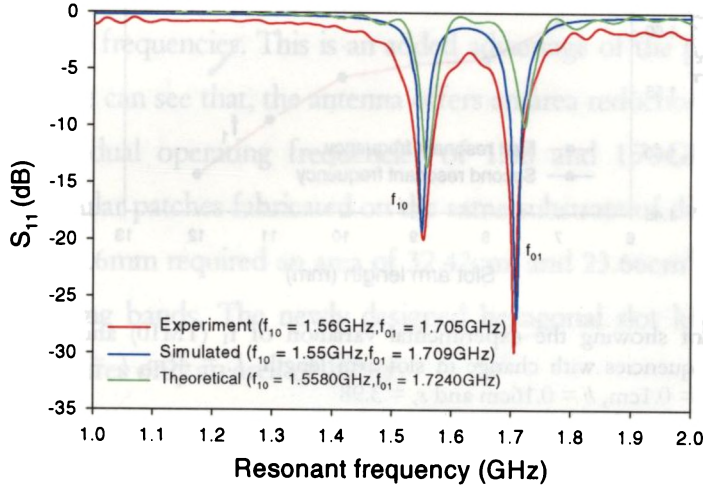


Figure 4.8 Theoretical (FDTD), simulated (IE3D) and measured return loss for the two resonant frequencies. The antenna dimensions are, $L = 4\text{cm}$, $l_1 = l_2 = 0.8\text{cm}$, $l_a = 1\text{cm}$, $w_a = 0.1\text{cm}$, $b = 0.16\text{cm}$ and $\epsilon_r = 3.98$

4.1.6.1 Frequency Tuning by Tailoring the Slot Arm Length

All the results and discussions stated above establish the ability of the novel design with optimized square patch and hexagonal slot to produce dual polarized dual frequencies when perturbed with a slot arm. Rigorous experimental investigations are then carried out to verify the frequency tuning mechanism of the proposed antenna by varying the slot arm dimensions. Care is taken to maintain the feed line position fixed, while taking return-loss measurements of the antenna with different slot arm lengths. The antenna is etched in a substrate of dielectric constant 3.98 and height 1.6mm with dimensions: $L = 4\text{cm}$ and $l_1 = l_2 = 0.8\text{cm}$. The slot arm length l_a is then varied from 7mm to 12mm, keeping the slot width $w_a = 1\text{mm}$ unchanged.

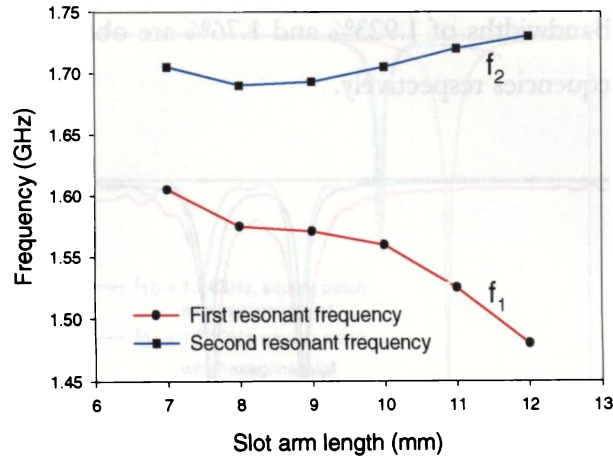


Figure 4.9 Plot showing the experimental variation of f_1 (TM10) and f_2 (TM01) frequencies with change in slot arm length. $L = 4\text{cm}$, $l_1 = l_2 = 0.8\text{cm}$, $w_a = 0.1\text{cm}$, $b = 0.16\text{cm}$ and $\epsilon_r = 3.98$

The change in dual frequency excitation with the different slot arm length is given in table 4.1. Fig. 4.9 shows the variation of first and second resonant modes with protruding slot arm length.

Table 4.1 Dual frequency performance of the proposed antenna with variation in slot arm slot length. The antenna parameters are: $L = 4\text{cm}$, $l_1 = l_2 = 0.8\text{cm}$, $w_a = 0.1\text{cm}$, $b = 0.16\text{cm}$ and $\epsilon_r = 3.98$

Slot arm length, l_a (mm)	f_1 (GHz)	f_2 (GHz)	% Impedance bandwidth		Frequency ratio, f_2/f_1
			f_1	f_2	
7	1.605	1.705	2.50	2.35	1.06
8	1.575	1.690	2.86	2.07	1.07
9	1.571	1.693	1.86	1.73	1.08
10	1.560	1.705	1.92	1.76	1.09
11	1.525	1.720	2.23	1.92	1.13
12	1.480	1.730	1.69	1.73	1.17

4.1.6.2 Improvement in Area Reduction

Besides the tuning effect, the increase in length of the slot arm also provides area reduction for the two resonant modes compared to standard rectangular patches operating at same frequencies. This is an added advantage of the proposed design. From table 4.2 we can see that, the antenna offers an area reduction of 50.65% and 32.38% for the dual operating frequencies of 1.48 and 1.73GHz respectively. Standard rectangular patches fabricated on the same substrate of dielectric constant 3.98 and height 1.6mm required an area of 32.42cm² and 23.66cm² respectively for the same operating bands. The newly designed hexagonal slot loaded single slot arm antenna requires only an area of 16cm².

Table 4.2 Percentage area reduction for the two resonant frequencies for different slot arm length, compared to standard rectangular patches. The antenna parameters are: $L = 4\text{cm}$, $l_1 = l_2 = 0.8\text{cm}$, $w_1 = 0.1\text{cm}$, $h = 0.16\text{cm}$ and $\epsilon_r = 3.98$

Slot arm length, l_s (mm)	f_1 (GHz)	f_2 (GHz)	% Area reduction		Frequency ratio, f_2/f_1
			f_1	f_2	
5	1.635	1.680	39.74	36.33	1.03
6	1.635	1.695	39.74	35.18	1.04
7	1.605	1.705	41.88	34.53	1.06
8	1.575	1.690	44.11	35.59	1.07
9	1.571	1.693	44.44	35.33	1.08
10	1.560	1.705	45.15	34.53	1.09
11	1.525	1.720	47.99	33.33	1.13
12	1.480	1.730	50.65	32.38	1.17

4.1.6.3 Variation of Input Impedance

As our aim is to develop a reconfigurable dual frequency microstrip antenna with a single feed excitation and devoid of any matching networks, the study of the input impedance of the antenna is a primary concern. HP 8510C Vector Network Analyzer is again used to find the antenna input impedances at different slot arm lengths. In the passive microstrip antenna experiments, with a single slot arm, it is noted that the antenna gives good impedance matching for both the excited resonant modes when the 50Ω microstrip feed line is essentially far away from the extended slot arm. This shows that, the change in length of this protruding slot arm hardly affects the impedance matching of the two resonant frequencies. In other words, we can say that the antenna input impedance is not very sensitive to small changes in the length of the extended slot arm. This remarkable property of the hexagonal slot loaded square microstrip passive antenna design greatly simplifies the design of the reconfigurable dual frequency microstrip antenna, where the extended slot arm length is switched to tune the operating frequencies. This is also the reason that no external matching network is needed for achieving better impedance matching for all the developed reconfigurable antennas. Table 4.3 gives the complex input impedance for the two orthogonal resonant modes, TM_{10} and TM_{01} at different slot arm lengths.

Table 4.3 Variation of complex input impedance for TM_{10} and TM_{01} resonant modes with slot arm length. The antenna parameters are: $L = 4\text{cm}$, $l_1 = l_2 = 0.8\text{cm}$, $w_s = 0.1\text{cm}$, $b = 0.16\text{cm}$ and $\epsilon_r = 3.98$. The feed position is kept unchanged as in figure 4.1.

Slot arm length, l_a (mm)	f_1 (GHz)	f_2 (GHz)	Input Impedance (Ω)			
			TM_{10}		TM_{01}	
			Re	Im	Re	Im
6	1.635	1.695	51	2	51	-11
7	1.605	1.705	50	30	47	-23
8	1.575	1.690	53	15	48	-13
9	1.571	1.693	44	29	47	-18
10	1.560	1.705	47	17	44	-13
11	1.525	1.720	44	-25	50	-23
12	1.480	1.730	49	19	46	-17

4.1.6.4 Variation of Frequency Ratio

As we excited the two orthogonal modes of the square patch, these frequencies are very much closer to each other giving low values for frequency ratio. Thus this type of design is very suitable for short link transmit- receive modules or vehicular-satellite communications, where a low frequency ratio is desirable [34]. The experimental and simulated (IE3D) variation of frequency ratio with slot arm length is depicted in fig. 4.10.

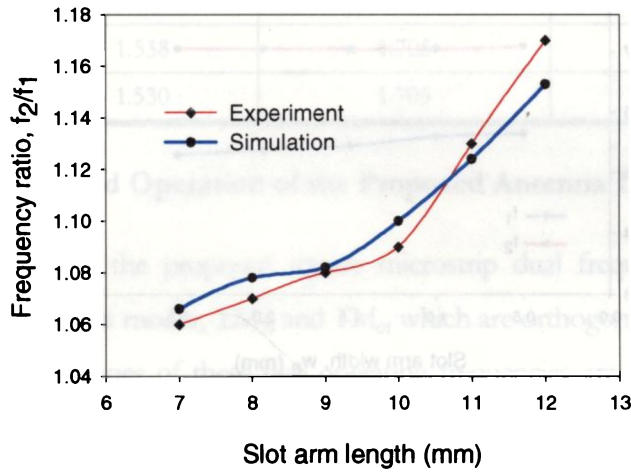


Figure 4.10 Variation of frequency ratio with change in slot arm length. $L = 4\text{cm}$, $l_1 = l_2 = 0.8\text{cm}$, $w_a = 0.1\text{cm}$, $b = 0.16\text{cm}$ and $\epsilon_r = 3.98$

The value of the ratio of frequencies, f_2/f_1 is roughly equal to the ratio of effective resonant length of the horizontal and vertical dimensions of the square patch, modified by the addition of hexagonal slot and protruding slot arm. The length of the slot arm mainly modifies the first resonant frequency (TM_{10}) and essentially leaves the second resonant frequency (TM_{01}) almost unchanged. A change in frequency ratio from 1.03 to 1.17 is observed when the slot arm length is varied from 5mm to 12mm.

4.1.6.5 Effect of Slot Arm Width, w_a

A slight variation in resonant frequencies is also observed when the width w_a is increased, but this change is found to be negligible compared to that of slot arm length l_a . The FDTD computed variation of the first and second resonant modes with the slot arm width is plotted in fig. 4.11.

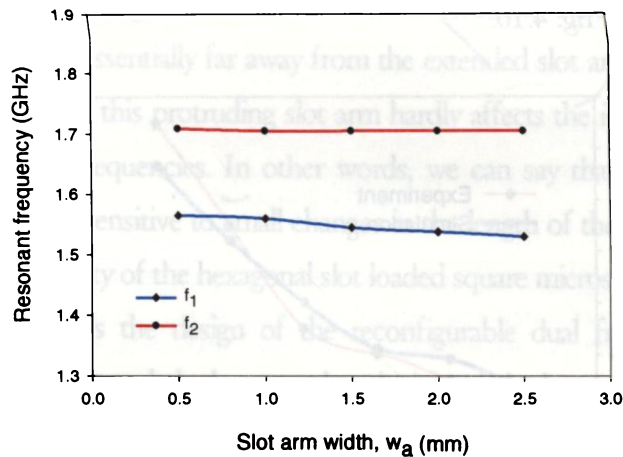


Figure 4.11 Plot showing the theoretically computed (FDTD) variation of f_1 (TM10) and f_2 (TM01) frequencies with change in slot arm width w_a . ($L = 4\text{cm}$, $l_1 = l_2 = 0.8\text{cm}$, $l_a = 1\text{cm}$, $b = 0.16\text{cm}$ and $\epsilon_r = 3.98$)

From the graph it is evident that the tuning of resonant frequencies by tailoring the slot arm width, w_a is not so efficient as in the case of slot arm length, l_a . By keeping the slot arm length unchanged ($l_a = 1\text{cm}$), the width w_a is varied from 0.5 to 2.5mm for the proposed configuration. A small decrease in f_1 is observed, as can be seen from table 4.4. The frequency ratio, f_2/f_1 varies in between 1.089 and 1.114 when w_a is varied from 0.5mm to 2.5mm. The tabulated results are given in table 4.4.

✓

Table 4.4 Dual frequency performance of the proposed antenna with variation in slot arm width w_s . The antenna parameters are: $L = 4\text{cm}$, $l_1 = l_2 = 0.8\text{cm}$, $l_a = 1\text{cm}$, $b = 0.16\text{cm}$ and $\epsilon_r = 3.98$

Slot arm width, w_s (mm)	First resonant frequency, f_1 (GHz)	Second resonant frequency, f_2 (GHz)	Frequency ratio, f_2/f_1
0.5	1.565	1.709	1.089
1.0	1.560	1.705	1.093
1.5	1.545	1.705	1.104
2.0	1.538	1.705	1.109
2.5	1.530	1.705	1.114

4.1.7 Dual Polarized Operation of the Proposed Antenna Design

As explained earlier, the proposed square microstrip dual frequency patch antenna generates two resonant modes, TM_{10} and TM_{01} which are orthogonal to each other. That is the polarization planes of these two operating frequencies are in orthogonal planes. This can be better derived from the transmission characteristics of the two resonant frequencies at mutually orthogonal planes.

The transmission characteristics are measured using HP8510C Vector Network Analyzer interfaced to a S310C Automatic Antenna Position Controller and an IBM PC. The designed square microstrip antenna is kept in the transmitting mode and a wide band standard horn is used as receiver. RF signal is applied to the microstrip antenna in the transmitting mode and the power received by the wide band horn, in the vertical plane is stored as a function of frequency for a particular PIN diode state. The transmitting antenna is then rotated 90° to record the received power as a function of frequency in the horizontal plane. The analysis of the recorded data in both the planes reveals that the two linearly polarized resonant frequencies are in orthogonal polarization planes. This is visible in the plot of measured data in two orthogonal planes in fig. 4.12.

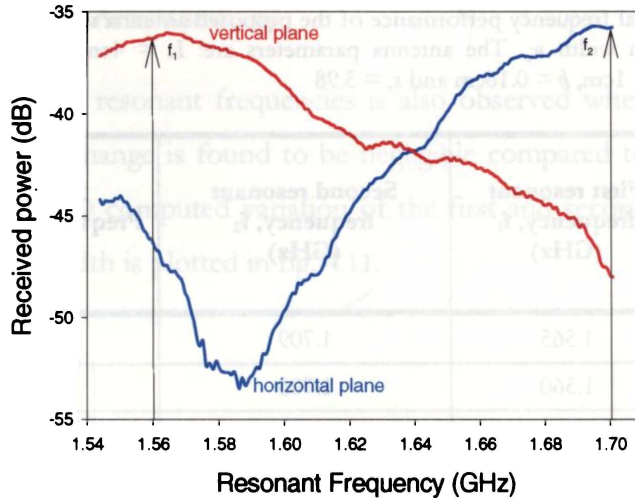


Figure.4.12 Variation of received power with frequency for the two orthogonal polarization planes for first and second resonant modes. The antenna dimensions are, $L = 4\text{cm}$, $l_1 = l_2 = 0.8\text{cm}$, $l_a = 1\text{cm}$, $w_a = 0.1\text{cm}$, $b = 0.16\text{cm}$ and $\epsilon_r = 3.98$

4.1.8 Radiation Pattern and Gain

The co-polar and cross-polar far-field radiation patterns of the newly proposed microstrip patch antenna in E and H principal planes are taken for both operating frequencies. The measured co-polar and cross-polar radiation pattern at the corresponding central frequencies of a typical antenna configuration ($L = 4\text{cm}$, $l_1 = l_2 = 0.8\text{cm}$, $l_a = 1\text{cm}$, $w_a = 0.1\text{cm}$, $b = 0.16\text{cm}$ and $\epsilon_r = 3.98$), is shown in fig. 4.13. The entire radiation pattern shows similar broad beam radiation characteristics with better cross polarization, similar to that of standard microstrip patch antennas. Thus the inclusion of the hexagonal slot and the extended slot arm by no means distorted the radiation patterns of the two resonant frequencies. Gain measurements are carried out using the gain comparison method with standard circular patches fabricated in the dielectric substrate of dielectric constant, $\epsilon_r = 3.98$. For the first resonant frequency the gain is found to be 4.63dBi and for second resonant frequency 4.57dBi, when the slot arm length is 1cm and width is 1mm. The slight reduction in gain compared to standard patches is due to the reduction in radiating area of the slot loaded square patch.

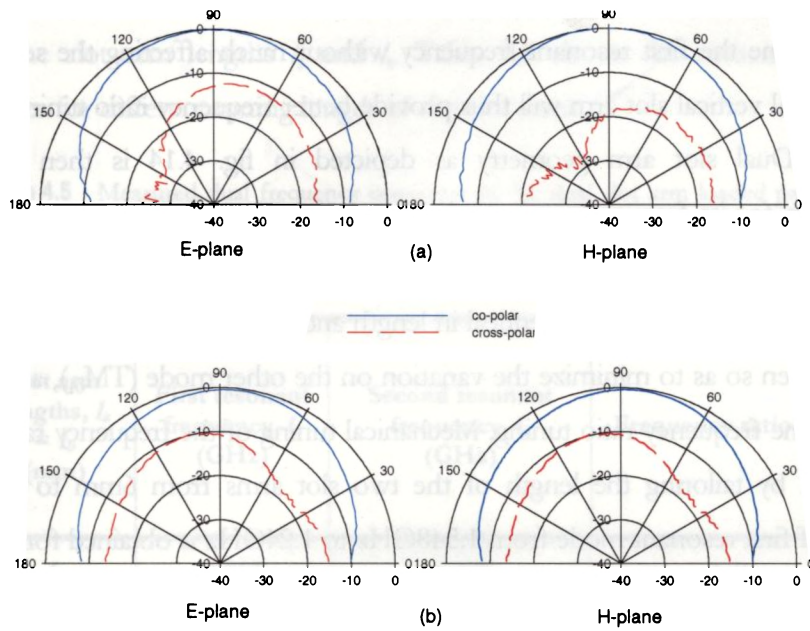


Figure.4.13 Measured E and H plane radiation pattern of the proposed antenna for (a) $f_1 = 1.56$ GHz and (b) $f_2 = 1.705$ GHz. The antenna dimensions are, $L = 4$ cm, $l_1 = l_2 = 0.8$ cm, $l_a = 1$ cm, $w_a = 0.1$ cm, $b = 0.16$ cm and $\epsilon_r = 3.98$

4.1.9 Dual Slot Arm Loaded Patch Antenna

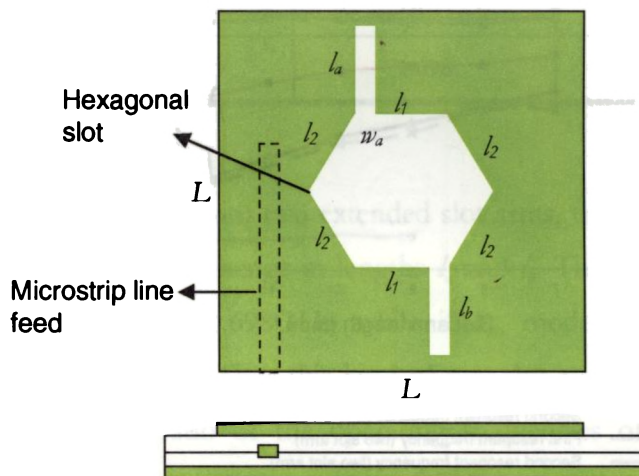


Figure 4.14 Geometry of the dual slot arm loaded square microstrip patch antenna. $L = 4$ cm, $l_1 = l_2 = 0.8$ cm, $w_a = 0.1$ cm, $b = 0.16$ cm and $\epsilon_r = 3.98$

From the studies conducted as above, it is concluded that the protruding slot arm can effectively tune the first resonant frequency without much affecting the second one. An additional vertical slot arm will thus provide better frequency ratio tuning and area reduction. Dual slot arm geometry as depicted in fig. 4.14 is then taken for investigation for its frequency ratio tuning capability. The configuration of the patch antenna is similar to that of the single slot arm loaded one, except a lower vertical arm of length, l_v . The two slots are identical in length and breadth. The location of the two slots is chosen so as to minimize the variation on the other mode (TM_{01}), and thereby increasing the frequency ratio tuning. Mechanical tuning of the frequency ratio is then carried out by tailoring the length of the two slot arms from 6mm to 12mm. A variation of first resonant mode from 1.548GHz to 1.24GHz is obtained for 6mm and 12mm slot lengths, respectively, whereas only a variation from 1.63 to 1.48 is observed with the single slot arm design. That is, f_1 is changing and f_2 unaffected. Thus frequency ratio tuning as well as improved size reduction is obtained with the inclusion of the lower vertical slot arm. This is evident from the plots in fig. 4.15,

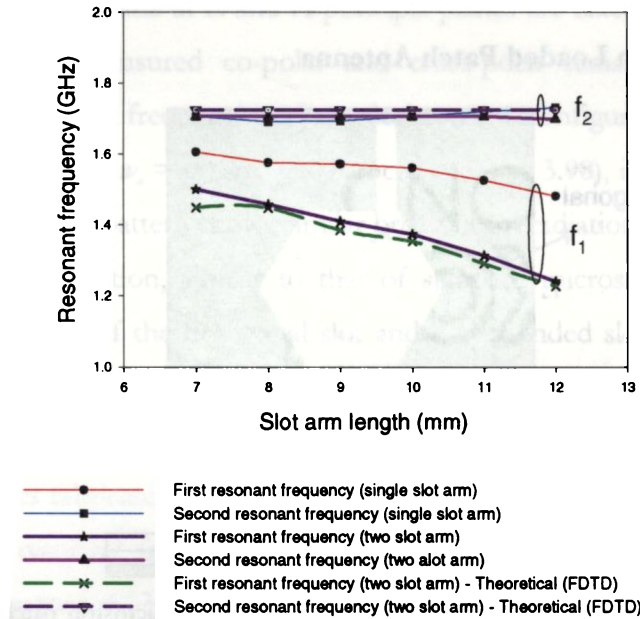
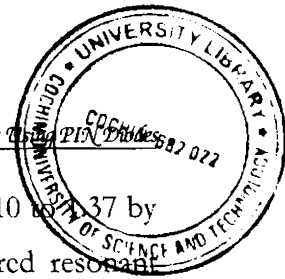


Figure 4.15 Comparison of frequency tuning between single and dual slot arm loaded square microstrip patch antennas. The common antenna parameters are $L = 4\text{cm}$, $l_1 = l_2 = 0.8\text{cm}$, $w_a = 0.1\text{cm}$, $b = 0.16\text{cm}$, $l_a = l_b$ and



The frequency ratio of this dual slot arm design can be varied from 1.10 to 1.37 by varying the slot arm lengths l_a and l_b . Table 4.5 shows the measured resonant frequencies for different tuning length of the slot arms.

Table 4.5 Measured dual frequency operation of the dual slot arm loaded patch with variation in slot arm length. The antenna parameters are: $L = 4\text{cm}$, $l_1 = l_2 = 0.8\text{cm}$, $l_c = l_b$, $h = 0.16\text{cm}$ and $\epsilon_r = 3.98$

Slot arm lengths, $l_a = l_b$ (mm)	First resonant frequency, f_1 (GHz)	Second resonant frequency, f_2 (GHz)	Frequency ratio, f_2/f_1
6	1.548	1.705	1.10
7	1.499	1.705	1.14
8	1.457	1.705	1.17
9	1.409	1.705	1.21
10	1.373	1.705	1.24
11	1.313	1.705	1.30
12	1.240	1.698	1.37

Thus in this novel design with two extended slot arms, the second resonant mode is almost unaffected with change in lengths l_a and l_b . The TM_{01} mode remains in between 1.705GHz and 1.698GHz while TM_{10} mode is varying in between 1.548GHz and 1.240GHz. Thus this kind of two slot arm design can be used for tuning the frequency ratio of the operating frequencies of the dual frequency microstrip patch antenna. A comparison of frequency ratio variation between the single and dual slot arm microstrip antenna configuration is given in fig. 4.16.

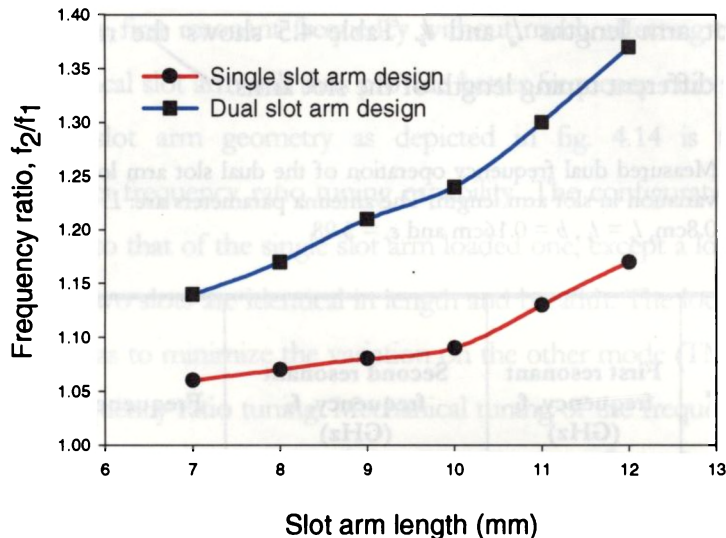


Figure 4.16 Frequency ratio variations with slot arm length for the proposed single and dual slot arm designs. The antenna dimensions are same as in fig. 4.14

The newly proposed dual slot arm microstrip antenna also offers greater area reduction, compared to the earlier single slot arm design. The separation of the two operating frequencies is also increased (see fig. 4.16) in this case. Thus electronic tuning of frequency ratio in a reasonable range is possible in this design with PIN and Varactor diode integration. The extended slot arms will serve as suitable places to integrate these switch/tuning devices. Detailed studies of electronically reconfigurable dual frequency antennas with dual slot arms and controlled by PIN diodes and Varactors are presented in sections 4.2.3 and 5.3 respectively.

4.1.10 Dual Frequency Patch with Orthogonal Slot Arms

In order to study the effects of slots in the orthogonal direction, a new design with two slots as in fig. 4.17 is constructed. For comparison with the single

slot arm design, the length l_a of the vertical arm is kept as a constant (10mm) and the length l_b is varied in between 9.5mm and 15.5mm. Since both the slot arms perturb the current densities of the TM_{10} and TM_{01} modes, the effective electrical lengths of these two resonant frequencies are much lower, giving enhanced area reduction compared to the single slot arm design. The measured resonant frequencies for different slot length combinations are given in table 4.6. Here both frequencies shift towards the lower frequency range when the orthogonal slot arm length l_b is increased. The frequency ratio variation is not much distinct as in the case of dual vertical slot arm design, because here, both frequencies are simultaneously changing. Thus the orthogonal slots design can be effectively used to tune both resonant frequencies by varying the length of the slots.

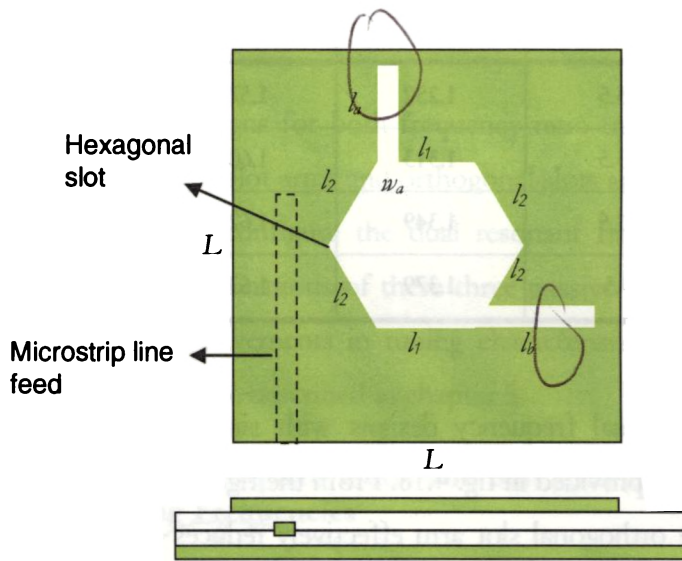


Figure 4.17 Geometry of the orthogonal slot arm loaded square microstrip patch antenna. $L = 4\text{cm}$, $l_1 = l_2 = 0.8\text{cm}$, $w_a = 0.1\text{cm}$, $b = 0.16\text{cm}$, $l_a = 1\text{cm}$ and $\epsilon_r = 3.98a$

Table 4.6 Measured dual frequency operation of the orthogonal slot arm loaded microstrip antenna. The antenna parameters are: $L = 4\text{cm}$, $l_1 = l_2 = 0.8\text{cm}$, $h = 0.16\text{cm}$ and $\epsilon_r = 3.98$

Vertical slot arm length, l_a (mm)	Slot arm lengths, l_b (mm)	First resonant frequency, f_1 (GHz)	Second resonant frequency, f_2 (GHz)	Frequency ratio, f_2/f_1
10	15.5	1.313	1.596	1.23
	14.5	1.349	1.602	1.19
	13.5	1.373	1.614	1.18
	12.5	1.415	1.626	1.15
	11.5	1.430	1.630	1.14
	10.5	1.445	1.638	1.13
	9.5	1.463	1.644	1.12
12	15.5	1.252	1.578	1.26
	13.5	1.313	1.602	1.22
	11.5	1.349	1.620	1.20
	9.5	1.379	1.638	1.19

A comparison of two dual frequency designs with single slot arm and dual orthogonal slot arms are provided in fig. 4.18. From the figure it is evident that the addition of one more orthogonal slot arm effectively reduces both the resonant frequencies of the dual frequency passive microstrip antenna giving more size reduction than the single slot arm design. The second resonant frequency now shows variations with the horizontal slot arm length l_b . The frequency ratio hardly shows much variation unlike the case of the design with two vertical slot arms.

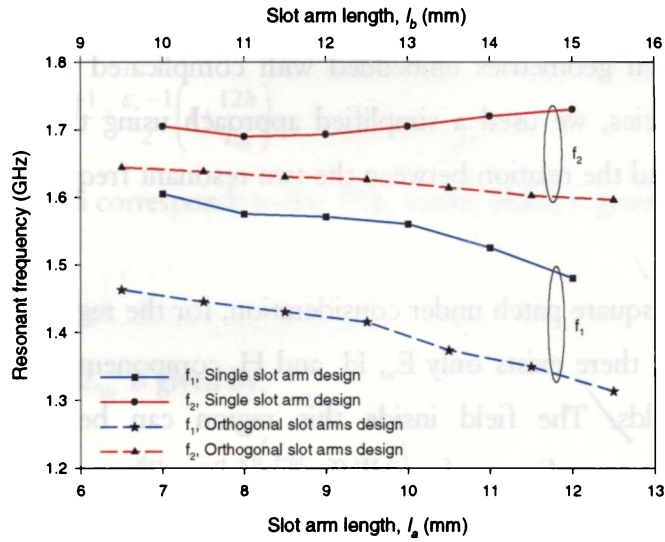


Figure 4.18 Plot showing the variation of two resonant frequencies of the proposed antenna with single and orthogonal slot arms. The antenna parameters are $L = 4\text{cm}$, $l_1 = l_2 = 0.8\text{cm}$, $w_a = 0.1\text{cm}$, $b = 0.16\text{cm}$, $l_a = 1\text{cm}$ and $\epsilon_r = 3.98$. l_a is kept constant at 10mm for later case.

Thus all the possible designs for both frequency ratio tuning and dual frequency tuning with single vertical slot arms and orthogonal slots are thoroughly explored in order to electronically reconfigure the dual resonant frequencies and frequency ratio. Moreover, the combinations of these three passive antenna designs are also utilized for further improvements in tuning characteristics using Varactors. The studies on these designs are described in chapter 5.

4.1.11 Determination of Square Patch and Slot Arm Lengths for Particular Dual Operating Frequencies

In order to find the original square patch and slot arm dimensions, we make use of the cavity model of the square microstrip patch antenna and the rigorous experiments carried out on the proposed dual frequency hexagonal slot loaded square microstrip patch. These equations can be used to find the square patch length and slot arm length combination for a set of dual resonant frequencies.

Since highly rigorous mathematical tools are required to develop accurate design equations for patch geometries embedded with complicated slots, with dual operating frequencies, we used a simplified approach using the experimental observations to find the relation between the two resonant frequencies with the slot geometries.

In the case of the square patch under consideration, for the region between the patch and ground, there exists only E_z , H_x and H_y components of the electric and magnetic fields. The field inside this region can be considered as independent of z -co-ordinate, for all frequencies. There is no normal component of electric current normal to the patch edge. Thus, the tangential component of magnetic field, H can be neglected. Thus this region becomes a cavity bounded by electric walls (above and below) and magnetic walls along the edges. Thus standard cavity model equations are used to find the resonant frequencies.

Let, L_{10} and L_{01} be the length of the lengths of the two orthogonal dimensions of the square patch corresponding to the given dual frequencies, f_{r10} and f_{r01} , respectively. Then,

$$L_{10} = \frac{c}{2 f_{r10}} \left(\frac{\epsilon_r + 1}{2} \right)^{-1/2} \quad (4.4)$$

where ϵ_r is the dielectric constant of the substrate. But, fringing fields makes the patch look wider, electrically compared to its physical dimensions. Since some of the waves travel in substrate and some in air, an effective dielectric constant ϵ_{reff} is introduced to account for the fringing and the wave propagation in the line.

or TM_{10} , we have,

$$\epsilon_{\text{reff}} = \frac{\epsilon_r + 1}{2} + \frac{\epsilon_r - 1}{2} \left(1 + \frac{12h}{L_{01}} \right) \quad (4.5)$$

Here L_{01} is the length corresponds to the TM_{01} mode, which is given by,

$$L_{10} = \frac{c}{2fr_{01}} \left(\frac{\epsilon_r + 1}{2} \right)^{1/2} \quad (4.6)$$

The line extension ΔL_{10} is given by,

$$\Delta L_{10} = 0.412h \frac{(\epsilon_{\text{reff}} + 0.3) \left(\frac{L_{01} + 0.264}{h} \right)}{(\epsilon_{\text{reff}} - 0.258) \left(\frac{L_{01} + 0.8}{h} \right)} \quad (4.7)$$

Similarly, for TM_{01} mode, ΔL_{10} is given by,

$$\Delta L_{01} = 0.412h \frac{(\epsilon_{\text{reff}} + 0.3) \left(\frac{L_{10} + 0.264}{h} \right)}{(\epsilon_{\text{reff}} - 0.258) \left(\frac{L_{10} + 0.8}{h} \right)} \quad (4.8)$$

The addition of the hexagonal slot and the line extension modifies L_{10} and L_{01} as,

$$L_{10\text{mod}} = \frac{c}{2fr_{10}\sqrt{\epsilon_{\text{reff}}}} - 2\Delta L_{10} - \frac{c}{52.2466fr_{10}} \quad (4.9)$$

The last term accounts for the effect of the hexagonal slot.

Similarly,

$$L_{01\text{mod}} = \frac{c}{2fr_{01}\sqrt{\epsilon_{\text{reff}}}} - 2\Delta L_{01} - \frac{c}{52.2466fr_{01}} \quad (4.10)$$

The dependence of fr_{10} and fr_{01} on the slot arm length is different and therefore empirical expressions are obtained for this length separately. For the TM_{10} mode, the slot arm length $s_{1,10}$ is given by,

$$s_{L10} = 1.761 \times 10^9 - \frac{fr_{10}}{2.175 \times 10^{10}} \quad (4.11)$$

For TM_{01} mode, the slot arm length is given by,

$$s_{L01} = \frac{fr_{01} - 1.6579 \times 10^9}{5.202 \times 10^9} \quad (4.12)$$

The reduced resonant lengths due to these slot arm for TM_{10} is,

$$L_{10red} = 4.999 \times 10^{-2} - 2.901 \times 10^{-11} \times fr_{10} \quad (4.13)$$

Similarly, for TM_{01} mode,

$$L_{01red} = 4.258 \times 10^{-2} - 2.445 \times 10^{-11} \times fr_{01} \quad (4.14)$$

Now, the side dimensions of the square patch can be calculated by the following equations. The length of the square patch corresponding to TM_{10} is,

$$L_{10sq} = L_{10mod} - L_{10red} \quad (4.15)$$

For TM_{01} mode, we have,

$$L_{01sq} = L_{01mod} - L_{01red} \quad (4.16)$$

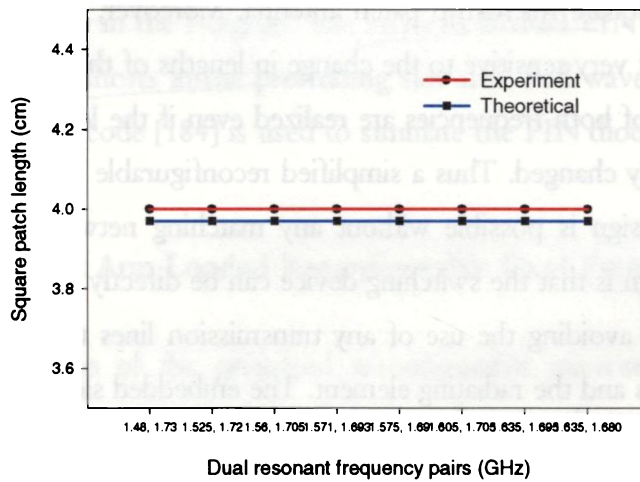
Taking the average for both modes, we get the dimension of the square patch for the given dual resonant modes as,

$$L = \frac{L_{10sq} + L_{01sq}}{2} \quad (4.17)$$

The length of the slot arm so as to generate the given dual resonant modes is obtained as,

$$l_a = \frac{s_{L10} + s_{L01}}{2} \quad (4.18)$$

The length of the square patch L and that of slot arm l_a for different dual resonant frequency combinations are then calculated using the above relations and compared with the experimental results. The experimental and theoretically predicted data are shown in fig. 4.19. The predicted data using the above described empirical relations closely follows the experimentally obtained results.



no L_{sc}
in the
Fig

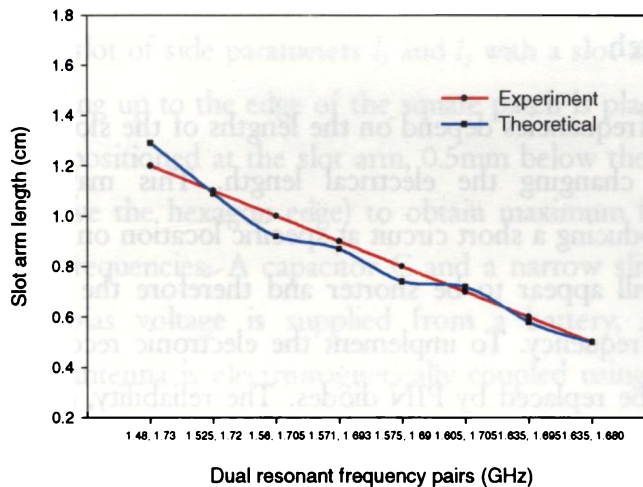


Figure 4.19 Graphs showing the variation of experimental and theoretical (FDTD) square patch and slot arm dimensions for different dual operating frequency pairs

4.2 Reconfigurable Dual Frequency Microstrip Antenna Design using PIN Diodes

The studies described in section 4.1 convincingly proved the novel concept of slot arm tuning mechanism which can be used either to reconfigure the dual operating frequencies or to tune the frequency ratio of the proposed dual frequency dual polarized single feed square microstrip patch antenna. Moreover, as the antenna input impedance is not very sensitive to the change in lengths of the extended slot arms, good matching of both frequencies are realized even if the lengths of these slot arms are drastically changed. Thus a simplified reconfigurable dual frequency microstrip antenna design is possible without any matching networks. Another advantage of this design is that the switching device can be directly implanted into the slot arms, thereby avoiding the use of any transmission lines to connect the non-linear components and the radiating element. The embedded slot arms, which extends to the periphery of the square patch thus proves to be an ideal place to integrate the PIN diodes.

4.2.1 PIN Diode Switch

As the dual resonant frequencies depend on the lengths of the slot arms, it can be easily tuned by changing the electrical length. This may be readily accomplished by introducing a short circuit at specific location on the slot arm. Then the slot arm will appear to be shorter and therefore the antenna will resonate at a higher frequency. To implement the electronic reconfigurability, the ideal short must be replaced by PIN diodes. The reliability, compactness, high switching speed, very small resistance and capacitance in the ON and OFF states, makes it most appropriate for the present application. A PIN diode is a semiconductor device that operates as a variable resistor at RF and microwave frequencies. The resistance value of the PIN diode is determined only by the

forward biased dc current. But in switch and attenuator applications, the PIN diode ideally controls the RF signal level without introducing distortion that might change the shape of the RF signal. An important additional feature of the PIN diode is its ability to control large RF signals while using much smaller levels of DC excitation. The performance of the PIN diode primarily depends on chip geometry and the nature of the semiconductor material in the finished diode, particularly in the I-region. The Siemens BAR63 PIN diodes are used to replace the ideal shorts in the protruding slot arm. Full wave analysis using the moment method code [184] is used to simulate the PIN diode in ON and OFF bias states.

4.2.2 Single Slot Arm Loaded Reconfigurable Dual Frequency Microstrip Antenna

The configuration of the proposed reconfigurable microstrip patch antenna with hexagonal slot and an extended slot arm for reconfigurable dual frequency operation is illustrated in fig. 4.20. A square microstrip patch antenna with side dimension L is fabricated on a substrate of thickness h and relative permittivity ϵ_r . A hexagonal slot of side parameters l_1 and l_2 with a slot arm of length l_a and width w_a extending up to the edge of the square patch is placed at its center. A pin diode D is positioned at the slot arm, 0.5mm below the square patch side (i.e. 0.7mm above the hexagon edge) to obtain maximum frequency shift for both resonant frequencies. A capacitor C and a narrow slit are used for DC isolation. DC bias voltage is supplied from a battery, through two chip inductors. The antenna is electromagnetically coupled using a 50Ω microstrip line. The feed line is kept unchanged through out the experiment, even when the PIN diode position is varied for achieving other reconfigurable dual frequency combinations.

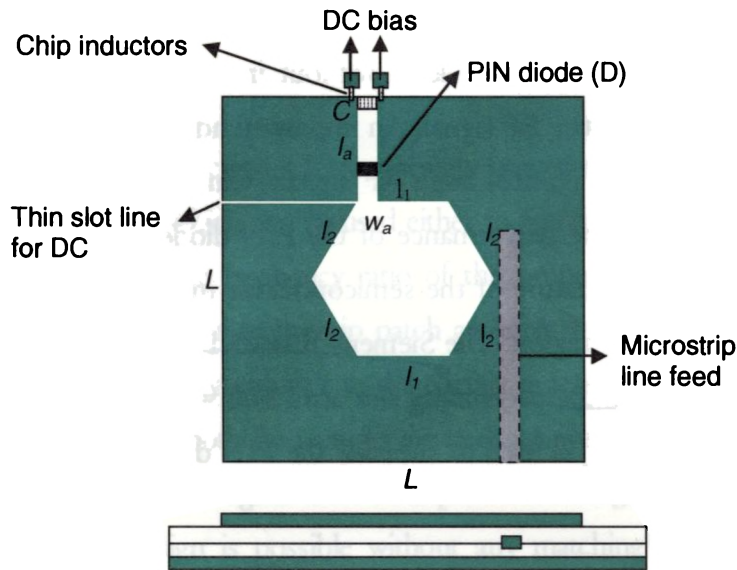


Figure 4.20 Geometry of the reconfigurable dual frequency dual polarized microstrip antenna controlled by a PIN diode. The antenna parameters are $L = 4\text{cm}$, $l_1 = l_2 = 0.8\text{cm}$, $l_a = 12\text{cm}$, $w_a = 0.1\text{cm}$, $b = 0.16\text{cm}$ and $\epsilon_r = 3.98$. PIN diode is placed at 0.7mm from the hexagon edge

The extended slot arm splits the fundamental resonant frequency of the square microstrip patch, with hexagon alone, into two separate resonant modes (TM_{10} and TM_{01}) with orthogonal polarization planes. These two excited frequencies can be tuned by changing the slot arm length. When the pin diode is ON, it essentially behaves as equivalent short circuit, thus driving the currents on the patch directly through it, reducing the effective length of the slot. When the diode is switched OFF, the currents have to flow through the capacitor C , with an increased current path, resulting in the shifting of resonant frequencies towards the lower frequency region. The position of the pin diode is so selected that it gives good matching for all the four excited resonant frequencies. The newly designed antenna gives good return loss characteristics and band width even when the position of the diode is

altered to achieve desired frequency values. Fig. 4.21 shows the measured return loss for the reconfigurable microstrip antenna at two PIN diode bias states.

To obtain correct biasing of the diode, the slot arm is open at one end with a small smd capacitor soldered to block the DC bias current and to provide good RF continuity. A narrow slit is designed at the bottom of the slot arm to switch the diode properly, without affecting patch currents. This narrow slit in the square patch effectively blocks the DC current while allowing the RF current density to pass through.

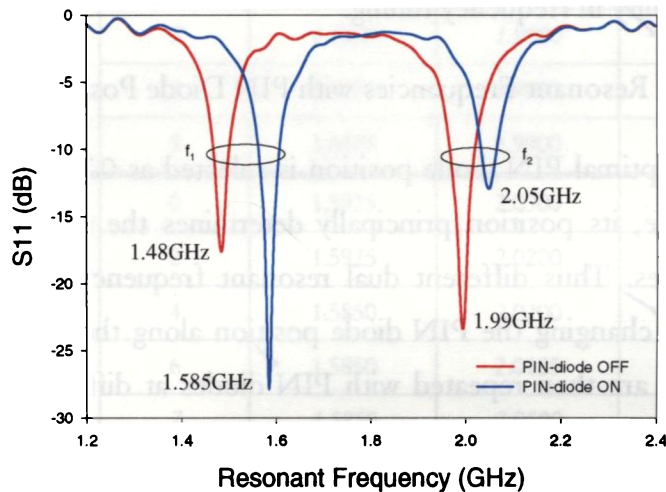


Figure 4.21 Measured reflection co-efficient of the reconfigurable dual frequency microstrip antenna for PIN diode ON and OFF states. The antenna parameters are $L = 4\text{cm}$, $l_1 = l_2 = 0.8\text{cm}$, $l_a = 12\text{cm}$, $w_a = 0.1\text{cm}$, $b = 0.16\text{cm}$ and $\epsilon_r = 3.98$. PIN diode is placed at 0.7mm from the hexagon edge.

The fundamental resonant frequency of the unslotted square patch is 1.885GHz . By embedding the hexagonal slot and the extended arm, two lower resonant frequencies can be excited due to the increase in the effective lengths of the two resonant modes (TM_{10} and TM_{01}) of the square patch.

When the diode is switched OFF, the antenna resonates at 1.48 GHz and 1.99 GHz with a frequency ratio 1.34. Once the diode is turned ON with a 1 volt DC bias, the first resonant frequency shifts by 105 MHz and second resonant frequency by 60 MHz, giving excitation at 1.585 GHz and 2.05 GHz, with a frequency ratio 1.29. In all these four operating frequencies, the antenna has a good matching at a single feed position. Fig. 4.21 shows the measured return loss (S_{11}), of the antenna with dimensions $L = 4\text{cm}$, $l_1 = l_2 = 0.8\text{cm}$, $l_a = 1.1\text{cm}$, $w_a = 0.1\text{cm}$, $b = 0.16\text{cm}$ and $\epsilon_r = 3.98$. The frequency ratio is tunable in the range 1.2684 to 1.3137 in the ON state and 1.3227 to 1.3779 in the OFF state, by changing the diode position along the slot arm, giving an added advantage of flexibility in frequency tuning.

4.2.2.1 Variation of Resonant Frequencies with PIN Diode Position

Even though the optimal PIN diode position is selected as 0.7mm above the hexagonal slot edge, its position principally determines the switchable dual resonant frequencies. Thus different dual resonant frequency combinations can be selected by changing the PIN diode position along the slot arm. The experiments above are then repeated with PIN diodes at different positions starting from 0mm from the bottom to 9mm along the slot arm. The results are tabulated in table 4.7. In the OFF state the frequency ratio shows only a feeble change between 1.33 and 1.34, which in turns indicates that the inclusion of the PIN diode in the slot arm, in the OFF states, ideally behaves like an open. On the other hand, in the ON state the frequency ratio varies in between 1.27 and 1.31. ✓

Table 4.7 Dual frequency operation of the single slot arm loaded antenna at different PIN diode position on the slot arm

PIN diode state	PIN diode position (mm)	First resonant frequency, f_1 (GHz)	Second resonant frequency, f_2 (GHz)	Frequency ratio, f_2/f_1
OFF	0	1.4725	1.9600	1.33
	2	1.4725	1.9600	1.33
	4	1.4725	1.9600	1.33
	6	1.4800	1.9600	1.32
	7	1.4800	1.9900	1.34
	8	1.4875	1.9900	1.34
	9	1.4875	1.9900	1.34
ON	0	1.5925	2.0300	1.27
	2	1.5925	2.0200	1.27
	4	1.5850	2.0200	1.27
	6	1.5850	2.0125	1.27
	7	1.5850	2.0500	1.29
	8	1.5550	1.9975	1.28
	9	1.5175	1.9900	1.31

The new design provides an area reduction of 61% for the first resonant frequency and 26% for the second, compared to standard rectangular patch antenna. Maximum bandwidths up to 3.3% and 4.27% respectively, have been obtained in the two modes, in ON and OFF states.

4.2.2.2 Loading Effect of PIN Diode on Antenna Resonant Frequencies

The experimental results obtained are then verified with the method of moment simulation tool. Although the previous results suggest that the input impedance of the proposed dual frequency microstrip antenna is almost unaffected when ideal switches are used, this is not the case when these ideal switches are substituted by PIN diodes. Even though the loading effects are small compared to that of the variations in resonant frequencies due to the electrical length variations of the slot arm, they are not negligible in the OFF and ON states. It can be seen from table 4.7 that the loading of the PIN diode causes slight shifts in operating frequencies compared to the passive design described in section 4.1.

The PIN diode loading primarily affects the resonant frequency and matching properties of the microstrip patch in the ON and OFF states. This can be understood by properly modeling the PIN diode in ON and OFF states. At high RF frequencies when a PIN diode is in the OFF state or reverse bias, it appears as a parallel plate capacitor, essentially independent of reverse voltage. When it is ON or forward biased, it in effect acts as a small resistance. Therefore full wave method of moment simulation tools is used to model the PIN diode in OFF and ON states. In the OFF state the PIN diode is modeled as a MIM capacitor while in the ON state as a thin film resistor. The ideal resistance and capacitance values are taken from the application notes of the PIN diode manufacturer.

The simulated and experimental results show good agreement for all the diode positions as seen in table 4.8. The typical return loss behavior of the newly designed reconfigurable microstrip antenna with the PIN positioned at 0.7mm is simulated and plotted in fig. 4.22. ($L = 4\text{cm}$, $l_1 = l_2 = 0.8\text{cm}$, $l_u = 1.1\text{cm}$, $w_a = 0.1\text{cm}$, $b = 0.16\text{cm}$ and $\epsilon_r = 3.98$). In the OFF state, the simulated resonant frequencies closely resemble the experimental ones. An error of 0.2082% and 2.7659% are observed for the first and second resonant frequencies, respectively in

the PIN diode ON state. The small discrepancy in the ON state second resonant frequency is mainly due to the neglected parasitic element effects which are important in higher frequencies.

Table 4.8 Comparison of experimental and simulated (IF3D) resonant frequencies for PIN diode ON and OFF states

Pin diode position (mm)	First resonant frequency, f_1 (GHz) - ON		% error, f_1	Second resonant frequency, f_2 (GHz) - ON		% error, f_2
	Experimental	Simulated		Experimental	Simulated	
0	1.5925	1.5917	0.0502	2.0300	1.9950	1.7241
2	1.5925	1.5909	0.0100	2.0200	1.9950	1.2376
4	1.5850	1.5843	0.0442	2.0200	1.9950	1.2376
6	1.5850	1.5750	0.6309	2.0125	1.9950	0.8696
7	1.5850	1.5817	0.2082	2.0500	1.9933	2.7659
8	1.5550	1.5513	0.2379	1.9975	1.9931	0.2203
9	1.5175	1.5200	-0.1647	1.9900	1.9930	-0.1508

Pin diode position (mm)	First resonant frequency, f_1 (GHz) - OFF		% error, f_1	Second resonant frequency, f_2 (GHz) - OFF		% error, f_2
	Experimental	Simulated		Experimental	Simulated	
0	1.4725	1.4820	-0.6452	1.9600	1.9990	-1.9897
2	1.4725	1.4820	-0.6452	1.9600	1.9990	-1.9897
4	1.4725	1.4820	-0.6452	1.9600	1.9990	-1.9897
6	1.4800	1.4820	-0.1351	1.9600	1.9990	-1.9897
7	1.4800	1.4820	-0.1351	1.9900	1.9990	-0.4523
8	1.4875	1.4820	0.3697	1.9900	1.9990	-0.4523
9	1.4875	1.4820	0.3697	1.9900	1.9990	-0.4523

It has been observed that the matching level of the dual operating frequencies deteriorates as the PIN diode resistance in ON state increases. However, this effect is insignificant in the experiment and good matching levels better than -18dB is observed for the dual resonant frequencies. Therefore, it is concluded that the matching properties of the proposed reconfigurable microstrip patch antenna solely

depend on the slot arm orientation and the position of the PIN diode on it. Thus no matching network is needed for the frequency switching.

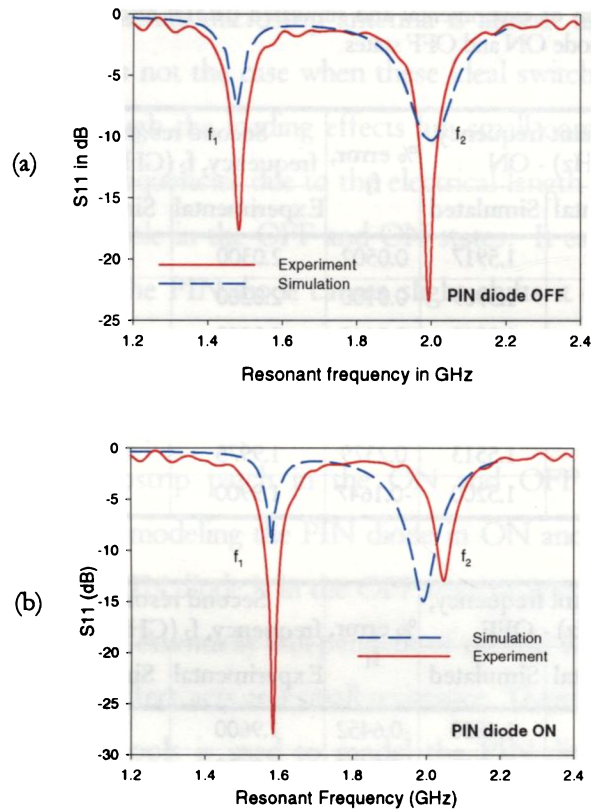


Figure 4.22 Experimental and simulated (IE3D) return loss of the PIN diode controlled reconfigurable microstrip antenna in (a) OFF and (b) ON states. The diode is positioned at 0.7mm from the hexagonal slot.

4.2.2.3 Theoretical Analysis of Reconfigurable Microstrip Antenna using FDTD

Theoretical analysis of the PIN diode controlled single slot arm hexagonal slot loaded microstrip antenna is carried out using the finite difference time domain (FDTD) method. Fine meshing with cell size 0.4mm for all three spatial directions are taken. When the PIN diode is in the OFF state, it is removed from the simulation and when the diode is in the ON state, it is modeled as a

metal tape with electric field components assigned with zero values. Gaussian pulse is then applied at the feed point and boundary conditions are defined as described earlier in chapter-3. The FDTD computed electric field distribution in the entire domain for the PIN diode ON state of the reconfigurable antenna is depicted in fig. 4.23.

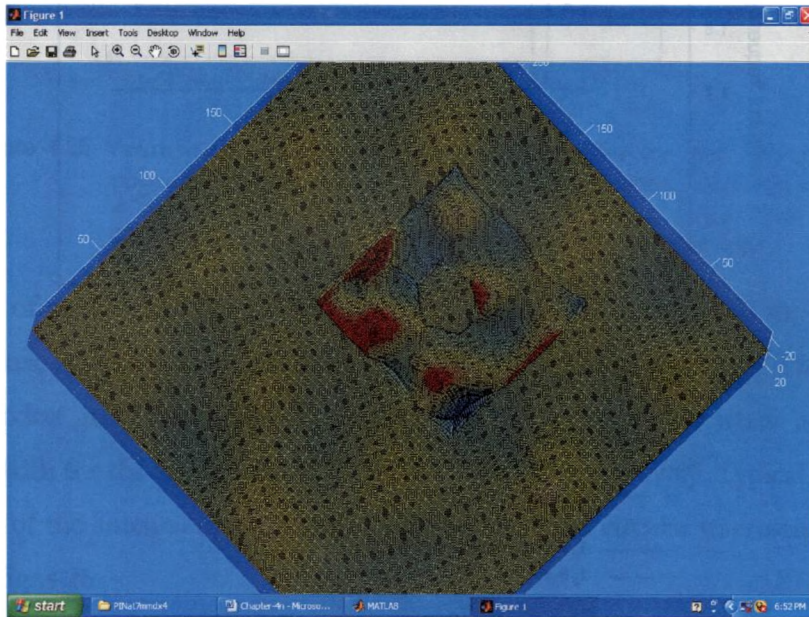


Figure 4.23 Theoretically computed (FDTD) surface electric field distribution in the entire computational domain when the PIN diode is in the ON state

Computed S11 for the dual resonant modes is then plotted against different PIN diode positions both in ON and OFF states. A comparison between the measured and theoretically calculated (FDTD) computed resonant frequencies are shown in fig. 4.24. Even though the first resonant mode shows close resemblance with the experimental values, some discrepancies occurred in the second resonant mode. This is mainly attributed to the assumption of perfect conducting metal tape or perfect 'open', made in the ON and OFF states of the

PIN diode, respectively. In reality, the PIN diode behaves as if it were a resistor in the ON state and as a capacitor in the OFF state.

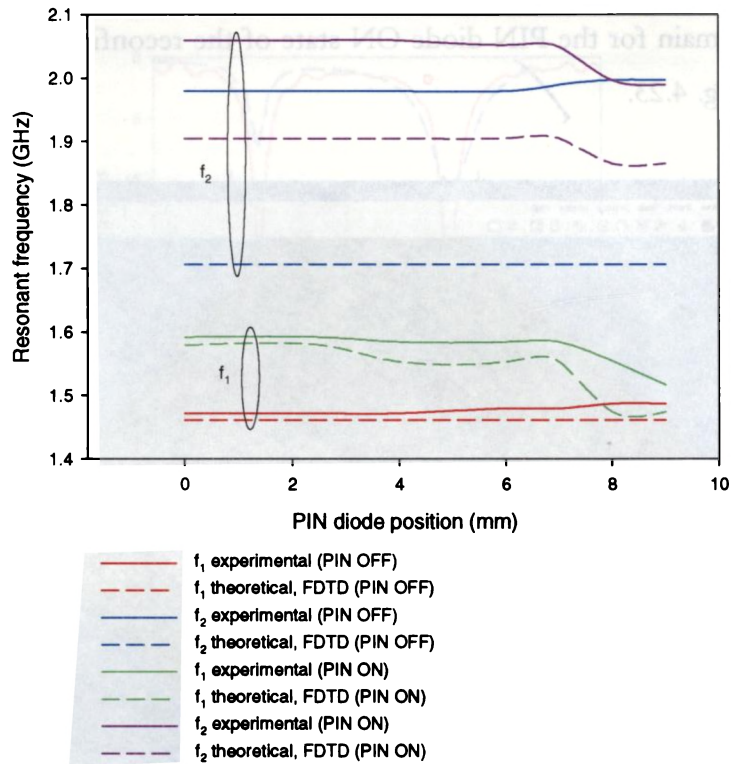


Figure 4.24 Comparison of experimental and theoretically (FDTD) computed dual resonant frequency values for PIN ON and PIN OFF states of the proposed reconfigurable antenna.

4.2.2.4 Polarization and Gain

The transmission characteristics (S12) of the designed reconfigurable microstrip antenna in two mutually orthogonal polarization planes are studied, for different diode states, in order to prove the dual polarization characteristics. The measured data is plotted in fig. 4.25. It can be seen that the polarization planes of the two resonant frequencies are mutually orthogonal in both states of the PIN diode.

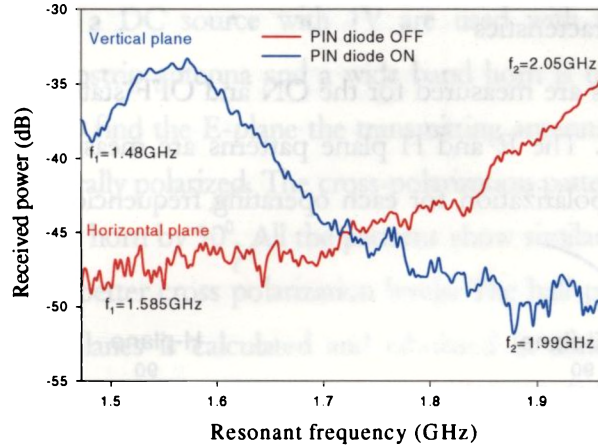


Figure 4.25 Variation of received power with frequency for the two orthogonal polarization planes for both diode states. The antenna parameters are $L = 4\text{cm}$, $l_1 = l_2 = 0.8\text{cm}$, $l_a = 12\text{cm}$, $w_a = 0.1\text{cm}$, $b = 0.16\text{cm}$ and $\epsilon_r = 3.98$. PIN diode is placed at 0.7mm from the hexagon edge.

The gain of the antenna for the dual operating frequencies is measured for both PIN diode states, using the gain comparison method described in chapter-3. The antenna offers modest gain of 2.852dBi and 3.121dBi for the first resonant mode and 3.1dBi and 3.434dBi for the second, for ON and OFF states, respectively. Typical measured gain plot of the antenna in comparison with the standard circular microstrip patch is given in fig. 4.26.

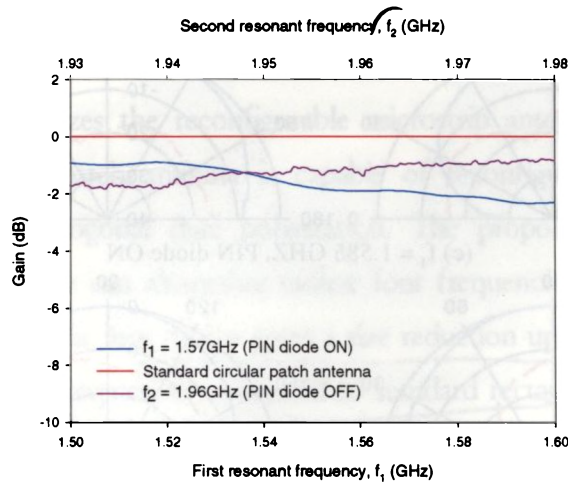


Figure 4.26 Measured gain of the single slot arm reconfigurable dual frequency microstrip antenna at $f_1=1.57\text{GHz}$ (PIN ON) and $f_2 = 1.96\text{GHz}$ (PIN OFF). The antenna parameters are $L = 4\text{cm}$, $l_1 = l_2 = 0.8\text{cm}$, $l_a = 12\text{cm}$, $w_a = 0.1\text{cm}$, $b = 0.16\text{cm}$ and $\epsilon_r = 3.98$. PIN diode is placed at 0.7mm from the hexagon edge.

4.2.2.5 Radiation Characteristics

The radiation patterns are measured for the ON and OFF states of the diode and displayed in fig. 4.27. The E and H plane patterns are measured as well as the corresponding cross-polarization for each operating frequencies in the PIN OFF and ON states.

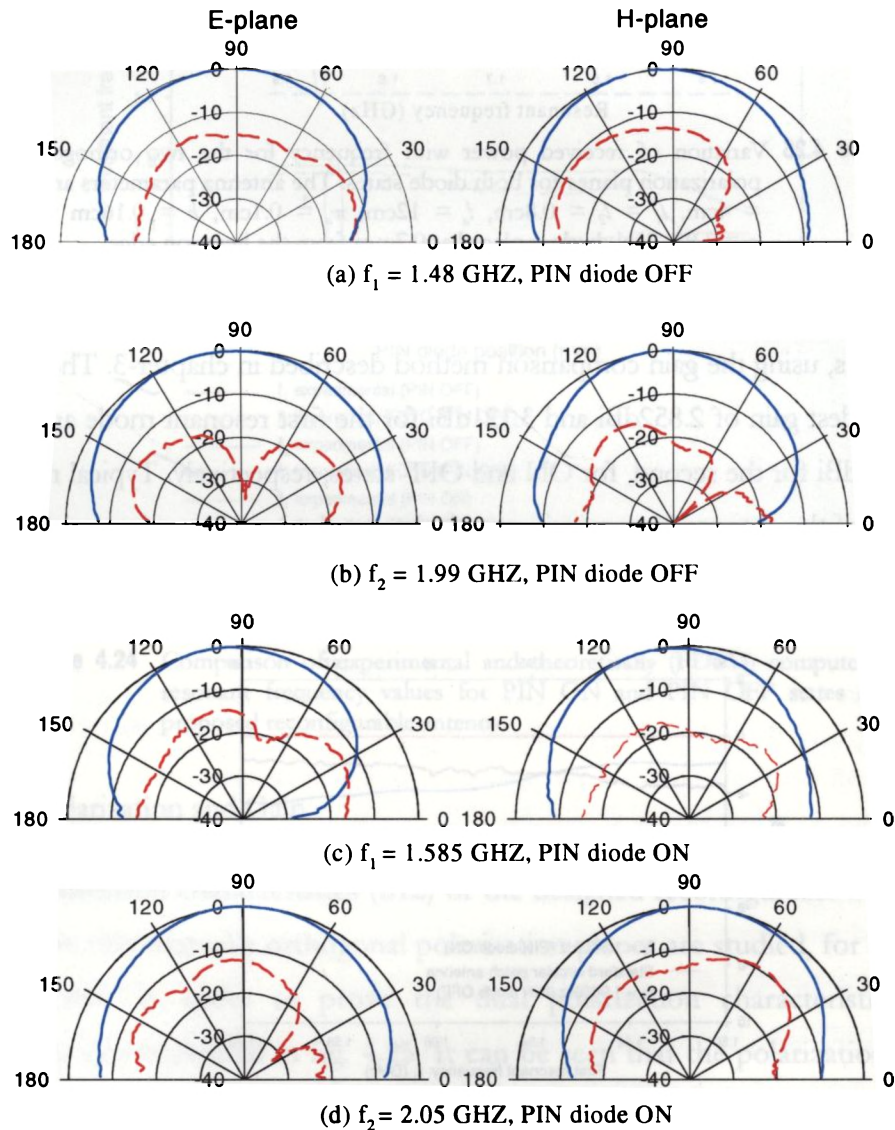


Figure 4.27 Measured radiation pattern of the single slot arm loaded reconfigurable antenna controlled by PIN diodes

An RF signal and a DC source with 1V are used with the newly designed reconfigurable microstrip antenna and a wide band horn is used as the receiving antenna. In order to find the E-plane the transmitting antenna is rotated until the electric field is vertically polarized. The cross-polarization patterns are measured by rotating the receiver horn by 90°. All the patterns show similar broadside radiation characteristics with better cross polarization levels. The half power beam-width in the two principal planes is calculated and tabulated in table 4.9. The radiation efficiency of the reconfigurable antenna is found to be 51% for f_1 and 60% for f_2 .

Table 4.9 Measured half-power beam-width in the two principal planes

Half-power Beam width (°)				
	First resonant frequency, f_1		Second resonant frequency, f_2	
	ON	OFF	ON	OFF
E-Plane	76	92	92	102
H-Plane	78	88	88	68

4.2.2.6 Summary of the Characteristics of Single Slot Reconfigurable Microstrip Antenna with PIN diode

Table 4.10 summarizes the reconfigurable microstrip antenna parameters. This novel, single feed patch antenna is capable of reconfigurable dual frequency operation, and orthogonal dual polarization. The proposed antenna with an integrated PIN diode can altogether radiate four frequencies with almost similar radiation patterns. The new design gives a size reduction up to 61% and 26% for the two resonating frequencies compared to standard rectangular patches. Also it gives considerable bandwidth up to 3.3% and 4.27%, for the two frequencies with a low operating frequency ratio in ON and OFF states of the PIN diode without much reduction in gain.

Table 4.10 Summary of single slot arm reconfigurable microstrip antenna parameters

Antenna parameters	Single slot arm loaded reconfigurable antenna	
Antenna geometry	$L = 4\text{cm}$, $l_1 = l_2 = 0.8\text{cm}$, $l_s = 12\text{cm}$, $w_s = 0.1\text{cm}$, $b = 0.16\text{cm}$ and $\epsilon_r = 3.98$	
Metallization area	13.64cm ²	
No. of slot arms	1	
Non-linear device used for switching	PIN diode – BAR63	
Antenna properties	TM ₁₀	TM ₀₁
Maximum % bandwidth	2.80	4.28
Maximum % area reduction	61	26
Maximum shift in frequency	105MHz	60MHz
% Tuning range	11.8	3.6

4.2.3 Dual Slot Arm Reconfigurable Microstrip Antenna Design for Tunable Frequency Ratio

Dual frequency multipolarization microstrip antennas have wide applications in satellite base communication, air route surveillance, GPS and mobile satellite personal communication systems. Reconfigurable microstrip antennas can be used to cover these multiple functions with a single antenna aperture. All these applications need a compact reconfigurable microstrip antenna having better bandwidth and easy switching capabilities. It has been proved in section 4.1.9 that the use of dual vertical slot arms can effectively tune the first resonant frequency without much affecting the second one. That is, the additional vertical slot arm will provide better frequency ratio tuning and size reduction. Dual slot arm geometry as described in fig. 4.14 is then studied for its tunable frequency ratio capability. The two slots are carved identical in length and breadth. The locations of the two slots are chosen with the help of method of moment software so as to minimize the variation on the other second resonant mode (TM₀₁), and thereby increasing the frequency ratio tuning.

Two PIN diodes are embedded in the arms of the central hexagonal slot to switch the two resonant frequencies of the antenna, considerably, by changing the electrical length of the slot. Thus multiple frequencies are generated in a single antenna aperture by controlling the DC bias of the two PIN diodes. Transmission lines are avoided in between the active components and the radiating element, so that, added noise and ohmic losses are suppressed and the resulting structure is more compact. The new design has the added advantage of high area reduction, better bandwidth and good matching for all operating frequencies compared to conventional microstrip patch antennas and offers a high flexibility in frequency tuning. Another attractive feature is that the antenna shows almost similar radiation patterns at all operating frequencies without much reduction in gain.

4.2.3.1 Antenna Configuration

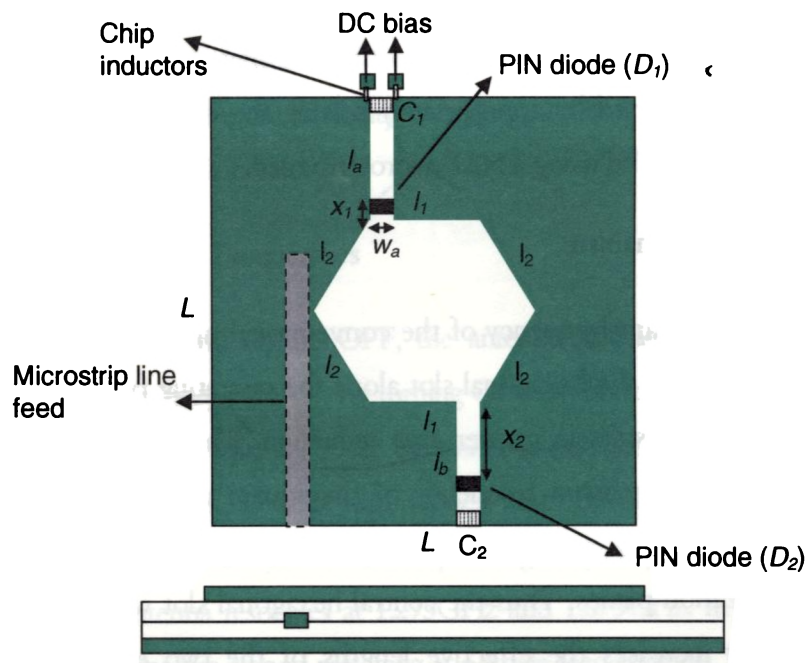


Figure 4.28 Layout of the dual slot arm loaded reconfigurable microstrip antenna. The antenna parameters are $L = 4\text{cm}$, $l_1 = l_2 = 0.8\text{cm}$, $x_1 = 0\text{cm}$, $x_2 = 0.8\text{cm}$, $l_a = l_b = 1.2\text{cm}$, $w_a = 0.1\text{cm}$, $b = 0.16\text{cm}$ and $\epsilon_r = 3.98$

The configuration of the proposed reconfigurable microstrip patch antenna with dual arm hexagonal slot is illustrated in the fig. 4.28. A square microstrip patch antenna with side dimension L is fabricated on a substrate of thickness b and relative permittivity ϵ_r . A hexagonal slot of side parameters l_1 and l_2 with two identical slot arms of length l_1 and l_2 and width w_s , extending up to the edge of the square patch is placed at its center. Two surface mount PIN diodes, D_1 and D_2 are positioned at the slot arms with distances x_1 and x_2 respectively from the hexagonal side. The positions of the diodes x_1 and x_2 can be suitably chosen to get the desired frequency ratio. Good DC isolation and RF continuity is obtained by embedding two smd capacitors C_1 and C_2 on the protruding slot arms as shown in the fig. 4.28.

DC bias voltage is applied to the patch through two chip inductors, which controls the PIN diode status. The diodes are placed in such a way that one is forward biased and the other in reverse at a time, so that resonant frequency of the antenna can be selected by appropriately biasing the diodes. The antenna is electromagnetically coupled using a 50Ω microstrip feed.

4.2.3.2 Operational Mechanism

The fundamental resonant frequency of the conventional unslotted square patch is 1.884GHz. By loading the hexagonal slot alone the operating frequency can be lowered to 1.74GHz, results in greater area reduction. The extended slot arms splits the fundamental resonant frequency of the square microstrip patch with hexagon alone, into two separate resonant modes, TM_{10} and TM_{01} with orthogonal polarization planes. Thus the central hexagonal slot with the two slot arms considerably increases the effective lengths of the two excited resonant modes, TM_{10} and TM_{01} , and the excited patch surface current densities are perturbed in such a way that these two modes can be excited for dual frequency operation with a single feed. The length of the slot arms determines the frequency

ratio of the two operating frequencies and a constant frequency ratio will be maintained for same slot arm lengths. Thus desired frequency reconfiguration can be readily achieved by switching the two slots with different lengths, by embedding the PIN diodes.

When the PIN diode is ON, it essentially behaves as equivalent short circuit, thus driving the currents on the patch directly through it, reducing the effective length of the slot. Since D_1 and D_2 are placed at x_1 and x_2 , in order to achieve different slot lengths, dual frequency generation is accomplished by different frequency ratios, depending on which diode is forward biased. When both diodes are off, the currents have to flow through the capacitors C_1 and C_2 , with an increased current path, resulting in the shifting of resonant frequencies towards lower frequency region with another frequency ratio. The advantage of this design is that the PIN diodes can be placed at any position of the two slot arms for different x_1 and x_2 values, without much affecting the good return loss characteristics and bandwidth, for a single feed position. This property of the design gives more flexibility in frequency tuning where frequency ratio varies in a wider range of 1.2 to 1.4.

4.2.3.3 Antenna Resonant Frequencies

When both diodes, D_1 and D_2 are OFF, the antenna resonates at 1.21GHz and 1.675GHz with a frequency ratio 1.4. By turning ON the diode D_1 , positioned at $x_1 = 0$ mm, the first resonant frequency shifts by 150MHz and second by 5MHz giving excitations at 1.36GHz and 1.67GHz with a much lower frequency ratio 1.2. Also by keeping D_2 ON, positioned at $x_2 = 8$ mm, the operating frequency ratio can be brought to 1.29, where the antenna resonates at 1.295GHz and 1.675GHz. In all these three diode states the antenna has a good matching at a single feed position. Fig. 4.29 shows the measured return loss (S11) of the antenna with dimensions $L = 4$ cm, $l_1 = l_2 = 0.8$ cm, $x_1 = 0$ cm, $x_2 = 0.8$ cm, $w_d = 0.1$ cm, $h = 0.16$ cm and $\epsilon_r = 3.98$.

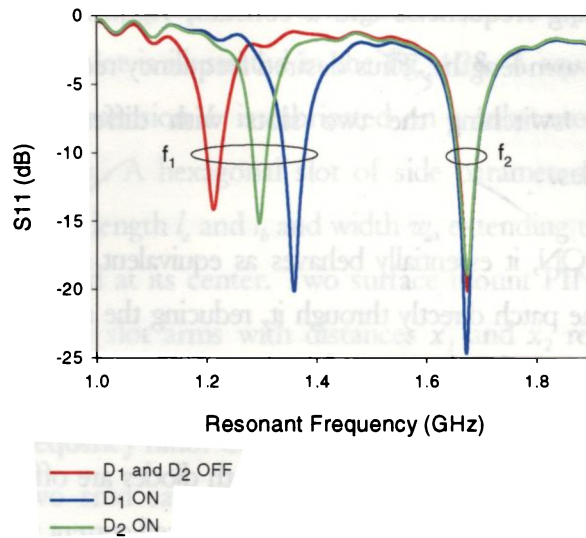


Figure 4.29 Measured return loss of the antenna for all the three PIN diode states. ($L= 4\text{cm}$, $l_1 = l_2= 0.8\text{cm}$, $x_1= 0\text{cm}$, $x_2= 0.8\text{cm}$, $w_a= 0.1\text{cm}$, $h= 0.16\text{cm}$ and $\epsilon_r= 3.98$).

Table 4.11 Measured resonant frequencies and corresponding -10dB bandwidths

PIN diode state	Resonant frequency (GHz)		% Bandwidth		Frequency ratio, f_2/f_1
	f_1	f_2	f_1	f_2	
D1 D2 OFF	1.210	1.675	2.250	2.190	1.4
D1 ON	1.360	1.670	2.820	2.415	1.2
D2 ON	1.295	1.675	2.050	2.203	1.3

The percentage bandwidths of the switchable resonant frequencies are better than 2% in all diode states. The experimental observations corresponding to each PIN diode bias configurations are given in table 4.11.

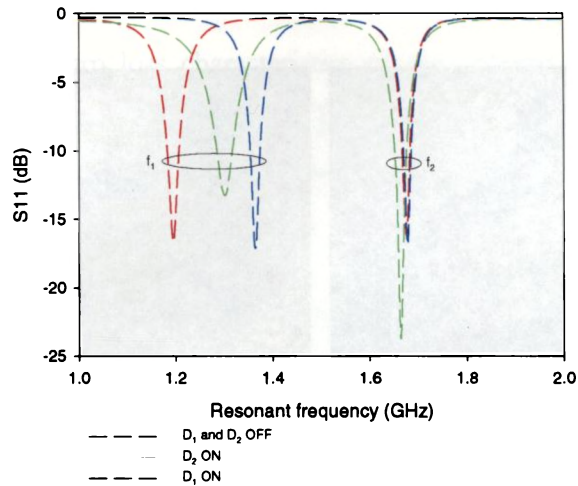


Figure 4.30 Simulated (IE3D) return loss of the antenna for all the three PIN diode states. ($L= 4\text{cm}$, $l_1 = l_2= 0.8\text{cm}$, $x_1= 0\text{cm}$, $x_2= 0.8\text{cm}$, $w_a= 0.1\text{cm}$, $h= 0.16\text{cm}$ and $\epsilon_r= 3.98$).

Figure 4.30 shows the simulated results for the dual slot arm loaded reconfigurable microstrip antenna and it almost strictly agrees with the experimental results. Here the PIN diode ON state is simulated as thin film resistor and OFF state as metal-insulator-metal (MIM) capacitor.

The theoretically (FDTD) computed surface current distribution at different PIN diode states are illustrated in fig. 4.31 and 4.32.

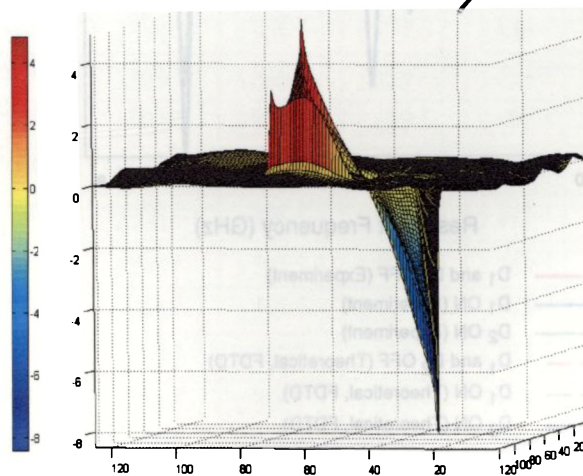


Figure 4.31 3-dimensional electric field distributions in the surface of the patch in D1 and D2 OFF state showing the excited resonant modes

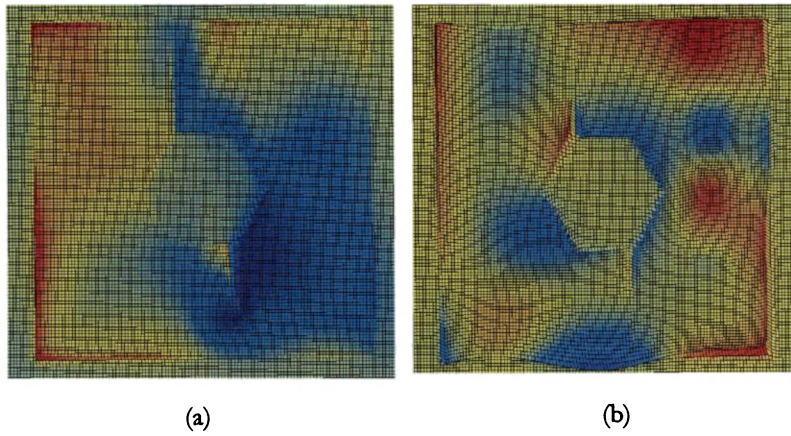


Figure 4.32 FDTD computed surface current distribution for (a) PIN D2 ON and (b) D1 & D2 OFF

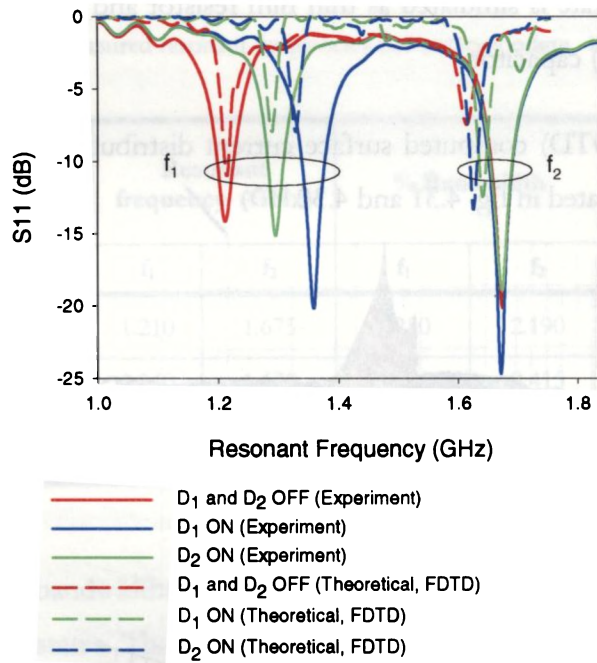


Figure 4.33 Measured and theoretical (FDTD) computed return loss behavior of the reconfigurable microstrip antenna with two vertical slot arms

The computed return loss characteristics of the antenna at different PIN diode configurations are given in fig. 4.33. The measured and computed results show almost close agreement. The discrepancy at the second resonant mode is mainly due to the absence of any loading effect in the FDTD model.

4.2.3.4 Study on reconfigurable resonant frequency variations with different x_1 and x_2 combinations

As stated earlier, it is confirmed that the selection of the PIN diode positions, x_1 and x_2 , in the protruding dual vertical slot arms mainly determines the operating dual resonant frequencies. Thus different switchable operating frequencies (and hence different frequency ratios), can be duly selected by choosing the right combination of x_1 and x_2 . A complete study on this is carried out and the findings are tabulated in table 4.12.

Table 4.12 Variation in dual frequency operation with PIN diode position (antenna shown in fig. 4.28)

Diode positions		Resonant frequencies					
		D ₁ D ₂ OFF		D ₁ ON		D ₂ ON	
x ₁ (mm)	x ₂ (mm)	f ₁ (GHz)	f ₂ (GHz)	f ₁ (GHz)	f ₂ (GHz)	f ₁ (GHz)	f ₂ (GHz)
10	0	1.210	1.675	1.245	1.670	1.370	1.670
	2	1.210	1.670	1.245	1.675	1.370	1.670
	4	1.215	1.670	1.245	1.670	1.360	1.670
	6	1.215	1.670	1.250	1.670	1.345	1.670
	8	1.220	1.670	1.255	1.670	1.315	1.675
	10	1.225	1.675	1.260	1.670	1.285	1.675
7	0	1.210	1.670	1.280	1.670	1.365	1.670
	2	1.210	1.675	1.285	1.670	1.360	1.670
	4	1.215	1.675	1.285	1.670	1.350	1.675
	6	1.215	1.670	1.290	1.670	1.335	1.670
	8	1.220	1.675	1.290	1.670	1.305	1.670
	10	1.225	1.675	1.295	1.670	1.275	1.675
5	0	1.205	1.665	1.305	1.665	1.365	1.670
	2	1.205	1.665	1.305	1.665	1.360	1.670
	4	1.205	1.665	1.310	1.670	1.350	1.665
	6	1.210	1.665	1.310	1.670	1.335	1.665
	8	1.215	1.670	1.315	1.665	1.305	1.665
	10	1.220	1.665	1.320	1.665	1.275	1.665
2	2	1.205	1.675	1.335	1.675	1.350	1.675
	4	1.210	1.675	1.340	1.670	1.340	1.670
	6	1.215	1.675	1.345	1.670	1.320	1.675
	8	1.215	1.675	1.350	1.670	1.295	1.675
	10	1.215	1.675	1.350	1.670	1.265	1.675
0	8	1.210	1.675	1.360	1.670	1.295	1.675
	10	1.215	1.675	1.365	1.675	1.265	1.675

Table 4.13 Variation in impedance bandwidth with PIN diode position (antenna shown in fig. 4.28)

Diode positions		% Bandwidth					
		D ₁ D ₂ OFF		D ₁ ON		D ₂ ON	
X ₁ (mm)	X ₂ (mm)	f ₁	f ₂	f ₁	f ₂	f ₁	f ₂
10	0	2.459	2.7021	2.590	2.860	1.817	3.000
	2	2.398	3.029	2.527	1.910	2.015	3.593
	4	2.595	3.353	2.643	3.659	1.870	3.793
	6	2.490	2.800	2.650	.754	1.911	2.800
	8	2.577	2.528	2.641	2.611	2.395	2.677
	10	2.531	2.660	2.587	2.546	2.286	2.746
7	0	2.314	2.259	2.620	2.326	1.573	2.390
	2	2.327	2.290	2.646	2.275	1.663	2.335
	4	2.331	2.300	2.665	2.302	1.745	2.300
	6	2.355	2.291	2.700	2.368	1.950	2.360
	8	2.410	2.329	2.731	2.326	2.187	2.360
	10	2.286	2.240	2.734	2.300	2.200	2.275
5	0	2.184	2.631	2.870	3.305	1.688	3.132
	2	2.249	3.070	2.790	3.104	1.100	3.642
	4	2.276	2.475	2.815	3.234	1.130	2.836
	6	2.271	2.909	2.879	3.600	0.900	2.800
	8	2.329	3.000	2.830	3.130	1.635	3.200
	10	2.361	2.787	2.864	3.271	1.834	3.171
2	2	2.178	2.209	2.854	2.388	1.585	2.300
	4	2.241	2.245	2.843	2.491	1.739	2.287
	6	2.243	2.201	2.806	2.364	1.980	2.215
	8	2.263	2.257	2.837	2.413	2.072	2.239
	10	2.315	2.328	2.864	2.473	2.121	2.353
0	8	2.250	2.190	2.820	2.415	2.050	2.203
	10	2.280	2.155	2.817	2.403	2.067	2.180

Table 4.14 Percentage area reduction of the dual slot arm reconfigurable antenna design (antenna shown in fig. 4.28)

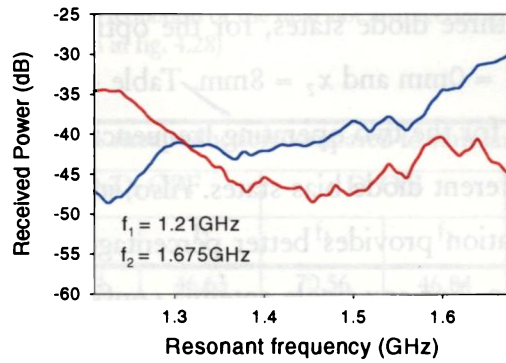
Diode positions		% Area reduction compared to standard circular patch					
		D ₁ D ₂ OFF		D ₁ ON		D ₂ ON	
X ₁ (mm)	X ₂ (mm)	f ₁	f ₂	f ₁	f ₂	f ₁	f ₂
10	0	72.21	46.63	70.56	46.84	64.32	46.84
	2	72.21	46.84	70.56	46.63	64.32	46.84
	4	71.93	46.84	70.56	46.84	64.83	46.84
	6	71.93	46.84	70.30	46.84	65.61	46.84
	8	71.73	46.84	70.03	46.84	67.14	46.63
	10	71.49	46.63	69.81	46.84	68.61	46.63
7	0	72.21	46.84	68.90	46.84	64.55	46.84
	2	72.21	46.63	68.61	46.84	64.83	46.84
	4	71.93	46.63	68.61	46.84	65.33	46.63
	6	71.93	46.84	68.37	46.84	66.10	46.84
	8	71.73	46.63	68.37	46.84	67.60	46.84
	10	71.49	46.63	68.13	46.84	69.11	46.63
5	0	73.00	47.15	67.60	47.15	64.55	46.84
	2	73.00	47.15	67.60	47.15	64.83	46.84
	4	73.00	47.15	67.39	46.84	65.33	47.15
	6	72.21	47.15	67.39	46.84	66.10	47.15
	8	71.93	46.84	67.14	47.15	67.60	47.15
	10	71.73	47.15	66.90	47.15	69.11	47.15
2	2	73.00	46.63	66.10	46.63	65.33	46.63
	4	73.00	46.63	65.83	46.84	65.83	46.84
	6	72.21	46.63	65.61	46.84	66.90	46.63
	8	71.93	46.63	65.33	46.84	68.13	46.63
	10	71.93	46.63	65.33	46.84	69.59	46.63
0	8	72.21	46.63	64.83	46.84	68.13	46.63
	10	71.93	46.63	64.55	46.63	69.59	46.63

Bandwidths up to 2.82% and 2.42% respectively, have been obtained in the two modes, in all the three diode states, for the optimized design with PIN diodes positioned at $x_1 = 0\text{mm}$ and $x_2 = 8\text{mm}$. Table 4.13 gives the measured percentage bandwidths for the two operating frequencies with different x_1 and x_2 combinations, at different diode bias states. Also, it must be noted that the dual slot arm configuration provides better percentage bandwidths than that of single slot arm design. For any single antenna configuration all frequencies have improved percentage bandwidths than the single slot arm design.

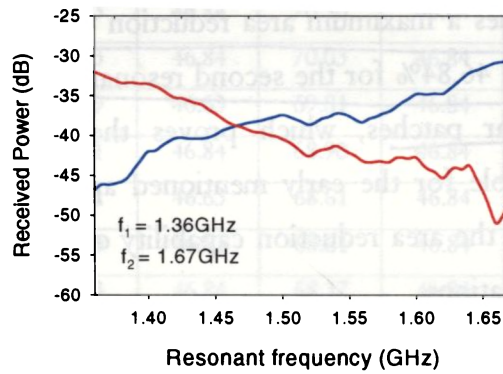
The new design provides a maximum area reduction of 72.21% for the first resonant frequency and 46.84% for the second resonant frequency, compared to standard rectangular patches, which proves the compactness of the proposed design, suitable for the early mentioned applications in L- band. Table 4.14 summarizes the area reduction capability of the designed antenna for all x_1 and x_2 combinations.

4.2.3.5 Antenna Polarization and Gain

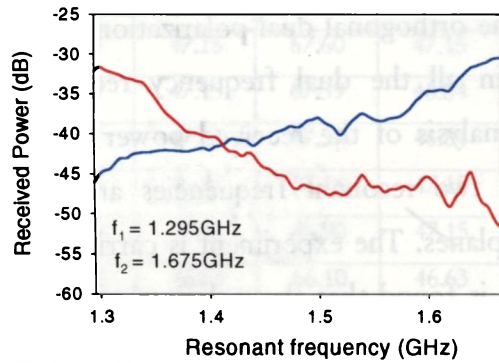
It is already said that the orthogonal dual polarization of the original passive antenna is preserved in all the dual frequency reconfigurable microstrip antenna designs. The analysis of the received power in the two orthogonal planes reveals that the two resonant frequencies are linearly polarized in mutually perpendicular planes. The experiment is carried out for all the three PIN diode states and it is found that the polarizations of the two operating frequencies are essentially same in all the diode states. The observations are plotted in fig. 4.34.



(a)



(b)



(c)

— Vertical plane
— Horizontal plane

Figure 4.34 Variation of received power with frequency for the two orthogonal polarization planes for all the three pin diode states. (a) D_1 and D_2 OFF (b) D_1 ON (c) D_2 ON

Gain measurements are carried out using the gain comparison method with standard circular patches fabricated in the dielectric substrate of $\epsilon_r = 3.98$. For the first resonant frequency the gain is found to be 3.63dBi and 3.57dBi respectively, when D_1 and D_2 are ON. In the case of second resonant frequency it is 5.6dBi and 5.4dBi when D_1 and D_2 are ON, respectively. When both the diodes are OFF, the measured gain for first resonant frequency is 3.38dBi and that of second resonant frequency is 5.07dBi.

4.2.3.6 Radiation Characteristics

The radiation patterns are measured for three diode states and plotted in fig. 4.35. All the patterns show similar broadside radiation characteristics without any distortion even after the diodes are turned ON, which is highly desirable for frequency reconfigurable antennas. Although the maximum radiation direction shows some slight variations, the power difference between them in all the diode states are below 0.4dB. The measured 3dB beam width for the two resonant frequencies in different PIN diode states are shown in table 4.15. Table 4.16 lists the variation of maximum radiation direction in degrees, for the two operating frequencies in different diode states.

Table 4.15 Measured half-power beam width in degrees for first and second resonant frequencies for all PIN-diode states

	First resonant frequency, f_1			Second resonant frequency, f_2		
	D_1 ON	D_2 ON	D_1 & D_2 OFF	D_1 ON	D_2 ON	D_1 & D_2 OFF
E-Plane	82°	76°	98°	112°	130°	156°
H-Plane	84°	84°	88°	86°	86°	102°

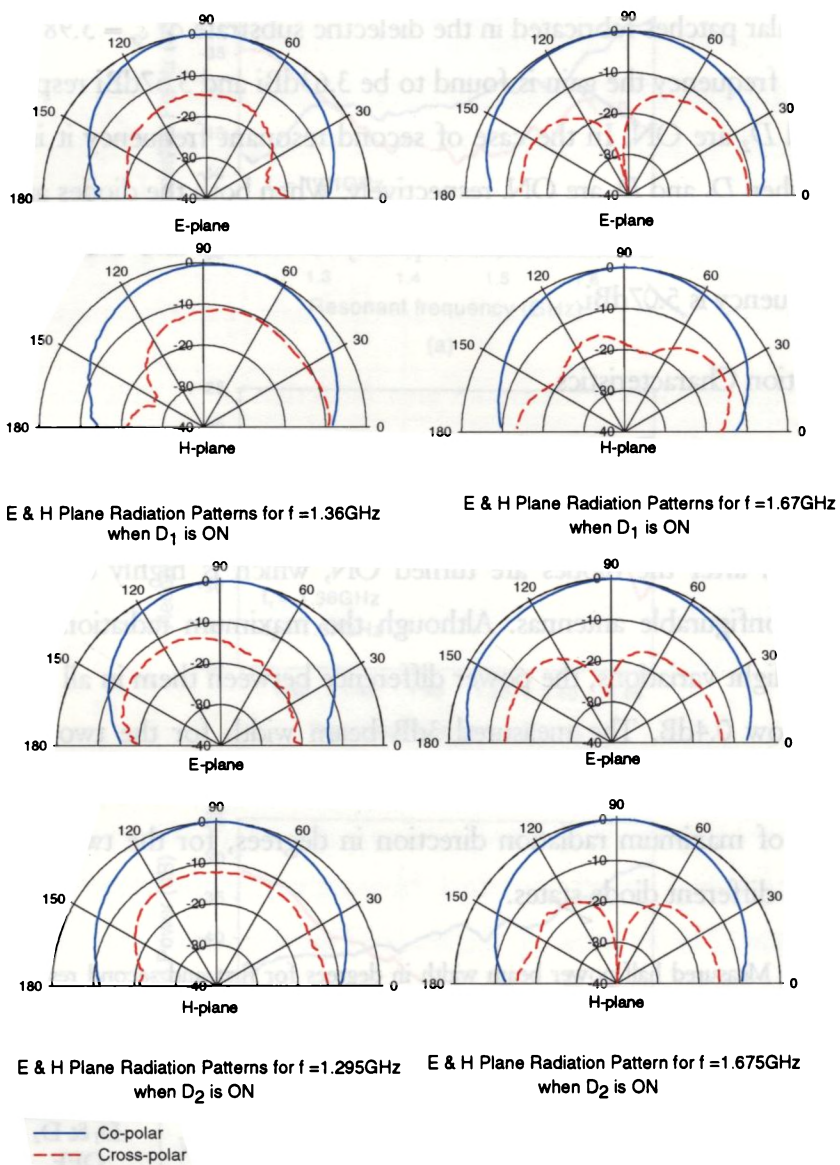


Figure 4.35 Measured E and H plane radiation patterns of the proposed antenna in different PIN diode states (contd. in next page.)

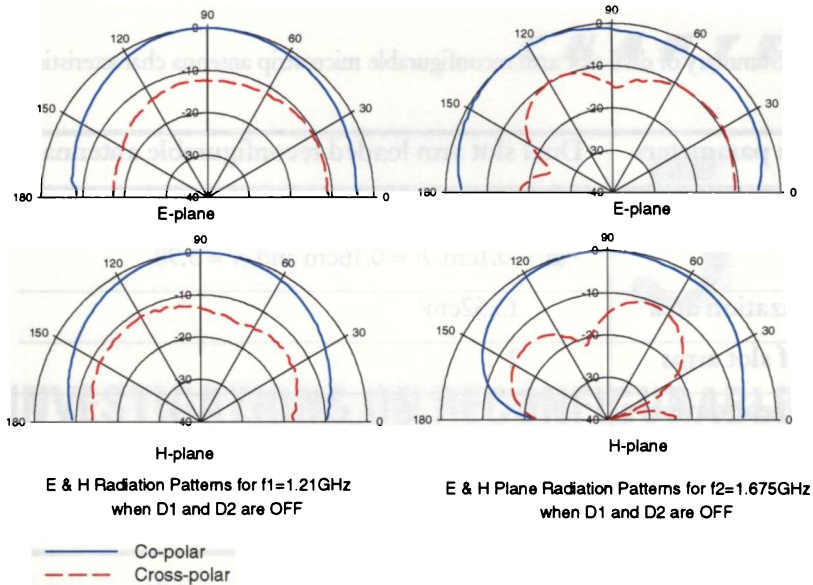


Figure 4.35 Measured E and H plane radiation patterns of the proposed antenna in different pin diode states (contd. from previous page.)

Table 4.16 Maximum radiation direction in degrees for first and second resonant frequencies for all PIN-diode states

	First resonant frequency, f_1			Second resonant frequency, f_2		
	D ₁ ON	D ₂ ON	D ₁ & D ₂ OFF	D ₁ ON	D ₂ ON	D ₁ & D ₂ OFF
E-Plane	83°	83°	91°	98°	87°	98°
H-Plane	77°	85°	87°	84°	85°	95°

The tuning mechanism of the dual slot arm loaded reconfigurable microstrip antenna now becomes more flexible with the choice of two PIN diodes and three different switching combinations. This design allows the electronic switching of first resonant frequency keeping the second mode almost unaltered, giving different frequency ratios. The PIN diodes are placed in such a way that a single bias supply can be used to switch the frequency ratios. Other antenna characteristics are summarized in table 4.17.

Table 4.17 Summary of dual slot arm reconfigurable microstrip antenna characteristics

Antenna parameters	Dual slot arm loaded reconfigurable antenna	
Antenna geometry	$L = 4\text{cm}, l_1 = l_2 = 0.8\text{cm}, l_a = lb = 12\text{cm},$ $w_t = 0.1\text{cm}, b = 0.16\text{cm}$ and $\epsilon_r = 3.98$	
Metallization area	13.52cm ²	
No. of slot arms	2	
Non-linear device used for switching	PIN diode – BAR63	
Antenna properties	TM ₁₀	TM ₀₁
Maximum % bandwidth	2.88	3.79
Maximum % area reduction	73	47
Maximum shift in frequency	150MHz	5MHz
% Tuning range	13.22	0.30

**INVESTIGATIONS ON RECONFIGURABLE DUAL
FREQUENCY MICROSTRIP ANTENNAS USING
VARACTOR DIODES****Contents**

5.1	<i>Varactor Controlled Single Slot Arm Loaded Reconfigurable Dual Frequency Microstrip Antenna</i>	142
5.1.1	<i>Frequency Tuning</i>	143
5.1.2	<i>Variation of Dual Resonant Frequencies with Varactor Reverse Bias</i>	144
5.1.3	<i>Antenna Size Reduction</i>	146
5.1.4	<i>Study of the Resonant Behavior of the Antenna at Different Varactor Positions</i>	146
5.1.5	<i>Polarization, Gain and Radiation Pattern</i>	147
5.2	<i>Computation of Resonant Frequencies of Varactor Tuned Reconfigurable Antenna</i>	150
5.3	<i>Varactor Controlled Reconfigurable Dual Frequency Microstrip Antenna Design for Frequency Ratio Tuning</i>	153
5.3.1	<i>Antenna Geometry</i>	153
5.3.2	<i>Variation of Resonant Frequencies with Varactor Reverse Bias</i>	154
5.3.3	<i>Polarization and Gain</i>	156
5.4	<i>Experimental Investigations on Varactor Loaded Reconfigurable Microstrip Antennas for Enhanced Dual Frequency Tuning and Area Reduction</i>	54
5.4.1	<i>Varactor Controlled Microstrip Antenna with Dual Orthogonal Slot Arms</i>	160
5.4.2	<i>Triple Slot Arm Loaded Reconfigurable Dual Frequency Microstrip Antenna Using Varactors</i>	164
5.4.3	<i>Four Slot Arm Loaded Varactor Controlled Reconfigurable Microstrip Antenna</i>	167
5.4.4	<i>Eight Slot Arm Loaded Varactor Controlled Reconfigurable Microstrip Antenna</i>	171
5.5	<i>Independent Frequency Tuning in Hexagonal Slot Loaded Microstrip Antenna Using Modified Slot Arm</i>	176
5.5.1	<i>C-Shaped Slot Loaded Reconfigurable Microstrip Antenna</i>	176
5.5.2	<i>Meandered Slot Arm Loaded Reconfigurable Microstrip Antenna</i>	181

One of the most important characteristics of frequency reconfigurable antennas is their flexibility in operation. That is, one can easily control their operating frequencies by simply selecting the desired external bias and without bothering about the antenna dimensions. Even though the PIN diode controlled reconfigurable antenna scheme described in the earlier section permits this, a more flexible frequency tuning scheme can be accomplished by replacing the PIN diodes with Varactor diodes.

Here Varactors are integrated with the extended slot arm of the dual frequency microstrip patch antenna. The Varactors provides various capacitive loadings to the microstrip patch. The Varactor junction capacitance varies against the bias voltage and can be calculated from the applied bias voltage as,

$$C = \frac{C_0}{\left(1 - \frac{V}{V_{bi}}\right)^\gamma} \quad (5.1)$$

where, C_0 is the Varactor capacitance at 0V DC bias, V is the applied bias voltage which is -ve for reverse bias, V_{bi} is the built-in potential and γ is a constant depending on the doping profile of the p-n junction [185]. The capacitance value can be decreased by reverse biasing the Varactor diode. These different capacitance loadings correspond to various electrical lengths of the protruding slot arm, thus giving different resonant frequencies. This dual frequency tuning scheme provides fast tuning over a wide frequency range, as is required for many applications. The various designs intended for both reconfigurable dual frequency operation and frequency ratio tuning are presented in detail.

5.1 Varactor Controlled Single Slot Arm Loaded Reconfigurable Dual Frequency Microstrip Antenna

The single slot arm loaded reconfigurable antenna geometry with Varactor diode is exactly similar to the single arm antenna in fig. 4.20, except that the PIN diode is replaced by a Varactor diode. Fig. 5.1 illustrates the antenna layout.

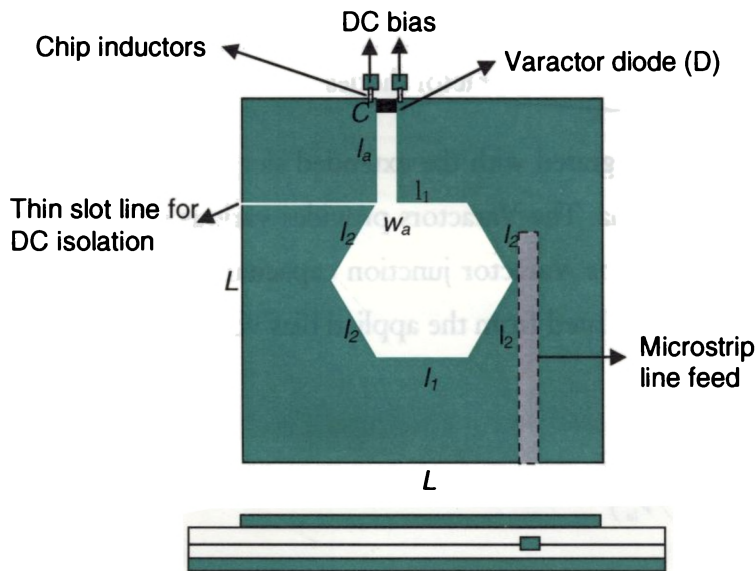


Figure 5.1 Geometry of the single slot arm reconfigurable dual frequency dual polarized microstrip antenna with Varactor diode. The antenna parameters are $L = 4\text{cm}$, $l_1 = l_2 = 0.8\text{cm}$, $l_a = 12\text{cm}$, $w_a = 0.1\text{cm}$, $b = 0.16\text{cm}$ and $\epsilon_r = 3.98$. Varactor diode is placed in the tip of the extending slot arm.

Varactor diode D is positioned at the extreme end of the slot arms in order to get maximum tuning range and better matching. The method of moment software is used to determine its exact position. DC bias voltage is supplied from a battery, through two chip inductors across D . The antenna is then electromagnetically coupled using a 50Ω microstrip line as shown in fig. 5.1. The Varactor diode placed in the protruding slot arm helps to control the current density of the TM_{01} mode which is strongly modified due to the presence of the slot arm.

Varactor embedded in the protruding slot arm provides various capacitive loadings across the slot arms in different reverse bias conditions. The junction capacitance of the Varactor varies against the reverse bias voltage applied and these different capacitive loadings correspond to different electrical lengths and thus different resonant frequencies.

5.1.1 Frequency Tuning

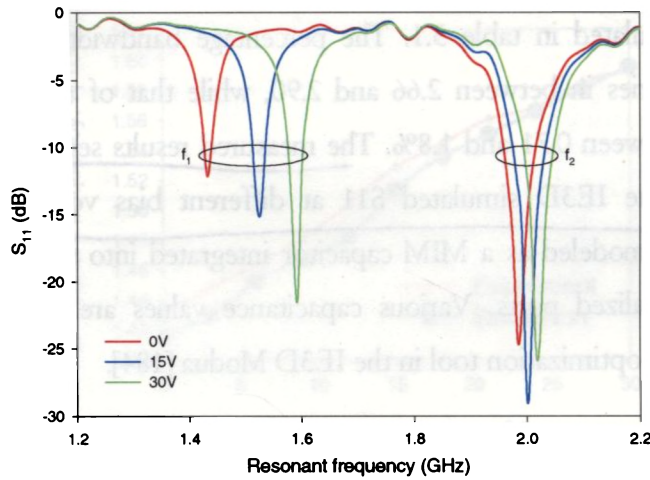


Figure 5.2 Measured return loss of the dual frequency Varactor controlled reconfigurable microstrip antenna for different bias voltage. ($L = 4\text{cm}$, $l_1 = l_2 = 0.8\text{cm}$, $l_s = 1.2\text{m}$, $w_s = 0.1\text{cm}$, $b = 0.16\text{cm}$ and $\epsilon_r = 3.98$)

The Varactor loaded reconfigurable antenna is tested using a HP 8510C Vector Network Analyzer. When the protruding slot arms are absent, the antenna shows a single resonant frequency at 1.74GHz, much lower than the fundamental resonant frequency (1.884GHz) of the unslotted square patch antenna. When the reverse bias is off, the Varactor loading in the two slot arm correspond to high capacitance and thus lower resonant frequencies at 1.432GHz and 1.984GHz with a frequency ratio 1.39. The reconfigurable antenna was then electronically tuned with a reverse DC voltage applied across the diodes. When the bias voltage is varied from 0 to -30V, the tuning range for the first resonant frequency is found to be 11.2% or 160MHz upwards (from 1.4320 to 1.5920GHz) and that of second resonant

frequency is 1.6% or 32MHz upwards (from 1.9840 to 2.0160GHz) as shown in fig. 5.2. At -30V the frequency ratio is found to be 1.27.

5.1.2 Variation of Dual Resonant Frequencies with Varactor Reverse Bias

Continuous tuning of the excited dual resonant frequencies is now possible by varying the applied reverse bias voltage of the Varactor diode. The variation of first and second resonant frequencies and the corresponding percentage bandwidths are measured and tabulated in table 5.1. The percentage bandwidth of the second resonant mode varies in between 2.66 and 2.90, while that of the first resonant mode varies in between 0.71 and 1.8%. The measured results seem to be in good agreement with the IE3D simulated S11 at different bias voltages. Here the Varactor diode is modeled as a MIM capacitor integrated into the extended slot arm with two localized ports. Various capacitance values are assigned to this capacitor using the optimization tool in the IE3D Modua [184].

Table 5.1 Resonant frequencies, percentage bandwidth and frequency ratio of the proposed Varactor tuned antenna with bias voltage

Tuning voltage (V)	Resonant frequency		% Bandwidth		Frequency ratio
	f ₁ (GHz)	f ₂ (GHz)	f ₁	f ₂	
0	1.432	1.984	0.71	2.90	1.39
3	1.448	1.992	0.95	2.90	1.38
6	1.464	1.992	1.06	2.90	1.36
9	1.48	1.992	1.15	2.90	1.35
12	1.504	2.000	1.35	2.92	1.33
15	1.528	2.000	1.50	2.90	1.31
18	1.544	2.008	1.60	2.90	1.30
21	1.56	2.008	1.67	2.81	1.29
24	1.568	2.016	1.74	2.77	1.29
27	1.584	2.016	1.76	2.70	1.27
30	1.592	2.016	1.80	2.66	1.27

Fig. 5.3 shows the dependence of first and second operating frequencies with the applied Varactor reverse bias voltage. In order to compare the measurement and simulated results more easily, the simulated and measured values of the dual operating frequencies are presented together in fig. 5.3. The maximum error between the simulated and measured value of the operating frequencies are 1.2% and 1.0% respectively, for the first and second bands.

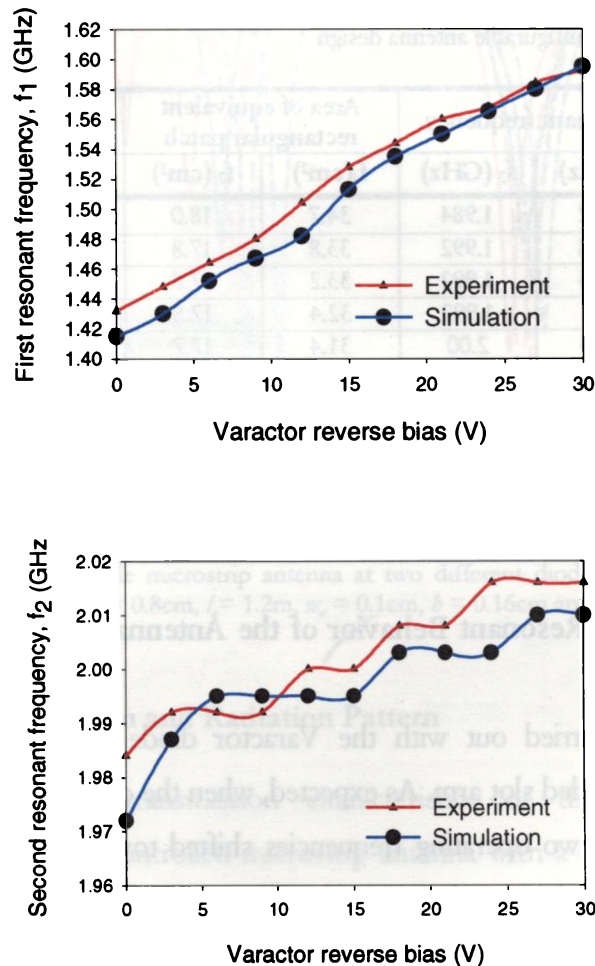


Figure 5.3 Experimental and simulated (IE3D) variation of resonant frequencies with Varactor reverse bias voltage, (a) First resonant frequency, f_1 (b) Second resonant frequency, f_2

5.1.3 Antenna Area Reduction

The area reduction provided by the proposed microstrip antenna at the dual operating frequencies are determined and tabulated in table 5.2. A maximum of 60.6% for the first resonant frequency and 24.1% for the second, compared to standard rectangular patches.

Table 5.2 Summary of percentage area reduction of the new dual slot arm reconfigurable antenna design

Tuning Voltage (V)	Resonant frequency		Area of equivalent rectangular patch		% Area reduction	
	f ₁ (GHz)	f ₂ (GHz)	f ₁ (cm ²)	f ₂ (cm ²)	f ₁	f ₂
0	1.432	1.984	34.7	18.0	60.6	24.1
3	1.448	1.992	33.8	17.8	59.7	23.5
6	1.464	1.992	33.2	17.8	58.9	23.5
9	1.48	1.992	32.4	17.8	57.9	23.5
12	1.504	2.00	31.4	17.7	56.6	22.8
15	1.528	2.00	30.4	17.7	55.2	22.8
18	1.544	2.008	29.8	17.5	54.3	22.3
21	1.56	2.008	29.1	17.5	53.2	22.3
24	1.568	2.016	28.8	17.4	52.7	21.7
27	1.584	2.016	28.3	17.4	51.8	21.7
30	1.592	2.016	28.0	17.4	51.3	21.7

5.1.4 Study of the Resonant Behavior of the Antenna at Different Varactor Positions

Experiments are carried out with the Varactor diode positioned at different location in the extended slot arm. As expected, when the diode is at 7mm from the hexagonal slot, the two operating frequencies shifted towards the higher side. A comparison between the two designs with different Varactor positions is depicted in fig. 5.4. From the plot it is clear that the diode position at the extreme end of the slot (12mm from hexagonal slot) will give better frequency tuning than at lower slot arm locations. At 7mm, the first resonant frequency varies from 1.57 to 1.6525GHz (82.5MHz upwards) and the second frequency from 2.0125 to

2.035GHz (22.5MHz upwards). The corresponding tuning ranges are 5.26% and 1.18%, respectively for the first and second mode. The frequency ratio varies in between 1.28 and 1.23, when the reverse bias is varied from 0 to 30V. The percentage size reduction is also less compared to the 12mm design (i.e. a maximum of 52.6% for f_1 and 21.9% for f_2).

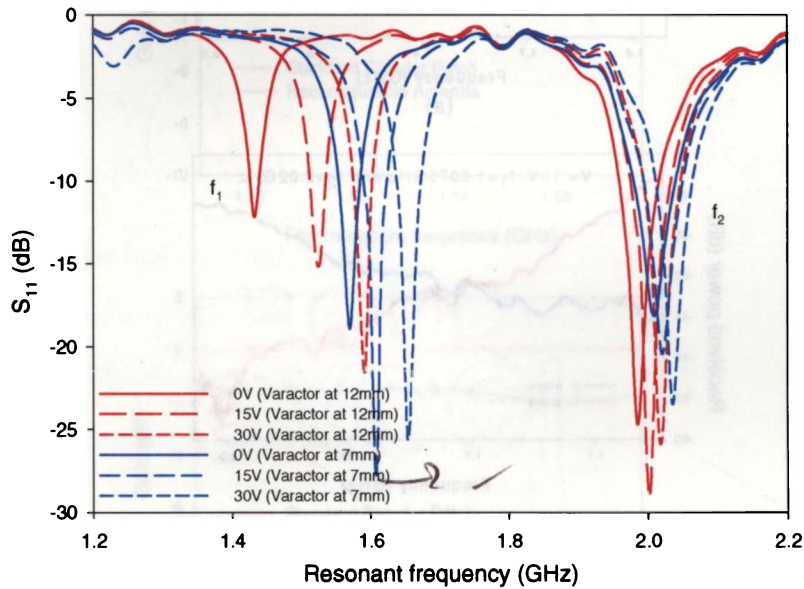
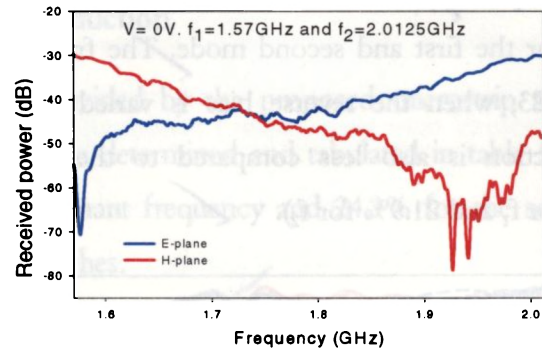


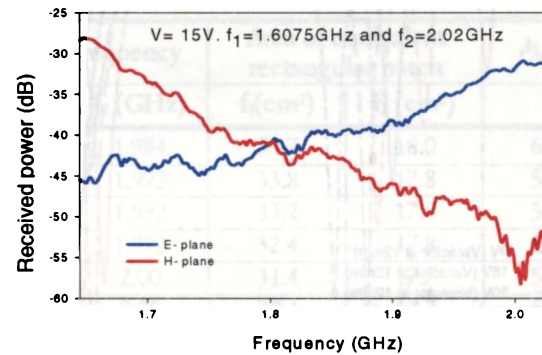
Figure 5.4 Measured return loss of the dual frequency Varactor controlled reconfigurable microstrip antenna at two different diode positions. ($L = 4\text{cm}$, $l_1 = l_2 = 0.8\text{cm}$, $l_s = 1.2\text{m}$, $w_s = 0.1\text{cm}$, $b = 0.16\text{cm}$ and $\epsilon_r = 3.98$)

5.1.5 Polarization, Gain and Radiation Pattern

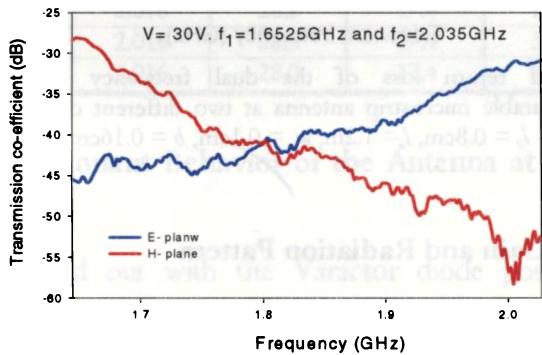
Fig. 5.5 portrays the transmission characteristics of the newly designed reconfigurable Varactor controlled microstrip antenna with a single extended slot arm, at different reverse bias voltages. It can be easily seen that the tuning of the microstrip antenna never alters the polarization of the two excited frequencies. The antennas dual orthogonal polarization is therefore kept preserved in the entire tuning range (0 to -30V).



(a)



(b)



(c)

Figure 5.5 Variation of received power with frequency for the two orthogonal polarization planes at different Varactor diode bias. (a) 0V (b) 15V (c) 30V



The gain of the antenna, at the two resonant frequencies for different Varactor reverse bias is 2.1dB and 1.8dB less respectively, compared to standard circular

patch. Typical gain plots for the antenna compared to standard circular patch operating at the same frequencies are shown in fig. 5.6.

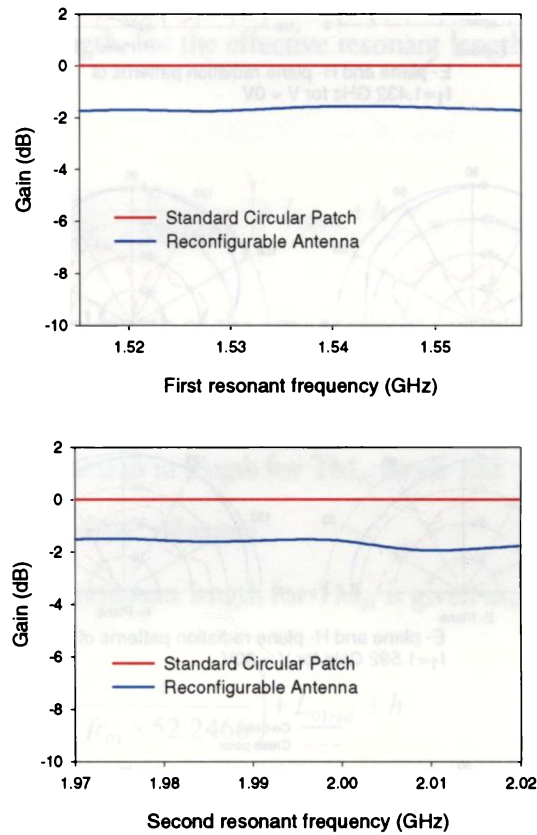


Figure 5.6 Measured gain plot of the antenna for first and second resonant frequencies

The radiation patterns at the principal planes for the dual resonant frequencies at different Varactor reverse bias voltages are shown in fig. 5.7. It is evident from the plots that the broad side radiation property of the antenna remains unchanged even after the reconfiguration.

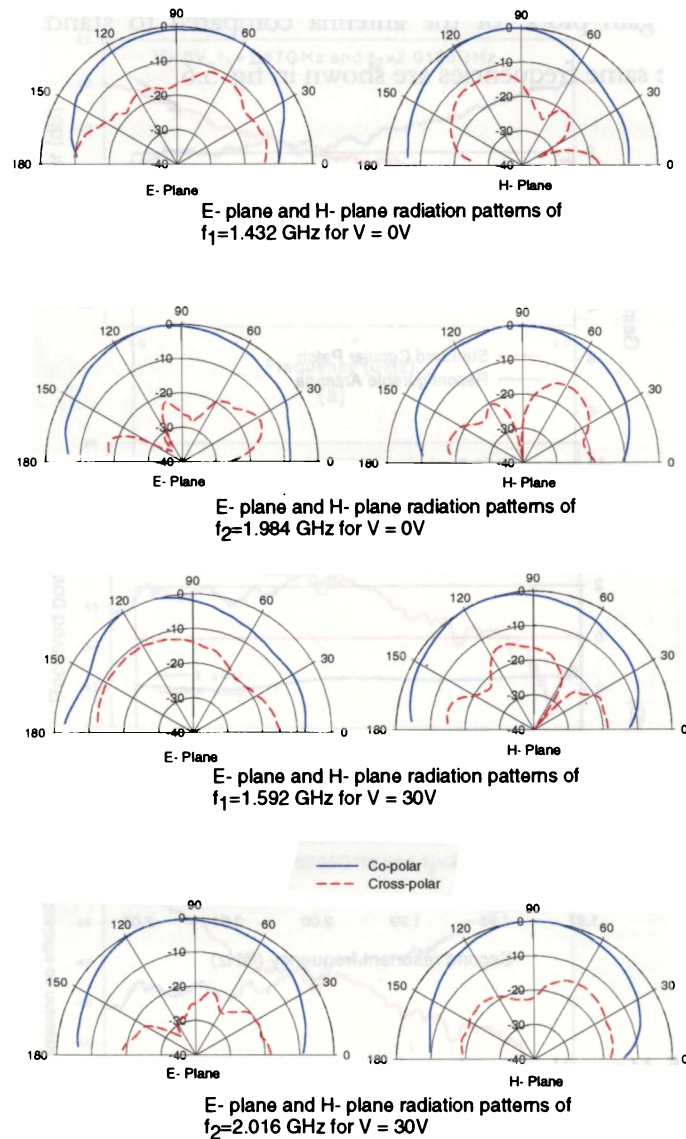


Figure 5.7 Measured E and H-plane radiation patterns of the proposed antenna for different varactor bias voltages

5.2 Computation of Resonant Frequencies of Varactor Tuned Reconfigurable Antenna

More insight into the Varactor controlled dual frequency microstrip antenna design with a single slot arm can be drawn from a simple transmission line model of the square patch. Since we are generating the dual resonant modes from the orthogonal

dimensions of the square patch, TM_{10} and TM_{01} , the two resonant frequencies can be expressed as if they are originating from two transmission lines of lengths L_1 and L_2 . Recalling the empirical relations derived in section 4.1.11 for the square patch length and slot arm length, for the effective resonant length for the TM_{10} mode, we can write,

$$L_1 = L + \left(\frac{c}{fr_{10} \times 52.2466} \right) + L_{10red} + h \quad (5.2)$$

Where, L is the physical length of the square patch,

fr_{10} is the first resonant frequency,

L_{10red} is the reduction in length for TM_{10} mode and

h is the height of the substrate.

Similarly, the effective resonant length for TM_{01} is given as,

$$L_2 = L + \left(\frac{c}{fr_{01} \times 52.2466} \right) + L_{01red} + h \quad (5.3)$$

Where, fr_{01} is the first resonant frequency.

The loading of the varactor diode across the slot arm is equivalent to an electrical length L_{var} which can be calculated from the capacitance of the varactor [186] as

$$L_{var} = C_v \times Z_0 \times \frac{c}{\sqrt{\epsilon_r}} \quad (5.4)$$

Where, c is the velocity of electromagnetic waves in vacuum,

Z_0 is the characteristic impedance,

ϵ_r is dielectric constant and

C_v is the capacitance of the varactor diode.

As the varactor junction capacitance varies with the applied reverse bias voltage V_{rev} , we can express C_V in terms of V_{rev} as,

$$C_V = \frac{C_0}{\left(1 - \frac{V_{rev}}{V_{bi}}\right)^\gamma} \quad (5.5)$$

Where, C_0 is the varactor junction capacitance at zero bias voltage,

V_{bi} is the built in potential for the semiconductor material used in the varactor and

γ is a constant depending on the doping profile of the varactor p-n junction.

Assuming that the varactor loading affects only the first resonant mode, we can modify the effective electrical length of the TM_{10} mode as,

$$L_1 = L + \left(\frac{c}{fr_{10} \times 52.2466} \right) + L_{inrad} + h + \left[\frac{C_0}{\left(1 - \frac{V_{rev}}{V_{bi}}\right)^\gamma} \times Z_0 \times \frac{c}{\sqrt{\epsilon_r}} \right] \quad (5.6)$$

Knowing L_1 and L_2 we can calculate the corresponding dual resonant frequencies for the varactor loaded reconfigurable patch antenna as,

$$\text{First resonant frequency} = \frac{c}{2L_1 \sqrt{\epsilon_{reff}}} \quad \text{and} \quad (5.7)$$

$$\text{Second resonant frequency} = \frac{c}{2L_2 \sqrt{\epsilon_{reff}}} \quad (5.8)$$

The comparison of experimental and theoretical results for the single slot arm loaded varactor controlled reconfigurable dual frequency microstrip antenna is given in fig.5.8.

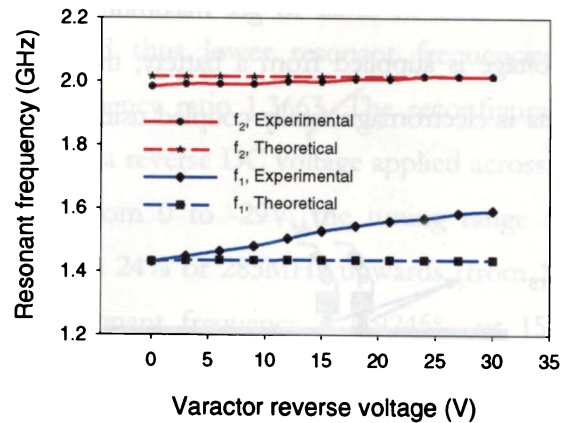


Figure 5.8 Plot showing the experimental and theoretical variation of first and second resonant frequencies with the applied varactor reverse bias

5.3 Varactor Controlled Reconfigurable Dual Frequency Microstrip Antenna Design for Frequency Ratio Tuning

As described in section 4.1.9, the dual vertical slot arm loaded design is used to tune the frequency ratio, electronically, by embedding two varactor diodes in the slot arms. Tunable frequency ratios varying in the range 1.1 to 1.37 is achieved. The proposed antenna can achieve a high tuning range of 24% for the first resonant frequency without much altering the second resonant frequency, with a single feed position. The design has an advantage of high flexibility in frequency tuning. Another advantage of this design is that the antenna shows almost similar radiation patterns for the two operating frequencies in the entire tuning range, without much affecting the gain, which is highly desirable for frequency reconfigurable antennas.

5.3.1 Antenna Geometry

The dual slot arm loaded reconfigurable antenna configuration is illustrated in fig. 5.9. A square microstrip patch antenna with side dimension L is fabricated on a substrate of thickness h and relative permittivity ϵ_r . A hexagonal slot of side parameters l_1 and l_2 with two slot arms of length l_a and l_b and width w_a , extending up to the edge of the square patch is placed at its center. Varactor diodes D_1 and D_2 are positioned at the

extreme end of the slot arms in order to get maximum tuning range and better matching. DC bias voltage is supplied from a battery, through two chip inductors across D_1 . The antenna is electromagnetically coupled using a 50Ω microstrip line as shown in fig. 5.9.

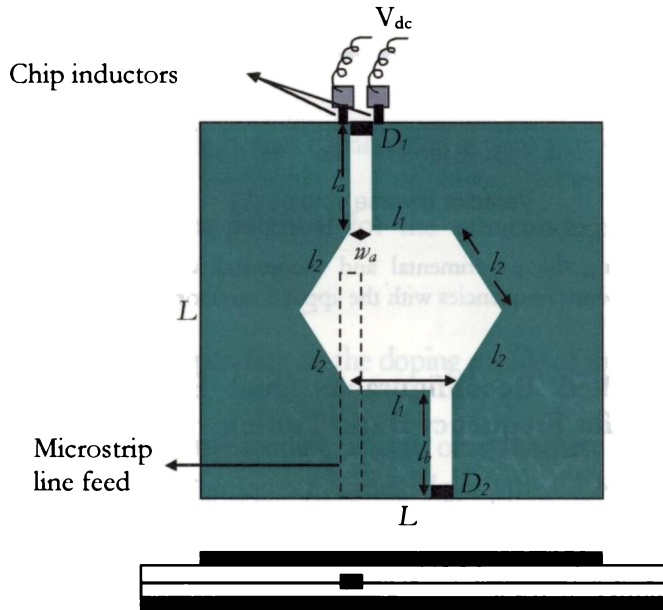


Figure 5.9 Reconfigurable dual frequency microstrip antenna controlled by varactor diodes for frequency ratio tuning. ($L = 4\text{cm}$, $l_1 = l_2 = 0.8\text{cm}$, $l_a = l_b = 1.1\text{cm}$, $w_a = 0.1\text{cm}$, $b = 0.16\text{cm}$ and $\epsilon_r = 3.98$).

5.3.2 Variation of Resonant Frequencies with Varactor Reverse Bias

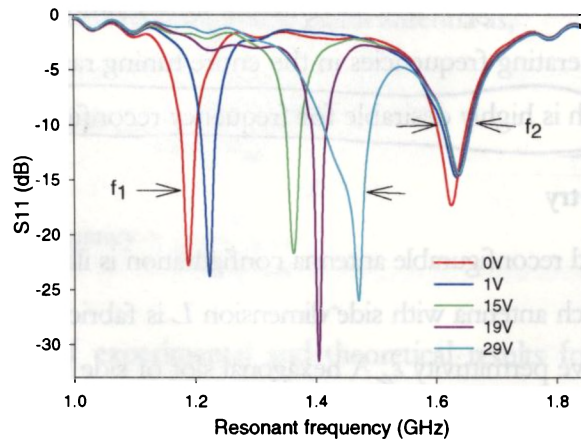


Figure 5.10 Measured return loss of the antenna for different varactor reverse bias voltages. ($L = 4\text{cm}$, $l_1 = l_2 = 0.8\text{cm}$, $l_a = l_b = 1.1\text{cm}$, $w_a = 0.1\text{cm}$, $b = 0.16\text{cm}$ and $\epsilon_r = 3.98$).

When the reverse bias is off, the varactor loadings in the two slot arms correspond to high capacitance and thus lower resonant frequencies at 1.1875GHz and 1.6225GHz with a frequency ratio 1.3663. The reconfigurable antenna was then electronically tuned with a reverse DC voltage applied across the diodes. When the bias voltage is varied from 0 to -29V, the tuning range for the first resonant frequency is found to be 24% or 285MHz upwards (from 1.1875 to 1.4725GHz) and that of second resonant frequency is 0.9245% or 15MHz upwards (from 1.6225 to 1.6375GHz) as shown in fig. 5.10. At -29V the frequency ratio is found to be 1.1008. The variation of first and second resonant frequencies (f_1 and f_2) with the applied varactor reverse bias voltage is measured and plotted in fig.5.11.

In fig. 5.11 second resonant mode is almost independent of the varactor bias voltage while the first resonant mode shows abrupt change. Thus it is proved that the design with two vertical slot arms controlled by varactors is best suitable for flexible frequency ratio tuning. Table 5.3 illustrates the measured frequency ratios at different bias voltages. The bandwidths of the two resonant modes are also measured at different bias voltages and given in table 5.3. Bandwidths of both operating frequencies remain essentially constant through out the tuning range.

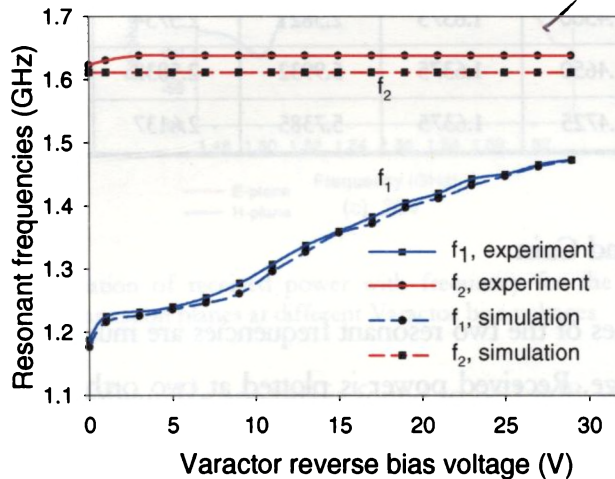


Figure 5.11 Experimental and simulated (IE3D) Variation of first and second resonant frequencies with varactor reverse bias.

Table 5.3 Measured frequency ratio and percentage bandwidths at different varactor bias

Tuning voltage (V)	Resonant frequencies		% Bandwidth		Frequency ratio
	f ₁ (GHz)	f ₂ (GHz)	f ₁ (GHz)	f ₂ (GHz)	
0	1.1875	1.6225	2.4867	3.2148	1.3663
1	1.2250	1.6300	2.3657	2.8371	1.3306
3	1.2325	1.6375	2.3140	2.7847	1.3286
5	1.2400	1.6375	2.3849	2.7181	1.3206
7	1.2550	1.6375	2.2892	2.6944	1.3048
9	1.2775	1.6375	2.2466	2.6571	1.2818
11	1.3075	1.6375	2.3962	2.6565	1.2524
13	1.3375	1.6375	2.1383	2.6137	1.2243
15	1.3600	1.6375	2.1103	2.5919	1.2040
17	1.3825	1.6375	2.0788	2.5783	1.1844
19	1.4050	1.6375	2.0641	2.5557	1.1655
21	1.4200	1.6375	2.1479	2.5527	1.1532
23	1.4425	1.6375	2.2693	2.5649	1.1352
25	1.4500	1.6375	2.3821	2.5734	1.1293
27	1.4650	1.6375	5.9932	2.5832	1.1177
29	1.4725	1.6375	5.7385	2.6137	1.1121

5.3.3 Polarization and Gain

The polarization planes of the two resonant frequencies are mutually orthogonal in the entire tuning range. Received power is plotted at two orthogonal planes, for different varactor bias voltages are given in fig. 5.12.

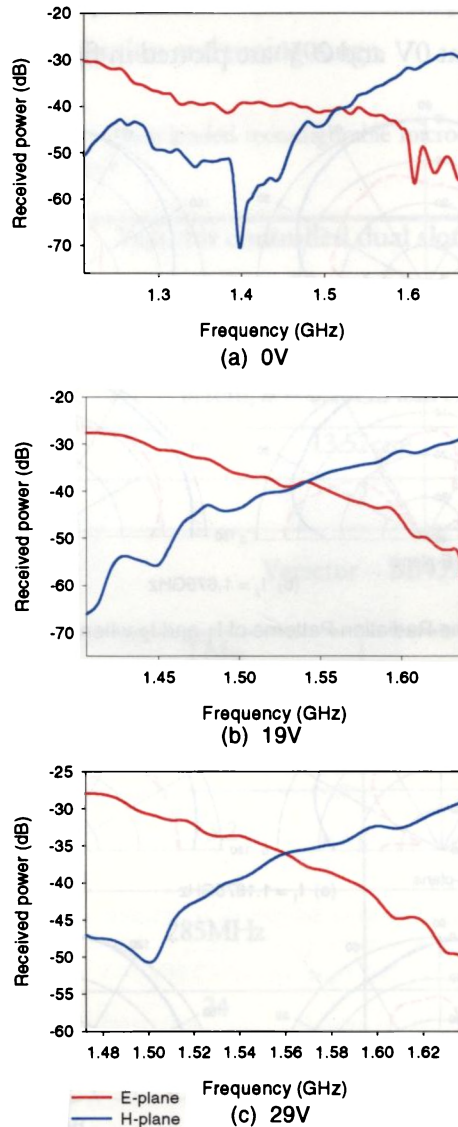


Figure 5.12 Variation of received power with frequency for the two orthogonal polarization planes at different Varactor bias voltages

The gain of the reconfigurable antenna is found to be 1.8dB and 0.4dB less for the first and second resonant frequencies respectively, compared to standard circular patch operating at the same frequencies. The new design offers an area reduction of 73.21% for the first resonant frequency and 49.86% for the second, compared

to standard rectangular patches. Measured E and H-plane radiation patterns of the reconfigurable antenna at 0V and 29V are plotted in fig. 5.13.

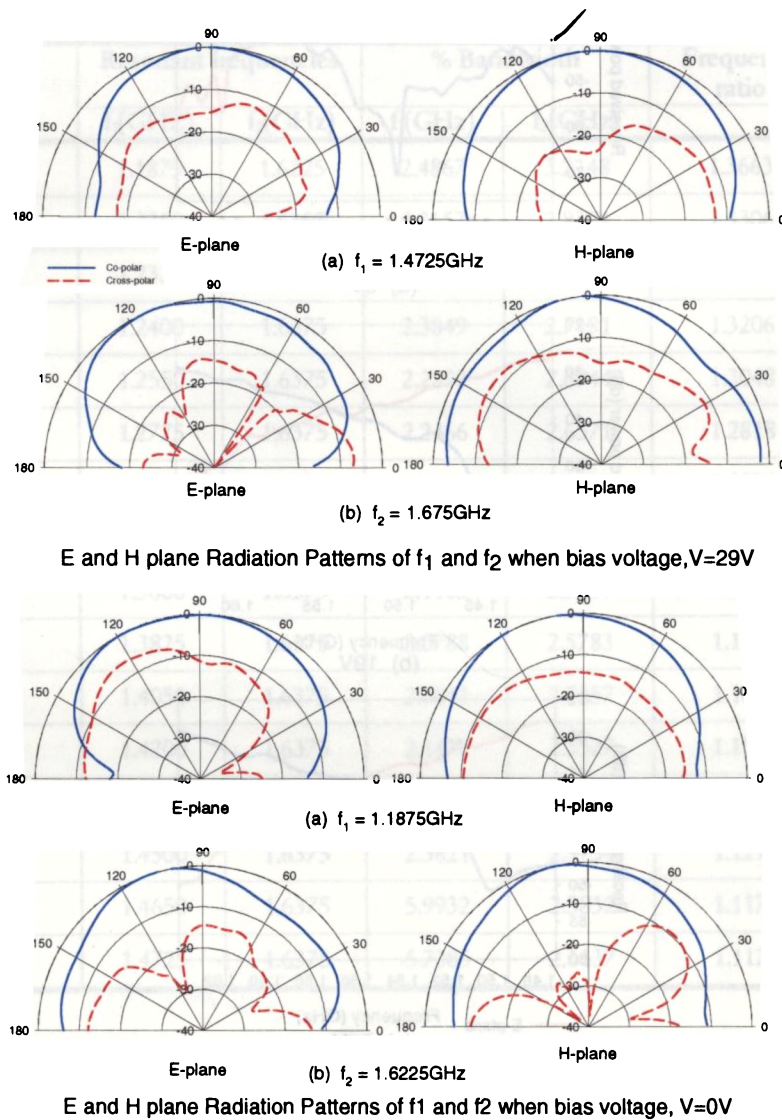


Figure 5.13 Measured E and H-plane radiation patterns of the reconfigurable antenna at 29V and 0V

The key properties of the proposed design in a nutshell are given in table 5.4. This dual slot arm design with varactor control proves to be a better candidate than the

dual slot arm loaded reconfigurable antenna with PIN diode switching, in terms of tunable frequency ratio, size reduction and tuning range.

Table 5.4 Overview of dual slot arm loaded reconfigurable microstrip antenna with varactor diode control

Antenna parameters	Varactor controlled dual slot arm loaded reconfigurable microstrip antenna	
Antenna geometry	$L = 4\text{cm}, l_1 = l_2 = 0.8\text{cm}, l_a = l_b = 1.2\text{cm}, w_1 = 0.1\text{cm}, b = 0.16\text{cm}$ and $\epsilon_r = 3.98$	
Metallization area	13.52cm ²	
No. of slot arms	2	
Non-linear device used for switching	Varactor – BB439	
Antenna properties	TM ₁₀	TM ₀₁
Maximum % bandwidth	5.7	3.2
Maximum % area reduction	73.2	49.9
Maximum shift in frequency (0-30V)	285MHz	15MHz
% Tuning range	24	0.9
Tunable frequency ratio	1.10 – 1.37	

5.4 Experimental Investigations on Varactor Loaded Reconfigurable Microstrip Antennas for Enhanced Dual Frequency Tuning and Area Reduction

Once the technique of reconfigurable dual frequency operation and frequency ratio tuning is established, studies are then extended to increase the tuning ranges of both the operating frequencies. Four modified designs are presented with two, three, four and eight

> fact ?

slot arms, respectively, in order to enhance the dual frequency tuning and area reduction.

5.4.1 Varactor Controlled Microstrip Antenna with Dual Orthogonal Slot Arms

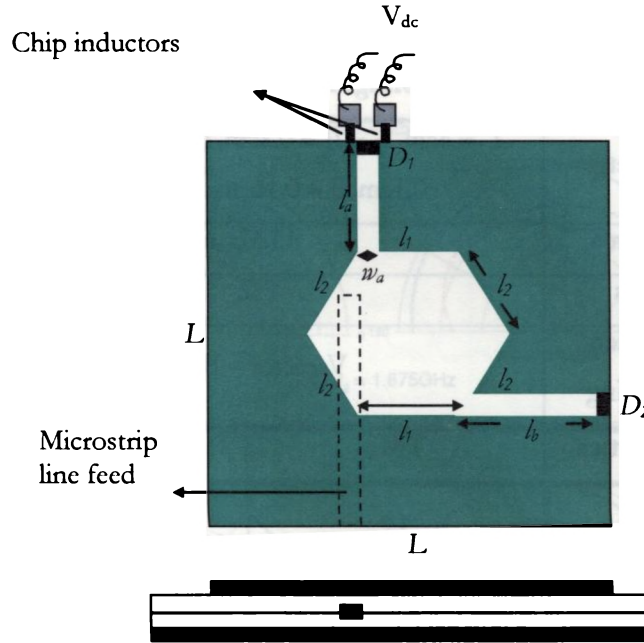


Figure 5.14 Reconfigurable dual frequency microstrip antenna configuration with orthogonal slot arms. ($L = 4\text{cm}$, $l_1 = l_2 = 0.8\text{cm}$, $l_a = 1.1\text{cm}$, $l_b = 1.5\text{cm}$, $w_a = 0.1\text{cm}$, $b = 0.16\text{cm}$ and $\epsilon_r = 3.98$).

The effect of two orthogonal slot arms in the dual operating frequencies for a passive hexagonal slot loaded square microstrip patch antenna is already discussed in section 4.1.10. Varactors are loaded in these slot arms to study the electronic tuning effect on both the resonant modes. The geometry of the orthogonal slot arm loaded antenna is illustrated in fig. 5.14. The design and feeding are exactly similar to the dual vertical slot arm microstrip antenna.

The second resonant mode TM_{01} , orthogonal to TM_{10} , is less affected by the length alteration in the vertical slot arm. Thus, the electrical length variation of a horizontal

slot arm of length l_s and width w_s introduced in the patch can effectively tune the second operating frequency. This is evident from the return loss curves in fig. 5.15, of the proposed design at different varactor reverse voltages.

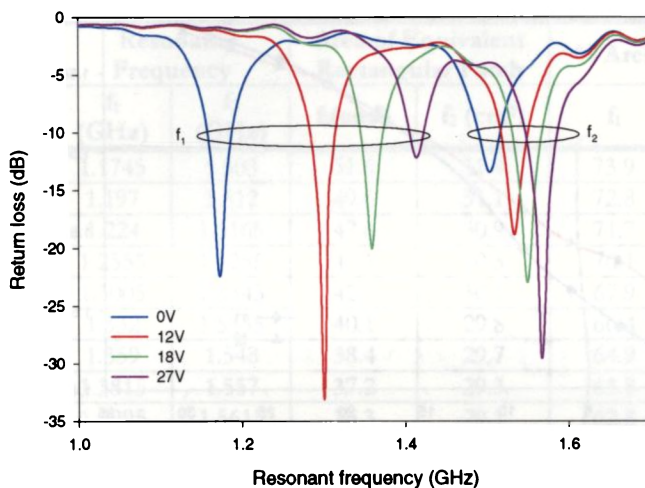


Figure 5.15 Return loss characteristics of the varactor tuned orthogonal slot arm loaded microstrip antenna

When the reverse bias is OFF, the varactor loadings in all the slot arms correspond to high capacitance and thus lower resonant frequencies at 1.1745GHz and 1.503GHz with a frequency ratio 1.2797. The reconfigurable antenna was then electronically tuned with a reverse DC voltage applied across the diodes as demonstrated in fig. 4.39. When the bias voltage is varied from 0 to -30V, the tuning range for the first resonant frequency is found to be 21.46% or 252MHz upwards (from 1.1745 to 1.4265GHz) and that of second resonant frequency is 4.49% or 67.5MHz upwards (from 1.503 to 1.5705GHz) as shown in fig. 5.15. At -30V the frequency ratio is found to be 1.1009. The variation of first and second resonant frequencies (f_1 and f_2) with the applied varactor reverse bias voltage is measured and plotted in fig. 5.16. Since the first resonant frequency is produced by perturbing the original patch current density of the TM_{01} mode, with a protruding slot arm, a change in length of the slot arms considerably affects the first resonant

frequency (TM_{01}) than the second resonant frequency (TM_{10}). The second resonant frequency mainly depends on the original patch current density which is unperturbed by the inclusion of the vertical slots.

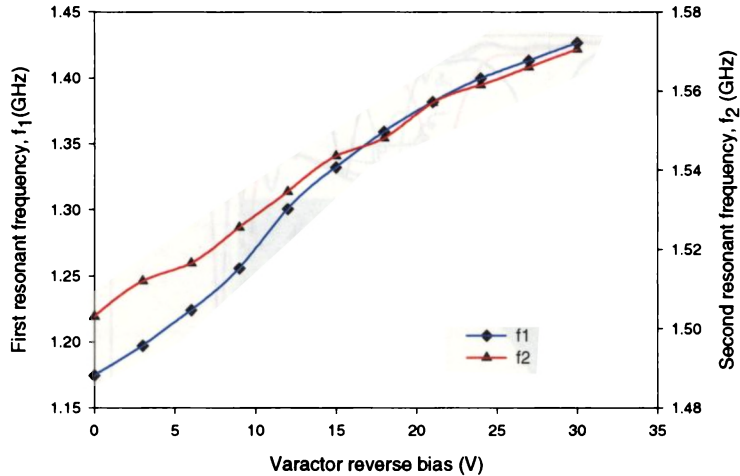


Figure 5.16 Variation of first and second resonant frequencies with varactor reverse bias.

Measured bandwidths and frequency ratio are given in table 5.5. The gain of the reconfigurable antenna with four slot arms is found to be nearly 2.1dB and 1.2dB less for the first and second resonant frequencies respectively, compared to standard square patch operating at the same frequencies.

Table 5.5 Measured bandwidths and frequency ratios

Tuning voltage (V)	Resonant frequency		% Bandwidth		Frequency ratio
	f_1 (GHz)	f_2 (GHz)	f_1	f_2	
0	1.1745	1.503	2.5443	1.7838	1.2797
3	1.197	1.512	2.6417	1.8534	1.2632
6	1.224	1.5165	2.6961	1.9321	1.2390
9	1.2555	1.5255	2.7903	2.0459	1.2151
12	1.3005	1.5345	2.3837	2.2033	1.1799
15	1.332	1.5435	2.1494	2.3032	1.1588
18	1.359	1.548	2.0456	2.3643	1.1391
21	1.3815	1.557	1.8820	2.4021	1.1270
24	1.3995	1.5615	1.6031	2.4541	1.1158
27	1.413	1.566	1.2102	2.5110	1.1083
30	1.4265	1.5705	0.7578	2.5497	1.1009

The size reduction offered by two resonant frequencies at different varactor reverse voltages are tabulated in table 5.6.

Table 5.6 Measured percentage area reduction for the two resonant modes

Tuning Voltage (V)	Resonant Frequency		Area of Equivalent Rectangular Patch		% Area Reduction	
	f ₁ (GHz)	f ₂ (GHz)	f ₁ (cm ²)	f ₂ (cm ²)	f ₁	f ₂
0	1.1745	1.503	51.6	31.4	73.9	57.1
3	1.197	1.512	49.6	31.1	72.8	56.6
6	1.224	1.5165	47.6	30.9	71.7	56.4
9	1.2555	1.5255	45.1	30.5	70.1	55.8
12	1.3005	1.5345	42.0	30.1	67.9	55.3
15	1.332	1.5435	40.1	29.8	66.4	54.8
18	1.359	1.548	38.4	29.7	64.9	54.5
21	1.3815	1.557	37.2	29.3	63.8	54.0
24	1.3995	1.5615	36.3	29.1	62.8	53.7
27	1.413	1.566	35.6	29.0	62.1	53.4
30	1.4265	1.5705	34.9	28.8	61.4	53.2

The polarization planes of the two resonant frequencies are mutually orthogonal in the entire tuning range. A typical received power vs. resonant frequency curve at two orthogonal polarization planes is given in fig. 5.17.

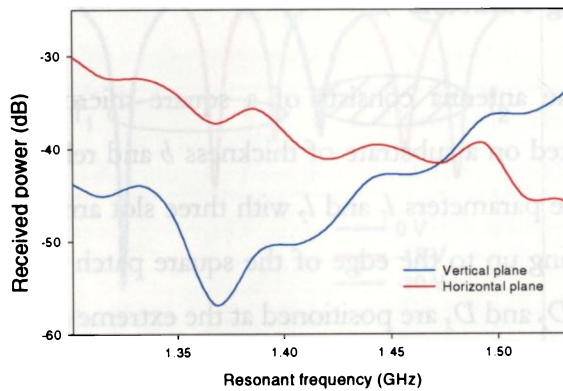


Figure 5.17 Measured received power in the two orthogonal polarization planes

The E and H-plane radiation patterns for the two reconfigurable antenna configurations are measured for different bias voltages. All the patterns show similar broadside radiation characteristics with good cross polarization levels even when the operating frequencies are shifted greatly by applying reverse bias. Typical radiation patterns for the resonant frequencies of two and four slot arm design are given in fig. 5.18.

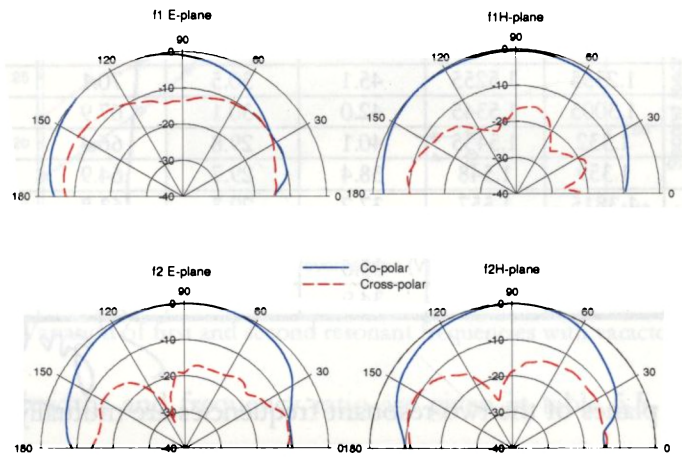


Figure 5.18 Measured radiation pattern for the dual modes

5.4.2 Triple Slot Arm Loaded Reconfigurable Dual Frequency Microstrip Antenna Using Varactors

The geometry of the antenna consists of a square microstrip patch with side dimension L fabricated on a substrate of thickness h and relative permittivity ϵ_r . A hexagonal slot of side parameters l_1 and l_2 with three slot arms of length l_a , l_b and l_c and width w_s extending up to the edge of the square patch is placed at its center. Varactor diodes D_1 , D_2 and D_3 are positioned at the extreme end of the slot arms in order to get maximum tuning range and better matching. A narrow slit is used to achieve good DC isolation. DC bias voltage is supplied from a battery, through two chip inductors across D_1 and D_2 . The antenna is electromagnetically coupled using a 50Ω microstrip line as shown in fig. 5.19.

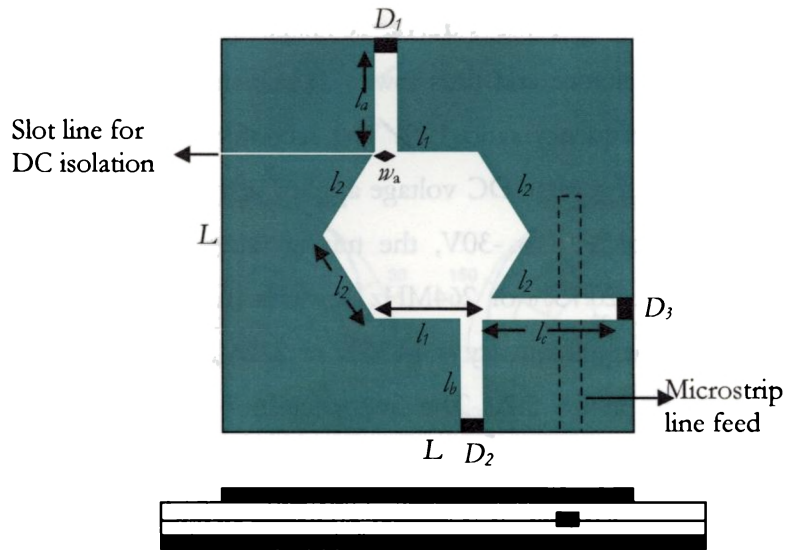


Figure 5.19 Geometry of the proposed varactor controlled microstrip antenna with three slot arms ($L = 4\text{cm}$, $l_1 = l_2 = 0.8\text{cm}$, $l_2 = l_b = 1.1\text{cm}$, $l_c = 1.5\text{cm}$, $w_a = 0.1\text{cm}$, $b = 0.16\text{cm}$ and $\epsilon_r = 3.98$).

The length of the upper and lower slot arms determines the first resonant frequency and a constant frequency ratio will be maintained for same slot arm lengths. In order to vary the second resonant frequency, a third slot arm is introduced orthogonal to the first two. Thus by varying the length of the three slot arms simultaneously, reconfigurable dual frequency operation with wide tuning range is achieved.

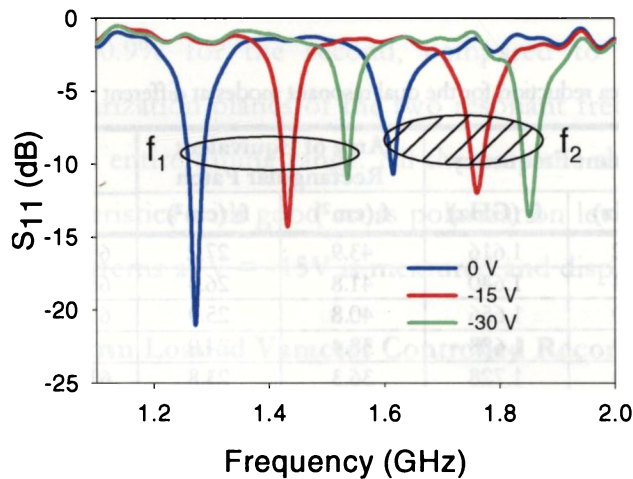


Figure 5.20 Measured return loss of the antenna for different varactor reverse bias voltages. ($L = 4\text{cm}$, $l_1 = l_2 = 0.8\text{cm}$, $l_2 = l_b = 1.1\text{cm}$, $l_c = 1.5\text{cm}$, $w_a = 0.1\text{cm}$, $b = 0.16\text{cm}$ and $\epsilon_r = 3.98$).

When the reverse bias is off, the varactor loadings in all the three slot arms correspond to high capacitance and thus lower resonant frequencies at 1.272GHz and 1.616GHz with a frequency ratio 1.27. The reconfigurable antenna was then electronically tuned with a reverse DC voltage applied across the diodes. When the bias voltage is varied from 0 to -30V, the tuning range for the first resonant frequency is found to be 20.75% or 264MHz upwards (from 1.272 to 1.536GHz) and that of second resonant frequency is 14.36% or 232MHz upwards (from 1.616 to 1.848GHz) as shown in fig. 5.20. The frequency ratio variation is very low in between 1.2 and 1.27. The variation of first and second resonant frequencies (f_1 and f_2) with the applied varactor reverse bias voltage is measured and plotted in fig. 5.21.

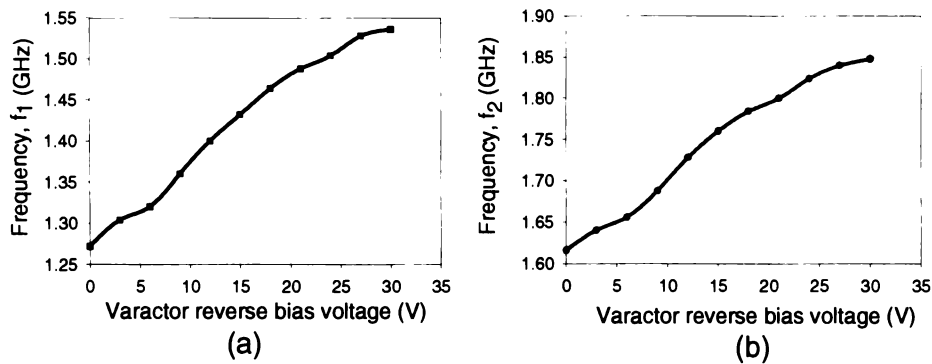


Figure 5.21 Variation of resonant frequencies with varactor reverse bias voltage, (a) f_1 (b) f_2

Table 5.7 Percentage area reduction for the dual resonant modes at different varactor bias voltages

Tuning Voltage (V)	Resonant Frequency		Area of Equivalent Rectangular Patch		% Area Reduction	
	f_1 (GHz)	f_2 (GHz)	f_1 (cm ²)	f_2 (cm ²)	f_1	f_2
0	1.272	1.616	43.9	27.2	69.6	50.9
3	1.304	1.640	41.8	26.4	68.1	49.4
6	1.320	1.656	40.8	25.9	67.3	48.4
9	1.360	1.688	38.4	24.9	65.3	46.4
12	1.400	1.728	36.3	23.8	63.2	43.8
15	1.432	1.760	34.7	22.9	61.5	41.7
18	1.464	1.784	33.2	22.3	59.8	40.1
21	1.488	1.800	32.1	21.9	58.4	38.9
24	1.504	1.824	31.4	21.3	57.5	37.4
27	1.528	1.840	30.4	20.9	56.0	36.0
30	1.536	1.848	30.1	20.7	55.6	35.6

The percentage area reduction offered by this design is tabulated for different frequencies and given in table 5.7.

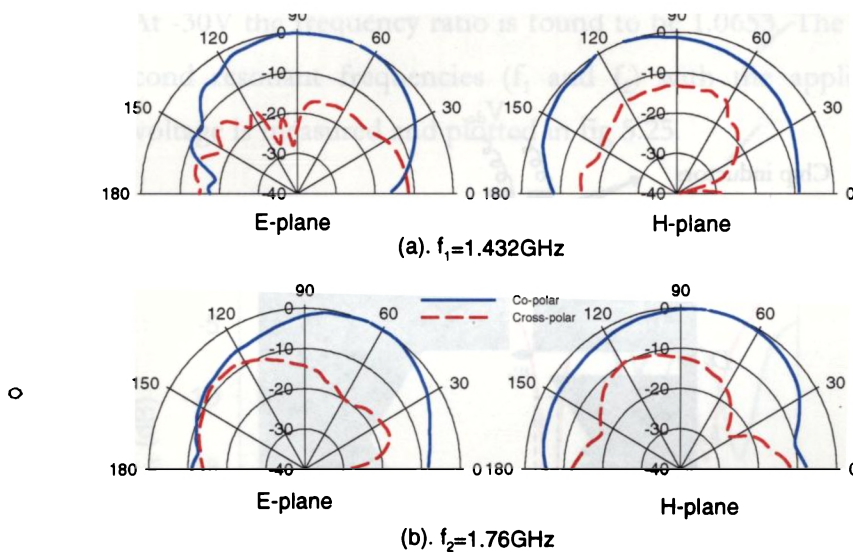


Figure 5.22 Measured E and H-plane radiation patterns at $f_1=1.432\text{GHz}$ and $f_2=1.76\text{ GHz}$ of the antenna, for $V= -15\text{volt}$

The new design provides an area reduction of 69.6% for the first resonant frequency and 50.9% for the second, compared to standard rectangular patches. The polarization planes of the two resonant frequencies are mutually orthogonal in the entire tuning range. All the patterns show similar broadside radiation characteristics with good cross polarization levels. Typical E and H-field radiation patterns at $V = -15\text{V}$ is measured and displayed in fig. 5.22.

5.4.3 Four Slot Arm Loaded Varactor Controlled Reconfigurable Microstrip Antenna

A symmetrical variation is made in the number and orientation of the slot arms in the design described in section 5.4.2, to device a four slot arm loaded varactor controlled reconfigurable microstrip antenna. Two slot arms each in

the vertical and horizontal directions are added to the central hexagonal slot, to tune both resonant frequencies. The antenna configuration is given in fig. 5.23.

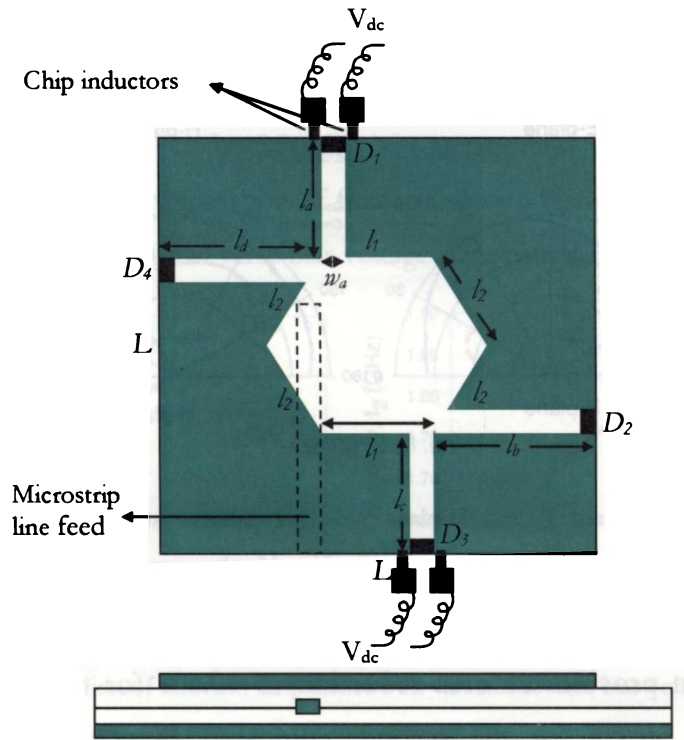


Figure 5.23 Four slot arm loaded reconfigurable dual frequency microstrip antenna controlled by varactor diodes. Antenna parameters are $L = 4\text{cm}$, $l_1 = l_2 = 0.8\text{cm}$, $l_a = l_c = 1.1\text{cm}$, $l_b = l_d = 1.5\text{cm}$, $w_a = 0.1\text{cm}$, $b = 0.16\text{cm}$ and $\epsilon_r = 3.98$.

When the varactor reverse bias is OFF, the varactor loadings in all the slot arms correspond to high capacitance and thus lower resonant frequencies at 1.037GHz and 1.359GHz with a frequency ratio 1.3105. The reconfigurable antenna was then electronically tuned with a reverse DC voltage applied across the diodes as demonstrated in fig 5.23. When the bias voltage is varied from 0

to -30V, the tuning range for the first resonant frequency is found to be 34.43% or 357MHz upwards (from 1.037 to 1.394GHz) and that of second resonant frequency is 9.2715% or 126MHz upwards (from 1.359 to 1.485GHz) as shown in fig. 5.24. At -30V the frequency ratio is found to be 1.0653. The variation of first and second resonant frequencies (f_1 and f_2) with the applied varactor reverse bias voltage is measured and plotted in fig 5.25.

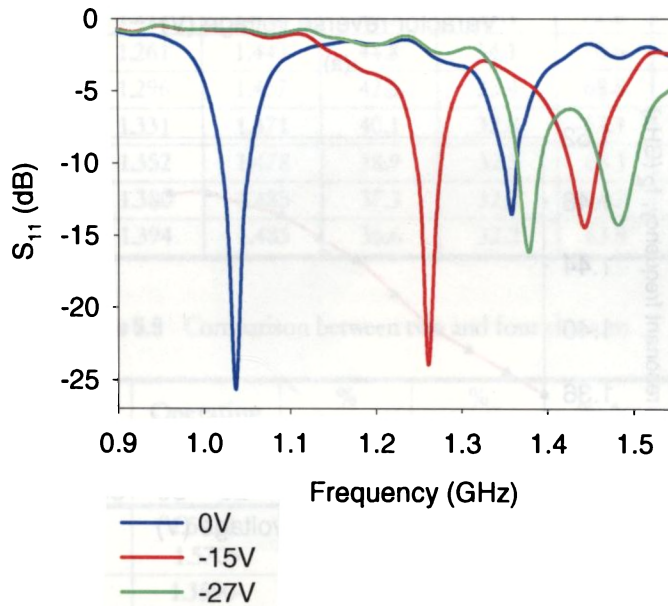
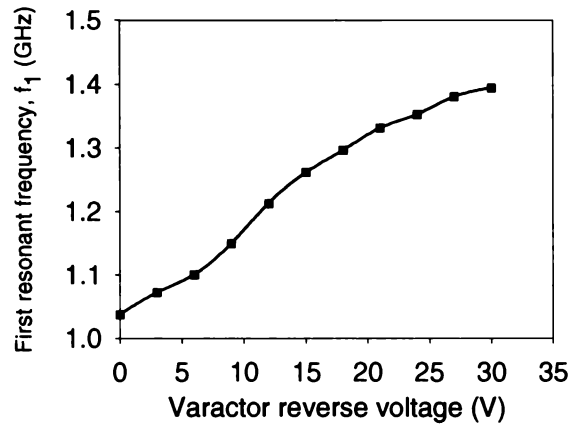
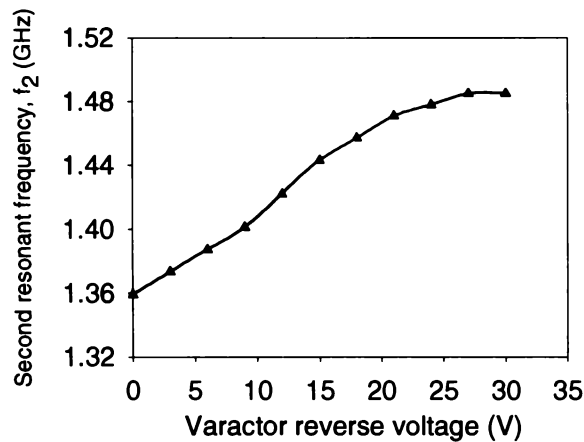


Figure 5.24 Measured return loss, (S_{11}) of the four slot arm antenna configuration for different varactor reverse bias voltages

The new design offers a maximum area reduction of 80.1053% for the first resonant frequency and 65.6912% for the second, compared to standard rectangular patches. Calculated area reduction for the two operating frequencies at different reverse bias voltages are given in table 5.8.



(a)



(b)

Figure 5.25 Variation of resonant frequencies for the four slot arm reconfigurable antenna design with varactors reverse voltage. (a) First resonant frequency, f_1 (b) Second resonant frequency, f_2

On the other hand, the design with two slot arms can provide only a tuning frequency range of 21.46% for the first resonant frequency and 4.49% for the second. The size reduction for this design is also less compared to four slot arm design; 73.8832% for the first resonant frequency and 57.0843% for the second, compared to standard rectangular patches. A comparison between the two and four slot arm antenna configurations is given in table 5.9.

Table 5.8 Area reduction at various reverse voltages

Tuning Voltage (V)	Resonant Frequency		Area of Equivalent Rectangular Patch		% Area Reduction	
	f_1 (GHz)	f_2 (GHz)	f_1 (cm ²)	f_2 (cm ²)	f_1	f_2
0	1.037	1.359	66.3	38.4	80.2	65.7
3	1.072	1.373	62.0	37.7	78.7	65.1
6	1.100	1.387	58.8	36.9	77.3	64.3
9	1.149	1.401	53.9	36.3	75.5	63.6
12	1.212	1.422	48.5	35.1	72.8	62.0
15	1.261	1.443	44.8	34.1	70.6	61.4
18	1.296	1.457	42.3	33.4	68.8	60.6
21	1.331	1.471	40.1	32.8	67.1	59.8
24	1.352	1.478	38.9	32.5	66.1	59.5
27	1.380	1.485	37.3	32.2	64.7	59.0
30	1.394	1.485	36.6	32.2	63.9	59.0

Table 5.9 Comparison between two and four slot arm

No. of slot arms	Operating band, f_1 (GHz)	Operating band, f_2 (GHz)	% Tuning range for f_1	% Tuning range for f_2	% Area reduction for f_1	% Area reduction for f_2
Two	1.1745-1.4265	1.5030-1.5705	21.46	4.49	73.88	57.08
Four	1.0370-1.3940	1.3590-1.4850	34.43	9.27	80.11	65.69

The E and H-plane radiation patterns for the two reconfigurable antenna configurations are measured for different bias voltages. All the patterns showed almost similar broadside radiation characteristics even when the operating frequencies are shifted greatly by applying reverse bias.

5.4.4 Eight Slot Arm Loaded Varactor Controlled Reconfigurable Microstrip Antenna

Eight protruding slot arms embedded with the central hexagonal slot generate dual frequencies with orthogonal polarization planes. Varactor diodes integrated with the extended slot arms are used to tune the operating

frequencies without much affecting the radiation characteristics and gain. Desired operating frequency values can be obtained electronically by varying the reverse bias voltage of the varactor diodes in between 0 to -30V. Varactor diodes D_1 , D_2 , D_3 , D_4 , D_5 , D_6 , D_7 and D_8 are positioned at the extreme end of the slot arms in order to get maximum tuning range and better matching. DC bias voltage is supplied from a battery, through two chip inductors across the varactors. The antenna is electromagnetically coupled using a 50Ω microstrip line as shown in fig. 5.26.

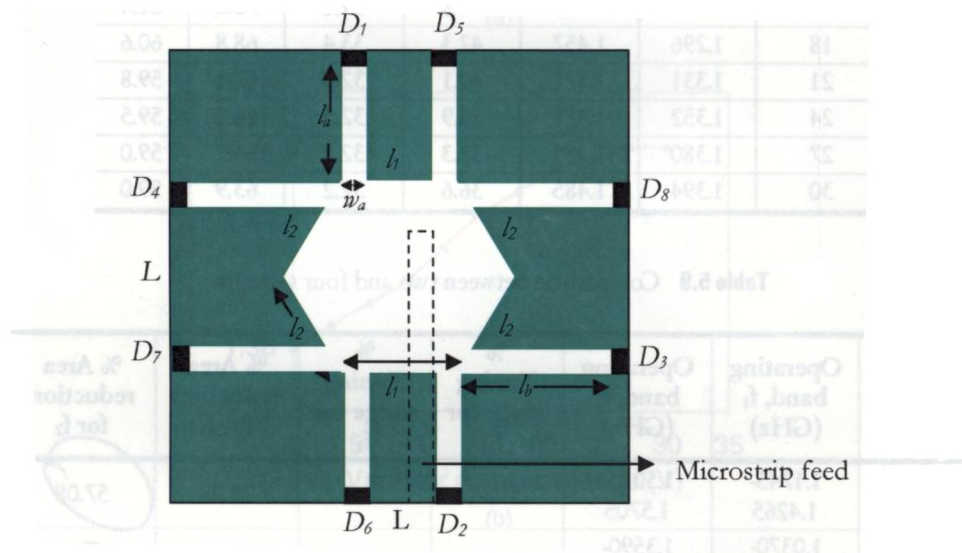


Figure 5.26 Geometry of the eight slot arm reconfigurable microstrip antenna controlled by varactor diodes

When the reverse bias is off, the varactor loadings in all the three slot arms correspond to high capacitance and thus lower resonant frequencies at 1.064GHz and 1.296GHz with a frequency ratio 1.0645. The reconfigurable antenna was then electronically tuned with a reverse DC voltage applied across the diodes. When the bias voltage is varied from 0 to -30V, the tuning range for the first resonant frequency is found to be 21.05% or 224MHz upwards (from 1.064 to 1.288GHz) and that of second resonant frequency is

12.96% or 168MHz upwards (from 1.296 to 1.464GHz) as shown in fig.5.27. The variation of first and second resonant frequencies (f_1 and f_2) with the applied varactor reverse bias voltage is measured and plotted in fig.5.28.

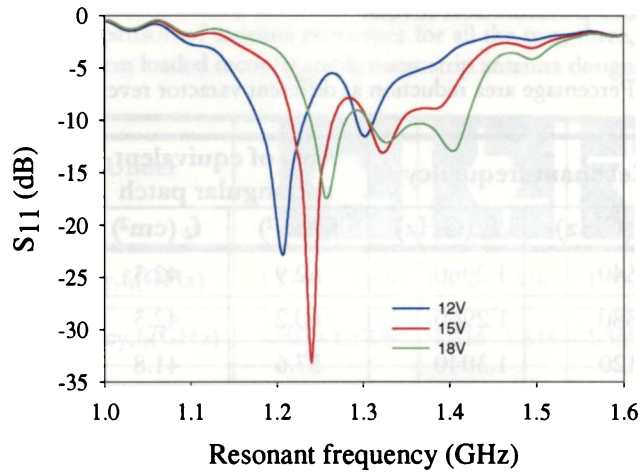


Figure 5.27 Measured return loss of the antenna for different varactor reverse bias voltages. ($L = 4\text{cm}$, $l_1 = l_2 = 0.8\text{cm}$, $l_a = 1.1\text{cm}$, $l_b = 1.5\text{cm}$, $w_a = 0.1\text{cm}$, $h = 0.16\text{cm}$ and $\epsilon_r = 3.98$).

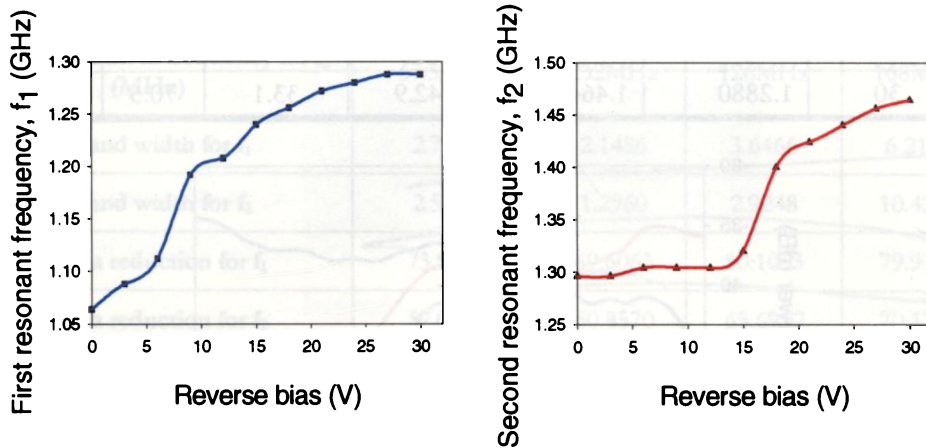


Figure 5.28 Variation of resonant frequencies with varactor reverse bias voltage, (a) f_1 (b) f_2

This design provides an area reduction of 80% for the first resonant frequency and 70.2% for the second, compared to standard rectangular patches. The detailed observation of the size reduction characteristics of the antenna is given in table

5.10. The polarization planes of the two resonant frequencies are mutually orthogonal in the entire tuning range. A typical plot of the antenna polarization is given in fig. 5.29. All the patterns showed similar broadside radiation characteristics with reasonable cross polarization levels.

Table 5.10 Percentage area reduction at different varactor reverse bias voltages

Tuning voltage (V)	Resonant frequency		Area of equivalent rectangular patch		% Area reduction	
	f_1 (GHz)	f_2 (GHz)	f_1 (cm ²)	f_2 (cm ²)	f_1	f_2
0	1.0640	1.2960	62.9	42.3	79.9	70.2
3	1.0880	1.2960	60.2	42.3	79.0	70.2
6	1.1120	1.3040	57.6	41.8	78.1	69.8
9	1.1920	1.3040	50.1	41.8	74.8	69.8
12	1.2080	1.3040	48.8	41.8	74.1	69.8
15	1.2400	1.3200	46.3	40.8	72.7	69.1
18	1.2560	1.4000	45.1	36.3	72.0	65.2
21	1.2720	1.4240	44.0	35.0	71.3	64.0
24	1.2800	1.4400	43.4	34.3	70.9	63.1
27	1.2880	1.4560	42.9	33.5	70.5	63.3
30	1.2880	1.4640	42.9	33.1	70.5	61.9

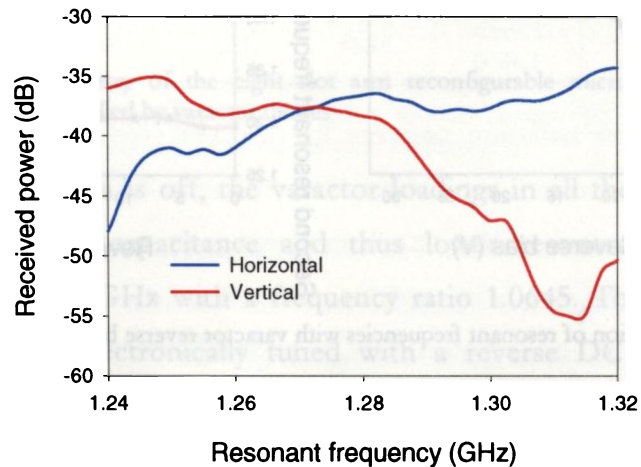






Figure 5.29 Variation received power with frequency in two orthogonal polarization planes for $V=15V$

A Comparison of all the two, three, four and eight slot arm designs studied is depicted in table 5.11.

Table 5.11 Comparison of antenna properties for all the two, three, four and eight slot arm loaded reconfigurable microstrip antenna designs

Antenna Parameter Under Consideration				
First resonant frequency, f_1(GHz)	1.1745-1.4265	1.272 -1.536	1.037-1.394	1.064-1.288
Second resonant frequency, f_2(GHz)	1.5030-1.5705	1.616 -1.848	1.359-1.485	1.296-1.464
Effective area of the antenna(cm²)	13.48	13.35	13.19	12.63
No. of slot arms used	2	3	4	8
Non-linear device used for switching	Varactor BB439	Varactor BB439	Varactor BB439	Varactor BB439
Maximum shift in frequency for f_1 (MHz)	252MHz	264MHz	357MHz	224MHz
Maximum shift in frequency for f_2 (MHz)	67.5MHz	232MHz	126MHz	168MHz
% band width for f_1	2.7903	2.1486	3.6466	6.2176
% band width for f_2	2.5497	1.2960	2.9248	10.4255
% area reduction for f_1	73.8832	69.6063	80.1053	79.9100
% area reduction for f_2	57.0843	50.8570	65.6912	70.1768
Tunable frequency ratio, f_2/f_1	1.2031 -1.2797	1.2344-1.2704	1.0653-1.3105	1.0645-1.2180
Operating band	L	L	L	L
% Tuning range for f_1	21.46	20.75	34.43	21.05
% Tuning range for f_2	4.49	14.36	9.27	12.96

5.5 Independent Frequency Tuning in Hexagonal Slot Loaded Microstrip Antenna Using Modified Slot Arm

Dual frequency patch antennas may provide an alternative to large-bandwidth antennas. The key to providing a flexible solution is to have the radiators relatively independent. We can achieve dual frequency microstrip antenna design with independent frequency selection, using a modified slot arm in the hexagonal slot loaded microstrip antenna. Dual frequency tuning has been realised using a varactor diode.

5.5.1 C-Shaped Slot Loaded Reconfigurable Microstrip Antenna

Fig. 5.30 shows the configuration of the proposed reconfigurable dual frequency microstrip antenna. The antenna structure consists of a square microstrip patch with two embedded slots. The hexagonal slot is selected in an attempt to reduce the two orthogonal resonant modes to lower frequencies. Dual frequency operation is achieved by perturbing the fundamental resonant mode of the patch with a 'C' shaped slot, thus splitting it into two distinct orthogonal resonant modes (TM_{10} and TM_{01}). A method of moment based software (IE3D) is used to optimize the dimension and orientation of the slots in the square patch. The 'C' shaped slot extends to the current density regions of TM_{10} and TM_{01} modes, respectively. Independent control of two resonant frequencies is realized by varying its vertical or horizontal dimensions by keeping the other unchanged.

Electromagnetic coupling with a 50Ω microstrip line is used to feed the patch. The antenna is fabricated on a substrate of thickness 1.6mm and $\epsilon_r = 3.95$. The optimized square patch for dual frequency L-band operation has dimension, $L=40\text{mm}$ with a regular hexagonal slot of side dimension $l_1=8\text{mm}$ inserted at its center. The 'C' shaped slot for dual frequency generation and control is etched out with width, $w_s = 1\text{mm}$ and lengths $x_1 = 10\text{mm}$ and $x_2 = 16\text{mm}$ as in fig. 5.30.

Electronic tuning of both modes is accomplished by a varactor diode integrated across the slot. The junction capacitance of the varactor varies against the reverse bias applied and these different capacitive loadings correspond to different electrical lengths and thus different resonant frequencies. DC bias is applied across the varactor through two chip inductors. A narrow slot line is carved in the patch for dc isolation. Transmission lines are avoided in between the nonlinear components and radiating element, so that, added noise and ohmic losses are suppressed and the resulting structure is more compact.

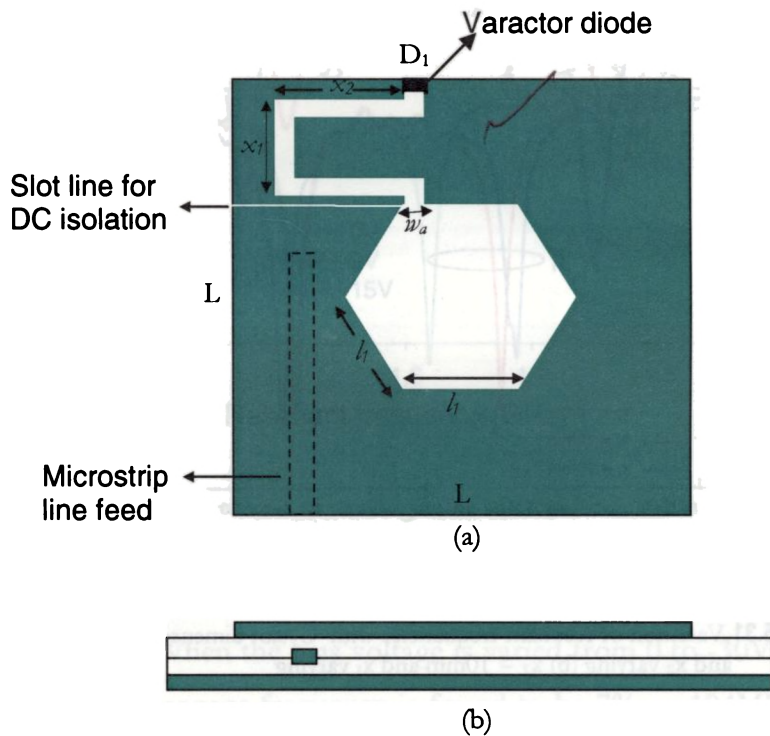


Figure 5.30 Schematic diagram of proposed reconfigurable microstrip antenna (a) Top view, (b) Side view. The antenna parameters are $L = 40\text{mm}$, $l_1 = 8\text{mm}$, $h = 1.6\text{mm}$, $w_a = 1\text{mm}$, $x_1 = 10\text{mm}$, $x_2 = 16\text{mm}$, $\epsilon_r = 3.95$

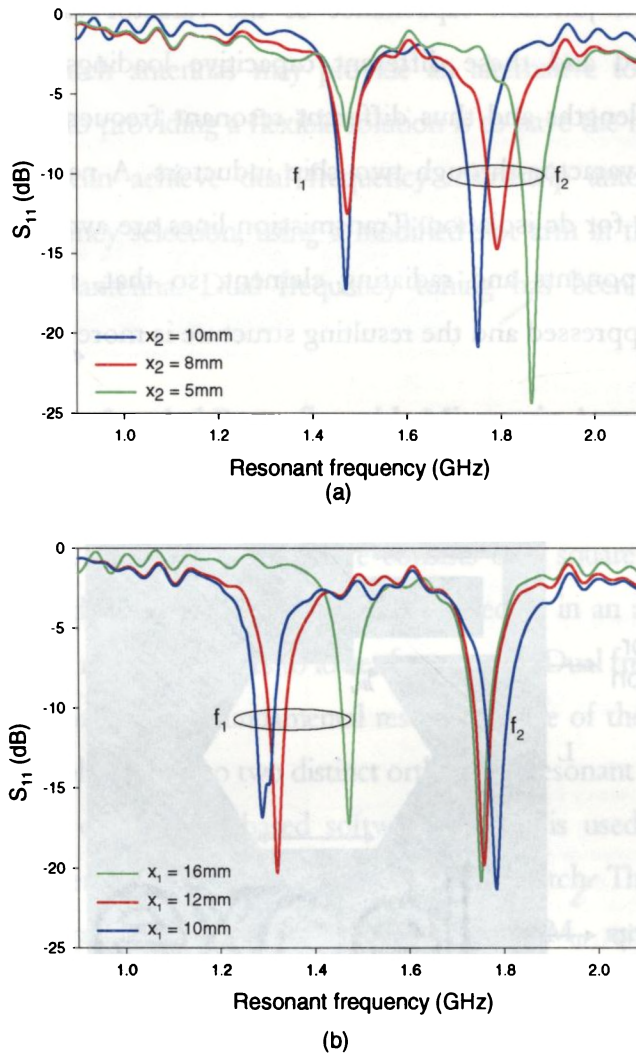


Figure 5.31 Variation of resonant frequencies with 'C' slot dimension (a) $x_1 = 16\text{mm}$ and x_2 varying (b) $x_2 = 10\text{mm}$ and x_1 varying

5.5.1.1 Independent Tuning of Dual Resonant Modes

The fundamental resonant frequency of the unslotted square patch is 1.885GHz. By etching the hexagonal slot at its center it reduces to 1.74GHz. With 'C' slot, two distinct resonant modes (TM_{10} and TM_{01}) at 1.472GHz and 1.752GHz have been

observed with a frequency ratio 1.19. Different 'C' slot dimensions, x_1 and x_2 , were tried to prove the independent frequency tuning capability of the proposed design. It was found that the first resonant frequency, f_1 can be tuned without affecting f_2 , by varying x_1 and keeping x_2 unchanged. Similarly, second resonant frequency, f_2 can be tuned by varying x_2 and keeping x_1 constant. The findings are depicted in fig. 5.31.

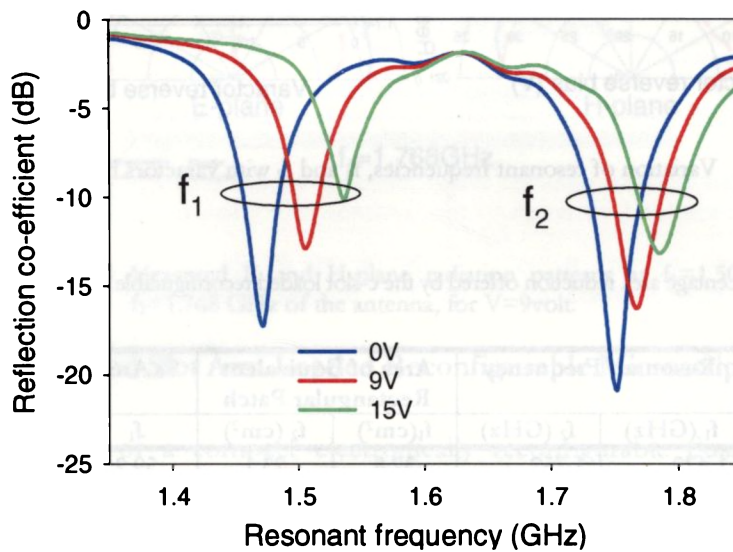


Figure 5.32 Return loss performance of reconfigurable antenna for $x_1 = 10\text{mm}$ and $x_2 = 16\text{mm}$

The antenna was then electronically tuned with a reverse dc voltage applied across the varactor. When the bias voltage is varied from 0 to -30V, the tuning range for the first resonant frequency is found to be 7% or 104MHz upwards (from 1.472 to 1.576GHz) and that of second resonant frequency is 4% or 72MHz upwards (from 1.752 to 1.824GHz) as shown in fig. 5.32. The variation of first and second resonant frequencies (f_1 and f_2) with the applied varactor reverse bias voltage is measured and plotted in fig.5.35. The gain of

the antenna for specific x_1 and x_2 values remained almost constant in the entire tuning range.

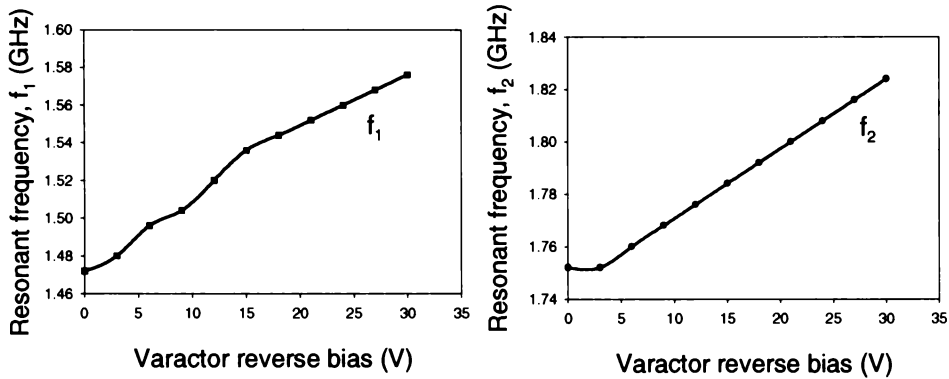


Figure 5.33 Variation of resonant frequencies, f_1 and f_2 with varactors bias voltage.

Table 5.12 Percentage area reduction offered by the c-slot loaded reconfigurable antenna design

Tuning Voltage (V)	Resonant Frequency		Area of Equivalent Rectangular Patch		% Area Reduction	
	f_1 (GHz)	f_2 (GHz)	f_1 (cm ²)	f_2 (cm ²)	f_1	f_2
0	1.472	1.752	32.8	23.1	59.2	42.2
3	1.480	1.752	32.4	23.1	58.7	42.2
6	1.496	1.760	31.8	22.9	57.9	41.6
9	1.504	1.768	31.4	22.7	57.4	41.1
12	1.520	1.776	30.8	22.5	56.5	40.5
15	1.536	1.784	30.1	22.3	55.5	39.9
18	1.544	1.792	29.8	22.1	55.1	39.3
21	1.552	1.800	29.4	21.9	54.5	38.8
24	1.560	1.808	29.2	21.7	54.1	38.4
27	1.568	1.816	28.8	21.5	53.6	37.8
30	1.576	1.824	28.6	21.3	53.2	37.2

Typical radiation plot is given in fig. 5.34. The design also offers a area reduction of 59 and 42% for f_1 and f_2 respectively, compared to standard rectangular patches. A detailed size reduction data is given in table 5.12. The polarisation planes of the two resonant frequencies are mutually orthogonal in the entire tuning range.

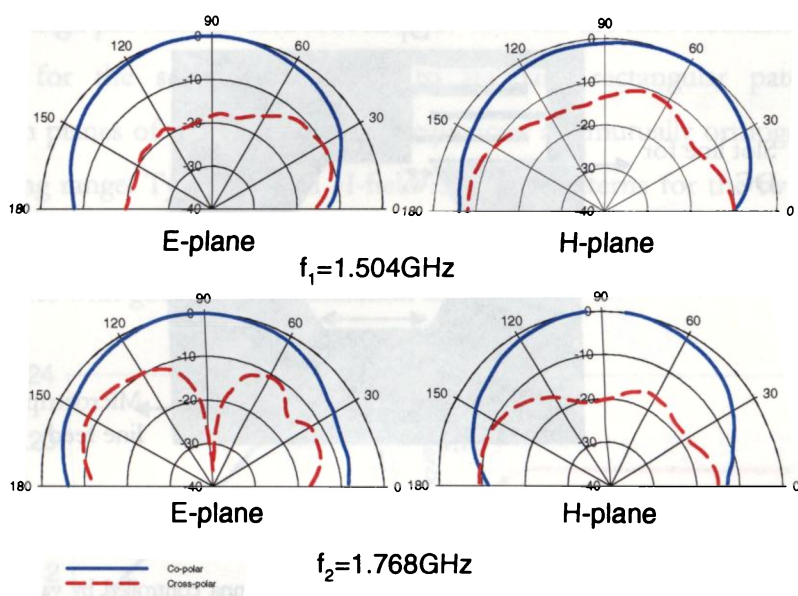


Figure 5.34 Measured E and H-plane radiation patterns at $f_1=1.504$ GHz and $f_2=1.768$ GHz of the antenna, for $V=9$ volt.

5.5.2 Meandered Slot Arm Loaded Reconfigurable Microstrip Antenna

A new design of a compact electronically reconfigurable dual frequency dual polarized single feed, meandered slot loaded microstrip antenna is also studied. A varactor diode is used to switch the operating frequencies considerably, without much affecting the radiation characteristics and gain. The antenna can work with a frequency ratio varying in a wide range from 1.36 to 1.53.

The geometry of the patch antenna is same as the C-shaped slot loaded design, except that a meandered line of dimension x_1 and x_2 is introduced in the center of the square patch, replacing the C-slot. (fig.5.35). Varactor diode D_1 is positioned at the extreme end of the slot arm in order to get maximum tuning range and better matching. A narrow slit is used to achieve good DC isolation. By electronically varying the length of the meandered slot line, using a varactor, the first resonant mode, TM_{10} can be tuned without much affecting the second resonant mode, giving different frequency ratios.

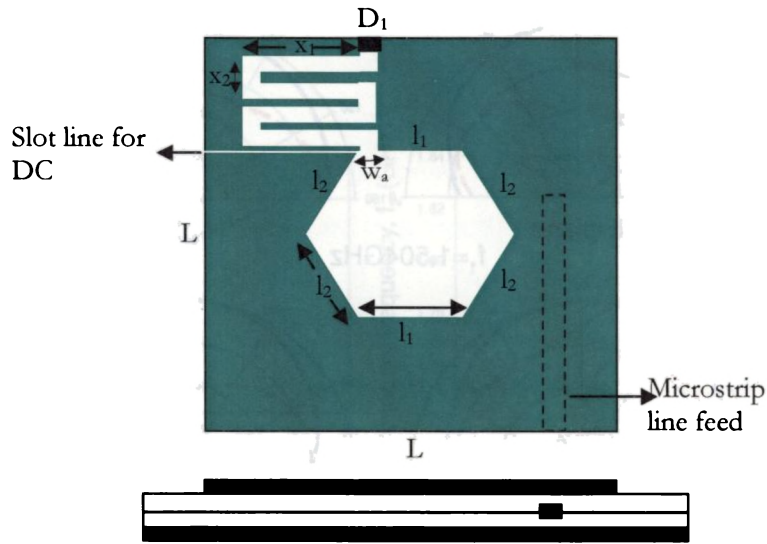


Figure 5.35 Geometry of the proposed tunable microstrip antenna controlled by varactor diode. ($L = 4\text{cm}$, $l_1 = l_2 = 0.8\text{cm}$, $x_1 = 1.6\text{cm}$, $x_2 = 0.4\text{cm}$, $w_a = 0.1\text{cm}$, $h = 0.16\text{cm}$ and $\epsilon_r = 3.98$)

When the bias voltage is varied from 0 to -30V, the tuning range for the first resonant frequency is found to be 12.4% or 136MHz upwards (from 1.096 to 1.232GHz) and that of second resonant frequency is 0.48% or 8MHz upwards (from 1.672 to 1.680GHz) as shown in fig. 5.36. The variation of first and second resonant frequencies (f_1 and f_2) with the applied varactor reverse bias voltage is measured and plotted in fig. 5.37.

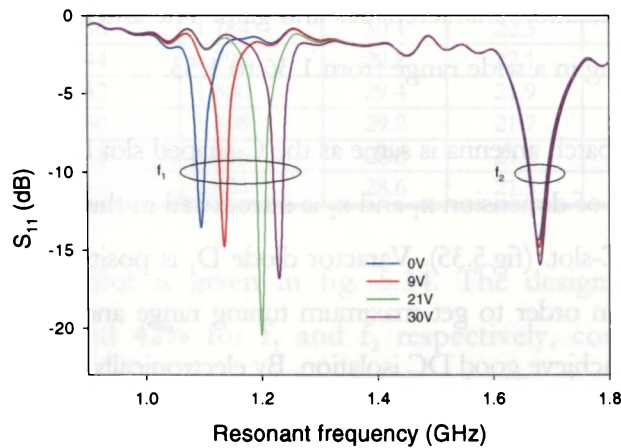


Figure 5.36 Measured return loss of the antenna for different varactor reverse bias voltages. ($L = 4\text{cm}$, $l_1 = l_2 = 0.8\text{cm}$, $x_1 = 1.6\text{cm}$, $x_2 = 0.4\text{cm}$, $w_a = 0.1\text{cm}$, $h = 0.16\text{cm}$ and $\epsilon_r = 3.98$).

The new design provides an area reduction of 78% for the first resonant frequency and 49% for the second, compared to standard rectangular patches. The polarization planes of the two resonant frequencies are mutually orthogonal in the entire tuning range. Typical E and H-field radiation patterns for the two resonant modes are displayed in fig. 5.38. All the patterns show similar broadside radiation characteristics with good cross polarization levels.

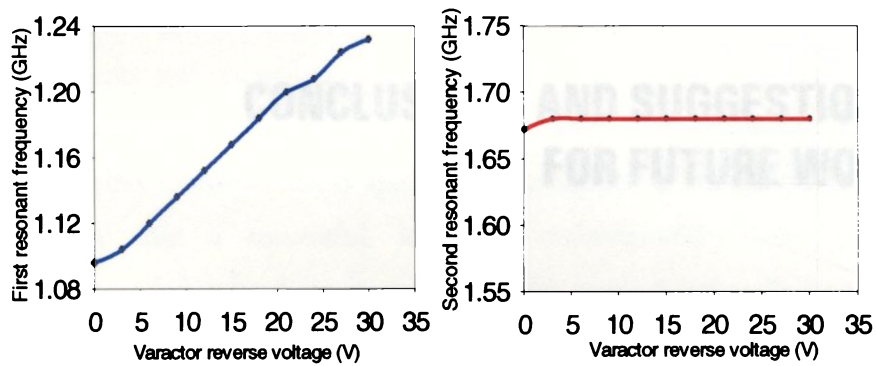


Figure 5.37 Variation of resonant frequencies with varactor reverse bias voltage, (a) f_1 (b) f_2

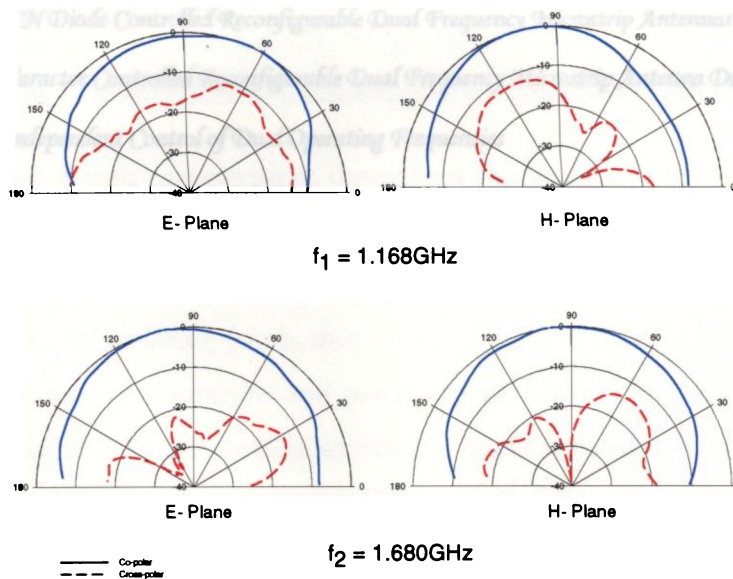


Figure 5.38 Measured E and H-plane radiation patterns at $f_1=1.168\text{GHz}$ and $f_2=1.68\text{GHz}$ of the antenna, for $V= -15\text{volt}$.

CHAPTER

6

CONCLUSIONS AND SUGGESTIONS FOR FUTURE WORK

Contents

6.1	<i>Inferences from Passive Dual-Frequency Microstrip Antenna</i>	187
6.2	<i>PIN Diode Controlled Reconfigurable Dual Frequency Microstrip Antennas</i>	188
6.3	<i>Varactor Controlled Reconfigurable Dual Frequency Microstrip Antenna Designs</i>	189
6.4	<i>Independent Control of Dual Operating Frequencies</i>	189
6.5	<i>Suggestions for Future Work</i>	190

This chapter presents the conclusions drawn from the detailed theoretical and experimental investigations performed on the newly proposed electronically reconfigurable dual frequency microstrip antenna and the scope for further research work. The goal of this thesis has been to develop and optimize compact single feed dual frequency microstrip antenna that would demonstrate an electronically reconfigurable dual-frequency of operation, without the use of any matching networks and complicated biasing circuitry. These antennas have been designed to operate in a very popular frequency range (L-band) where a great number of wireless communication applications exist. From this analysis, it has been concluded that a successful, low cost reconfigurable dual-frequency microstrip antenna design has been introduced to the wireless and radio frequency design community. The strict requirements of constant input impedance, gain, radiation pattern and polarization are achieved by carefully designing the passive antenna structure and the tuning. PIN diodes and Varactor diodes are used for the switching/tuning mechanism.

6.1 Inferences from Passive Dual-Frequency Microstrip Antennas

The important design considerations throughout this study are compactness of the patch, tuning of operating frequencies in a comparatively wide range without the use of any matching networks and simplified switching/tuning mechanism directly integrated into the radiating patch, thus avoiding the use of any transmission lines between non-linear components and patch. All are realized by suitably designing the hexagonal slot loaded square microstrip patch antenna with a single feed excitation for dual frequency operation. The integrated slot arms not only provided a flexible frequency tuning facility but also enhanced the compact feature of the reconfigurable antenna design. The design and theoretical analysis of the initial passive patch are carried out using the indigenously developed full wave analysis,

FDTD and with a commercially available Moment Method electromagnetic simulator, IE3D. The theoretical, simulated and the experimental results are in good agreement.

important conclusion

As both the FDTD and the IE3D results proved the dual polarized dual frequency operation of the proposed design, rigorous experiments are conducted to study the mechanical tuning of the antenna by varying the slot arm length. The idea of dual frequency tuning and frequency ratio tuning is incorporated into these designs by suitably embedding additional slot arms. Single and dual orthogonal slot arm loaded designs proved to be capable of dual frequency tuning, while, dual vertical slot arm loaded designs are meant for frequency ratio tuning.

6.2 PIN Diode Controlled Reconfigurable Dual Frequency Microstrip Antennas

The dual resonant frequencies depend on the lengths of the slot arms, and therefore they are tuned by changing the electrical length of the protruding slot arm. This is readily accomplished by introducing a short circuit at specific location on the slot arm. To implement the electronic reconfigurability, the ideal short is replaced by a PIN diode. When the diode is switched OFF, the antenna resonates at 1.48 GHz and 1.99 GHz with a frequency ratio 1.34. Once the diode is turned ON with a 1 volt DC bias, the first resonant frequency shifts 105 MHz and second resonant frequency, 60 MHz, giving excitation at 1.585 GHz and 2.05 GHz with a frequency ratio 1.29. In all these four operating frequencies, the antenna has a good matching at a single feed position.

Two pin diodes are then embedded in the dual vertical arms of the central hexagonal slot to switch the two resonant frequencies of the antenna, considerably, by changing the electrical length of the slot. Thus multiple frequencies are generated in a single antenna aperture by controlling the DC bias of the two PIN diodes. This design is well suited for frequency ratio tuning.

6.3 Varactor Controlled Reconfigurable Dual Frequency Microstrip Antenna Designs

More flexible reconfigurable dual frequency operation is achieved by replacing the PIN diodes with Varactor diodes. The basic biasing circuitry and the feeding mechanism used for the PIN diode switched reconfigurable antennas are kept unaltered. Rigorous studies are carried out to demonstrate the reconfigurable dual frequency operation and frequency ratio tuning by suitably selecting the slot arms and their orientation. Varactor tuned independent reconfigurable antenna designs are studied with one to eight slot arms embedded with the central hexagonal slot. The design with two vertical slot arms can achieve a tunable frequency ratio 1.1 to 1.37. The triple slot arm loaded design has a tuning range of 20.8% and 14.4% for the first and second resonant frequencies, respectively with a very feeble change of 1.2 to 1.27% in frequency ratio. A maximum of 34.4% tuning in the first resonant frequency alone is obtained in the four slot arm antenna configuration.

6.4 Independent Control of Dual Operating Frequencies

Compact electronically reconfigurable dual frequency microstrip antenna design with independent control of the two operating frequencies is proposed and experimentally verified. Independent frequency selection is made possible by including a 'C' shaped slot in the hexagonal slot. The technique described uses a highly simplified varactor tuning circuit without any transmission lines. The design also offers a size reduction of 59 and 42% for f_1 and f_2 respectively, compared to standard rectangular patches.

A meandered slot arm is then used with the central hexagonal slot to enhance the area reduction of the square patch reconfigurable antenna. An area reduction of 78% and 48.8% are obtained for the first and second resonant frequencies, respectively compared to standard rectangular patches.

6.5 Suggestions for Future Work

A novel method for designing affordable, compact, electronically reconfigurable dual frequency microstrip antennas with single feed excitation operating in the entire L-band is proposed in this thesis.

For more accurate design and analysis of the hexagonal slot loaded reconfigurable antenna, Conformal FDTD method with Berenger's PML boundary conditions can be used in place of 3D-FDTD with staircase approximation. PIN diodes and Varactors can be replaced with RF-MEMS in order to minimize the loading effect.

A modification of the same frequency reconfigurable antenna design with both radiation pattern and polarization reconfigurability is also an interesting topic for future research.

REFERENCES

References

1. M. S. Longair, *Theoretical Concepts in Physics*, Cambridge University Press, 1984
2. J. D. Kraus, *Antennas: Our Electronic Eyes and Ears*, Microwave Journal, January 1989
3. David M. Pozar, *Microstrip Antennas*, Proceedings of IEEE, vol-80, no-1, January 1992
4. K.R. Carver and J.M. Mink, *Microstrip Antenna Technology*, IEEE Antennas and Propagation, vol-AP-29, No-1, January 1981
5. Lewin, *Spacious Radiation from Microstrip*, Proceedings of IEE, vol-125, no-7, July 1978
6. E.V. Byron, *A New Flush Mounted Antenna Element for Phased Array Applications*, Proceedings of Phased Array Antenna Symposium, 1970, pp. 187-192.
7. R.E Munson, *Single Slot Cavity Antennas*, US patent no-3713162, January 22, 1973
8. J.Q Howell, *Microstrip Antennas*, Dig. International Symposium Antennas Propagation Society, Williamsburg, VA, Dec 1972, pp. 177-180
9. G. W. Garwin, R. E. Munson, L. T. Ostwald and K. G. Schroeder, *Low Profile Electrically Small Missile Base Mounted Microstrip Antennas*, Dig. International Symposium Antennas Propagation Society, Urbana, IL, June 1975, pp. 244-247
10. J. Q. Howell, *Microstrip Antennas*, IEEE Transactions on Antennas and Propagation, vol-AP-23, no-1, pp. 90-93, January 1975
11. H. D. Weinschel, *A Cylindrical Array of Circularly Polarized Microstrip Antennas*, Dig. International Symposium Antennas Propagation Society, Urbana, IL, June 1975, pp. 177-180
12. J. R. James and G. J. Wilson, *New Design Techniques for Microstrip Antenna Arrays*, Proceedings of 5th European Microwave Conference, Hamburg, September 1975, pp. 102-106
13. Ramesh Garg, P. Bhartia, I. Bhal and A. Ittipiboon, *Microstrip Antenna Design Handbook*, Artech House, 2001
14. C. H. Chen et al, *Broadband Two Layer Microstrip Antenna*, IEEE Antennas and Propagation Symposium Digest, 1984, pp. 251-254
15. Y. Quian et al, *Microstrip Patch Antenna Using Novel Photonic Bandgap Structures*, Microwave Journal, vol-42, January 1999, pp. 66-76
16. I. J Bhal and P. Bhartia, *Microstrip Antennas*, Artech House
17. J.R. James, P.S. Hall and C. Wood, *Microstrip Antenna Theory and Design*, Peter Petergrins, 1981

18. Bhattacharya, L. Shafai, and R. Garg, *Microstrip antenna- A Generalized Transmission Line*, Progress in Electromagnetics Research, vol-4, 1991, pp. 45-84
19. Y. T. Lo et al, *Theory and Experiments on Microstrip Antennas*, IEEE Transactions on Antennas and Propagation, vol-AP-27, 1979, pp. 137-145.
20. W. F. Richards et al, *An Improved Theory for Microstrip Antennas and Applications*, IEEE Transactions on Antennas and Propagation, vol-AP-29, 1981, pp. 38-46
21. D. M. Pozar and B. Kaufman, *Increasing the Bandwidth of a Microstrip Antenna by Proximity Coupling*, Electronics Letters, vol-23, pp. 368-369, April 1987
22. D. M. Pozar, *A Microstrip Antenna Aperture Coupled to a Microstrip Line*, Electronics Letters, vol-21, pp. 49-50, January 1985
23. G. Gronau and I. Wolff, *Aperture Coupling of a Rectangular Microstrip Resonator*, Electronic Letters, vol-22, pp. 554-556, May 1986.
24. D. M. Pozar, *Radiation and Scattering from a Microstrip Patch on a Uniaxial Substrate*, IEEE Transactions on Antennas and Propagation, vol-AP-35, 1987, pp. 613-621
25. M. D. Deshpande and M. C. Bailey, *Input Impedance of Microstrip Antennas*, IEEE Transactions on Antennas and Propagation, vol-AP-30, 1982, pp. 645-650.
26. J. R. Mosig and F. E. Gardiol, *A Dynamic Radiation Model for Microstrip Structures*, Advances in Electronics and Electron Physics, vol-59, 1982, pp. 139-234.
27. A. Taflove, *Computational Electrodynamics: The Finite Difference Time Domain Method*, Artech House, Norwood, MA, 1995
28. K. S. Yee, *Numerical Solution of Initial Boundary Value Problems Involving Maxwell's Equations in Isotropic Media*, IEEE Transactions on Antennas and Propagation, vol-AP-14, 1966, pp. 302-307
29. S. A. Long and M. D. Walton, *A Dual Frequency Stacked Circular Disc Antenna*, IEEE Transactions on Antennas and Propagation, vol-AP-27, 1979, pp. 1281-1285.
30. J. S. Dahele, K. F. Lee, D. P. Wong, *Dual Frequency Stacked Annular Ring Microstrip Antenna*, IEEE Transactions on Antennas and Propagation, vol-AP-35, 1987, pp. 137-145
31. J. Wang, R. Fralich, C. Wu, L. Litva, *Multifunctional Aperture Coupled Stack Antenna*, Electronics Letters, 26, 25, December 1990, pp. 2067-2068
32. W. F. Richards, S. E. Davidson, S. A. Long, *Dual Band Reactively Loaded Microstrip Antenna*, IEEE Transactions on Antennas and Propagation, vol-AP-33, 1985, pp. 556-560
33. S. E. Davidson, S. A. Long, W. F. Richards, *Dual Band Microstrip Antenna with Monolithic Reactive Loading*, Electronics Letters, 21, 21, 1985, pp. 936-937

34. S. Maci and G. Biffi Gentili, *Dual Frequency Patch Antennas*, IEEE Antennas and Propagation Magazine, vol-39, No-6, December 1997, pp. 13-20
35. J. S. Chen and K. L. Wong, *A Single Layer Dual Frequency Rectangular Microstrip Patch Antenna Using a Single Probe Feed*, Microwave and Optical Technology Letters, 11, 2, 1996, pp. 38-42
36. Y. M. M. Antar, A. I. Ittipiboon, A. K. Bhattacharya, *A Dual Frequency Antenna Using a Single Patch and an Inclined Slot*, Microwave and Optical Technology Letters, 8, 6, 1995, pp. 1906-1907
37. M. Piessis du, J. H. Cloete, *Tuning Stubs for Microstrip Patch Antennas*, IEEE Antennas and Propagation Society Magazine, Vol-36, No-6, 1994, pp. 52-55
38. D. H. Schaubert et al, *Microstrip Antennas with Frequency Agility and Polarization Diversity*, IEEE Transactions on Antennas and Propagation, vol-AP-29, 1981, pp. 118-121
39. J. S. Dahele, K. F. Lee, *Theory and Experiment on Microstrip Antennas with Air gaps*, IEE Proceedings , Vol. 132, 1985, pp. 455-460
40. A. Henderson, J. R James, D. Fray, *Magnetized Microstrip Antenna with Pattern Control*, Electronics Letters, vol-24, June 9, 1988, pp. 45-47
41. D. M Pozar and V. Sanchez, *Magnetic Tuning of a Microstrip Antenna on a Ferrite Substrate*, Electronics Letters, vol-24, June 9, 1988, pp. 729-731
42. N. Fayyaz, S. Safavi-Naeini, E. Shin, N. Hodjat, *A Novel Electronically Tunable Rectangular Patch Antenna with One Octave Bandwidth*, Proceedings of IEEE Canadian Conference on Electrical and Computer Engineering, 1998, vol-1, pp. 25-28
43. S. H. Al-Charchafchi, M. Frances, *Electronically Tunable Microstrip Patch Antennas*, IEEE Antennas and Propagation Symposium Digest, 1998, vol-1, pp. 304-307
44. P. J. Rainville, F. J. Harackewicz, *Magnetic Tuning of a Microstrip Patch Antenna Fabricated on a Ferrite Film*, IEEE Microwave and Guided Wave Letters, 1992, vol-2, pp. 483-485
45. S. Kawasaki, T. Itoh, *A Slot Antenna with Electronically Tunable Length*, IEEE Antennas and Propagation Symposium Digest, 1991, vol-1, pp. 130-133
46. D. J. Roscoe, L. Shafai, A. Ittipiboon, M. Cuhaci, R. Douville, *Tunable Dipole Antennas*, IEEE Antennas and Propagation Symposium Digest, 1972, vol-2, pp. 672-675
47. Aly E. Fathy et al, *Silicon Based Reconfigurable Antennas - Concepts, Analysis, Implementation and Feasibility*, IEEE Transactions on Microwave Theory and Techniques, vol-51, no-6, pp. 1650-1660, June 2003

48. G. H. Huff, J. Feng, S. Zhang, J. T. Bernhad, *A Novel Radiation Pattern and Frequency Reconfigurable Single Turn Square Microstrip Spiral Antenna*, IEEE Microwave and Wireless Components Letters, vol-13, no-2, pp. 57-59, February 2003
49. G. A. Deschamps, *Microstrip Microwave Antennas*, 3rd USAF Symposium on Antennas, 1953
50. H. Gutton and G. Baissinot, *Flat Aerial for Ultra high Frequencies*, French Patent No. 703113, 1955
51. L. Lewin, *Radiation From Discontinuities in Stripline*, Proceedings of Institution of Electronic Engineers, vol-107, pp. 163-170, February 1960
52. H. D. Weinschel, *Progress Report on Development of Microstrip Cylindrical Arrays for Sounding Rockets*, Physic. and Sci. Lab., New Mexico State University, 1973
53. G. G. Sanford, *Conformal Microstrip Phased Array for Aircraft tests with ATS-6*, Proceedings of National Electronic Conference, vol-29, pp. 252-257, October 1974
54. R. E. Munson, *Conformal Microstrip Antennas and Microstrip Phased Arrays*, IEEE Transactions on Antennas and Propagation, vol-AP-22, January 1974, pp. 74-77
55. A. G. Derneryd, *Linear Microstrip Array Antennas*, Technical Report, Chalmers University of Technology, Sweden, TR 7505, October 1975
56. K. R. Carver, *The radiation Pattern of a Microstrip Disc Antenna*, Physic. and Sci. Lab., Tech. Memo., New Mexico State University, 1976
57. Y. T. Lo, D. D. Harrison, D. Solomon, G. A. Deschamps and F. R. Ore, *Study of microstrip Antennas, Microstrip Phased Arrays and Microstrip Feed Networks*, Rome Air Development Center, Technical Report, TR-77-406, October 1977
58. A. G. Derneryd, *A Theoretical Investigation of the Rectangular Microstrip Antenna Element*, Rome Air Development Center, Technical Report, TR-77-206, June 1977
59. L. C. Chen and S. A. Long, *Low Profile Printed Circuit Antennas*, Dept. of Electrical Engineering, University of Houston, TX, DAAG-29-75-0187, October 1977
60. K. R. Carver and E. L. Coffey, *Theoretical Investigation of the Microstrip Antenna*, Physic. and Sci. Lab., Tech. Memo., PT-00929, New Mexico State University, 1976
61. D. H. Schaubert and F. G. Farrar, *Some Conformal Printed Circuit Antenna Designs*, Proceedings of Workshop on Printed Circuit Antenna Technology, New Mexico State University, pp. 5/1-21, October 1979
62. E. H. Newman and D. M. Pozar, *Electromagnetic Modeling of Composite Wire and Surface Geometries*, IEEE Transactions on Antennas and Propagation, vol-AP-26, no-6, 1978, pp. 784-789
63. E. L. Newman, *Strip Antennas in a Dielectric Slab*, IEEE Transactions on Antennas and Propagation, vol-AP-26, no-5, 1978, pp. 647-653

64. E. L. Coffey and K. R. Carver, *Towards the Theory of Microstrip Antenna Patterns*, Proceedings of Antenna Application Symposium, Allerton Park, IL, 1977
65. E. L. Coffey and T. H. Lehman, *A New Analysis Technique for Calculating the Self and Mutual Impedance of Microstrip Antennas*, Proceedings of Workshop on Printed Circuit Antenna Technology, New Mexico State University, pp. 31/1-21
66. K. R. Carver, *A Modal Expansion Theory for the Microstrip Antenna*, Dig. Int. Symposium on Antenna and Propagation Society, Seattle, WA, June 1979, 101-104
67. K. R. Carver, *Practical Analytical Techniques for the Microstrip Antenna*, Proceedings of Workshop on Printed Circuit Antenna Technology, New Mexico State University, pp. 7/1-20, October 1979
68. J. H. Richmond, *A Wire Grid Model for Scattering by Conducting Bodies*, IEEE Transactions on Antennas and Propagation, vol-AP-14, 1966, pp. 782-786
69. J. R. James and P. S. Hall, *Handbook of Microstrip Antennas*, Peter Peregrinus, 1989
70. D. H. Schaubert, D. M. Pozar, A. Adrian, *Effect of Microstrip Antenna Substrate Thickness and Permittivity*, IEEE Transactions on Antennas and Propagation, vol-AP-37, 1989, pp. 677-682
71. W. C. Chew and J. A. Kong, *Analysis of Circular Microstrip Disc Antenna with a Thick Dielectric Substrate*, IEEE Transactions on Antennas and Propagation, vol-AP-29, 1981, pp. 68-76
72. J. T. Aberle and D. M. Pozar, *Analysis of Infinite Arrays of One and Two Probe Fed Circular Patches*, IEEE Transactions on Antennas and Propagation, vol-AP-38, 1990, pp. 421-432
73. M. C. Bailey and M. D. Deshpande, *Analysis of Elliptical and Circular Microstrip Antennas Using Moment Method*, IEEE Transactions on Antennas and Propagation, vol-AP-33, 1985, pp. 954-959
74. M. Haneishi and Y. Suzuki, *Circular Polarization and Bandwidth*, in Handbook of Microstrip Antennas, vol-1, J. R. James and P. S. Hall, Peter Peregrinus, London, 1989
75. Y. Suzuki, N. Miyano, T. Chiba, *Circularly Polarized Radiation from Singly Fed Equilateral Triangular Microstrip Antenna*, in Microstrip Antenna Design, K. C. Gupta and A. Benalla, Artech House, 1988, pp. 338-342
76. K. K. Tsang and R. J. Langley, *Design of Circular Patch Antennas on Ferrite Substrate*, IEE Proceedings of Microwave Antennas and Propagation, vol-145, no-1, 1998, pp. 49-55
77. L. C. Schen, *The Elliptical Microstrip Antenna with Circular Polarization*, IEEE Transactions on Antennas and Propagation, vol-AP-29, 1981, pp. 90-94

78. S. A. Long et al, *An Experimental Study of the Circular Polarized Elliptical Printed Circuit Antenna*, IEEE Transactions on Antennas and Propagation, vol-AP-29, 1981, pp. 95-99
79. M. Haneishi and S. Yoshida, *A Design Method of Circularly Polarized Rectangular Microstrip Antenna by One-Point Feed*, in , K. C. Gupta and A. Benalla, Artech House, 1988, pp. 313-321
80. J. Huang, *A Technique for an Array to Generate Circular Polarization with Linearly Polarized Elements*, IEEE Transactions on Antennas and Propagation, vol-AP-34, 1986, pp. 1113-1124
81. D. M. Pozar, *A Microstrip Antenna Aperture Coupled to a Microstrip Line*, Electronics Letters, vol-21, 1985, pp. 49-50
82. P. L. Sullivan and D. H. Schaubert, *Analysis of an Aperture Coupled Microstrip Antenna*, IEEE Transactions on Antennas and Propagation, vol-AP-34, 1986, pp. 977-984
83. D. M. Pozar, *A reciprocity Method of Analysis for Printed Slot and Slot Coupled Microstrip Antennas*, IEEE Transactions on Antennas and Propagation, vol-AP-34, 1986, pp. 1439-1445
84. D. M. Pozar and S. M. Voda, *A Rigorous Analysis of a Microstrip Line Fed Patch Antenna*, IEEE Transactions on Antennas and Propagation, vol-AP-35, 1987 pp. 1343-1350
85. S. D. Targonski and D. M. Pozar, *Design of Wide Band Circularly Polarized Aperture Coupled Microstrip Antennas*, IEEE Transactions on Antennas and Propagation, vol-AP-41, 1993, pp. 214-220
86. M. Himdi, J. P. Daniel and C Terret, *Analysis of Aperture Coupled Microstrip Antenna Using Cavity Method*, Electronics Letters, vol-25, 1989, pp. 391-392
87. M. A. Saed, *Efficient Method for Analysis and Design of Aperture Coupled Rectangular Microstrip Antennas*, IEEE Transactions on Antennas and Propagation, vol-AP-41, 1993, pp. 986-988
88. M. Yazidi, H. Himidi and J. P. Daniel, *Aperture Coupled Microstrip Antenna for Dual Frequency Operation*, Electronics Letters, vol-29, 1993, pp. 1506-1508
89. M. Himdi, J. P. Daniel and C Terret, *Transmission Line Analysis of Aperture Coupled Microstrip Antenna*, Electronics Letters, vol-25, 1989, pp. 1229-1230
90. M. Yazidi, H. Himidi and J. P. Daniel, *Transmission Line Analysis of Non Linear Slot Coupled Microstrip Antenna* , Electronics Letters, vol-28, 1992, pp. 1406-1408
91. A. Ittipiboon et al, *A Modal Expansion Method of Analysis and Measurement on Aperture Coupled Microstrip Antenna*, IEEE Transactions on Antennas and Propagation, vol-AP-39, 1991, pp. 1567-1574

92. R. Q. Lee et al, *Characteristics of a Two Layer Electromagnetically Coupled Microstrip Patch Antenna*, Electronics Letters, vol-23, 1987, pp. 1070-1072
93. F. Croq, G. Kossiavas and A. Papiernik, *Stacked Resonators for Bandwidth Enhancement: A Comparison of Two Feeding Techniques*, IEE Proceedings, vol-140, 1993, pp. 303-308
94. C. H. Tsao et al, *Aperture Coupled Patch Antennas with Wide Bandwidth and Dual Polarization Capabilities*, IEEE Antennas and Propagation Symposium Digest, 1988, pp. 936-939
95. F. Croq and D. M. Pozar, *Millimeter Wave Design of Wide Band Aperture Coupled Stacked Microstrip Antennas*, IEEE Transactions on Antennas and Propagation, vol-AP-39, 1991, pp. 1770-1776
96. G. Kumar and K. C. Gupta, *Broadband Microstrip Antennas Using Additional Resonators Gap Coupled to the Radiating Edges*, IEEE Transactions on Antennas and Propagation, vol-AP-32, 1984, pp. 1375-1379
97. E. Entsehladen and U. Nagel, *Microstrip Patch Array Antenna*, Electronics Letters, vol-20, 1984, pp. 931-933
98. C. K. Aanandan, P. Mohanan and K. G. Nair, *Broadband Gap Coupled Microstrip Antenna*, IEEE Transactions on Antennas and Propagation, vol-AP-38, 1990, pp. 1581-1586
99. H. F. Pues and A. R. Van de Capelle, *An Impedance Matching for Increasing the Bandwidth of Microstrip Antennas*, IEEE Transactions on Antennas and Propagation, vol-AP-37, 1989, pp. 1345-1354
100. D. A. Paschen, *Practical Examples of Integral Broadband Matching of Microstrip Antenna Elements*, Proceedings of Antenna Applications Symposium, 1986, pp. 199-217
101. K. L. Wong and Y. F. Lin, *Small Broadband Rectangular Microstrip Antenna with Chip Resistor Loading*, Electronics Letters, vol-33, 1997, pp. 1593-1594
102. K. L. Wong and Y. F. Lin, *Microstrip Line Fed Compact Microstrip Antenna with Broadband Operation*, IEEE Antennas and Propagation Symposium Digest, 1998, pp. 1120-1123
103. G. Kossiavas et al, *The CPatch – A Small Microstrip Element*, Electronics Letters, vol-25, 1989, pp. 253-254
104. G. A. E. Vandenbosch, *Capacitive Matching of Microstrip Antennas*, Electronics Letters, vol-31, no-18, 1995, pp. 1535-1536
105. R. R. Corbett and R. D. Murch, *A Capacitively Loaded PIFA for Compact Mobile Telephone Handsets*, IEEE Transactions on Antennas and Propagation, vol-45, no-5, May 1997, pp. 837-842

106. K. L. Wong and S. Cheng Pan, *Compact Triangular Microstrip Antenna*, Electronics Letters, vol-33, no-6, 1997, pp. 433-434
107. J. H. Lu, C. L. Tang and K. L. Wong, *Slot Coupled Small Triangular Microstrip Antenna*, Microwave and Optical Technology Letters, vol-16, no-6, December 1997, pp. 371-374
108. K. L. Wong and Y. F. Lin, *Small Broadband Rectangular Microstrip Antenna with Chip Resistor Loading*, Electronics Letters, vol-33, no-19, 1997, pp. 1593-1594
109. C. Y. Huang, J. Y. Wu and K. L. Wong, *Slot Coupled Microstrip Antenna for Broadband Circular Polarization*, Electronics Letters, vol-30, no-9, 1995, pp. 835-836
110. K. M. Luk, R. Chair and K. F. Lee, *Small Rectangular Patch Antenna*, Electronics Letters, vol-34, no-25, 1998, pp. 2366-2367
111. Wen-Hsiu Hsu and K. L. Wong, *Circularly Polarized Disk – Sector Microstrip Antenna*, Electronics Letters, vol-34, no-23, 1998, pp. 2188-2190
112. S. K. Satpathy, G. Kumar and K. P. Ray, *Compact Shorted Variations of Triangular Microstrip Antennas*, Electronics Letters, vol-34, no-8, 1998, pp. 709-711
113. R. Chair, K. M. Luk and K. F. Lee, *Small Dual Patch Antenna*, Electronics Letters, vol-35, no-10, 1999, pp. 762-764
114. J. Y. Sze and K. L. Wong, *Single Layer Single Patch Broadband Rectangular Microstrip Antenna*, Microwave and Optical Technology Letters, vol-22, no-4, August 20, 1999, pp. 234-236
115. Cheng – Shong Hong, *Small Annular Slot Antenna with Capacitor Loading*, Electronics Letters, vol-36, no-2, 2000, pp. 110-111
116. M. C. Liang, Y. L. Kuo, Y. M. Yen and W. C. Lai, *Capacitor Loaded Frequency Control Scheme for Circular Patch Antenna*, Electronics Letters, vol-36, no-21, 2001, pp. 1757-1758
117. Y. J. Wang, C. K. Lee and N. C. Karmakar, *A Novel Microstrip Patch Antenna for 3G IMT – 200 Mobile Handsets*, Microwave and Optical Technology Letters, vol-31, no-6, December 20, 2001, pp. 488-490
118. Jaume Anguera, Carles Puente, Carmen Borja, Gisela Font and Jordi Soler, *A Systematic Method to Design Single Patch Broadband Microstrip Patch Antennas*, Microwave and Optical Technology Letters, vol-31, no-2, November 5, 2001, pp. 185-188
119. J. P. Lee and Seong – Ook Park, *The Meander Line Antenna for Bluetooth*, Microwave and Optical Technology Letters, vol-34, no-2, July 20, 2002, pp. 149-151
120. Y. J. Wang, Y. B. Gan and C. K. Lee, *A Broadband and Compact Microstrip Antenna for IMT-2000, DECT and Bluetooth Integrated Handsets*, Microwave and Optical Technology Letters, vol-32, no-3, February 5, 2002, pp. 204-207

121. Aaron K. Schakelford, K. F. Lee and K. M. Luk, *Design of Small Size Wide Bandwidth Microstrip Patch Antennas*, IEEE Antennas and Propagation Magazine, vol-45, no-1, February 2003, pp. 75-83
122. S. K. Roy, *Performance of the Transmission Line Model for the Microstrip Elements*, International Journal of Electronics, vol-87, no-6, pp. 703-707
123. Martin Schubler, Jens Freese and Rolfy Jakoby, *Design of Compact Planar Antennas Using LH-Transmission Lines*, 2004 IEEE MTT – S Digest, pp. 209-212
124. B. F. Wang and Y. T. Lo, *Microstrip Antennas for Dual Frequency Operation*, IEEE Transactions on Antennas and Propagation, vol-32, May 1984, pp. 938-943
125. C. Salvador, L. Boreselli, A. Falciani and S. Maci, *Dual Frequency Planar Antenna at S and X Bands*, Electronics Letters, vol-31, no-20, 1995, pp. 1706-1707
126. K. L. Wong and G. B. Hsieh, *Dual Frequency Circular Microstrip Antenna with a Pair of Arc – Shaped Slots*, Microwave and Optical Technology Letters, vol-19, no-5, December 20, 1998, pp. 410-412
127. K. L. Wong and W. S. Chen, *Slot Loaded BowTie Microstrip Antenna for Dual Frequency Operation*, Electronics Letters, vol-34, no-18, 1998, pp. 1713-1714
128. W. Chen, *Single Feed Dual Frequency Rectangular Microstrip Antenna with Square Slot*, Electronics Letters, vol-34, no-3, 1998, pp. 231-232
129. E. Lee, P. S. Hall and P. Gardner, *Compact Dual-Band Dual-Polarization Microstrip Patch Antenna*, Electronics Letters, vol-35, no-13, 1999, pp. 1034-1036
130. J. H. Lu and K. L. Wong, *Dual Frequency Rectangular Microstrip Antenna with Embedded Spur Lines and Integrated Reactive Loading*, Microwave and Optical Technology Letters, vol-21, no-4, May 20, 1999, pp. 272-275
131. Jui – Han Lu, *Novel Dual – Frequency Design of Single Feed Equilateral Triangular Microstrip Antenna*, Microwave and Optical Technology Letters, vol-22, no-2, July 20, 1999, pp. 133-136
132. Y. X. Guo, K. M. Luk and K. F. Lee, *Dual – Band Slot Loaded Short – Circuited Patch Antenna*, Electronics Letters, vol-36, no-4, 2000, pp. 289-291
133. J. H. Lu, *Slot – Loaded Rectangular Microstrip Antenna for Dual – Frequency Operation*, Microwave and Optical Technology Letters, vol-24, no-4, February 20, 2000, pp. 235-237
134. Xue – Xia Yang and S. Zhong, *Analysis of Two Dual – Polarization Square – Patch Antennas*, Microwave and Optical Technology Letters, vol-26, no-3, August 5, 2000, pp. 153-156
135. C. Tang, J. Y. Chiou and K. L. Wong, *Broadband Dual – Frequency V – Shape Patch Antenna*, Microwave and Optical Technology Letters, vol-25, no-2, April 20, 2000, pp. 121-123

136. M. M. Vazquez, M. Geissler, D. Heberling, A. M. Gonzalez and David Hernandez, *Compact Dual Band Antenna for Mobile Handsets*, Microwave and Optical Technology Letters, vol-32, no-2, January 20, 2002, pp. 87-88
137. G. S. Binoy, C. K. Aanandanan, P. Mohanan and K. Vasudevan, *Slot Coupled Square Microstrip Antenna for Compact Dual Frequency Operation*, Microwave and Optical Technology Letters, vol-32, no-1, January 5, 2002, pp. 7-9
138. S. Kawasaki and T. Itoh, *A Slot Antenna with Electronically Tunable Length*, 1991 IEEE Antennas and Propagation Symposium Digest, vol-1, pp. 130-133
139. P. J. Rainville and F. J. Harackiewicz, *Magnetic Tuning of Microstrip Patch Antenna Fabricated on a Ferrite Film*, IEEE Microwave and Guided Wave Letters, vol-2, no-12, December 1992, pp. 483-485
140. D. J. Roscoe, L. Shafai, A. Ittipiboon, M. Cuhaci and R. Douville, *Tunable Dipole Antennas*, 1993 IEEE Antennas and Propagation Symposium Digest, vol-2, pp. 672-675
141. Egor Alekseev, K. Hong, D. Pavlidis, D. Sawadai and A. Samelis, *InGaAs/InP PIN diodes for Microwave and Millimeter Wave Switching and Limiting Applications*, IEEE International Semiconductor Device Research Symposium – 1996
142. M. A. Forman and Z. B. Popovic, *A Tunable Second-Resonance Cross-Slot Antenna*, 1997 IEEE Antennas and Propagation Symposium Digest, vol-1, pp. 18-21
143. S. H. Al-Charchafchi and M. Frances, *Electronically Tunable Microstrip Patch Antennas*, 1998 IEEE Antennas and Propagation Symposium Digest, vol-1, pp. 304-307
144. Elliott R. Brown, *RF-MEMS Switches for Reconfigurable Integrated Circuits*, IEEE Transactions on Microwave Theory and Techniques, vol-46, no-11, November 1998, pp. 1868-1880
145. N. Fayyaz, S. Safavi-Naeini and N. Hodjat, *A Novel Electronically Tunable Rectangular Patch Antenna with One Octave Bandwidth*, IEEE Canadian Conference on Electrical and Computer Engineering, vol-1, 1998, pp. 25-28
146. A. T. Kolsrud, M. Y. Li and Kai Chang, *Dual-Frequency Electronically Tunable CPW-Fed CPS Dipole Antenna*, Electronics Letters, vol-34, no-7, 1998, pp. 609-611
147. S. Sharma and B. R. Vishvakarma, *MOS Capacitor Loaded Frequency Agile Microstrip Antenna*, International Journal of Electronics, vol-86, no-8, 1999, pp. 979-990
148. W. H. Weedon, W. J. Payne, G. M. Rebeiz, J. S. Herd and M. Champion, *MEMS-Switched Reconfigurable Multi-Band Antenna: Design and Modeling*, Proceedings of the Antenna Applications Symposium, Monticello, IL, 1999
149. B. C. C. Chang, Y. Qian and T. Itoh, *A Reconfigurable Leaky Mode/Patch Antenna Controlled by PIN Diode Switches*, IEEE Antennas and Propagation Symposium Digest, 1999

150. W. H. Weedon, W. J. Payne and G. M. Rebeiz, *MEMS – Switched Reconfigurable Antennas*, IEEE Antennas and Propagation Society International Symposium, 2001, pp. 654-657
151. Fan Yang and Yahya Rahmat-Samii, *Patch Antenna with Switchable Slot: Dual – Frequency Operation*, Microwave and Optical Technology Letters, vol-31, no-3, November 5, 2001, pp. 165-168
152. D. Peroulis, K. Sarabandi and L. P. B. Katehi, *A Planar VHF Reconfigurable Slot Antenna*, Proceedings of IEEE Antennas and Propagation Society International Symposium, 2001, vol-1, pp. 154-157
153. Fan Yang and Yahya Rahmat-Samii, *A Reconfigurable Patch Antenna Using Switchable Slots for Circular Polarization Diversity*, IEEE Microwave and Wireless Components Letters, vol-12, no-3, March 2002, pp. 95-98
154. J. M. Laheurte, H. Tosi and J. L. Dubard, *Microstrip Antenna Controlled by PIN Diodes: Influence of the Bias Current on the Antenna Efficiency*, Microwave and Optical Technology Letters, vol-33, no-1, April 5, 2002, pp. 44-47
155. G. H. Huff, J. Feng and J. T. Bernhard, *A Novel Radiation and Frequency Reconfigurable Single Turn Square Spiral Microstrip Antenna*, IEEE Microwave and Wireless Components Letters, vol-13, no-2, February 2003, pp. 57-59
156. Aly Fathy, A. Rosen, H. S. Owen, F. McGinty, D. J. McGee, G. C. Taylor, R. Amantea, P. K. Swain, S. M. Perlow and M. Elsherbiny, *Silicon-Based Reconfigurable Antennas – Concepts, Analysis, Implementation and Feasibility*, IEEE Transactions on Microwave Theory and Techniques, vol-51, no-6, June 2003, pp. 1650-1660
157. W. H. Chen, Z. H. Feng, M. Y. Fan and Y. Furuya, *Dual-Band Reconfigurable Antenna for Wireless Communications*, Microwave and Optical Technology Letters, vol-40, no-6, March 20, 2004, pp. 503-505
158. D. Peroulis, K. Sarabandi and L. P. B. Katehi, *Design of Reconfigurable Slot Antennas*, IEEE Transactions on Antennas and Propagation, vol-53, no-2, February 2005, pp. 645-654
159. A. Reineix and B. Jecko, *Analysis of Microstrip Patch Antennas Using Finite Difference Time Domain Method*, IEEE Transactions on Antennas and Propagation, vol-37, no-11, November 1989, pp. 1361-1369
160. P. Leveque, A. Reineix and B. Jecko, *Modeling Dielectric Losses in Microstrip Patch Antennas: Application of FDTD Method*, Electronics Letters, vol-28, no-6, 1992, pp. 539-540
161. C. Wu, K. L. Wu, Z. Q. Bi and J. Litva, *Accurate Characterization of Planar Printed Antennas Using Finite Difference Time Domain Method*, IEEE Transactions on Antennas and Propagation, vol-40, no-5, 1992, pp. 526-533

162. K. Uehara and K. Kagoshima, *FDTD Method Analyses of Mutual Coupling Between Microstrip Antennas*, IEICE Transactions on Communications, E-76B, 7, 1993, pp. 762-764
163. T. Oonishi, T. Kashiva and I. Fukai, *Analyses of Microstrip Antennas on a Curved Surface Using the Conformal Grids FDTD Method*, Electronics and Communications in Japan, Part 1, 76, 12, 1993, pp. 73-81
164. T. Kashiwa, T. Onishi and I. Fukai, *Analyses of Microstrip Antennas on a Curved Surface Using the Conformal Grids FDTD Method*, IEEE Transactions on Antennas and Propagation, vol-42, no-3, 1994, pp. 423-427
165. R. Luebbers, L. Chen, T. Uno and S. Adachi, *FDTD Calculation of Radiation Patterns, Impedance and Gain for a Monopole Antenna on a Conducting Box*, IEEE Transactions on Antennas and Propagation, vol-40, no-12, 1992, pp. 1577-1583
166. L. Chen, T. Uno, S. Adachi and R. Luebbers, *FDTD Analysis of a Monopole Antenna Mounted on a Conducting Box Covered with a Layer of Dielectric*, IEICE Transactions on Communications, E-76B, 12, 1993, pp. 1583-1586
167. D. M. Sheen, S. M. Ali, M. D. Abouzahra and J. A. Kong, *Application of the Three Dimensional Finite Difference Time Domain Method to the Analyses of Planar Microstrip Circuits*, IEEE Transactions on Microwave Theory and Techniques, vol-38, no-7, 1990, pp. 849-857
168. Bilge Belentepe, *Modeling and Design of Electromagnetically Coupled Microstrip-Patch Antennas and Antenna Arrays*, IEEE Antennas and Propagation Magazine, vol-37, no-1, February 1995, pp. 31-38
169. D. Lee and S. Lee, *Design of a Coaxially Fed Circularly Polarized Rectangular Microstrip Antenna Using a Genetic Algorithm*, Microwave and Optical Technology Letters, vol-26, no-5, September 5, 2000, pp. 288-291
170. H. T. Chen and K. L. Wong, *Analysis of Probe-Fed Spherical-Circular Microstrip Antennas Using Cavity Model Theory*, Microwave and Optical Technology Letters, vol-7, no-7, 1994, pp. 309-312
171. D. L. Sengupta, *Resonant Frequency of a Tunable Rectangular Patch Antenna*, Electronics Letters, vol-20, no-15, July 1984, pp. 614-615
172. B. Beker, G. Cokkinides and A. Templeton, *Analysis of Microwave Capacitors and IC Packages*, IEEE Transactions on Microwave Theory and Techniques, vol-42, no-9, 1994, pp. 1759-1764
173. C. C. Huang and T. H. Chu, *Radiation and Scattering Analysis of a Slot-Coupled Patch Antenna Loaded with a MESFET Oscillator*, IEEE Transactions on Antennas and Propagation, vol-43, no-3, 1995, pp. 291-298

174. R. J. Luebbers and H. S. Langdon, *A Simple Feed Model that Reduces Time Steps Needed for FDTD Antenna and Microstrip Calculations*, IEEE Transactions on Antennas and Propagation, vol-44, no-7, 1996, pp. 1000-1005
175. Mehmet Kara, *Formulas for the Computation of the Far-Field Radiation Patterns of Rectangular Microstrip Antenna Elements with thick Substrates*, Microwave and Optical Technology Letters, vol-14, no-6, 1997, pp. 360-367
176. K. M. Krishnaiah and C. J. Railton, *Passive Equivalent Circuit of FDTD: An Application to Subgridding*, Electronics Letters, vol-33, no-15, July 1997, pp. 1277-1278
177. M. J. White, M. F. Iskander and Z. Huang, *Development of a Multigrid FDTD Code for Three Dimensional Applications*, IEEE Transactions on Antennas and Propagation, vol-45, no-10, 1997, pp. 1512-1517
178. F. Bilotti, F. Castellana and L. Vegni, *Multi-Frequency Patch Antenna Design via the Method of Moment and Genetic Algorithm*, Microwave and Optical Technology Letters, vol-35, no-3, 2002, pp. 184-186
179. F. Kung and H. T. Chuah, *Modeling of Bipolar Junction Transistor in FDTD Simulation of Printed Circuit Board*, Progress in Electromagnetic Research, PIER-36, 2002, pp. 179-192
180. P. B. Katehi and N. G. Alexopoulos, *On the Modeling of Electromagnetically Coupled Microstrip Antennas – The Printed Strip Dipole*, IEEE Transactions on Antennas and Propagation, vol-32, 1984, pp. 1179-1186
181. AppCAD, version 3.0, September – 2002, Hewlett-Packard, USA
182. Product Manual HP8510C VNA, Hewlett Packard Co USA
183. Matlab™ V-7, Mathworks Inc, USA
184. Zealand IE3D version 8.0. Zealand Inc, USA
185. I. Bhal and P. Bhartia, *Microwave Solid State Circuit Design*, John Wiley & Sons, New York.
186. C.R.Rowell, and R.D Murch, *A Capacitively Loaded PIFA for Compact Mobile Telephone Handsets*, IEEE Transactions on Antennas and Propagation, vol-AP-45, 1997, pp. 837 - 842

List of Publications of the Author

International Journals

1. **Shynu S.V**, Gijo Augustin, C.K Aanandan, P. Mohanan and K. Vasudevan, "C-shaped slot loaded reconfigurable microstrip antenna", *Electronics Letters, IEE, UK* Vol-42, Issue-6, March-2006.
2. **Shynu S.V**, Gijo Augustin, C.K Aanandan, P. Mohanan and K. Vasudevan, " Design of Compact Reconfigurable Dual Frequency Microstrip Antennas Using Varactor Diodes", *Progress in Electromagnetics Research, PIER, USA*, 60, 2006
3. **Shynu S.V**, Gijo Augustin, C.K Aanandan, P. Mohanan and K. Vasudevan, " Development of a Varactor Controlled Dual Frequency Reconfigurable Microstrip Antenna", *Microwave and Optical Technology Letters, USA*, 20 August 2005.
4. **Shynu S.V**, Gijo Augustin, C.K Aanandan, P. Mohanan and K. Vasudevan, " A Reconfigurable Dual Frequency Slot Loaded Microstrip Antenna Controlled by PIN Diode", *Microwave and Optical Technology Letters, USA*, 20 February 2005
5. **Shynu S.V**, Gijo Augustin, C.K Aanandan, P. Mohanan and K. Vasudevan, "A Compact Electronically Reconfigurable Dual Frequency Microstrip Antenna for L- Band Applications", *International Journal on Wireless and Optical Communications*, December 2004.
6. Gijo Augustin, **Shynu S.V**, C.K Aanandan, P. Mohanan and K. Vasudevan, "Compact Dual Band Antenna for Wireless Access Point", *Electronics Letters, IEE, UK* Vol-42, Issue-10, March-2006.
7. Gijo Augustin, **Shynu S.V**, C.K Aanandan, P. Mohanan and K. Vasudevan, "Reactive loaded Slot Line Leaky-Wave antenna for low cost beam steering applications", *Microwave and Optical Technology Letters, USA*, 2006.
8. Gijo Augustin, **Shynu S.V**, C.K Aanandan, P. Mohanan and K. Vasudevan, "A Novel Electronically Scannable Log-periodic Leaky Wave Antenna", *Microwave and Optical Technology Letters, USA*, 20 April 2005

International Conference

1. Shynu S. V, Gijo Augustin, CK Aanandan, P. Mohanan and K. Vasudevan. "Meandered Slot Arm Loaded Electronically Tunable Microstrip Antenna Using Varactors", *Proc. of IEEE APS International Symposium, Albuquerque, USA, July-2006*
2. Shynu S. V, Gijo Augustin, CK Aanandan, P. Mohanan and K. Vasudevan. "Triple Slot Arm Loaded Reconfigurable Dual Frequency Antenna Using Varactors", *Proc. of IEEE APS International Symposium, Washington, USA, July-2005*
3. Shynu S. V, Gijo Augustin, CK Aanandan, P. Mohanan and K. Vasudevan. "A Novel Reconfigurable Hexagonal Slot Loaded Microstrip Antenna" *URSI General Assembly- 2005 International Symposium, New Delhi, India, July-2005*
4. Shynu S. V, Rohith K. Raj, Anupam R. Chandran, Aanandan C. K, Mohanan P. and Vasudevan K. "Single Feed Dual Frequency Dual Polarized Microstrip Antenna with Hexagonal Slot" *Proc. of IEEE APS International Symposium, Monterey, CA, USA, June 20-25, 4380-4383*
5. Gijo Augustin, Shynu S. V, CK Aanandan, P. Mohanan and K. Vasudevan. "An Electronically Scannable Wide Band Leaky – Wave Antenna Using Varactor Diodes" *URSI General Assembly- 2005 International Symposium, New Delhi, India, July-2005*
6. Gijo Augustin, Shynu S. V, CK Aanandan, P. Mohanan and K. Vasudevan. "Wide Band Electronically Steerable Leaky Wave Antenna for Beam Steering Applications" *Asia Pacific Microwave Conference-2005, International Symposium, Suschou, China, December-2005*
7. Gijo Augustin, Shynu S. V, CK Aanandan, P. Mohanan and K. Vasudevan. "A Novel Leaky Wave Antenna Capable for Electronic Beam Steering", *IEEE APS International Symposium, Albuquerque, USA, July-2006*
8. Gijo Augustin, Shynu S. V, CK Aanandan, P. Mohanan and K. Vasudevan "A Novel Compact Monopole Antenna for Wireless Modules", *International Conference on Computers and Devices for Communication (CODEC-06) December, 2006, Kolkata, India*
9. Gijo Augustin, Shynu S. V, CK Aanandan, P. Mohanan and K. Vasudevan "Multiband Antenna for Short Range Wireless Communications", *International Conference on Microwaves, Antenna, Propagation and Remote Sensing (ICMARS-2006) December 18-22, 2006, Jodhpur, India*
10. Rohith K. Raj, Sona O. Kundukulam, Shynu S.V, CK. Aanandan, K. Vasudevan, P. Mohanan and Praveen Kumar "Compact Slotted Active Microstrip Antenna", *International Conference on Computers and Devices for Communication (CODEC-04) January 1-3, 2004, Kolkata, India*

National Conference

1. Shynu S.V, Gijo Augustin, C.K Aanandan, P. Mohanan and K. Vasudevan “Electronically Reconfigurable Dual Frequency Microstrip Antenna Using Varactor Diode” *Proc. of the National Symposium on Antennas and Propagation (APSYM-2004)*, 21-23 Dec. 2004, 131-134, Cochin University of Science and Technology, Kochi
2. Shynu S.V, Gijo Augustin, C.K Aanandan, P. Mohanan and K. Vasudevan, “A Varactor Controlled Electronically Reconfigurable Dual Frequency Microstrip Antenna”, *Emerging and Futuristic Communication Systems-EFCoS-2005 Symposium*, IETE, Bangalore, India
3. Gijo Augustin, Shynu S.V, C.K Aanandan, P. Mohanan and K. Vasudevan “Electronically Reconfigurable Dual Frequency Microstrip Antenna Using Varactor Diode” *Proc. of the National Symposium on Antennas and Propagation (APSYM-2004)*, 21-23 Dec. 2004, 127-130, Cochin University of Science and Technology, Kochi

Shynu S.V

STEC Senior Research Fellow
Centre for Research in Electromagnetics and Antennas
Department of Electronics
Cochin University of Science and Technology
Cochin-22, Kerala, India
Tel: +91-484-2576418
Fax: +91-484-2575800
Email: shynusv@cusat.ac.in

Objective:

To pursue research activities in the field of electronically reconfigurable microstrip antennas, leaky-wave antennas and electromagnetic computation

Research Experience

1. Worked as JRF in the Centre for Research in Electromagnetics and Antennas (CREMA), Department of Electronics, Cochin University of Science and Technology, Cochin from March 2003 – February 2006
2. Working as Project Fellow in the UGC sponsored project entitled, “Development of Electronically Reconfigurable Microstrip Antennas for Mobile and Satellite Communication Systems” at Department of Electronics, Cochin University of Science and Technology, Cochin from August 2006 – till date.

Publications

International Journal	8
International Conference	10
National Conference	3

Citation in International Journals

1. A Directivity Diversity Microstrip Antenna Array in Millimeter Wave , M.Caillet et. al., *Microwave and Optical Technology Letters*, USA, Vol. 48, Issue -6, June 2006, pp 1190 – 1194.
2. A New Bi-faced Log Periodic Printed Antenna., E. Avila – Navarro et.al., *Microwave and Optical Technology Letters*, USA, Vol. 48, Issue -2, February 2006, pp 402 –405.

Education

M.Sc Applied Physics

Mahatma Gandhi University

Specialization: Optoelectronics & Optical Fiber Communication

Duration: 1999-2001

Percentage: 66.1% (First Class, University IV-Rank)

B.Sc Physics

University of Kerala

Duration: 1996-1999

Percentage: 87.4% (First class with Distinction)

Pre-Degree

University of Kerala

Duration: 1994 -1996

Percentage: 77.2% (First class)

SSLC

Board of Public Examinations (1994)

Govt. of Kerala, India

Percentage: 78.2% (First Class)

Awards Obtained:

Awarded with Junior Research Fellowship (JRF) by Science Technology and Environment Department (STEC), Govt. of Kerala, India.

Computer proficiency

Languages

C++, FORTRAN, Matlab, Assembly Languages for Intel 8085 Microprocessor

Operating Systems

Windows 9x, Windows 2000, Windows XP, Redhat-Linux, Fedora-Linux

RF Tools

Zealand IE3D, HFSS, Ansoft Designer, AWR Microwave Office, Flomerics Microstripes, Agilent ADS, CST Microwave Studio

A

absorbing boundary, 17, 70, 71, 73
 alumina, 51
 anechoic chamber, 55, 57
 aperture coupling, 14
 AppCAD, 54

B

bandwidth, 22, 23, 25, 32, 33, 34, 35,
 36, 37, 38, 40, 44, 54, 56, 57, 78, 89,
 114, 122, 123, 125, 134
 beam width, 121, 136
 biconical antenna, 3
 built-in potential, 141

C

capacitors, 19, 46, 124, 125,
 cavity model, 8, 31, 32, 42, 46
 chamber reflectivity, 55
 chip inductors , 110, 124, 142, 154,
 164, 177
 circular patch, 30, 32, 96, 136
 circular polarization, 5
 coaxial feed, 12, 13
 coplanar waveguide, 11, 15
 coupling constant, 12, 13
 courant stability, 67
 CPW, *see Coplanar waveguide*
 C-shaped slot, 176, 181

D

DECT mobile system , 36
 developer solution, 52
 dielectric constant, 9, 21, 36, 46, 51,
 82, 83, 85, 89, 91, 96, 105, 151
 dielectric substrate, 4, 6, 7, 9, 15, 29,
 51, 82, 83, 85, 89, 91, 96, 105
 dipole, 3, 9, 10, 40, 41, 42
 dominant mode, 12
 dual polarization, 5, 19

E

electromagnetic coupling, 53, 84, 176
 electromagnetic interference, 55
 electronic intelligence, 3, 24
 electronic tuning, 20, 21, 22, 40, 78,
 79, 87, 100
 electronic surveillance, 77

F

FDTD, 16, 24, 25, 29, 45, 47, 60, 61,
 62, 63, 69, 72, 73, 108, 117,
 ferrite, 21, 32, 40
 ferromagnetic, 51
 FFT, 60, 62
 Fourier-Transform, *see* FFT
 FR4, 52
 frequency ratio, 38, 39, 43, 122, 123,
 124, 125, 126, 130, 138, 141, 143,
 144, 147, 153, 154, 155, 156
 frequency tuning, 20, 21, 43, 45, 78,
 85, 89, 99, 103, 112, 123, 125, 141,
 143, 153, 159, 160, 176, 179

G

gain, 5, 9, 22, 24, 25, 36, 44, 56, 59,
 61, 72, 96, 97, 118, 141, 148, 149, 153
 gaussian pulse, 61, 68, 69, 71, 73, 117
 GPS, 3, 23, 33, 37
 Green's function, 15, 16
 GSM, 39

H

half-wave dipole, 3
 Hertz, 3
 hexagonal slot, 60, 62, 73
 horn antenna, 57, 58, 59
 HP 8510C, 51, 55, 56, 92
 HP-BASIC, 55
 HPIB, 55

I

IE3D, 25, 73, 80, 83, 85, 86, 88, 89,
93, 115, 116, 127, 144, 145, 155, 176
InGaAs, 41
InP, 41
input impedance, 8
Inverse Fourier Transform, 54

L

L-band, 24, 30
loss-tangent, 8

M

magnetic tuning, 20, 21
Matlab, 61
Maxwell, 3, 16, 60, 63, 64, 65
meander slot line, 181
mechanical tuning, 20, 21, 87, 98
MEMS, 22, 41, 42, 43, 190
method of moment, 25, 31, 46, 47,
80, 114, 123, 142, 176
Mgrid, 74
microstrip antenna, 4, 5, 6, 7, 9, 11,
12, 15, 16, 17, 19, 21, 22, 23, 24, 25,
29, 30, 31, 32, 33, 34, 35, 36, 37, 38,
39, 40, 45, 46, 47, 77, 78, 79, 80, 83,
84, 92, 95, 100, 102, 108, 109, 110,
11, 112, 115, 116, 117, 119, 177, 181,
187, 188
microstrip line, 53, 62, 70, 85, 110
MIM Capacitor, 114
MMIC, 15, 22
mobile communications, 33
modal expansion method, 32
Modua, 74
MPIE, 16
Mur, 70

N

network analyzer, 54, 55, 56, 57, 92,
95, 143

O

optical lithography, *see photolithography*
orthogonal mode, 17, 18, 31, 93, 147
orthogonal polarization, 85, 147, 148,
157, 163, 171, 174

P

patch antenna, 9, 19, 79, 97
PEC, 73
photolithography, 52
photo mask, 52, 53
photo resist, 52
PIFA, 33, 39
PIN Diode, 42, 43, 44, 44, 78, 95,
109, 110, 111, 112, 113, 114, 115,
116, 117, 118, 119, 120, 121, 122,
123, 124, 125, 126, 127, 130, 131,
132, 134, 135, 136, 137, 138, 139,
141, 142, 159, 187, 188, 189, 190
p-n junction, 141, 152
polarization diversity, 4, 43, 78
polyolefin, 51
polyphenylene, 51
polystyrene, 51
printed slot antennas, 9, 10
probe coupling, 12
proximity coupling, 14, 53, 80
PTFE, 51

Q

quartz, 51

R

radar, 3, 5, 24, 37
radiation, 3, 4, 5, 6, 7, 8, 9, 10, 12, 13,
15, 17, 19, 21, 23, 24, 25, 29, 30, 31,
32, 35, 37, 38, 39, 40, 42, 43, 44, 45,
46, 47, 56, 57, 58, 59, 60, 71, 73, 74,
77, 78, 79, 80, 96, 97, 120, 121, 122,
123, 136, 137, 138, 147, 149, 150,

7394

153, 158, 164, 167, 171, 172, 174,
180, 181, 183, 187, 190
radiation efficiency, 51
radiometer, 5
reactive loading, 5, 39
rectangular patch, 6, 8, 10, 12, 19, 30,
32, 33, 35, 38, 39, 40, 41, 42, 45, 46,
47, 79, 87, 91, 114, 122, 134, 146,
158, 163, 166, 167, 169, 170, 171,
173, 174, 180, 183, 189
RF Stimulus, 55
RLC Network, 8
rutile, 51

S

sapphire, 51
scatterometer, 37
semiconductor, 51, 53, 109, 152
semiconductor diodes, 22, 29
slot antenna, 9, 10, 11, 35, 40, 41, 43,
44
SMA Connector, 12
Smith chart, 55
Sommerfield's potential, 16
S-parameter, 55, 56, 57, 60, 74
spectral domain, 16, 32
square patch, 36, 78, 80, 81, 82, 83,
84, 85, 87, 88, 89, 93, 97, 104, 106,
107, 108, 109, 110, 111, 112, 124,
125, 143, 150, 151, 153, 162, 164,
176, 178, 181, 189
staircase approximation, 60, 61, 81,
83, 190
synthetic aperture radar, 24, 37

T

TE-Mode, 11
transmission line model, 7, 8, 25, 30,
31, 32, 37, 41, 46, 150
travelling wave antenna, 11

U

UAV, 24
UV Light, 52

V

varactor diode, 22, 24, 25, 41, 42, 53,
74, 100, 141, 142, 144, 146, 148, 151,
153, 154, 159, 164, 168, 171, 172,
176, 177, 181, 182, 189

W

wireless communication, 3, 23, 44,
187
WLAN, 3, 37

Y

Yee's Cell, 68
YIG, 55

Z

Zealand, 74

